SYNTHESIS, CHARACTERIZATION AND BIOLOGICAL ACTIVITY OF COPPER(II) AND ZINC(II) COMPLEXES OF THIOSEMICARBAZONES AND THEIR N(4)-SUBSTITUTED DERIVATIVES DERIVED FROM 2,4-DIHYDROXYBENZALDEHYDE

TAN KONG WAI

FACULTY OF SCIENCE

UNIVERSITY MALAYA

KUALA LUMPUR

2010

SYNTHESIS, CHARACTERIZATION AND BIOLOGICAL ACTIVITY OF COPPER(II) AND ZINC(II) COMPLEXES OF THIOSEMICARBAZONES AND THEIR N(4)-SUBSTITUTED DERIVATIVES DERIVED FROM 2,4-DIHYDROXYBENZALDEHYDE

TAN KONG WAI

THESIS SUBMITTED IN FULFILLMENT OF THE

REQUIREMENT FOR THE DEGREE OF

DOCTOR OF PHILOSOPHY

FACULTY OF SCIENCE

UNIVERSITY MALAYA

KUALA LUMPUR

2010

ACKNOWLEDGEMENTS

I would like to express my heartfelt gratitude and appreciation to both my supervisors, Prof. Dato' Dr. Mohd. Jamil Maah from Chemistry Department, Faculty of Science, Universiti Malaya and Assoc. Prof. Dr. Ng Chew Hee from Department of Chemistry, Faculty of Engineering and Science, University Tunku Abdul Rahman for their encouragement, guidance and the precious time that they have devoted to this research. I would also like to thank them for their patience and many hours of hardwork in giving suggestions and proof reading this dissertation.

I also would like to thank Prof. Dr. Ng Seik Weng for solving all the crystal structures and his critical comments throughout my tenure as a student. His comments have helped me to reflect on my shortcomings that need to be overcome in order to be a better chemist. I am also thankful to the Head of Department, Prof. Dr. Zanariah Abdullah, all the lecturers and staff at Chemistry Department who have supported and helped me in my research in Universiti Malaya.

I am also very grateful to the Ministry of Higher Education (MOHE) and Universiti Malaya for their financial support through SLAI Fellowship and various research grants (PS197/2008A and FS316/2008C).

I am also very thankful to my parents and siblings for their love, understanding and support during all these years. I owe my achievement to them. I also need to thank Ms. Seng Hoi Ling, Ms. Von Sze Tin, Ms. Lim Fei Shen and Mr. James Chong for all their help and guidance in the biological studies. Many thanks to Mr. Lee Guan Serm, Ms. Hong Sok Lai and Mr. Mohd. Rizal Razalli for their friendship, help and motivations during my study.

Last but not least, I would like to dedicate my work to my beloved wife, Sim Bean for her patience, love and understanding all these years. She has helped me to become a better person. With her support, my endeavor has become more meaningful and purposeful.

ABSTRACT

Four thiosemicarbazones ligands (**1-4**) have been prepared with good yield by refluxing 2,4-dihydroxybenzaldehyde with thiosemicarbazide or N(4)-substituted thiosemicarbazide in ethanol or methanol. From these four ligands, 16 new ternary metal complexes (**5-20**) with the general formulation of M(B)L have been prepared from the reactions of metal acetates with 2,4-dihydroxybenzaldehyde N(4)-substituted thiosemicarbazone in the presence of *N*,*N*-heterocyclic base (M^{2+} = Zn^{2+} or Cu^{2+}; B = 2,2'-bipyridine, (bpy); 1,10-phenanthroline, (phen); L^{2-} = doubly deprotonated thiosemicarbazones = 2,4-dihydroxybenzaldehyde thiosemicarbazonato, (HT); 2,4-dihydroxybenzaldehyde 4-methylthiosemicarbazonato, (HM); 2,4-dihydroxybenzaldehyde 4-ethylthiosemicarbazonato, (HE) and 2,4-dihydroxybenzaldehyde 4-phenylthiosemicarbazonato, (HP)) These compounds have been characterized by elemental analyses, IR, UV-Vis, NMR and magnetic susceptibility. The structures for ligands (**2, 3, 5)** and complexes (**8, 9, 11, 13** and **18**) have been solved by single crystal X-ray crystallography. Results from spectroscopic data and crystal structure analysis show that all the free ligands exist in the **thione form**. The complexes are mononuclear and five coordinated with the doubly deprotonated thiosemicarbazone as a tridentate ligand coordinating through the phenolic oxygen, azomethine nitrogen and thiolate sulfur while 2,2'-bipyridine or 1,10-phenanthroline as the *N,N'*-bidentate ligand**.** The coordination geometries vary from distorted square pyramidal to distorted trigonal bipyramidal. The effect of varying the N(4) substituent from methyl, ethyl to phenyl, metal ions and polpyridyl ligand towards the chemical and biological properties of these compounds (DNA duplex and G-quadruplex binding, nucleolytic, topoisomerase I inhibition and antimicrobial) have been studied. Results from our biological studies show that compounds with more hydrophobic ligands generally have better biological properties. The nucleolytic efficiency of the copper(II) complexes are better than their zinc analogs. Interestingly, complexes Cu(phen)(HM) **18** and Cu(phen)(HE) **19** can induce oxidative DNA cleavage in the absence of exogenous agent.

ABSTRAK

Empat ligan tiosemikarbazon (**1-4**) telah berjaya disediakan dengan hasil yang baik dengan kaedah refluks campuran 2,4-dihidroksibenzaldehid dengan tiosemikarbazida atau dengan tiosemikarbazida N(4)-tertukarganti dalam metanol atau etanol. Daripada empat ligan ini, 16 kompleks logam ternari (**5-20)** dengan formula umum, M(B)(L) telah disediakan melalui tindak balas antara asetat logam dan 2,4-dihidroksibenzaldehid tiosemikarbazon N(4)-tertukarganti dengan kehadiran bes N,N'-heterosiklik (M^{2+} = Zn^{2+} atau Cu^{2+}; B = 2,2'-bipiridina, (bpy); 1,10'-phenantrolin, (phen); L^{2-} = tiosemikarbazon ternyahproton = 2,4-dihidroksibenzaldehid tiosemikarbazonato, (HT); 2,4-dihidroksibenzaldehid 4-metiltiosemikarbazonato, (HM); 2,4-dihidroksibenzaldehid4-etiltiosemikarbazonato, (HE) and 2,4-dihidroksibenzaldehid 4-feniltiosemikarbazonato, (HP)). Sebatian yang terhasil telah dicirikan dengan kaedah analisis unsur, spektroskopi seperti infra merah, ultra-lembayung nampak, resonans magnet nukleus dan kerentanan magnet. Struktur untuk ligan-ligan (**2**, **3** dan **5**) dan kompleks (**8, 9, 11, 13** and **18**) telah ditentukan dengan kaedah kristalografi sinar-X. Data spektroskopi dan analisis struktur hablur menunjukkan bahawa semua ligan bebas wujud dalam bentuk tion. Kompleks yang terhasil adalah mononuklear dan terkoordinat lima. Tiosemikarbazon yang ternyahproton bertindak sebagai ligan tridentat yang mengkoordinat melalui oksigen fenolik, nitrogen azometina dan sulfur tiolat manakala 2,2'-bipiridina atau 1,10-phenantrolin bertindak sebagai ligan bidentat-N,N'. Kompleks yang terhasil mempunyai geometri piramid segiempat terherot atau trigonal bipiramid terherot. Kesan mengubah kumpulan penukarganti N(4) dari metil, etil ke fenil serta ion logam dan ligan polipiridil terhadap sifat kimia dan aktiviti biologi (pertambatan DNA, nukleolitik, perencatan toposiomerase I dan antimikrob) sebatian-sebatian ini telah dikaji. Kajian aktiviti biologi menunjukkan bahawa secara kebiasaannya, sebatian yang mengandungi ligan yang lebih hidrofobik memiliki aktiviti biologi yang lebih baik. Aktiviti nukleolitik kompleks kuprum(II) adalah lebih baik berbanding dengan analog zink. Kompleks Cu(phen)(HM) **18** dan Cu(phen)(HE) **19** boleh mengaruhkan pembelahan DNA oksidatif tanpa kehadiran agen eksogenus.

TABLE OF CONTENTS

			PAGE
ACKNOWLEDGEMENT			I
ABSTRACT			II
ABSTRAK			III
TABLE OF CONTENTS			IV
LIST OF TABLES			IX
LIST OF FIGURES			XII
LIST OF SYMBOLS AND ABBREVIATIONS			XX
CHAPTER			
1	**Introduction**		
	1.1	**Metal ions in biological system**	1
	1.2	**Metal complexes with anticancer properties: Designs and improvements**	2
	1.2.1	Improving platinum based anticancer agents	3
	1.2.2	Utilization of prodrugs	8
	1.2.3	Non-platinum DNA targeting drugs	10
	1.2.4	DNA intermediates as target	12
	1.2.5	Metal complexes targeting protein and enzyme	16
	1.2.6	Conclusion	19
	1.3	**Thiosemicarbazones in general**	20
	1.4	**Anticancer properties of thiosemicarbazone and their metal complexes**	23
	1.5	**Thiosemicarbazones with polyhydroxybenzaldehyde**	25
	1.6	**Purpose of research**	25

2	**Synthesis, characterization and biological properties of zinc(II) complexes of 2,4-dihydroxybenzaldehyde N^4-substituted thiosemicarbazones and 2,2'-bipyridine**		28
	2.1	**Introduction**	28
	2.2	**Experimental**	30
	2.2.1	Materials and solutions	30
	2.2.2	Physical measurements	31
	2.2.3	Syntheses	32
	2.2.4	X-ray crystallography	38
	2.2.5	DNA binding	39
	2.2.6	Nucleolytic study	39
	2.2.7	Human Topoisomerase I inhibtion assay	40
	2.2.8	Antibacterial and antifungal assay	42
	2.3	**Results and discussion**	43
	2.3.1	Synthesis of ligands and complexes	43
	2.3.2	Crystal structure analysis	46
	2.3.3	Infrared and electronic spectra	65
	2.3.4	^{1}H and ^{13}C NMR spectra	71
	2.3.5	DNA binding	76
	2.3.6	Nucleolytic study	93
	2.3.7	Topoisomerase I inhibition assay	96
	2.3.8	Antibacterial and antifungal assay	99
	2.4	**Conclusion**	104

3 Synthesis, characterization and biological properties of zinc(II) complexes of 2,4-dihydroxybenzaldehyde N^4-substituted thiosemicarbazones and 1,10-phenanthroline 106

3.1 Introduction 106

3.2. Experimental 107

3.2.1 Materials and solutions 107

3.2.2 Physical measurements 107

3.2.3 Syntheses 108

3.2.4 X-ray crystallography 110

3.2.5 DNA binding 111

3.2.6 Nucleolytic study 111

3.2.7 Human Topoisomerase I inhibtion assay 112

3.2.8 Antibacterial and antifungal assay 112

3.3 Results and discussion 112

3.3.1 Synthesis of the complexes 112

3.3.2 Crystal structure analysis 114

3.3.3 Infrared and electronic spectra 125

3.3.4 ^{1}H and ^{13}C NMR spectra 129

3.3.5 DNA binding 131

3.3.6 Nucleolytic study 142

3.3.7 Topoisomerase I inhibition assay 144

3.3.8 Antibacterial and antifungal assays 147

3.4 Conclusion 151

4	**Synthesis, characterization and biological properties of copper(II) complexes of 2,4-dihydroxybenzaldehyde N^4-substituted thiosemicarbazones and 2,2'-bipyridine**		154
	4.1	**Introduction**	154
	4.2	**Experimental**	155
	4.2.1.	Materials and solutions	155
	4.2.2	Physical measurements	155
	4.2.3	Syntheses	156
	4.2.4	X-ray crystallography	158
	4.2.5	DNA binding	158
	4.2.6	Nucleolytic study	158
	4.2.7	Human Topoisomerase I inhibtion assay	158
	4.2.8	Antibacterial and antifungal assay	159
	4.3	**Results and discussion**	159
	4.3.1	Synthesis of the complexes	159
	4.3.2	Crystal structure analysis	161
	4.3.3	Infrared and electronic spectra	167
	4.3.4	DNA binding	171
	4.3.5	Nucleolytic study	185
	4.3.6	Topoisomerase I inhibition assay	191
	4.3.7	Antibacterial and antifungal assay	195
	4.4	**Conclusion**	200
5	**Synthesis, characterization and biological properties of copper(II) complexes of 2,4-dihydroxybenzaldehyde N^4-substituted thiosemicarbazones and 1,10-phenanthroline**		202
	5.1	**Introduction**	202

5.2 Experimental 203

5.2.1. Materials and solutions 203

5.2.2 Physical measurements 203

5.2.3 Syntheses 203

5.2.4 X-ray crystallography 205

5.2.5 DNA binding 206

5.2.6 Nucleolytic study 206

5.2.7 Human Topoisomerase I inhibtion assay 206

5.2.8 Antibacterial and antifungal assay 206

5.3 Results and discussion 206

5.3.1 Synthesis of the complexes 206

5.3.2 Crystal structure analysis 209

5.3.3 Infrared and electronic spectra 214

5.3.4 DNA binding 218

5.3.5 Nucleolytic study 226

5.3.6 Topoisomerase I inhibition assay 239

5.3.7 Antibacterial and antifungal assay 240

5.4 Conclusion 244

6 Conclusion 246

6.1 Syntheses and characterization of the ligands and complexes 246

6.2 Biological activities 248

6.3 Suggestions 254

References 255

Appendix 271

LIST OF TABLES

Table No.		PAGE
2.1	Stoichiometries, colours and partial elemental analyses of the ligands and zinc(II) complexes	45
2.2	Crystal data and structure refinement parameters for compounds **2, 3, 5** and **8**	49
2.3	Selected bond lengths (Å) and angles (˚) for H_3M (**2**)	50
2.4	Hydrogen-bond geometry (Å, °) for H_3M (**2**)	50
2.5	Selected bond lengths (Å) and angles (˚) for H_3E (**3**)	53
2.6	Hydrogen-bond geometry (Å, °) for H_3E (**3**)	53
2.7	Selected bond lengths (Å) and angles (˚) for [Zn(bpy)(HT)](**5**)	58
2.8	Hydrogen-bond geometry (Å, °) for [Zn(bpy)(HT)](**5**)	58
2.9	Selected bond lengths (Å) and angles (˚) for [Zn(bpy)(HP)].2H $_2$O (**8**)	64
2.10	Hydrogen-bond geometry (Å, °) for [Zn(bpy)(HP)].2H_2O (**8**)	65
2.11	IR spectral assignments for the ligands and their zinc(II) complexes	70
2.12	Electronic spectral assignments (cm^{-1}) for the ligands and their zinc(II) complexes in DMF	71
2.13	^{1}H NMR spectral assignments for the thiosemicarbazone ligands and their zinc(II) complexes in DMSO	73
2.14	^{13}C spectral assignments for the thiosemicarbazone ligands in DMSO	76
2.15	CD spectral bands of duplex oligo or quadruplex + zinc complex: wavelength, λ (molar ellipcity)	79

2.16	Mean MIC value (µg/mL) towards microbes tested.	100
2.17	Mean MIC value (µg/mL) towards fungi tested.	103
3.1	Stoichiometries, colors and partial elemental analyses of the zinc(II) complexes	114
3.2	Crystal data and structure refinement parameters for complex **9a** and **11a.**	119
3.3	Selected bond lengths (Å) and angles (°) for [Zn(phen)(HT)].H2O. DMSO (**9a**)	120
3.4	Hydrogen-bond geometry (Å, °) for [Zn(phen)(HT)].H_2O. DMSO (**9a**)	120
3.5	Selected bond lengths (Å) and angles (°) for [Zn(phen)(HE)].H_2O.DMF (**11a**)	124
3.6	Hydrogen-bond geometry (Å, °) for [Zn(phen)(HE)].H_2O.DMF (**11a**)	124
3.7	IR spectral assignments (cm^{-1}) for the ligands and their zinc(II) complexes	127
3.8	Electronic spectral assignments (cm^{-1}) for the ligands and their zinc(II) complexes in DMF	128
3.9	^{1}H NMR spectral assignments for the ligands and their zinc(II) complexes in DMSO	129
3.10	CD spectral bands of duplex oligo or quadruplex + copper complex: wavelength, λ (molar ellipcity)	138
3.11	Mean MIC value (µg/mL) towards microbes tested.	147
3.12	Mean MIC value (µg/mL) towards fungi tested	151
4.1	Stoichiometries, colors and partial elemental analyses of the copper(II) complexes	160
4.2	Crystal data and structure refinement parameters for complex **13a**	165
4.3	Selected bond lengths (Å) and angles (°) for [Cu(bpy)(HT)].DMF (**13a**)	166
4.4	Hydrogen-bond geometry (Å, °) for [Cu(bpy)(HT)].DMF (**13a**)	166

4.5	IR spectral assignments (cm^{-1}) for the ligands and their copper(II) complexes	169
4.6	Electronic spectral assignments (cm^{-1}) for the ligands and their copper(II) complexes in DMF	171
4.7	CD spectral bands of duplex oligo or quadruplex + copper complex: wavelength, λ (molar ellipcity)	180
4.8	Mean MIC value (µg/mL) towards microbes tested.	196
4.9	Mean MIC value (µg/mL) towards fungi tested	199
5.1	Stoichiometries, colors and partial elemental analyses of the copper(II) complexes	208
5.2	Crystal data and structure refinement parameters for complex **18a**	212
5.3	Selected bond lengths (Å) and forangles (°) [Cu(phen)(HM)].H_2O.DMSO (**18a**)	213
5.4	Hydrogen-bond geometry (Å, °) for [Cu(phen)(HM)].H_2O.DMSO (**1a**)	213
5.5	IR spectral assignments (cm^{-1}) for the ligands and their copper(II) complexes	216
5.6	Electronic spectral assignments (cm^{-1}) for the ligands and their copper(II) complexes in DMF	218
5.7	CD spectral bands of duplex oligo or quadruplex + copper complex: wavelength, λ (molar ellipcity)	223
5.8	Mean MIC value (µg/mL) towards microbes tested	242
5.9	Mean MIC value (µg/mL) towards fungi tested	244

Figure No. **LIST OF FIGURES**

1.1	Platinum(IV) complex bound to SWNT	5
1.2	Trinuclear platinum complex, BBR3464	6
1.3	Polynuclear platinum(II) complex, TriplatinNC	7
1.4	*Trans*-dihydroxy platinum(IV) prodrugs	9
1.5	*Trans, trans, trans*-$[Pt(N_3)_2(OH)_2(NH_3)(py)]$	9
1.6	Assembly of the $[Fe_2L_3]^{4+}$ ($L=C_{25}H_{20}N_4$) tetracationic supramolecular helicate	13
1.7	The saturated iron triple helicate binds to a three-way DNA junction	13
1.8	Substituted salicylidene phenylenediamine-nickel(II) complex	15
1.9	Pentacationic manganese(III) porphyrin	16
2.1	Proposed structures for all the compounds	44
2.2	Thermal ellipsoid (Barbour, 2001) plot of **2** drawn at the 70% probability level. Hydrogen atoms are drawn as spheres of arbitrary radii.	46
2.3	Thione-thiol tautomerization for the ligands	46
2.4	Hydrogen bond interactions for compound **2**	47
2.5	Intermolecular O2—H2O···S hydrogen bonds for compound **2**	47
2.6	Intermolecular N2—H2N···O1 hydrogen bonds for compound **2**	48
2.7	Unit cell packing diagram of **2** along c axis	48
2.8	Thermal ellipsoid (Barbour, 2001) plot of **3** drawn at the 70% probability level. Hydrogen atoms are drawn as spheres of arbitrary radii.	51
2.9	Hydrogen bonding interactions for compound **3**	52
2.10	Unit cell packing diagram of **3** along c axis	52
2.11	Thermal ellipsoid (Barbour, 2001) plot of **5** drawn at the 70% probability level. Hydrogen atoms are drawn as spheres of	54

	arbitrary radii.	
2.12	Simplified hydrogen bonding interactions for complex **5.** Bipyridine carbons have been omitted for clarity.	56
2.13	Unit cell packing diagram of complex **5** along c axis.	57
2.14	Thermal ellipsoid (Barbour, 2001) plot of **8** drawn at the 70% probability level. Hydrogen atoms are drawn as spheres of arbitrary radii.	59
2.15	Zig-zag chain formed from N3-H3---O2 hydrogen bonding interactions for complex **8**	61
2.16	Water molecules (green) bridging the adjacent mononuclear complexes into a three-dimensional network through hydrogen bonding.	62
2.17	Unit cell packing diagram of **8** view along b axis.	63
2.18	IR spectra for the ligands	66
2.19	IR spectra of all the complexes	67
2.20	CD spectra of 15 µM of oligonucleotide in the absence and presence of 120 µM of complex **5**	80
2.21	CD spectra of 15 µM of oligonucleotide in the absence and presence of 120 µM of complex **6**	80
2.22	CD spectra of 15 µM of oligonucleotide in the absence and presence of 120 µM of complex **7**	81
2.23	CD spectra of 15 µM of oligonucleotide in the absence and presence of 120 µM of complex **8**	81
2.24	CD spectra of 10 µM of oligonucleotides in the absence and presence of 120 µM of complex **5**	84
2.25	CD spectra of 10 µM of oligonucleotides in the absence and presence of 120 µM of complex **6**	84
2.26	CD spectra of 10 µM of oligonucleotides in the absence and presence of 120 µM of complex **7**	85
2.27	CD spectra of 10 µM of oligonucleotides in the absence and	85

	presence of 120 μM of complex **8**	
2.28	CD spectra of 20 μM of G-quadruplex in the absence and presence of 120 μM of complex	89
2.29	CD spectra of 20 μM of G-duplex in the absence and presence of 120 μM of complex	91
2.30	Electrophoresis results of incubating pBR322 (0.5 μg/μL) in the presence of complex **6** in TN buffer (5 mM Tris, 50 mM NaCl) pH 7.5 at 37 ^{o}C for 24 h.	94
2.31	Electrophoresis results of incubating pBR322 (0.5 μg/μL) in the presence of complex **8** in TN buffer (5 mM Tris, 50 mM NaCl) pH 7.5 at 37 ^{o}C for 24 h.	94
2.32	Electrophoresis results of incubating pBR322 (0.5 μg/μL) with $ZnCl_2$ or complex **5-8** in TN buffer (5 mM Tris, 50 mM NaCl) pH 7.5 at 37 ^{o}C for 2 h in the absence and presence of exogenous agents	95
2.33	Human topoisomerase I inhibition assay by gel electrophoresis. Electrophoresis results of incubating human topoisomerase I (1 unit/21μL) with pBR322 in the absence or presence of 40 μM of complex	97
2.34	Effect of sequence of mixing for the human topoisomerase I inhibition assay of complex **8**. Electrophoresis results of incubating human topoisomerase I (1 unit/21μL) with pBR322	99
3.1	Proposed structure for all the compounds	113
3.2	Thermal ellipsoid (Barbour, 2001) plot of **9a** drawn at the 70% probability level. Hydrogen atoms are drawn as spheres of arbitrary radii.	115
3.3	Hydrogen bonding interactions for complex **9a**	117
3.4	Unit cell packing diagram of **9a** along b axis.	118
3.5	Thermal ellipsoid (Barbour, 2001) plot of **11a** drawn at the 70% probability level. Hydrogen atoms are drawn as spheres of arbitrary radii.	121
3.6	Hydrogen bonding interactions for complex **11a**	122

3.7	Unit cell packing diagram of **11a** view down in between a and c axes.	123
3.8	IR spectra of the zinc complexes	126
3.9	CD spectra of 15 μM of oligonucleotide in the absence and presence of 120 μM of complex **10**	133
3.10	CD spectra of 15 μM of oligonucleotide in the absence and presence of 120 μM of complex **11**	133
3.11	CD spectra of 10 μM of oligonucleotides in the absence and presence of 120 μM of complex **10**	136
3.12	CD spectra of 10 μM of oligonucleotides in the absence and presence of 120 μM of complex **11**	136
3.13	CD spectra of 20 μM of G-quadruplex in the absence and presence of 120 μM of complex	140
3.14	CD spectra of 20 μM of G-duplex in the absence and presence of 120 μM of complex	141
3.15	Electrophoresis results of incubating pBR322 (0.5 μg/μL) in the presence of complex **10** in TN buffer (5 mM Tris, 50 mM NaCl) pH 7.5 at 37 ^{o}C for 24 h	143
3.16	results of incubating pBR322 (0.5 μg/μL) in the presence of complex **11** in TN buffer (5 mM Tris, 50 mM NaCl) pH 7.5 at 37 ^{o}C for 24 h.	143
3.17	Effect of sequence of mixing for the human topoisomerase I inhibition assay of complex **10**. Electrophoresis results of incubating human topoisomerase I (1 unit/21μL) with pBR322	145
3.18	Effect of sequence of mixing for the human topoisomerase I inhibition assay of complex **11**	146
4.1	Proposed structure for all the compounds	159
4.2	Thermal ellipsoid (Barbour, 2001) plot of **13a** drawn at the 70% probability level. Hydrogen atoms are drawn as spheres of arbitrary radii.	161
4.3	Linear chain formed from N3—H32···O2 hydrogen bonding	163

	interactions for complex **13a** view down from b axis.	
4.4	Zig-zag chain from N3—H31···O1 hydrogen bonding interactions for complex **13a** view down from c axis.	164
4.5	Packing diagram of **13a** along b axis.	164
4.6	IR spectra of complexes **13-16**	168
4.7	Thione-thiol tautomerization for the ligands	169
4.8	CD spectra of 15 µM of oligonucleotide in the absence and presence of 120 µM of complex **13**	173
4.9	CD spectra of 15 µM of oligonucleotide in the absence and presence of 120 µM of complex **14**	174
4.10	10 CD spectra of 15 µM of oligonucleotide in the absence and presence of 120 µM of complex **15**	174
4.11	CD spectra of 15 µM of oligonucleotide in the absence and presence of 120 µM of complex **16**	175
4.12	CD spectra of 10 µM of oligonucleotides in the absence and presence of 120 µM of complex **13**	178
4.13	CD spectra of 10 µM of oligonucleotides in the absence and presence of 120 µM of complex **14**	178
4.14	CD spectra of 10 µM of oligonucleotides in the absence and presence of 120 µM of complex **15**	179
4.15	CD spectra of 10 µM of oligonucleotides in the absence and presence of 120 µM of complex **16**	179
4.16	CD spectra of 20 µM of G-quadruplex in the absence and presence of 120 µM of complex **13-16**	182
4.17	CD spectra of 20 µM of G-duplex in the absence and presence of 120 µM of complex	184
4.18	Electrophoresis results of incubating pBR322 (0.5 µg/µL) with $CuCl_2$ or complex **13-16** in TN buffer (5 mM Tris, 50 mM NaCl) pH 7.5 at 37 ^{o}C for 2 h in the absence and presence of exogenous agents	186

4.19	Electrophoresis results of incubating pBR322 (0.5 μg/μL) with $CuCl_2$ or complex **13-16** in TN buffer (5 mM Tris, 50 mM NaCl) pH 7.5 at 37 ^oC for 2 h in the absence and presence of increasing hydrogen peroxide concentrations	188
4.20	Electrophoresis results of incubating pBR322 (0.5 μg/μL) with complex **16** in TN buffer (5 mM Tris, 50 mM NaCl) pH 7.5 at 37 ^oC for 2 h in the presence of sodium ascorbate and scavenging agents	189
4.21	Electrophoresis results of incubating pBR322 (0.5 μg/μL) with complex **16** in TN buffer (5 mM Tris, 50 mM NaCl) pH 7.5 at 37 ^oC for 2 h in the presence of hydrogen peroxide and scavenging agents	191
4.22	Human topoisomerase I inhibition assay by gel electrophoresis. Electrophoresis results of incubating human topoisomerase I (1 unit/21μL) with pBR322 in the absence or presence of 40 μM of complex	193
4.23	Effect of sequence of mixing for the human topoisomerase I inhibition assay of complex **13** and **16**. Electrophoresis results of incubating human topoisomerase I (1 unit/21μL) with pBR322	195
5.1	Proposed structure for all the complexes	207
5.2	Thermal ellipsoid (Barbour, 2001) plot of **18a** drawn at the 70% probability level. Hydrogen atoms are drawn as spheres of arbitrary radii.	209
5.3	Hydrogen bonding interactions for complex **18a**	211
5.4	Unit cell packing diagram of **18a** view in between c and a axis.	211
5.5	IR spectra of all the complexes	215
5.6	Thione-thiol tautomerization for the ligands	214
5.7	CD spectra of 15 μM of oligonucleotide in the absence and presence of 120 μM of complex **18**	220
5.8	CD spectra of 15 μM of oligonucleotide in the absence and presence of 120 μM of complex **19**	220
5.9	CD spectra of 10 μM of oligonucleotides in the absence and	222

	presence of 120 μM of complex **18**	
5.10	CD spectra of 10 μM of oligonucleotides in the absence and presence of 120 μM of complex **19**	222
5.11	CD spectra of 20 μM of G-quadruplex in the absence and presence of 120 μM of complex **18** and **19**	224
5.12	CD spectra of 20 μM of G-duplex in the absence and presence of 120 μM of complex	226
5.13	Electrophoresis results of incubating pBR322 (0.5 μg/μL) in the presence of complex **18** in TN buffer (5 mM Tris, 50 mM NaCl) pH 7.5 at 37 ^{o}C for 24 h	227
5.14	Electrophoresis results of incubating pBR322 (0.5 μg/μL) in the presence of complex **19** in TN buffer (5 mM Tris, 50 mM NaCl) pH 7.5 at 37 ^{o}C for 24 h	228
5.15	Electrophoresis results of incubating pBR322 (0.5 μg/μL) with complex **18** in TN buffer (5 mM Tris, 50 mM NaCl) pH 7.5 at 37 ^{o}C for 72 h in the presence of scavenging agents	230
5.16	Electrophoresis results of incubating pBR322 (0.5 μg/μL) with complex **19** in TN buffer (5 mM Tris, 50 mM NaC) pH 7.5 at 37 ^{o}C for 72 h in the presence of scavenging agents	232
5.17	Electrophoresis results of incubating pBR322 (0.5 μg/μL) with $CuCl_2$ or complex **10, 11, 18 and 19** in TN buffer (5 mM Tris, 50 mM NaC) pH 7.5 at 37 ^{o}C for 2 h in the absence and presence of exogenous agents	234
5.18	Electrophoresis results of incubating pBR322 (0.5 μg/μL) with $CuCl_2$ or complex (**10, 11, 18** or **19)** in TN buffer (5 mM Tris, 50 mM NaCl) pH 7.5 at 37 ^{o}C for 2 h in the absence and presence of increasing hydrogen peroxide concentrations	235
5.19	Electrophoresis results of incubating pBR322 (0.5 μg/μL) with complex **19** in TN buffer (5 mM Tris, 50 mM NaC) pH 7.5 at 37 ^{o}C for 2 h in the presence of exogenous agent and scavenging agents	237
5.20	Electrophoresis results of incubating pBR322 (0.5 μg/μL) with complex **19** in TN buffer (5 mM Tris, 50 mM NaCl) pH 7.5 at 37 ^{o}C for 2 h in the presence of exogenous agent and scavenging	237

agents

5.21 Electrophoresis results of incubating pBR322 (0.5 μg/μL) with complex **18** in TN buffer (5 mM Tris, 50 mM NaC) pH 7.5 at 37 ^{o}C for 2 h in the presence of hydrogen peroxide and scavenging agents 238

5.22 Electrophoresis results of incubating pBR322 (0.5 μg/μL) with complex **19** in TN buffer (5 mM Tris, 50 mM NaC) pH 7.5 at 37 ^{o}C for 2 h in the presence of hydrogen peroxide and scavenging agents 238

5.23 Human topoisomerase I inhibition assay by gel electrophoresis. Electrophoresis results of incubating human topoisomerase I (1 unit/21μL) with pBR322 in the absence or presence of 40 μM of complex 239

LIST OF SYMBOLS AND ABBREVIATIONS

These following abbreviations were used at various parts in the subsequent text:

B.M	Bohr Magneton
bpy	2,2'-bipyridine
DMF	N,N-Dimethylformamide
DMSO	Dimethylsulphoxide
G	Guanine
HE	2,4-dihydroxybenzaldehyde 4-ethylthiosemicarbazonato
HM	2,4-dihydroxybenzaldehyde 4-methylthiosemicarbazonato
HT	2,4-dihydroxybenzaldehyde thiosemicarbazonato
HP	2,4-dihydroxybenzaldehyde 4-phenylthiosemicarbazonato
ORTEP	Oak Ridge Thermal-Ellipsoid Plot Program
phen	1,10'-phenanthroline
Tris	Tris-(hydroxymethyl)aminomethane

Chapter 1

Introduction

1.1 Metal ions in biological system

Metal ions and their coordination compounds can be found in various biological systems. Iron for example, can be found in hemoglobin, a molecule responsible for carrying oxygen to the cells in animals (Orvig and Abrams, 1999). In addition, iron is also found in ribonucleotide reductase, an enzyme involved in the rate limiting step of DNA synthesis **(**Reichard, 1988; Fan *et al.* 1998). Metal ions such as zinc provide the structural framework for the zinc fingers that regulate the functions of genes in the nuclei of cells. Zinc is also a natural component of insulin, a substance that regulates sugar metabolism. Metal ions such as copper, zinc, iron, nickel and manganese are incorporated into various metalloenzymes, catalytic proteins which promotes a multitude of chemical reactions crucial for life (Orvig and Abrams, 1999). Meanwhile, the chlorophyll essential for photosynthesis in plants is actually a coordination compound of magnesium and porphyrin (Fleming, 1967). These metal cations or metal-containing complex species function by interacting with various inorganic molecules or biomolecules, such as protein, DNA and RNA, through electrostatic interaction, covalent bonding, hydrogen bonding, and van der Waals forces.

Since metal ions play many important roles in biological system, it is essential to maintain adequate concentration of metal ions in the system for the organism to function healthily. There are many complications that can arise due to deficiency of metal ions. Anemia in mammals is due to the deficiency of iron (Lozoff *et al.* 1987; Guyatt *et al.* 1992), while the lack of calcium could lead to osteoporosis (Tilyard *et al.* 1992; Nordin,

1997; Heaney, 2000). Although metal ions are essential to animals, it can also induce toxicity if present in excess. Iron overload can lead to thalassemia and Friedrich's ataxia (Galanello *et al.* 2003; Wagner *et al.* 2003; Neufeld, 2006) while copper(II) has been implicated in diseases such as Wilson's, Menkes, Alzheimer's, Parkinson's and other neurodegenerative diseaseS (Linder and Hazegh, 1996; Sarkar, 1999; Lyons et al, 1999; Gaggelli *et al.* 2006). Excess free metal ions can participate in Fenton chemistry and produce reactive oxygen species (ROS) such as hydroxyl radical, resulting in oxidative insults to critical biomolecules like protein, DNA and lipids that will cause impaired cellular functions (Valko *et al.* 2006; Kozlowski *et al.* 2009).

Given the wide importance of metal ions and their coordination compound in living system, it is understandable why the field of inorganic biochemistry and medicinal inorganic chemistry are growing in prominence. Synthesis of new metal complexes of biological importance and elucidation of their properties are increasingly attracting attention because adequate knowledge in these fields is vital in the search of treatments for metal related disease, metal-based drugs and to gain a better understanding on how nature works.

1.2 Metal complexes with anticancer properties: Designs and improvements

The usage of metal ions in medicinal chemistry has a history of about 5000 years (Orvig, and Abrams, 1999). However, the true potential of metal ions in medicinal chemistry was only fully acknowledged and explored with the serendipitous discovery of the antitumor activity of cisplatin (Rosenberg *et al.* 1969). Cisplatin still remains as one of the leading metal-based anticancer drug, being especially effective in treatments of genitourinary

tumors such as testicular cancer. However, the clinical use of cisplatin is severely limited by dose limiting side effects such as neuro-, hepato- and nephrotoxicity (Zhang and Lippard, 2003; Zutphen and Reedjik, 2005). Besides high systemic toxicity, the second problem seems to be the acquired resistance of cancer cell towards platinum-based drugs. In order to develop metal-based anticancer drugs with higher specificity and reduced side effectS, a departure from the cisplatin paradigm of activity is necessary. Much effort has been put into overcoming toxicity and drug resistance. The alternative strategies include development of more selective delivery or activation of cisplatin related prodrugs, development of non-platinum metal-based drugs, discovery of new non-covalent interactions with DNA (intercalator or groove binder) and looking at other molecular target besides DNA (Bruijnincx and Sadler, 2008).

1.2.1 Improving platinum-based anticancer agents

Problems like toxic side effects and acquired drug resistance do not dampen the interest of scientist towards developing platinum complexes as potential anticancer agents, owing to the huge success of cisplatin. Instead, numerous effort have been reported on designing drug delivery system capable of delivering platinum to tumor cells only and preventing binding to non-pharmacological targets. In addition, platinum complexes with different binding modes from that of cisplatin are of current interest and may provide higher antitumor activity against cisplatin-resistant cancer cells (Zhang and Lippard, 2003).

Recently, Yang *et al.* (2007) have developed a method of delivering platinum drugs to the tumor cells only by encapsulating cisplatin and carboplatin in the hollow protein cage of the iron storage protein ferritin, which can be internalized by some tumor tissues. The

drug-loaded protein showed cytotoxic activity against the rat pheochromocytoma cell line (PC12). Meanwhile, MacDiamird *et al.* (2007) have utilized some bacterially derived 400 nm particles for encapsulation and cancer cell targeting of chemotherapeutics. Chemotherapeutics such as cisplatin were packed in the minicells and labeled with bispecific antibodies. These bispecific antibodies (BsAb) have two arms with different functions. One of these arms recognizes the O-antigen component of the minicell surface LPS whereas the other arm is a cell-surface receptor specific for the mammalian cell to be targeted. For example, EGFR or HER2/neu receptor targets breast and ovarian cancer cells, respectively. These minicells specifically target the tumor cell-surface receptors via its bispecific antibody coating. Receptor engagement results in minicell endocytosis, intracellular degradation, and ultimately drug release in cancer cells.

Previously, in an attempt to improve the delivery of platinum(IV) prodrugs, Lippard's group synthesized an estrogen tethered platinum(IV) complex based on the observation that estrogen receptor-positive, ER(+), breast cancer cells treated with estrogen are sensitized to cisplatin. This approach is successful in inducing up regulation of high mobility group (HMG) domain protein upon intracellular reduction of the prodrug. The domain protein, HMGB1 shields platinated DNA from nucleotide excision repair (Barnes *et al.*, 2004).

In another approach, Lippard *et al.* have circumvented the problem of drug delivery by attaching a Pt(IV) prodrug to a functionalized water soluble single-walled carbon nanotubes (SWNT), highly effective carriers that can transport various cargos across the cell membrane through clathrin-dependent endocytosis. The platinum(IV) complex has

two different axial ligands, Fig. 1.1 and binds non-covalently to the nanotube surface and one SWNT longboat carries on average 65 platinum complexes. The conjugate shows increased cellular uptake and substantial increase in cytotoxicity compared to the untethered complex and to cisplatin (Feazell *et al.*, 2007). Along a similar vein, Dhar *et al.* (2008) have further improved this approach by attaching a folic acid derivative to the second axial ligand of the platinum(IV) complex as a homing device. This complex specifically targets folate receptor-enriched tumor cells and has enhanced cell killing properties when conjugated to SWNT. This compound is more active than cisplatin by a factor of 8.6.

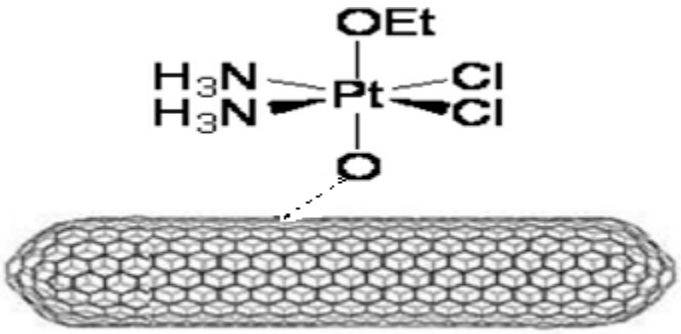

Fig. 1.1 Platinum(IV) complex bound to SWNT (Feazell *et al.*, 2007).

Attempt to overcome cancer cells resistant to cisplatin led to development of platinum complexes with distinctively different DNA binding mode such as *trans*-platin and multinuclear platinum complexes. Reports of *trans*-platinum complexes showing favorable cytotoxicity against cancer cells, especially cisplatin-resistant cells have been reviewed by Natile and Coluccia (2001). A series of *trans*-Pt(II)-piperazine compounds were reported by Najajreh *et al.* (2002). These cationic complexes are more water soluble and bind more rapidly to DNA compared with cisplatin and displayed significant cytotoxicity against cisplatin-resistant ovarian cancer cells.

Multinuclear platinum complexes containing two, three or four platinum centers with both *cis* and/or *trans* configurations also bind to DNA differently from cisplatin. These complexes are generally connected by polyamines linkers. An example of this class of compounds is BBR3464, Fig. 1.2, a trinuclear complex which has entered a phase II clinical trial and exhibits activity against pancreatic, lung and melanoma cancers. Furthermore, this complex is effective against human tumor mouse xenografts containing the mutant p53 gene (Pratesi *et al.* 1999). The p53 gene is a tumor suppressor encoding a nuclear phosphoprotein that mediates cellular response towards genotoxic stress including cisplatin treatment. Over 60% of human cancers are characterized by nonfunctional p53 (Zamble *et al.* 1998). The ability of BBR3464 to target cells with mutant p53 renders it a potent anticancer drug. BBR3464 can bind to DNA rapidly, forming various long-range interstrand and intrastrand cross-links because it is a highly charged 4+ species.

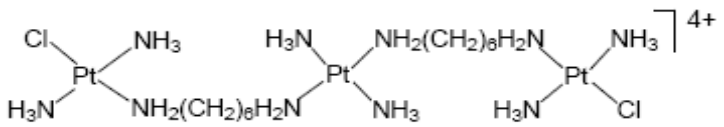

BBR3464

Fig 1.2 Trinuclear platinum complex, BBR3464

Recently, Komeda *et al.* (2006) have reported a new mode of binding between a polynuclear platinum complex, TriplatinNC (Fig. 1.3) and DNA. TriplatinNC does not intercalate nor does it bind in either groove. Instead, it binds to phosphate oxygen atoms through specific hydrogen bonding interactions called phosphate clamps and thus associates with the backbone. The new binding mode was observed in the crystal structure of a

double-stranded B-DNA dodecamer with TriplatinNC. Another feature of TriplatinNC is that the cellular uptake is significantly enhanced over the "parent" BBR3464 due to the increase of charge. TriplatinNC also displays micromolar activity against human ovarian cancer cell lines (Harris *et al.*, 2005). The binding of a small molecule to DNA is greatly enhanced in the presence of positive charge. This is attributed to the increase in electrostatic interaction between the positively charged molecule and the negatively charged DNA backbone.

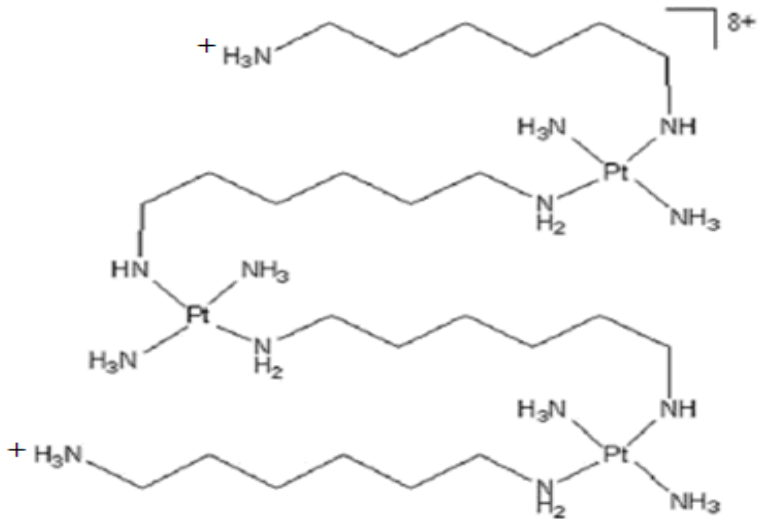

Fig. 1.3 Polynuclear platinum(II) complex, TriplatinNC (Harris *et al.*, 2005).

Another strategy is to develop Pt(IV) complexes that are kinetically inert under biological conditions as prodrugs. These prodrugs are only activated upon reduction and provide a good mean of delivering cisplatin or its analog to tumor cells. The delivery of these prodrugs has been mentioned earlier (Feazell *et al.*, 2007; Barnes *et al.*, 2004). Detailed example of the prodrugs strategy will be discussed in the next section.

1.2.2 Utilization of prodrugs

In overcoming toxicity of a therapeutic agent, one of the useful strategies is to develop a prodrug. Prodrugs are modified versions of substances that are administered in their inactive form with improved delivery features and need to be transformed *in vivo* to release the active drug. This strategy allowed for site selective drug delivery and minimizes the damaged to non-cancerous cells. Activation can occur either chemically, enzymatically or through photo irradiation (Bruijnicx and Sadler, 2007; Zutphen and Reedijk, 2005).

Platinum(IV) complexes are widely studied as prodrugs to tackle problems normally encountered in the use of Pt(II) complexes because they are kinetically inert under biological conditions and can undergo two electron reduction to form reactive square planar Pt(II) complexes. Most of the Pt(IV) prodrugs undergo intracellular reduction to exert their cytotoxicity (Feazell *et al.*, 2007; Barnes *et al.*, 2004).

Photochemical activation of platinum(IV) drugs to release active antitumor agents, rather than spontaneous intracellular reduction is a strategy that can provide localized treatment of cancers accessible to irradiation. Mackay *et al.* (2006) have discovered that a photoactivated *trans*-diammine platinum complex is as cytotoxic as cisplatin. The *trans*-dihydroxy platinum(IV) prodrugs, Fig. 1.4 are non-toxic in the dark and incorporate two azide ligands, *trans* to each other. Irradiation results in growth inhibition of human bladder cancer cells and cytotoxicity towards human skin cells (HaCaT keratinocytes). The potency of this complex can be elevated by introduction of a pyridine ligand, Fig. 1.5 (Mackay *et al.*, 2007).

Fig. 1.4 *Trans*-dihydroxy platinum(IV) prodrugs

Fig. 1.5 *trans, trans, trans*-[$Pt(N_3)_2(OH)_2(NH_3)(py)$]

Designing non-toxic prodrugs that can selectively be activated by enzymes at the tumor open up another opportunity for the development of targeted therapies. Based on the knowledge that a number of enzymes are found at elevated concentration around tumor tissue has led to the use of prodrug monotherapy (PMT) that involves a single administration of a prodrug, which is activated locally to yield the active drug. An example of this approach is the activation of cephalosporin-platinum complex by B-lactamases (Hanessian *et al.*, 1993) and a B-glucuronyl-platinum conjugate by B-glucuronuidase (Tromp *et al.*, 2004). In both cases, the enzymes managed to activate the prodrug resulting in the release of a modified oxaliplatin type species. Meanwhile, Kageyama *et al.* (2004) have made platinum compounds with hydrophobic side chains link *via* an ester bond that

show improved cell permeability with respect to cisplatin. These compounds are activated by ester hydrolysis and show a 10-fold difference in activity between the (R) and (S)-enantiomers.

1.2.3 Non-platinum DNA targeting drugs

The desire to overcome significant side effects and drug resistance associated with the use of platinum-based drugs for the treatment of cancer has spurred chemists to look for non-platinum DNA targeting drugs. This class of compound that can bind to DNA either through covalent binding or non-covalent (groove binder or intercalator or electrostatic interaction), or a combination of these modes of interaction are anticipated to have different mechanism in leading to cell death.

Among the non-platinum anticancer drugs, ruthenium holds a promising future. A variety of ruthenium complexes which interact with the classical target, DNA have been reported recently (Ang & Dyson, 2006; Liu *et al.*, 2006). Yan *et al.* (2005) has synthesized a family of ruthenium(II)-arene complexes that exhibits high *in vitro* and *in vivo* anticancer activity. The complex synthesized by Liu *et al.* (2006) is not cross-resistant to cisplatin. This may be explained by the ability of the complexes to induce different DNA structural distortions compared to cisplatin. In addition, direct coordinative binding to N7 of G bases in DNA, this complex also intercalates with the DNA through the biphenyl ligand and forms specific hydrogen bonds with C6O of guanine *via* its ethylenediamine NH_2 groups.

Transition metal complexes that can bind and cleave DNA under physiological conditions open up another exciting opportunity for developing non-platinum DNA

targeting drugs. The binding of one class of compound is normally achieved by introduction of an intercalating ligand. The mode of interaction is non-covalent and involves intercalation between nucleobase or binding to the major or minor groove of DNA. A second ancillary ligand is normally introduced to form a ternary complex, which often acts either as a bioactive moiety itself, a photosensitizer, or a homing device to target a specific sequence of DNA or to modulate the redox properties of the metal ion. Cleavage of DNA can be achieved by targeting its basic constituents like base and/or sugar by an oxidative pathway or by hydrolysis of phosphoester linkages. Iron and copper complexes are known to be useful for oxidative cleavage of DNA involving nucleobase oxidation and/or degradation of sugar by abstraction of deoxyribose hydrogen atom(s), while complexes containing strong Lewis acids like copper(II) and zinc(II) are suitable for hydrolytic cleavage of DNA. Oxidative cleavage of DNA could take place by chemical or photochemical means (Ng *et al.*, 2008; Seng *et al.*, 2008; Chakravarty, 2006).

An example of ternary copper(II) complex of 1,10-phenanthroline with L-threonine that utilize this strategy has been reported by Zhang *et al.* (2004). The complex exhibited highly *in vitro* cytotoxic effects toward HL-60 and SGC-7901 tumor cell lines and was more potent than cisplatin at most experimental concentrations. The complex was shown to intercalate into DNA and cleave pBR322 DNA efficiently in the presence of ascorbate with hydroxyl radicals as the active species. The introduction of L-threonine in the copper complex gave rise to potential selective interactions with DNA, which may result in the variation of nuclease activity of the Cu–phen system as well as its cytotoxicity towards tumor cell lines.

1.2.4 DNA intermediates as target

The paradigm shift towards the targeting of intermediate DNA structures other than the form in which DNA is stored, and design of compounds with specificity for certain DNA forms, may open up access to the targeting of certain types of biological activity. In eukaryotic cells, DNA is stored in its supercoiled duplex form and is arranged in supramolecular structures that are stabilized by ancillary proteins. However, during activation toward processes such as replication and transcription, this stable storage complex is rearranged and the DNA may form structures that differ from the Watson–Crick-induced B-DNA duplex. The most studied and well-known of these structures is the Holliday (four-way) junction, which is the key intermediate in nearly all recombination processes, although three-way forks also occur in major steps of both RNA and DNA metabolism. As they are landmarks of pivotal events in the cell cycle, these transient conformations are attractive targets to control diseases at the source (Oleksi *et al., 2006; Boer et al., 2008).*

An example of complex that recognizes the DNA three way junction (3WJ) by a supramolecular helicate was reported by Oleksi *et al.* (2006) recently. The interaction mode observed involves a highly stable complex between the DNA junction and the 'helicate', a compound that consists of three organic stranded ligands wrapped around two Fe^{2+} atoms, as shown in Fig. 1.6. The helicate combines the two positively charged centers with an extensive hydrophobic surface formed by four aromatic rings of each respective ligand. The X-ray structure that was determined, illustrated in Fig. 1.7, shows that the positive charge of the helicate, together with the large hydrophobic surface of the aromatic rings (with π-stacking potential), are the driving forces behind this specific interaction. This

unprecedented mode of non-covalent DNA recognition shows that three-way junctions, naturally occurring both in DNA and RNA can be new structural targets for the design of novel and highly specific drugs.

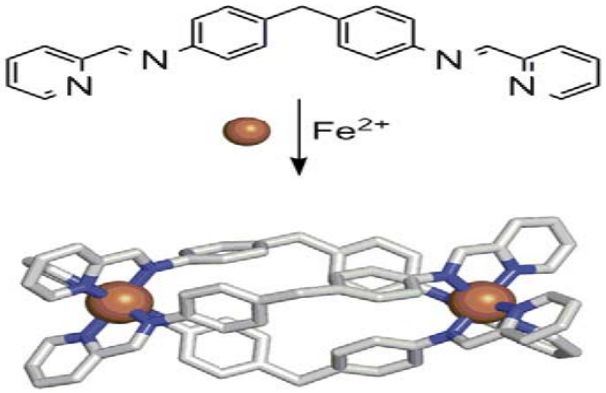

Fig. 1.6 Assembly of the $[Fe_2L_3]^{4+}$ ($L=C_{25}H_{20}N_4$) tetracationic supramolecular helicate (Oleksi *et al.* 2006)

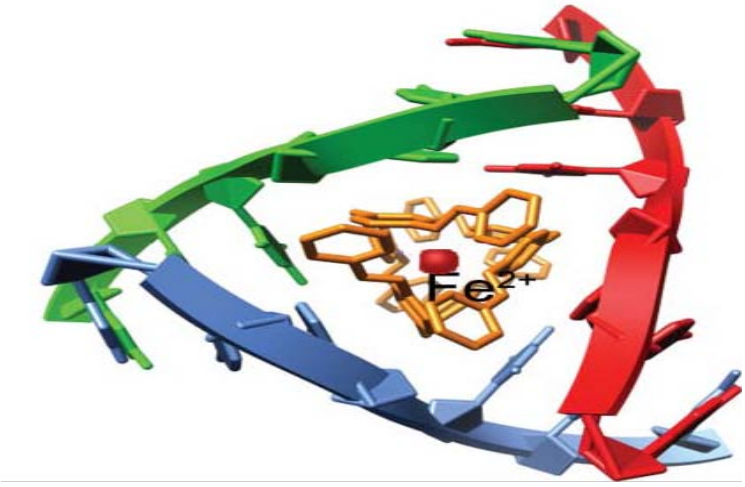

Fig 1.7 The saturated iron triple helicate binds to a three-way DNA junction (Oleksi *et al.* 2006)

Based on the same strategy, Pascu et. al. (2007) have synthesized a ruthenium metallohelicate which induces a similar bending/coiling effect, further illustrating that the helicate is responsible in recognizing the three-way DNA junction. The Ru triple helicate

exhibits cytotoxicity towards human breast cancer HBL-100 and T47D cells, which is 2–5-fold less potent than cisplatin. Meanwhile, a related unsaturated dinuclear ruthenium double helicate, capable of classic coordinative binding to DNA, show greatly improved cytotoxicity towards the same cell lines (30-fold more active than cisplatin). These complexes illustrate the many possibilities of using metallosupramolecular architectures that target unique DNA structure in anticancer drugs design (Hotze *et al.*, 2006).

Another DNA intermediate that deserves attention as a new anticancer target is telomere. Telomere recognition and regulation has been marked as an important potential target for cancer therapy because the behavior of these regions differs in somatic and cancer cells. In a normal cell, telomeric DNA shortens after every cell division and after critical shortening of the telomeres (upon reaching the Hayflick limit) cells stop dividing and commit suicide. In contrast, telomere lengths are actively maintained at a certain length in cancer cells due to the over expression of telomerase, an enzyme responsible in maintaining the length of the telomeric DNA. This renders the cancer cells with the ability to replicate indefinitely and thus proliferate (Neidle and Parkinson, 2002).

Single-stranded ends of human telomeric DNA, which consists of guanine-rich TTAGGG repeats known to fold into G-quadruplex structures. Since telomerase accepts only the single-stranded overhang, stabilization of the G-quadruplexes provides an attractive means of inhibiting the telomerase. The desirable features of these stabilizing molecules are:

(1) a π-delocalized system that is able to stack on the face of a guanine quartet

(2) a partial positive charge that is able to lie in the center of the quartet, increasing stabilization by substituting the cationic charge of the potassium or sodium that would normally occupy that site

(3) positively charged substituents to interact with the grooves and loops of the quadruplex and the negatively charged backbone phosphates.

A recent example of stabilization of G-quadruplex DNA and inhibition of telomerase activity by square-planar nickel(II) complexes has been reported by Reed *et al.* (2006). The substituted salicylidene phenylenediamine-nickel(II) complex , Fig. 1.8, is water soluble in slightly acidic pH and fulfills the main requirements of a G-quadruplexes stabilizing molecule. These compounds induce high degree of quadruplex DNA stabilization and telomerase inhibition with $^{tel}EC_{50}$ in the range of 0.1 uM.

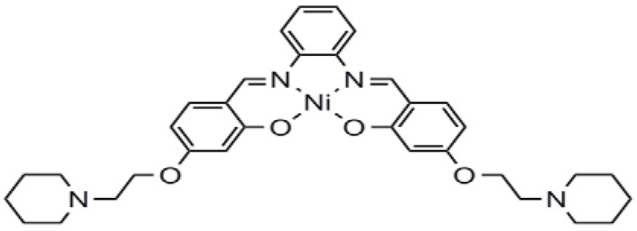

Fig. 1.8 Substituted salicylidene phenylenediamine-nickel(II) complex
(Reed *et al.* 2006)

Riding on the previous success of Reed *et al.* (2006), Dixon *et al.* (2007) have developed a metalloporphyrin, Fig. 1.9, that shows both a very high affinity and an excellent selectivity for G-quadruplex DNA over GC-rich or AT-rich DNA . This compound shows an exceptional 10,000-fold selectivity for quadruplex over duplex DNA

(IC_{50} of around 0.6 mM) , while the Ni(II)–salphen complex, Fig 1.8 only shows selectivity of >50-fold. These results illustrate the potential of metal complexes as telomere-targeted chemotherapeutics.

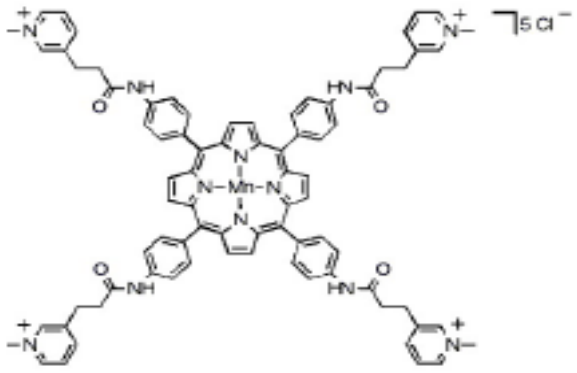

Fig. 1.9 Pentacationic manganese(III) porphyrin
(Dixon *et al.* 2007)

1.2.5 Metal complexes targeting protein and enzyme

The advents of genomics and proteomics have resulted in a wealth of information concerning the biology of cancer cells that were not known previously. The data have greatly facilitated the development of targeted therapies, an approach of designing novel agents that target cellular signaling pathways specific to cancer cells. Interestingly, cancer cells normally have an elevated level of particular enzymes or metal ions compared to normal cells. Approaches that focus on the differences between healthy and cancer cells are more selective and are anticipated to overcome the drawbacks of the traditional DNA-targeting anticancer drugs that affect cancer and healthy cells as well (Bruijnicx and Sadler,

2007; Zhang and Lippard, 2003; Dyson and Sava, 2006). A few examples of protein and enzymes as target will be illustrated.

Gold complexes well known for treatment of rheumatoid arthritis are also active as antitumor agents. These complexes display a wide spectrum of antitumor activity *in vivo*, especially in some cisplatin-resistant cell lines. Mechanistic studies suggest that, in contrast to cisplatin, DNA is not the primary target of these complexes. Rather, their cytotoxicity is mediated by their ability to alter mitochondrial function and inhibit protein synthesis (Mckeage *et al.*, 2002; Plilasertty *et al.*, 2003). A recent example of gold-containing anticancer agents are the gold(III) porphyrins studied by Sun *et al.* (2007). These complexes exhibit potent *in vitro* and *in vivo* anticancer activity towards hepatocellular and nasopharyngeal carcinoma by targeting the mitochondrial death pathway.

Human thioredoxin reductase (hTrxR) is associated with many cellular processes such as antioxidant defence and redox homeostasis. The hTrxR is an interesting target for anticancer drugs because it is found at elevated levels in human tumor cell lines and it is strongly associated with tumor proliferation (Urig *et al.*, 2006a). Urig *et al.* (2006b) have developed a series of gold(I) complexes that are potent inhibitors of hTrxR, a feature attributable to the high electrophilicity of Au(I) and its preference for the selenocysteine residue of hTrxR.

Another non-DNA target is proteasome. It is a protein responsible for degrading a large number of cellular protein. It is an interesting target in cancer therapy due to the over expression of proteasome activities in cancer cells. Proteasome inhibition could lead to

rapid and selective induction of apoptosis in oncogened transformed cells but not in healthy cells. Milacic *et al.* (2006) have synthesized a gold(III) thiocarbamate compound which inhibits proteasome that is more cytotoxic *in vitro* than cisplatin, including intrinsically resistant cell lines. However, the mode of action in proteasome inhibition is yet to be understood.

Instead of targeting DNA like most ruthenium anticancer drugs, Meggers's group has pioneered the development of organometallic ruthenium complexes that mimic organic enzyme inhibitors. Structural variation by simple substitution of the ligands on the metal to optimize the enzyme-inhibitor interactions has resulted in the discovery of nanomolar and even picomolar protein kinase inhibitors. This class of complexes illustrates the possibilities of using the metal as a scaffold instead of a reactive centre in anticancer drug design. In this method, metals can be used as building blocks for well-defined, three-dimensional constructs with unique stereochemistry and orientation of organic ligands and structures which are not accessible through purely organic, carbon-based compounds. (Mergers *et al.*, 2007; Bregman *et al.*, 2006).

Another biological target is topoisomerase. Topoisomerases are enzymes that break and rejoin DNA strands required for cells to divide and grow, are becoming promising target in anticancer drugs. Since the initial discovery that $[Ru(\eta^6\text{-}C_6H_6)(DMSO)Cl_2]$ can inhibit topoisomerase II activity, Gopal *et al.* (2002) have prepared three new derivatives by replacing the DMSO ligand with 3-aminopyridine, p-aminobenzoic acid or aminoguanidine. These analogs show improved efficacy as topoisomerase II inhibitors and

have higher cytotoxicity against breast and colon carcinoma cells compared to the parent compound.

Other ruthenium complexes that deserves attention are [Ru(Im)(Me_2SO)Cl_4] (NAMI) and its analog (ImH)*trans*-[Ru(Im)(Me_2SO)Cl_4] (NAMI-A) that posses antimetastatic properties by interfering with type IV collagenolytic activity (Clarke, 2003). Type IV collagenolytic activity is a process of breaking down collagen found primarily in the basal lamina. These compounds which are devoid of *in vitro* cytotoxicity but capable of *in vivo* metastasis inhibition have led to development of new metallopharmacheuticals by identifying metastasis as target (Bergamo and Saya, 2007). These examples should be a wake up call for the needs of developing new assays that look beyond traditional *in vitro* cytotoxicity tests (Dyson and Sava, 2006).

1.2.6 Conclusion

Metal-based drugs have and will continue to play important roles in treating cancers. These examples show that many creative approaches have been taken in designing and improving metal complexes with anticancer properties. The main objectives are to design compounds with higher selectivity, reduced side-effects and to overcome drug resistance. Platinum-based drugs still remain the most widely used metal based drugs even though there are a few downsides such as toxicity and acquired resistance. There is still a long way to go for the commercialization of emerging non-platinum anticancer agents because drug approval still required vigorous testing to understand the mechanism of action and potential side effects. Ruthenium and gold complexes are emerging rapidly as promising candidates with mode of action that departs from the cisplatin paradigm of activity. Targeted delivery and

utilization of prodrugs offer a future of more selective and effective treatments of cancer with lesser side effects. To discover new compounds and new targets like DNA intermediates, enzymes and protein as well as to gain understanding on mechanism of action of drugs in the post-genomic era, there is a need to rely heavily on interdisciplinary collaboration. All these examples show that there is light at the end of the tunnel for those who are interested in developing metal based anticancer agents.

1.3 Thiosemicarbazones in general

Thiosemicarbazones are a class of Schiff base formed from the condensation of a carbonyl compound with a thiosemicarbazide. Thiosemicarbazone are normally named by placing the name of the ketone or aldehyde as the prefix followed by thiosemicarbazone as the suffix (Casas *et al.*, 2000). Thiosemicarbazones are well known for wide range of biological activities and are widely used in industrial and analytical fields. The presence of an intact =NNH(CS)NH— moiety is essential for their chemical properties and biological activities (Casas *et al.*, 2000; West *et al.*, 1993).

Thiosemicarbazones are one class of versatile ligands that are of interest to many researchers because of its ability to chelate to metal. Thiosemicarbazones are widely used in coordination chemistry because of their abilities to form complexes, in which they are monodentate, bidentate or multidentate ligands (Padye and Kaufman, 1985). The thiosemicarbazone moiety without substituents attached to the thione sulfur coordinates as either a neutral or anionic NS bidentate ligand. Depending on the method of complex preparation a third coordinating atom often gives ONS (e.g. 2-hydroxybenzaldehyde thiosemicarbazones) or NNS (e.g. 2-acetylpyridine thiosemicarbazones) tridentate ligands.

Some examples of higher denticity involving one or more thiosemicarbazone moieties, as well as monodentate thiosemicarbazone have been reported (West *et al.*, 1993; Campbell, 1975).

Due to the tendency of thiosemicarbazone ligands to form complexes with metals, it has been widely used in analytical applications. The basic mode of action is through the formation of colored chelates. Reddy *et al.* (2003) have determined the presence of Cu(II) and Ni(II) simultaneously with spectrophotometric methods by using 1-phenyl-1,2-propanedione-2-oxime thiosemicarbazone as a reagent. The presence of sulphur, a soft base, in thiosemicarbazone enhances its affinities to soft acids like Hg^{2+} and Ag^{+}. Majahan *et al.* (2003) have prepared the first ion selective electrode for Hg^{2+} by using neutral salicylaldehyde thiosemicarbazone as an ionophore. This electrode displays good selectivity towards Hg^{2+} over alkali metal and a few transition metal ions. The low cost of thiosemicarbazones as well as their easy preparative methods could provide a major attraction for the development of analytical reagents for a wide range of metal ions.

A survey of the literature reveals that thiosemicarbazones and their metal complexes posses a wide range of biological activities such as antibacterial, antifungal, antitumor, and antiviral owing to their property to diffuse through the semi permeable membrane of the cell lines (Lobana *et al.*, 2009; Beraldo and Gambino, 2004; West *et al.*, 1993).

The discovery that the intermediate in the antitumor activity of 3-ethoxy-2-oxobutyraldehyde bis(thiosemicarbazone) was the 4-coordinate copper chelate (Petering and Giessen, 1966), has inspired the search for bioactive metal complexes of

thiosemicarbazones. The enhanced effect may be attributed to the increased lipophilicity of the complexes compared to the ligand alone. Lipophilicity, which controls cells permeability, is modified by coordination (Farrel, 2002). The mechanism of action can involve binding to a metal *in vivo* or the metal complex may be a vehicle for activation of the ligand as the cytotoxic agent. Chelating agents are often powerful inhibitors of metalloenzymes so that the ligands may act by inhibiting the enzymes whose activity depends on metals (Fahmi and Singh, 1996).

The following examples are just a small illustration of the wide range of biological activites of thiosemicarbazones and their metal complexes. Dittes *et al.* (1997) show that bismuth complexes of thiosemicarbazone are active towards *Helicobacter pylori*, a bacterium responsible for gastric and peptic ulcer. 2-Benzoylpyridine thiosemicarbazone, and its copper(II) complexes exhibit antifungal activity against various strains of the pathogenic fungi. The activity varied with the nature of the substituent at the amino nitrogen of thiosemicarbazone. 2-Benzoylpyridine-*N*(1)-isopropyl thiosemicarbazone as well as its square pyramidal complex, $[Cu(HL)Cl_2]$ where HL is undeprotonated Schiff base were fungitoxic against the human pathogenic fungi, *A. niger* and *P. variotti* (West *et al.*, 1995). Meanwhile the antiviral activity of thiosemicarbazone against meurovaccinal infection in mice was first reported in 1950 by Hamre *et al.* It has since prompted the investigations by other groups and the results have been reviewed by Baeur (1972). Singh *et al.* (2000) have prepared metal complexes of thiosemicarbazone with d^3 metal ions. *In vitro* and *in vivo* antitumor testing showed that complexation can enhance the cytotoxicity. Since our main focus is to develop metal complexes with anticancer properties, more

examples of some thiosemicarbazones or their complexes with significant anticancer properties will be discussed in the next section.

1.4 Anticancer properties of thiosemicarbazone and their metal complexes

Since the antileukemic effect of 2-formylpyridine thiosemicarbazone was reported by Brockman *et al.* in 1956, a tremendous amount of thiosemicarbazones and their complexes were subjected to screening in search of a compound with better anticancer properties and lower systemic toxicity. Vigorous testing has led to the discovery of thiosemicarbazones with potent anticancer properties and a better understanding of their modes of action (West *et al.*, 1993; Beraldo and Gambino; 2004; Kalinowski and Richardson, 2007).

Even though thiosemicarbazone is a class of very old compound and their biological activities have been extensively studied, a survey of the literature still shows a resurgence interest is this class of compounds in the last ten years. The discovery of Triapine (3-aminopyridine-2-carboxaaldehyde thiosemicarbazone) as a potent inhibitor of ribonucleotide reductase by Finch *et al.* (1999), may have sparked off this interest. Beside the cleavage of DNA, an anticancer drug can also work by inhibiting ribonucleotide reductase that is essential to DNA repair and synthesis. Recently, some researchers discovered that Triapine that has completed phase I clinical trial, can actually induce apoptosis in ovarian cancer cell. Apoptosis has been identified as the key mechanism by which chemotherapeutic agents like carboplatin and paclitaxel induce cell death (Alvero *et al.*, 2006). This discovery further substantiates the fact that the thiosemicarbazone class of compound, well known for a wide spectrum of biological activities, has good potential to

be developed as anticancer drugs. Triapine is currently in phase II clinical trial for various cancers.

In addition, Adsule *et al.* (2006) have discovered that copper complexes of quinoline-2 carboxaldehyde thiosemicarbazone are proteasome inhibitor in human prostate cancer cells. A proteasome is a large protein complex that helps destroy other cellular proteins when they are no longer needed. Proteasome is an interesting target in cancer therapy because proteasome inhibition could induce apoptosis rapidly and selectively in oncogene transformed cells but not in healthy cells.

Besides proteasome inhibition, Chen *et al.* (2004) have developed a class of 1,2-naphthoquinone thiosemicarbazone and metal derivatives which are cytotoxic towards MCF-7 human breast cancer cells. These compounds exert their cytotoxicity by inhibition of topoisomerase. These compounds stabilize the cleavable complex of DNA and Topo II, and turned the complex into an enzymatic DNA cleavage agent. This happened when the compound poisoned an essential enzyme such as topoisomerase and stripped off its ability to religate the DNA strand after uncoiling it in the first place.

The above illustrates the potential of thiosemicarbazones and their metal complexes as anticancer agents that targets enzymes and proteins similar to those compounds discussed earlier in section 1.2.5. Targeted therapy may offer a more selective treatment of cancer with fewer side-effects.

1.5 Thiosemicarbazones with polyhydroxybenzaldehyde

The coordination chemistry and biological properties of salicylaldehyde thiosemicarbazones have been extensively studied. However, polyhydroxybenzaldehye thiosemicarbazones are less well known.

Zhu *et al.* (1997) have prepared some Fe(II) and Ni(II) complexes with 3,4-dihydroxybenzaldehyde thiosemicarbazone. Biological activity tests show that the complexes exhibit strong superoxide dismutase activity and inhibitory actions towards *Escherichia coli, Bacillus subtilis, Staphylococcus aureus* and *Cryptococcus neoforms*. The complexes are more active than the free ligand and the nickel complex is less active compared to the iron complex.

The catalytic oxidation of 3,5-di-tert-butylcatechol into the corresponding o-benzoquinone by copper(II) complexes of 2,3-dihydroxybenzaldehyde N(4)-substituted thiosemicarbazone have been reported in the presence of H_2O_2 or t-butylhydroperoxide as co-oxidants by Al-Kubaisi (2002). Dang *et al.* (2002) have developed a new method for the spectrophotometric detection of trace copper ion by using 2,4-dihydroxybenzaldehyde thiosemicarbazone (DBT). But to the best of our knowledge there are no reports on anticancer properties and DNA interaction of binary and ternary complexes from polyhydroxybenzaldehyde.

1.6 Purpose of research

The purpose of our research is to synthesize and characterize various mononuclear and polynuclear transition metal complexes with both polypyridyl ligands and ligands derived

from polyhydroxybenzaldehye thiosemicarbazone. Some biological properties (e.g DNA binding, nucleolytic, topoisomerase I inhibition and antimicrobial) of the above complexes and ligands and the factors influencing such properties will also be investigated.

Our interest in thiosemicarbazones stems from the fact that it has the potential as anticancer agents that can target protein and enzyme. In addition, we were inspired by the work of Thomas *et al.* (2004) that ternary copper complexes of thiosemicarbazone can exhibit light induced DNA cleavage at 312 nm and 532 nm. Their complexes can bind to the DNA minor groove and major groove. In the ternary complexes, the thiosemicarbazone, dipyridoquinoxaline and dipyridophenazine moiety can actually act as photosensitizers, while the planar heterocyclic bases are binders to DNA. Compounds that can cleave DNA upon light activation can be utilized in photo dynamic therapy (PDT).

At the same time, we are interested in Schiff base derived from polyhydroxybenzaldehye because it was reported by Tonde *et al.* (2006) that copper(II) complexes of hydroxyl-rich ligands with anthralinic acid are capable of cleaving DNA without any exogenous agent or light activation. Self activating nucleases such as these are interesting because they can be used as diagnostic or therapeutic agent that cleave DNA in parts of the biological system which are not accessible to exogenous agent or light activation. Furthermore, thiosemicarbazone derived from polyhydroxybenzaldehyde, unlike the salicylaldehyde derivatives, would have uncoordinated hydroxyl group that can enhance the solubility of the compound in common solvent to facilitate biological testing. The uncoordinated hydroxyl group also offers the opportunity for further derivatization to

form bimetallic complexes. It can also be utilize to interact with DNA or other biomolecules through hydrogen bonding.

By combining some or all the features in one compound, we hope to design a molecule that contains an intercalator (i.e. 1,10'-phenanthroline) that can bind to DNA through non-covalent interactions, a thiosemicarbazide moiety that can act as a photosensitizer or bioactive moiety that may inhibit ribonucleotide reductase, topoisomerase or proteasome. The presence of uncoordinated hydroxyl group may render the molecule with higher solubility or self-activating nuclease property.

Chapter 2

Synthesis, characterization and biological properties of zinc(II) complexes of 2,4-dihydroxybenzaldehyde N^4-substituted thiosemicarbazones and 2,2'-bipyridine

2.1. Introduction

Thiosemicarbazones are a class of Schiff bases that have been evaluated for various biological properties such as anticancer, antimicrobial and antiviral properties (Padyhe and Kaufman, 1985; Liberta and West, 1992; Beraldo and Gambino, 2004). Research on the biological properties of thiosemicarbazones, as well as on those of their metal complexes, has recently revealed the abilities of these compounds to act as ribonucleotide reductase (Attia *et al.* 2008; Odenike *et al.* 2008; Ma *et al.* 2008), topoisomerase (Afrasiabi *et al.* 2004; Chen *et al.* 2004; Wei *et al.* 2006; Rao *et al.* 2009) and proteasome (Adsule *et al.* 2006; Barve *et al.* 2006) inhibitors. In particular, the metal complexes of salicylaldehyde N^4-substituted thiosemicarbazones have been most studied (West *et al.* 1993; Latheef *et al.* 2007 & 2008; Seena and Kurup, 2007 & 2008; Lobana *et al.* 2008). On the other hand, the polyhydroxybenzaldehyde thiosemicarbazones derivatives (Zhu *et al.* 1997) have been less studied. To the best of our knowledge, there is no report of ternary Zn(II) complexes of 2,2'-bipyridine and 2,4-dihydroxybenzaldehyde N(4)-substituted thiosemicarbazone.

As the metal complexes themselves are Lewis acceptors, the coordination chemistry of their adducts, particularly the *N*-heterocycles, can yield information on the mode of biological activity. A suitable metal for this purpose is zinc, whose ion is involved in many enzymatic reactions and is relatively less toxic compared with other metal ions (Vallee and

Auld 1990; Waterborg *et al*. 1982). Zinc is also known to enhance antitumor activity of thiosemicarbazones (Kovala-Demertzi *et al*. 2006 & 2008). The IC_{50} value for HAcTsc against the MCF-7 cell line is 3.29 µM and for the zinc(II) complexes of HAcTsc, the IC_{50} value is 1.36 and 0.88 µM for $[ZnCl_2(HAcTsc)]$ and $[Zn(AcTsc)_2]$ respectively (Kovala-Demertzi *et al*. 2006 & 2008).

Metal complexes containing 2,2'-bipyridine have been extensively studied for their ability to bind to DNA (Carter *et al*. 1989; Pyle *et al.* 1989; Jenkins *et al*. 1992; Tysoe *et al*. 1993; Lincoln & Nordén, 1998). These studies normally utilized the 2,2'-bipyridine heterocycle as a primary ligand bound to metal as a control. Further variations were carried out by using bipyridine derivatives or additional secondary ligands to study the effect of shape or hydrophobicity on DNA binding. Metal complexes derived from polyhydroxybenzaldehyde thiosemicarbazones would have an additional uncoordinated hydroxyl group, directed away from the coordination sphere,that can help to enhance solubility in common polar solvents and to interact with DNA through hydrogen bonding in contrast to salicylaldehyde derivatives. This class of compound may also act as a self-activating nuclease that can cleave DNA without any activation as reported by Tonde *et al*. (2006) for copper(II) complexes of Schiff base derived from polyhydroxybenzaldehyde and anthralinic acid. Normally, cleavage of DNA by metal complexes proceeds in the presence of exogenous agents such as hydrogen peroxide or sodium ascorbate and some may occur through activation by light. Self-activating nuclease reported by Tonde *et al.* (2006) most likely involves singlet oxygen or a singlet oxygen-like moiety as the reactive species responsible for the cleavage of plasmid pBR322 DNA. These radicals were generated by

sequence of reactions involving concomitant copper and hydroquinone redox cycles. Antineoplastic activity of thiosemicarbazones are highly dependent on the substituent at the N(4) position. For example, palladium(II) complexes of 2-benzoylpyridine thiosemicarbazone with a phenyl substituent at the N(4) is the most cytostatic compared to the methyl substituted and non-substituted derivatives (Rebolledo *et al*. 2005).

Therefore in this chapter, the study of the effect of varying the N(4) substituent of the thiosemicarbazone ligand from hydrogen, methyl, ethyl to phenyl towards the chemical and biological properties (DNA binding, nucleolytic, topoisomerase I inhibition and antimicrobial) of ternary Zn(II) complexes containing this 2,2'-bipyridine ligand as the heterocyclic base is described.

2.2. Experimental

2.2.1. Materials and solutions

The solvents were purchased from Merck and the reactants for syntheses were from Sigma. The pBR322, gene ruler 1 kb DNA ladder, 6x loading buffer and Tris-(hydroxymethyl)aminomethane (Tris) were procured from BioSyn Tech (Fermentas). Analytical grade agarose powder was obtained from Promega. PAGE grade self-complimentary 12-mer oligonucleotides $(CG)_6$, $(AT)_6$, (CGCGAATTCGCG), (CGCGATATCGCG), HPLC grade human telomeric sequence 22-mer oligonucleotide 5'-AGGGTTAGGGTTAGGGTTAGGG-3', and 17-mer complementary oligonucleotides 5'-CCAGTTCGTAGTAACCC-3, 3'-GGTCAAGCATCATTGGG-5' were purchased from

1st BASE and Eurogentec Ait. The respective duplex or quadruplex were annealed as specified by the supplier. Sodium chloride, human DNA topoisomerase I and ethidium bromide were purchased from Sigma Chemical Co. (USA). The aqueous solutions for DNA experiments were prepared with ultra-pure water from an Elga PURELAB ULTRA Bioscience water purification system with a UV light accessory. The Tris-NaCl (TN) buffer was prepared from the combination of Tris-(hydroxymethyl)aminomethane (Tris) base and NaCl dissolved in water and its pH was adjusted with hydrochloric acid (HCl) solution to pH 7.5. The Tris-NaCl buffer pH 7.5 contains Tris at 5 mM and NaCl at 50 mM. All stock solutions of aqueous H_2O_2 and sodium ascorbate in deionized water and the test compounds in *N*,*N*-dimethylformamide (DMF) were freshly prepared daily.

2.2.2. Physical measurements

IR spectra were recorded as KBr pellets by using a Perkin-Elmer Spectrum RX-1 spectrophotometer. NMR spectra were recorded in deuterated DMSO-d6 on a JEOL JNM-LA400 or ECA 400 MHz instrument. Elemental analyses were performed on a Thermo Finnigan Eager 300 CHNS elemental analyzer. UV–visible spectroscopic measurements were carried out on a Perkin–Elmer Lambda 40 spectrophotometer. The circular dichroism study of the interaction of metal complexes with ds(oligonucleotide) or G-quadruplex was carried out with a 1.0 cm or 1.0 mm quartz cell respectively, using a Jasco J-810 spectropolarimeter.

2.2.3 Syntheses

2.2.3.1 Synthesis of 2,4-dihydroxybenzaldehyde thiosemicarbazone, H_3T **(1)**

The ligand was synthesized by minor modification to the procedure reported by Zhu *et al.* (1997). Thiosemicarbazide (0.09 g, 1 mmol) and 2,4-dihydroxybenzaldehyde (0.14 g, 1 mmol) were heated in an ethanol/water mixture (20/5 ml) for 3 hours. Slow evaporation of the solvent yielded yellow crystals. The crystals were filtered, washed with cold methanol and ether, dried in air and kept in a desiccator over silica gel.

(Yield: 0.18 g, 85%). Anal. Calc. for $C_8H_9N_3O_2S$: C, 45.49; H, 4.29; N, 19.89. Found: C, 45.98; H, 3.94; N, 20.01%. IR (KBr disc, cm^{-1}): 3478 m, 3342 m, 3174s , 2997 w, 1625 s, 1555 s, 1507 s, 1379 m, 1317 m, 1287 m, 1239 s, 1165 s, 1122 s, 864 m, 810 m, 792 m, 482 m, 452 m (s, strong; m, medium ; w, weak).

Characteristic ^{1}H-NMR signals (DMSO-d6, TMS, p.p.m.): 11.49 (s, 1H, NHCS), 9.75 (s, 2H, OH), 8.20 (s, 1H, CH=N), 7.92 (s, 1H, NH_2), 7.71 (s, 1H, NH_2), 7.64 (d, 1H, aromatic, J = 8 Hz), 6.26 (s, 1H, aromatic), 6.21(d, 1H, aromatic, J = 8 Hz). Characteristic ^{13}C-NMR signals (DMSO-d6, TMS, p.p.m.): 177.40 (C=S), 161.04 (C-O), 158.56 (C-O), 140.97 (C=N), 128.67 112.11, 108.26, 102.80 (C-aromatic).

2.2.3.2 Synthesis of 2,4-dihydroxybenzaldehyde 4-methylthiosemicarbazone, H_3M **(2)**

4-Methylthiosemicarbazide (0.11 g, 1 mmol) and 2,4-dihydroxybenzaldehyde (0.14 g, 1 mmol) were heated in ethanol (10 ml) for 1 h. Slow evaporation of the solvent yielded

yellow crystals. The crystals were filtered, washed with cold methanol and ether, dried in air and kept in a desiccator over silica gel.

(Yield: 0.20 g, 89%). Anal. Calc. for $C_9H_{11}N_3O_2S$: C, 47.99; H, 4.92; N, 18.65. Found: C, 48.28; H, 5.21; N, 18.98%. IR (KBr disc, cm^{-1}): 3342m, 3249m, 3127 w, 1625 s, 1573 s, 1521 m, 1459 w, 1331 s, 1270 m, 1231 s, 1166m, 1125 m, 1019 m, 967 w, 868 m, 817 m, 780 w, 670 m, 635 m, 586 w, 547 w, 497w, 374w (s, strong; m, medium ; w, weak).

Characteristic ^{1}H-NMR signals (DMSO-d6, TMS, p.p.m.): 11.18 (s, 1H, NHCS), 9.88 (s, 1H, OH), 9.74 (s, 1H, OH), 8.20 (s, 1H, CH=N), 8.24 (d, 1H, N***H***CH_3, J = 4 Hz), 7.68 (d, 1H, aromatic, J = 8 Hz), 6.26 (s, 1H, aromatic), 6.24 (d, 1H, aromatic, J = 8 Hz), 2.95 (d, 3H, NC***H*****$_3$**, J = 4 Hz). Characteristic ^{13}C-NMR signals (DMSO-d6, TMS, p.p.m.): 177.61 (C=S), 160.87 (C-O), 158.40 (C-O), 140.54 (C=N), 128.67, 112.45, 108.19, 102.80 (C-aromatic), 31.28 (N-CH_3).

2.2.3.3 Synthesis of 2,4-dihydroxybenzaldehyde 4-ethylthiosemicarbazone, H_3E **(3)**

4-Ethylthiosemicarbazide (1.19 g, 10 mmol) and 2,4-dihydroxybenzaldehyde (1.38 g, 10 mmol) were refluxed in ethanol (40 ml) for 3 h. Slow evaporation of the solvent yielded yellow crystals. The crystals were filtered, washed with cold methanol and ether, dried in air and kept in a desiccator over silica gel.

(Yield: 2.05 g, 86%). Anal. Calc. for $C_{10}H_{13}N_3O_2S$: C, 50.19; H, 5.48; N, 17.56. Found: C, 50.32; H, 5.28; N, 17.78%. IR (KBr disc, cm^{-1}): 3382 m, 3295 m, 3163 s, 2979w, 1626 s, 1579 m, 1551 s, 1499 s, 1401 m, 1302 s, 1241 s, 1166 s, 1126 m, 1099 m, 938 w, 867 w, 820 w, 801 w, 741 w, 642 w, 621 w, 522 m (s, strong; m, medium ; w, weak).

11.16 (s, 1H, NHCS), 9.76 (s, 2H, OH), 8.26 (s, 1H, CH=N), 8.31 (d, 1H, N***H***CH_2-, J = 4 Hz), 7.72 (d, 1H, aromatic, J = 8 Hz), 6.32 (s, 1H, aromatic), 6.30 (d, 1H, aromatic, J = 8 Hz), 3.57 (m, 2H, NC***H₂***-, J = 4 Hz) 1.14 (d, 3H, NCH_2C***H₃***, J = 4 Hz). Characteristic ^{13}C-NMR signals (DMSO-d6, TMS, p.p.m.): 176.34 (C=S), 160.84 (C-O), 158.40 (C-O), 140.99 (C=N), 128.88, 112.34, 108.32, 102.81 (C-aromatic), 32.20 (N-**C**H_2-), 15.21 (NCH_2**C**H3*).*

2.2.3.4 Synthesis of 2,4-dihydroxybenzaldehyde 4-phenylthiosemicarbazone, H_3P **(4)**

4-Phenylthiosemicarbazide (0.17 g, 1 mmol) and 2,4-dihydroxybenzaldehyde (0.14 g, 1 mmol) were heated in ethanol (20 ml) for 3 h. Slow evaporation of the solvent yielded yellow crystals. The crystals were filtered, washed with cold methanol and ether, dried in air and kept in a desiccator over silica gel.

(Yield: 0.23 g, 80%). Anal. Calc. for $C_{14}H_{13}N_3O_2S$: C, 58.52; H, 4.56; N, 14.62. Found: C, 58.38; H, 4.26; N, 14.29%. IR (KBr disc, cm^{-1}): 3331 m, 3144m, 2974 m, 1629 s, 1542 s, 1223 m, 1264 s, 1210 s, 1121 s, 978 m, 838 w, 743 w, 694 w(s, strong; m, medium ; w, weak).

Characteristic ^{1}H-NMR signals (DMSO-d6, TMS, p.p.m.): 11.54 (s, 1H, NHCS), 9.93 (s, 1H, OH), 9.89 (s, 1H, OH), 8.72 (s, 1H, N**H**C_6H_5), 8.34 (s, 1H, CH=N), 7.82 (d, 1H, aromatic, J = 8 Hz), 7.53 (d, 2H, aromatic, J = 8), 7.33 (t, 12H, aromatic, J = 8), 7.16 (t, 1H, aromatic, J = 8), 6.29 (s, 1H, aromatic), 6.27 (d, 1H, aromatic, J = 4 Hz). Characteristic ^{13}C-NMR signals (DMSO-d6, TMS, p.p.m.): 175.57 (C=S), 161.21 (C-O), 158.75 (C-O), 141.73 (C=N), 139.64, 129.25, 126.06, 125.66, 112.23, 108.38, 102.84 (C-aromatic).

2.2.3.5 Synthesis of (4-Hydroxy-2-oxidobenzaldehyde thiosemicarbazonato)-(2,2'-bipyridine)zinc(II) , [Zn(bipy)(HT)] **(5)**

Zinc acetate dihydrate (0.22 g, 1 mmol) and 2,2'-bipyridine (0.16 g, 1 mmol) were heated in ethanol (20 ml) for 1 hour followed by addition of 2,4-dihydroxybenzaldehyde thiosemicarbazone, H_3T (0.21 g, 1 mmol) in hot ethanol (20 ml) and the mixture was refluxed for another 3 hours. The yellow complex that formed was filtered, washed with cold methanol and ether, dried in air and kept in a desiccator over silica gel. (Yield: 0.28 g, 65 %). Anal. Calc. for $C_{18}H_{15}N_5O_2SZn$: C, 50.18; H, 3.51; N, 16.26. Found: C, 50.43; H, 3.26; N, 16.54 %. IR (KBr disc, cm^{-1}): 3428 w, 3316 m, 3142 w, 3070 w, 3069w, 1604 s, 1478 s, 1444 m, 1315 m, 1252 m, 1219 s, 1175s m, 1122 m, 842 w, 763 m, 553 w, 420 w (s, strong; m, medium ; w, weak).

Characteristic ^{1}H-NMR signals (DMSO-d6, TMS, p.p.m.): 9.47 (s, broad, 1H, OH), 8.62 (d, 2H, bipy, J = 4 Hz), 8.42 (d, 2H, bipy, J = 8 Hz), 8.18 (s, 1H, CH=N), 7.98 (t, 2H, bipy, J = 8 Hz), 7.48 (d, 2H, bipy, J = 4 Hz), 6.92 (s, broad, 1H, aromatic), 6.30 (s, broad, 1H, aromatic), 6.02 (s, broad, 1H, aromatic + 2H, -N**H$_2$**)

2.2.3.6 Synthesis of (4-Hydroxy-2-oxidobenzaldehyde 4-methylthiosemicarbazonato)-(2,2'-bipyridine)zinc(II) trihydrate, [Zn(bipy)(HM)]. $3H_2O$ **(6)**

Zinc acetate dihydrate (0.22 g, 1 mmol) and 2,2'-bipyridine (0.16 g, 1 mmol) were heated in ethanol (20 ml) for 1 hour followed by addition of 2,4-dihydroxybenzaldehyde 4-methylthiosemicarbazone, H_3M (0.23 g, 1 mmol) in hot ethanol (20 ml) and the mixture

was refluxed for another 3 hours. The yellow complex that formed was filtered, washed with cold methanol and ether, dried in air and kept in a desiccator over silica gel.

(Yield: 0.40 g, 80%). Anal. Calc. for $C_{19}H_{23}N_5O_5SZn$: C, 45.74; H, 4.65; N, 14.04. Found: C, 4.53; H, 4.21; N, 13.59%. IR (KBr disc, cm^{-1}): 3378 m (broad), 3236 m, 3075 w, 1602 s, 1441 m, 1405 m, 1332 m, 1273 m, 1220 m, 1175 m, 849 w m, 765 m, 652 w 551 w, 450 w (s, strong; m, medium ; w, weak).

Characteristic ^{1}H-NMR signals (DMSO-d6, TMS, p.p.m.): 8.54 (s, 2H, bipy), 8.45 (d, 2H, bipy, J = 8 Hz), 8.27 (s, 1H, CH=N), 8.05 (s, broad, 2H, bipy), 7.57 (s, broad, 2H, bipy), 6.94 (d, 1H, aromatic, J = 4 Hz), 6.40 (s, broad, 1H, -N**H**-CH_3), 6.27 (s, broad, 1H, aromatic), 6.01 (s, broad, 1H, aromatic), 2.71 (s, 3H, NC***H*****$_3$**)

2.2.3.7 Synthesis of (4-Hydroxy-2-oxidobenzaldehyde 4-ethylthiosemicarbazonato)-(2,2'-bipyridine)zinc(II) trihydrate, [Zn(bipy)(HE)].3H_2O **(7)**

Zinc acetate dihydrate (0.22 g, 1 mmol) and 2,2'-bipyridine (0.16 g, 1 mmol) were heated in ethanol (20 ml) for 1 hour followed by addition of 2,4-dihydroxybenzaldehyde 4-ethylthiosemicarbazone, H_3E (0.24 g, 1 mmol) in hot ethanol (20 ml) and the mixture was refluxed for another 3 hours. The yellow complex that formed was filtered, washed with cold methanol and ether, dried in air and kept in a desiccator over silica gel.

(Yield: 0.38 g, 75 %). Anal. Calc. for $C_{20}H_{25}N_5O_5SZn$: C, 46.83; H, 4.91; N, 13.65. Found: C, 47.09; H, 4.42; N, 13.30%. IR (KBr disc, cm^{-1}): 3400 m, 3221 m, 3064 w, 2974 m, 1603 s, 1442 m, 1336 m, 1268 m, 1227 m, 1172 m, 853 m, 799 m, 762 m, 591 m, 420 w,(s, strong; m, medium ; w, weak).

Characteristic ^{1}H-NMR signals (DMSO-d6, TMS, p.p.m.): 8.61(d, 2H, bipy, J = 4 Hz), 8.45 (d, 2H, bipy, J = 8 Hz), 8.22 (s, 1H, CH=N), 8.01 (s, broad, 2H, bipy), 7.51 (s, broad, 2H, bipy), 6.94 (d, 1H, aromatic, J = 4 Hz), 6.30 (s, broad, 1H, aromatic), 6.25 (t, 1H, -N**H**-CH_2CH_3), 6.01 (s, broad, 1H, aromatic), 3.21 (m, 2H, -NHC-**H_2**CH3, J = 4 Hz), 1.01 (t, 3H, -$NHCH_2$C-**H_3,** J = 4 Hz)

2.2.3.8 Synthesis of (4-Hydroxy-2-oxidobenzaldehyde 4-phenylthiosemicarbazonato)-(2,2'-bipyridine)zinc(II) dihydrate, [Zn(bipy)(HP)].2 H_2O **(8)**

Zinc acetate dihydrate (0.22 g, 1 mmol) and 2,2'-bipyridine (0.16 g, 1 mmol) were heated in ethanol (20 ml) for 1 hour followed by addition of 2,4-dihydroxybenzaldehyde 4-phenylthiosemicarbazone, H_3P (0.29 g, 1 mmol) in hot ethanol (20 ml), and the mixture was refluxed for another 3 hours. The yellow complex that formed was filtered, washed with cold methanol and ether, dried in air and kept in a desiccator over silica gel.

(Yield: 0.44 g, 81 %). Anal. Calc. for $C_{24}H_{23}N_5O_4SZn$: C, 53.09; H, 4.27; N, 12.90. Found: C, 53.54; H, 4.31; N, 12.55%. IR (KBr disc, cm^{-1}): 3620 w, 3327 m, 3109 w, 3070 w, 1598 m, 1484 s, 1429 m, 1313 m, 1217 m. 1172 m, 846 m, 755 m, 588 w, 568 w, 508 w, 450 w (s, strong; m, medium ; w, weak).

Characteristic ^{1}H-NMR signals (DMSO-d6, TMS, p.p.m.): 9.61 (s, broad, 1 H, OH), 8.64 (d, 2H, bipy, J = 4 Hz), 8.41 (d, 2H, bipy, J = 8 Hz), 7.96 (t, 2H, bipy, J = 8 Hz), 7.76 (d, 2H, bipy, J = 8 Hz), 7.47 (t, 2H, aromatic, J = 4 Hz), 7.15 (t, 2H, aromatic, J = 8 Hz), 7.01 (s, broad, 1H, aromatic), 6.79 (t, 1H, aromatic, J = 4 Hz), 6.38 (s, broad, 1H, aromatic), 5.92 (s, broad, 1H, aromatic)

2.2.4 X-ray crystallography

Yellow crystal of compound **2** and compound **3** were grown from slow evaporation from their ethanolic solutions. While yellow crystals for complex **5** and green crystal for complex **8** were recrystallised from dimethylsulphoxide (DMSO) and dimethylformamide (DMF), respectively. The unit cell parameters and the intensity data were collected on a Bruker SMART APEX CCD diffractometer, equipped with a Mo Kα X-ray source (λ=0.71073 Å). The APEX2 software was used for data acquisition and the SAINT software for cell refinement and data reduction (Bruker, 2007). Absorption corrections on the data were made using SADABS (Sheldrick, 1996). The structures were solved and refined by SHELXL97 (Sheldrick, 2008). Molecular graphics were drawn by using XSEED (Barbour, 2001). Material for publication was prepared using publCIF (Westrip, 2009). The structures were solved by direct-methods and refined by a full-matrix least-squares procedure on F^2 with anisotropic displacement parameters for non-hydrogen atoms. Carbon-bound H-atoms for compound **2,** were placed in calculated positions (C—H 0.95 to 0.98 Å) and were included in the refinement in the riding model approximation, with Uiso>(H) set to 1.2-1.5 Ueq(C). Whereas, the hydroxy and amino H-atoms were located in a difference Fourier map, and were refined with distance restraints of O–H = 0.84.01 and N–H = 0.88.01 Å; their temperature factors were freely refined. Hydrogen atoms for compounds **3**, **5** and **8** were placed in their calculated positions and refined using a riding model.

2.2.5 DNA binding

PAGE grade self-complimentary 12-mer oligonucleotides $(CG)_6$, $(AT)_6$, (CGCGAATTCGCG), (CGCGATATCGCG), HPLC grade human telomeric sequence 22-mer oligonucleotide 5'-AGGGTTAGGGTTAGGGTTAGGG-3', and 17-mer complementary oligonucleotides 5'-CCAGTTCGTAGTAACCC-3, 3'-GGTCAAGCATCATTGGG-5' were annealed to give the respective duplex or quadruplex, as specified by the supplier, 1st BASE and Eurogentec Ait. The circular dichroism spectra were obtained by scanning Tris-NaCl buffered solutions of the DNA without and with the complexes.

2.2.6 Nucleolytic study

Agarose gel electrophoresis experiments were carried out on supercoiled plasmid DNA pBR322 (4.4 kb) using a horizontal gel system. For the cleavage studies, each 20 µL sample consisted of the zinc(II) complex (5 mM) dissolved in DMF, DNA, and the required volume of additional buffer. All samples were incubated in the dark in an oven incubator at a temperature of 37 ^{o}C. The reaction mixtures (20 uL) were prepared as follows: compounds or salt with different concentration were added to a standard mixture of 0.5 µl of supercoiled plasmid DNA pBR322 (0.25 µg/µl) and Tris-NaCl buffer pH 7.5. The reactions were performed after incubating the reaction mixture at 37 °C for 2 or 24 hours. 3 µl of 6x loading buffer was added to 20 µl of the reaction mixtures and electrophoresis was performed at 80 V for 90 minutes in Tris-acetate-EDTA (TAE) buffer, pH 8.1, using 1.5 % agarose gel. After electrophoresis, the agarose gel was stained with ethidium bromide

solution (0.5 μg/ml). For the oxidative or reductive cleavage studies, incubation of the samples were similarly carried out in the presence of H_2O_2 or sodium ascorbate. The DNA cleavage profile was analyzed using 1.5% agarose gel in a horizontal gel tank set with a running time of 2 hours, at a constant voltage of 80 V. Each reaction mixture consisted of 0.5 μg/μl DNA and Tris-NaCl buffer pH 7.5 unless otherwise mentioned. The resultant DNA bands after the electrophoresis step for each set of experiments were stained with ethidium bromide before being photographed under UV light using a Syngene Bio Imaging system and the digital image was viewed with Gene Flash software.

2.2.7 Human Topoisomerase I inhibtion assay

The human DNA topoisomerase I inhibitory activity was determined by measuring the relaxation of supercoiled plasmid DNA pBR322. A positive result is indicated by the reduction of the nicked band (containing nicked and fully relaxed DNA) (Form II) and formation of various faster moving bands of topoisomers with different degree of relaxation as compared to the Topoisomerase I with DNA control. For measurement of human topoisomerase I activity, the reaction mixture was comprised of 10 mM Tris-HCl, pH 7.5, 100 Mm NaCl, 1mM phenylmethylsulfonyl fluoride (PMSF), α-toluenesulfonyl fluoride, and 1 mM 2-mercaptoethanol, 0.25 μg plasmid DNA pBR322, 1 unit of human DNA topoisomerase I, and metal complex with final concentration of 40 μM . All reactions were conducted at a final volume of 20 μl and were prepared on ice. Upon enzyme addition, reaction mixtures were incubated at 37^{o}C for 30 minutes. The reactions were terminated by the addition of 2 μl of 10% sodium dodecyl sulphate (SDS) and then followed by 3 μl of dye solution comprising 0.02% bromophenol blue and 50% glycerol. SDS is required to

observe a linear DNA fragment and to denature topoisomerase I, preventing further functional enzymatic activity, and thus DNA is prevented from being relegated by topoisomerase. The mixtures were applied to 1.2% agarose gel and electrophoresed for 5 hours at 33 V with running buffer of Tris-acetate EDTA (TAE) at pH 8.1. The gel was stained, destained, and photographed under UV light using a Syngene Bio Imaging system and the digital image was viewed with Gene Flash software.

In the Human DNA topoisomerase I inhibition condition study, the same protocol was applied. This study is designed to investigate the effect of the metal complex on topoisomerase I and DNA, and to do a preliminary study on the mode of action of metal complex in the Human DNA topoisomerase I inhibition study. The sequence of addition of the main components (human DNA topoisomerase I, plasmid DNA pBR322, and metal complex) was varied. Two conditions were studied in this assay. For the first condition, human DNA topoisomerase I with the metal complex was incubated at 37 ^{o}C for 30 minutes before the addition of DNA. This mixture was incubated for another 30 minutes at the same temperature after the addition of DNA. As for the second condition, the metal complex and DNA was incubated for 30 minutes at 37 ^{o}C first, and then followed by the addition of topoisomerase I. This mixture was incubated for another 30 minutes at 37 ^{o}C after the addition of topoisomerase I.

2.2.8 Antibacterial and antifungal assay

The antibacterial and antifungal activities of the ligands and complexes were assessed against several strains of Gram-positive bacteria, Gram-negative bacteria and fungi. A colorimetric broth microdilution method using *p*-iodonitrotetrazolium violet (INT) as the growth indicator was employed to quantify the minimum inhibitory concentration (MIC) value of the complexes in the antibacterial and antifungal assay. The test was performed as serial two fold dilutions on sterile, 96 well u-bottom plate. The complexes were tested with concentration range of 0.49 to 250 μg/ml. The complexes (1000 μg) are dissolved in 1 ml 80% DMF because at this concentration, DMF does not show inhibition towards the microorganisms tested.

The inocula were each diluted in broth to a final concentration of 5×10^5 CFU/ml where CFU stands for colony forming unit. In the antibacterial assay, bacteria that were 24 hours old were prepared to match the turbidity of a McFarland standard corresponding to (1×10^8 CFU/ml) at 625 nm. The inocula were each diluted in broth to a final concentration of 5×10^5CFU/ml. Mueller Hilton Broth was used as the broth medium. The concentrations of the antibacterial drug Chloramphenicol, which was as the positive control was between 0.25 to 128 μg/ml. In the antifungal assay, 24 hour old *candida* species and 48 hour old *c. neoformans* and *a. niger* were prepared to match the turbidity of a McFarland standard corresponding to (1×10^6 CFU/ml) at 530 nm. The inocula of *candida* species were each diluted in broth to a final concentration of 0.5-2.5 x 10^3 CFU/ml, *c. neoformans* at 0.5-2.5 x 10^4 CFU/ml and *a. niger* at 0.5-2.5 x 10^5 CFU/ml. RPMI - 1640 with L-glutamine, without bicarbonate and buffered at pH 7 with 3-(N-morpholino) propanesulfonic acid was used as

the broth medium. The concentrations of the antifungal drug fluconazole (positive control) were between 0.63 to 32 μg/ml. After incubation for 24 hours for bacteria and *candida* species and 48 hours for *c. neoformans* and *a. niger*, the MIC in μg/ml was defined as the lowest concentration of solvent in which there was no microbial growth, evidenced by no color change.

2.3. Results and discussion

2.3.1 Synthesis of ligands and complexes

Proposed structures for all the compounds with IUPAC numbering scheme are shown in Fig. 2.1. The stoichiometries, colors and partial elemental analyses of the ligands and complexes are shown in Table 2.1. Results from partial elemental analyses are in good agreement with the proposed formulation of Zn(bipy)L where bipy = 2,2'-bipyridine and L is the doubly deprotonated thiosemicarbazones. Complexes **6** and **7** contain three hydrated water molecules while complex **8** exist as a dihydrate. All the complexes are yellow in appearance except **8**, which is green. Ligands **1-4** are prepared in high yield from the condensation of 2,4-dihydroxybenzaldehyde and the various thiosemicarbazides in refluxing ethanol while the complexes are prepared in high yield by refluxing zinc acetate dihydrate, 2,2'-bipyridine and the thiosemicarbazones in ethanol. Spectroscopic and crystallographic data show that all the free ligands exist in the thione tautomer form in both solid and solution. However, all the complexes were isolated with the ligands coordinating in the thiolate form. This implies that the presence of acetate in the reaction mixture facilitate the formation of the ligand in the thiolate form by deprotonating the thiol proton.

Once the ligand was deprotonated and coordinated to the metal in the thiolate form, it cannot tautomerize back to the thione form. In the absence of acetate, reaction of similar ligands with zinc chloride has led to formation of a dinuclear complex with the thiosemicarbazone moiety coordinating in the thione form (Tan *et al.* 2009).

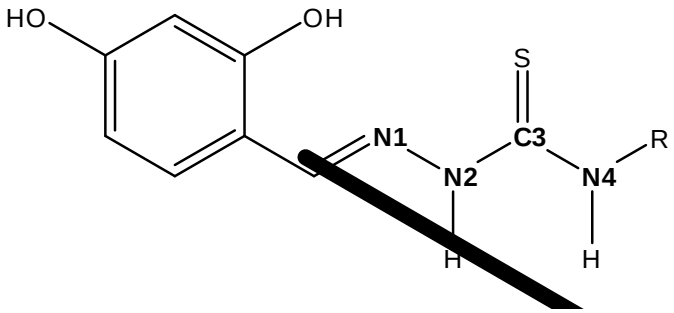

1 R = H **2** R = -CH_3 **3** R = -C_2H_5 **4** R = -C_6H_5

5 R = H **6** R = -CH_3 **7** R = -C_2H_5 **8** R = -C_6H_5

Fig. 2.1 Proposed structures for all the compounds

Table 2.1

Stoichiometries, color and partial elemental analyses of the ligands and zinc(II) complexes

Compound	Stoichiometries	Color	Anal. Calc. (Found)%		
			C	H	N
H_3T **(1)**	$C_8H_9N_3O_2S$	Pale yellow	45.49 (45.98)	4.29 (3.94)	19.89 (20.01)
H_3M **(2)**	$C_9H_{11}N_3O_2S$	Pale yellow	47.99 (48.88)	4.92 (5.21)	18.65 (18.98)
H_3E **(3)**	$C_{10}H_{13}N_3O_2S$	Pale yellow	50.19 (50.32)	5.48 (5.28)	17.65 (17.78)
H_3P **(4)**	$C_{14}H_{13}N_3O_2S$	Yellow green	58.52 (58.38)	4.56 (4.26)	14.62 (14.29)
[Zn(bipy)(HT)] **(5)**	$C_{18}H_{15}N_5O_2SZn$	Yellow	50.18 (50.43)	3.51 (3.26)	16.26 (16.54)
[Zn(bipy)(HM)].3H_2O **(6)**	$C_{19}H_{23}N_5O_5SZn$	Yellow	45.74 (45.53)	4.65 (4.21)	14.04 (13.59)
[Zn(bipy)(HE)].3H_2O **(7)**	$C_{20}H_{25}N_5O_5SZn$	Yellow	46.83 (47.09)	4.91 (4.42)	13.65 (13.30)
[Zn(bipy)(HP)].2H_2O **(8)**	$C_{24}H_{23}N_5O_4SZn$	Yellow green	53.09 (53.54)	4.27 (4.31)	12.90 (12.55)

Complexes **6** and **7** are soluble in methanol, DMF and DMSO. While complexes **5** and **8** are insoluble in common polar and non-polar solvents but are soluble in DMF and DMSO. None of the complexes are sufficiently soluble in DMSO for acquisition of ^{13}C NMR spectra. The compounds synthesized were subjected to biological tests before recrystallization. Therefore, the absolute structure of the compounds in solution, used for biological tests, may not be exactly identical compared to those determined crystallographically. The numbers and type of solvent molecules in the crystal packing may affect the absolute structure in the solid state.

2.3.2 Crystal structure analysis

2.3.2.1 Crystal structure of H_3M (**2**)

Ligand **2** crystallised into a monoclinic lattice with space group symmetry *Cc*. The perspective view of the compound with numbering scheme is shown in Fig. 2.2.

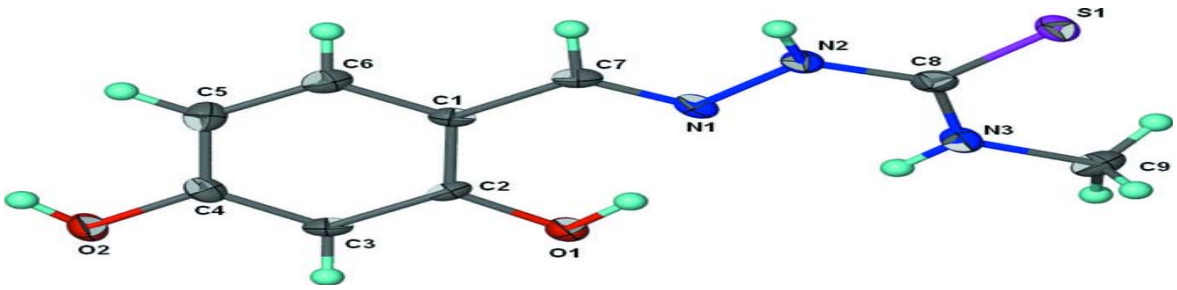

Fig. 2.2 Thermal ellipsoid (Barbour, 2001) plot of **2** drawn at the 70% probability level. Hydrogen atoms are drawn as spheres of arbitrary radii.

Selected bond lengths and angles are presented in Table 2.3. Compound **2** adopts an E configuration about the C=N bond. The N1-C7 bond length of 1.283 (4) Å is characteristic of azomethine linkage in Schiff base. The N2-C8 bond length of 1.354 (4) Å and C8-S1 bond length of 1.699 (3) Å indicates that the ligand exists in the thione tautomer form. Formation of thiol tautomer is indicated by decrease in N2-C8 bond length and increase of C8-S1 bond length due to the gain and loss in double bond character accompanying tautomerization (Fig 2.3).

Fig. 2.3 Thione-thiol tautomerization for the ligands

Hydrogen bonding interactions for compound **2** is shown in Fig. 2.4 while hydrogen bonding parameters are shown in Table 2.4. Each molecule is connected to four adjacent molecules through hydrogen bonds. The essentially planar ligand is stabilized by O1—H1O---N1 intramolecular hydrogen bond. The molecule is linked to adjacent molecules by O2—H2O···S hydrogen bonds to form a zigzag chain as shown in Fig. 2.5.

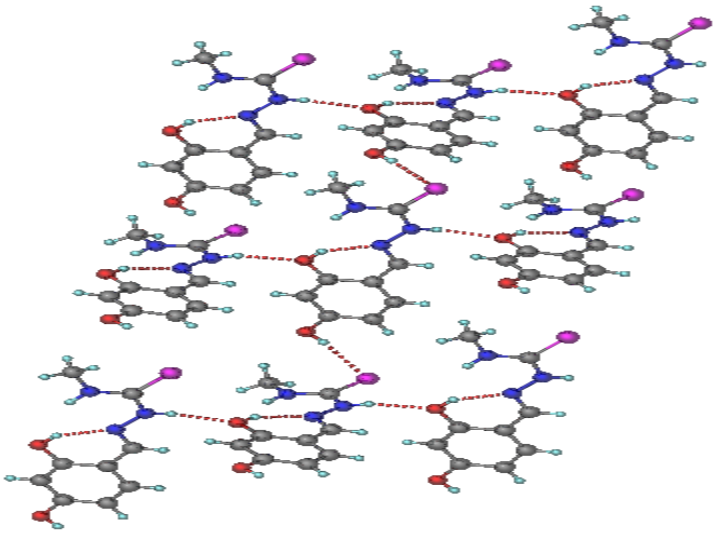

Fig. 2.4 Hydrogen bond interactions for compound **2**

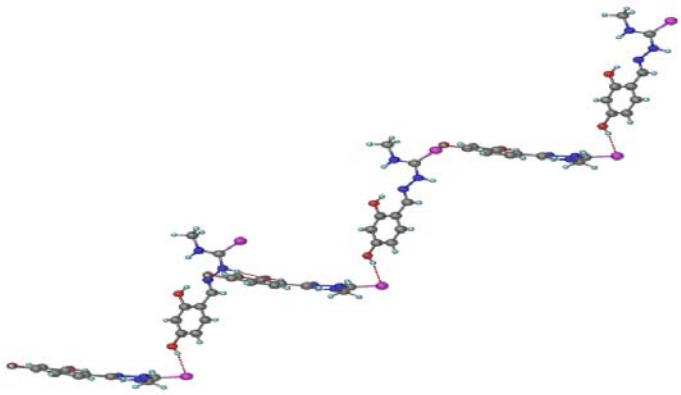

Fig. 2.5 Intermolecular O2—H2O···S hydrogen bonds for compound **2**

These adjacent chains are consolidated by N2—H2N···O1 hydrogen bonds into a two dimensional array intermolecular hydrogen bonding contacts as shown in Fig. 2.6.

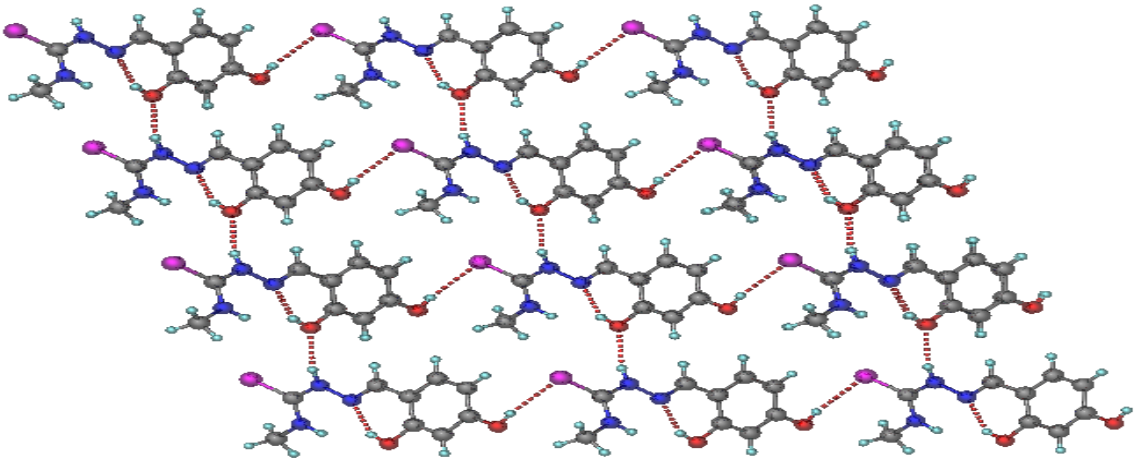

Fig. 2.6 Intermolecular N2—H2N···O1 hydrogen bonds for compound **2**

Packing diagram for compound **2** is shown in Fig. 2.7. The packing of molecules in the unit cell is stabilised by hydrogen bonding interactions.

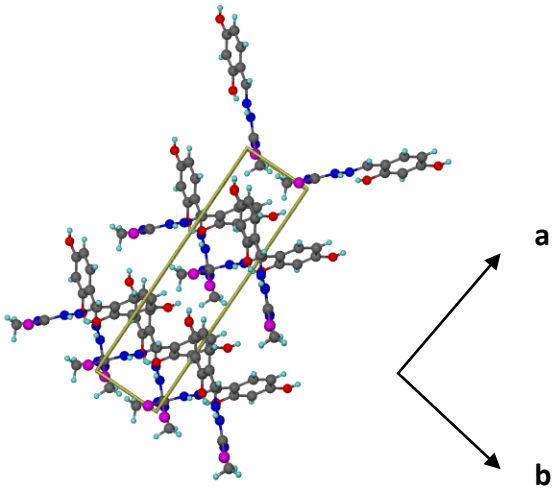

Fig. 2.7 Unit cell packing diagram of **2** along c axis.

Table 2.2

Crystal data and structure refinement parameters for compounds **2, 3, 5** and **8.**

Compound	H_3M (**2**)	H_3E (**3**)	[Zn(bipy)(HT)] (**5**)	[Zn(bipy)(HP).$2H_2O$ (**8**)
Empirical formula	$C_9H_{11}N_3O_2S$	$C_{10}H_{13}N_3O_2S$	$C_{18}H_{15}N_5O_2$ S Zn	$C_{24}H_{23}N_5O_4$ S Zn
Formula weight	225.27	239.29	430.78	542.90
Crystal system	Monoclinic	Monoclinic	Monoclinic	Orthorhombic
Space group	*Cc*	$P2_1/n$	$P2_1/c$	*Pbca*
Unit cell dimensions				
a (Å)	18.0046 (6)	4.6592 (6)	16.1256 (4)	17.9569 (9)
b (Å)	4.64360 (10)	24.067 (3)	7.0478 (2)	12.9769 (7)
c (Å)	12.2842 (4)	10.0466 (13)	17.6387 (5)	20.4834 (11)
β (°)	106.695 (2)	99.060 (2)	113.646 (2)	90
Volume, V ($Å^3$)	983.74 (5)	1112.5 (2)	1836.33 (9)	4773.1 (4)
Z	4	4	4	8
F(0 0 0)	472	504	880	2240
Density (calculated), (mg m^{-3})	1.521	1.429	1.558	1.511
Absorption coefficient, μ (mm^{-1})	0.31	0.28	1.48	1.16
Temperature, T (K)	100 (2)	100 (2)	100(2)	100 (2)
Crystal size (mm)	0.09 × 0.06 × 0.03	0.40× 0.12 × 0.06	0.10 × 0.04 × 0.02	0.35 × 0.25 × 0.15
Reflections collected	4390	6303	15773	25918
Independent reflections	2128	2517	4191	5481
	[R(int) = 0.034]	[R(int)= 0.028]	[R(int) = 0.086]	[R(int) = 0.029]
Data/restraints/parameters	2128/6/153	2517/0/148	4191/24/245	5481/20/350
$R[F^2 > 2\sigma(F^2)]$	0.038	0.039	0.062	0.028
$wR(F^2)$	0.109	0.109	0.195	0.076
S	1.11	1.08	1.04	1.03
Largest difference peak and hole (e $Å^{-3}$)	0.31 and -0.22	0.38 and -0.25	0.88 and -0.96	0.34 and -0.33

Table 2.3

Selected bond lengths (Å) and angles (°) for H_3M (**2**)

Bond lengths		Bond angles	
S1—C8	1.699 (3)	O1—C2—C3	117.7 (3)
O1—C2	1.367 (4)	O1—C2—C1	121.6 (3)
O1—H1O	0.838 (10)	O2—C4—C3	117.9 (3)
O2—C4	1.360 (4)	O2—C4—C5	121.6 (3)
O2—H2O	0.836 (10)	N1—C7—C1	123.2 (3)
N1—C7	1.283 (4)	N3—C8—N2	118.3 (3)
N1—N2	1.392 (3)	N3—C8—S1	123.4 (2)
N2—C8	1.354 (4)	N2—C8—S1	118.3 (2)
N2—H2N	0.871 (10)		
N3—C8	1.328 (4)		
N3—C9	1.451 (4)		
N3—H3N	0.880 (10)		

Table 2.4
Hydrogen-bond geometry (Å, °) for H_3M (**2**)

D—H···*A*	*D*—H	H···*A*	*D*···*A*	*D*—H···*A*
O1—H1O···N1	0.840 (10)	1.93 (3)	2.694 (3)	151 (6)
O2—H2O···S1^{i}	0.840 (10)	2.540 (10)	3.365 (2)	170 (4)
N2—H2N···O1^{ii}	0.870 (10)	2.110 (10)	2.950 (4)	162 (3)

Symmetry codes: (i) *x*+1/2, −*y*−1/2, *z*+1/2; (ii) *x*, −*y*, *z*−1/2.

2.3.2.2 Crystal structures of H_3E (**3**)

Ligand **3** crystallised into a monoclinic lattice with space group symmetry $P2_1/n$. The perspective view of the compound with numbering scheme is shown in Fig. 2.8. Selected bond lengths and angles are presented in Table 2.5.

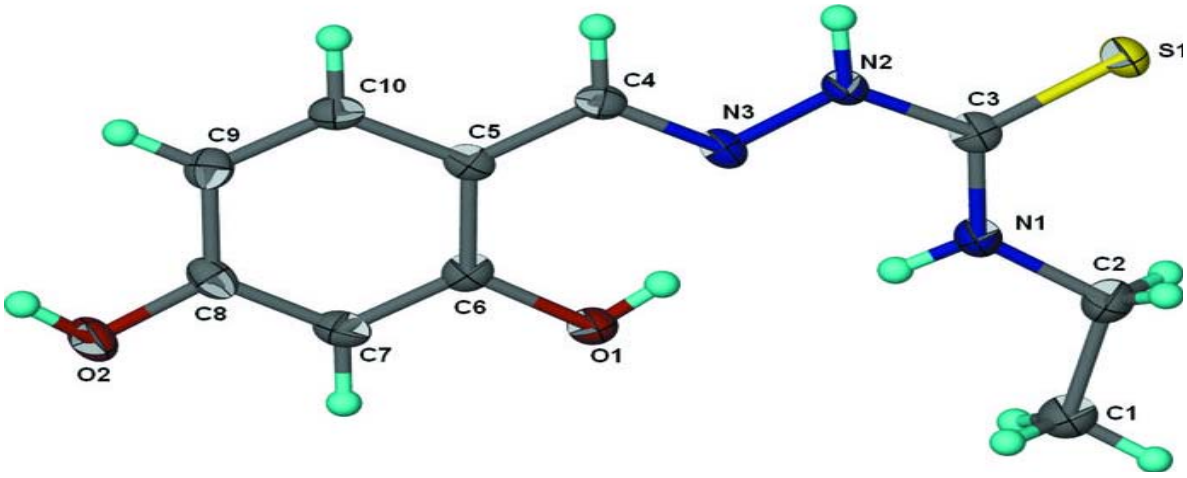

Fig. 2.8 Thermal ellipsoid (Barbour, 2001) plot of **3** drawn at the 70% probability level. Hydrogen atoms are drawn as spheres of arbitrary radii.

As for ligand **2**, ligand **3** similarly adopts an E configuration about the C=N bond (C4-N3). The essentially planar ligand is stabilized by O1—H1O---N3 intramolecular hydrogen bond. The N3-C4 bond length of 1.291 (2) Å is characteristic of azomethine linkage in Schiff base. The N2-C3 bond length of 1.357 (2) Å and C3-S1 bond length of 1.6826 (19) Å indicates that the ligand exist in the thione tautomer form similar to compound **2.**

Hydrogen bonding interactions for compound **3** is shown in Fig. 2.9 and hydrogen bonding parameters are shown in Table 2.6. Adjacent molecules are linked by O2—H2···O1 hydrogen bonds to furnish a zigzag chain as shown in Figs. 2.9 and 2.10. The

assembly of the molecules in the unit cell is stabilised by hydrogen bonding as shown in Fig. 2.10.

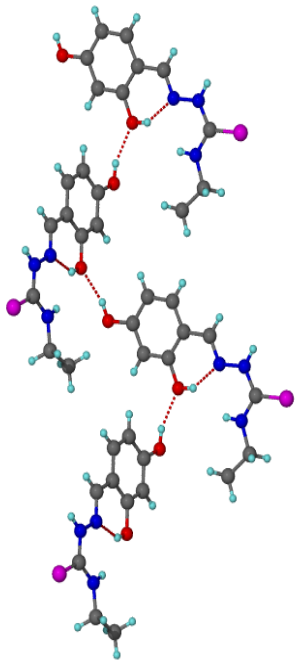

Fig. 2.9 Hydrogen bonding interactions for compound **3**

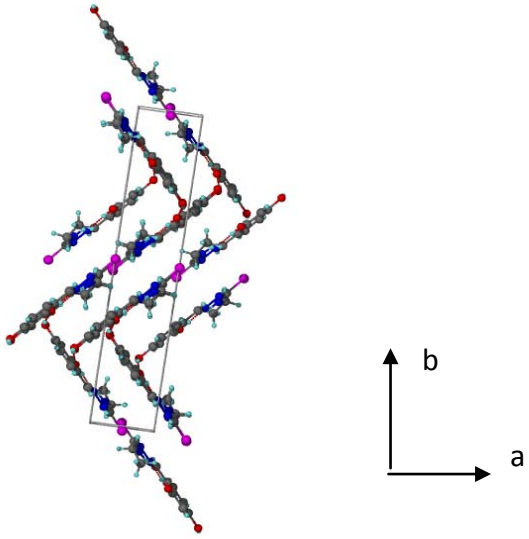

Fig. 2.10 Unit cell packing diagram of **3** along c axis.

Table 2.5

Selected bond lengths (Å) and angles (˚) for H_3E (**3**)

Bond lengths		Bond angles	
S1—C3	1.6826 (19)	N1—C3—N2	116.86 (17)
O1—C6	1.367 (2)	N1—C3—S1	123.11 (14)
O2—C8	1.355 (2)	N2—C3—S1	120.03 (14)
N1—C3	1.333 (2)	N3—C4—C5	120.45 (16)
N1—C2	1.458 (2)	O1—C6—C7	117.76 (17)
N2—C3	1.357 (2)	O1—C6—C5	120.57 (17)
N2—N3	1.374 (2)	O2—C8—C7	116.98 (17)
N3—C4	1.291 (2)	O2—C8—C9	123.01 (17)

Table 2.6
Hydrogen-bond geometry (Å, °) for H_3E (**3**)

D—H···*A*	*D*—H	H···*A*	*D*···*A*	*D*—H···*A*
O1—H1···N3	0.84	1.84	2.583 (2)	147
O2—H2···O1^{i}	0.84	1.92	2.7139 (18)	158

Symmetry codes: (i) $x-1/2, -y+1/2, z+1/2$. Hydrogen atoms are placed at calculated positions.

2.3.2.3 Crystal structures of [Zn(bipy)(HT)](**5**)

Complex **5** crystallised into a monoclinic lattice with space group symmetry $P2_1/c$. The perspective view of the complex with numbering scheme is shown in Fig. 2.11. Selected bond lengths and angles are presented in Table 2.7.

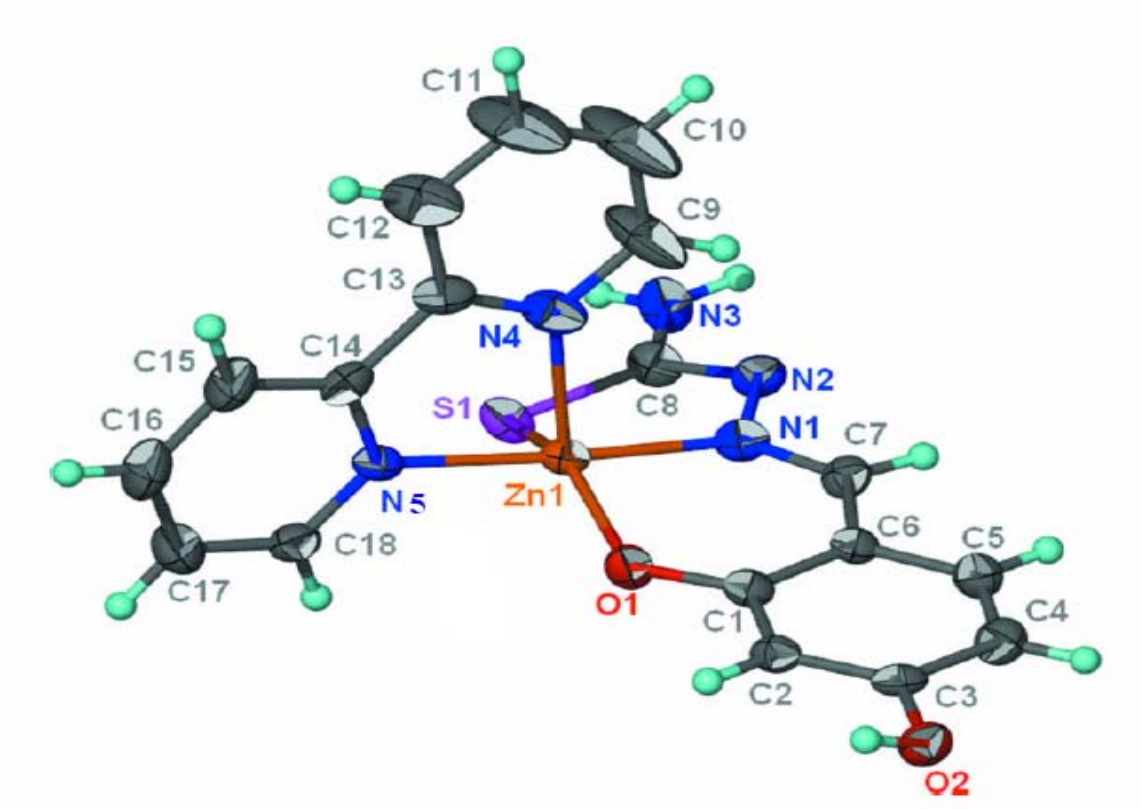

Fig. 2.11 Thermal ellipsoid (Barbour, 2001) plot of **5** drawn at the 70% probability level. Hydrogen atoms are drawn as spheres of arbitrary radii.

The complex **5** is mononuclear and five-coordinated with the doubly deprotonated thiosemicarbazone as a tridentate ligand coordinating through one phenolic oxygen, azomethine nitrogen and thiolate sulfur while the 2,2'-bipyridine is coordinated as the *N*,*N*'-bidentate ligand. A five coordinated complex can adopt either square pyramidal or trigonal bipyramidal geometry and are known to interconvert through a process known as pseudo-Berry rotation. However, five coordinated complexes are also known to adopt intermediate coordination geometry between square pyramidal or trigonal bipyramidal. Therefore to effectively illustrate the distortion from ideal coordination geometry, the index of trigonality were proposed by Addison *et al.* in 1984. In a five-coordinate system, the index of trigonality is defined by the angular structural parameter (τ). The value of τ is calculated

by the formula τ = ($\beta-\alpha$)/60, where β(the greatest basal angle) = N1—Zn1—N6 = 175.77 (18)˚ and α(the second greatest angle) = O1—Zn1—S1 = 146.44(12)˚ . The values of τ are zero and unity for perfect square pyramidal and trigonal bipyramidal geometries respectively. Since distortion from ideal geometry can be distorted square pyramidal, distorted trigonal bipyramidal or intermediate between the two, we classified a complex with τ < 0.33 as having distorted square pyramidal geometry. In this thesis, a complex with τ value between 0.33 and 0.66 is described as trigonal bipyramidal distorted square based pyramid (TBDSBP) whereas complex with τ > 0.66 is assigned with distorted trigonal bipyramidal geometry. The trigonality index τ of 0.49 for **5** indicates that the coordination geometry around zinc is intermediate between trigonal bipyramidal and square pyramidal geometries and is better described as trigonal bipyramidal distorted square based pyramid (TBDSBP).

The deviation from an ideal stereochemistry may due to the restricted bite angle imposed by both the thiosemicarbazone and bipy ligands (Seena and Kurup, 2008). The bite angle around the metal for *N*,*N'*-heterocycle of 77.46(19)˚ may be considered normal when compared with an average value of 77˚ reported in the literature for zinc complexes with 2,2'-bipyridine (Chang and Janiak, 2001; Seena and Kurup, 2008). Zn –$N_{azomethine}$ bond length of 2.045(5) Å is shorter than the Zn-N_{bipy} bond length of 2.109(5) and 2.112(5) Å. This indicates that the azomethine nitrogen is coordinated more strongly to zinc compared to the bipyridine nitrogen and the thiosemicarbazone moiety dominates equatorial bonding. The Zn–N_{bipy} bond lengths are similar to those reported for mononuclear zinc(II) complexes (Chang and Janiak, 2001; Seena and Kurup, 2008). The imine bond formation is

evidenced from N1-C7 and N2-C8 distances of 1.306(7) Å and 1.310(7)Å. The C-N bond length of 1.306(7) Å and C-S bond length of 1.746(6) is similar to those reported for coordination of thiosemicarbazone in the thiolate form (Seena and Kurup, 2008; Demirci, 2008).

Hydrogen bonding interactions for complex **5** is shown in Fig. 2.12 and hydrogen bonding parameters are shown in Table 2.8.

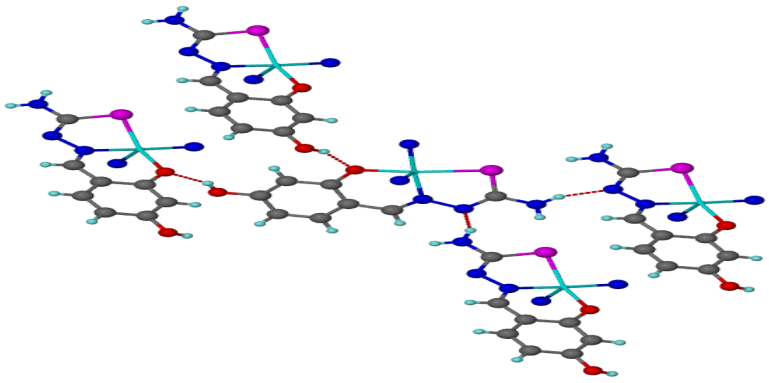

Fig. 2.12 Simplified hydrogen bonding interactions for complex **5.** Bipyridine carbons have been omitted for clarity.

Each mononuclear molecule is linked to four adjacent molecules through N-H---N and O-H---O hydrogen bonds to form a 2-dimensional layer structure. The packing of the molecules are stabilized by hydrogen bonding as shown in Fig. 2.13. No obvious π-π interactions were observed in the crystal packing.

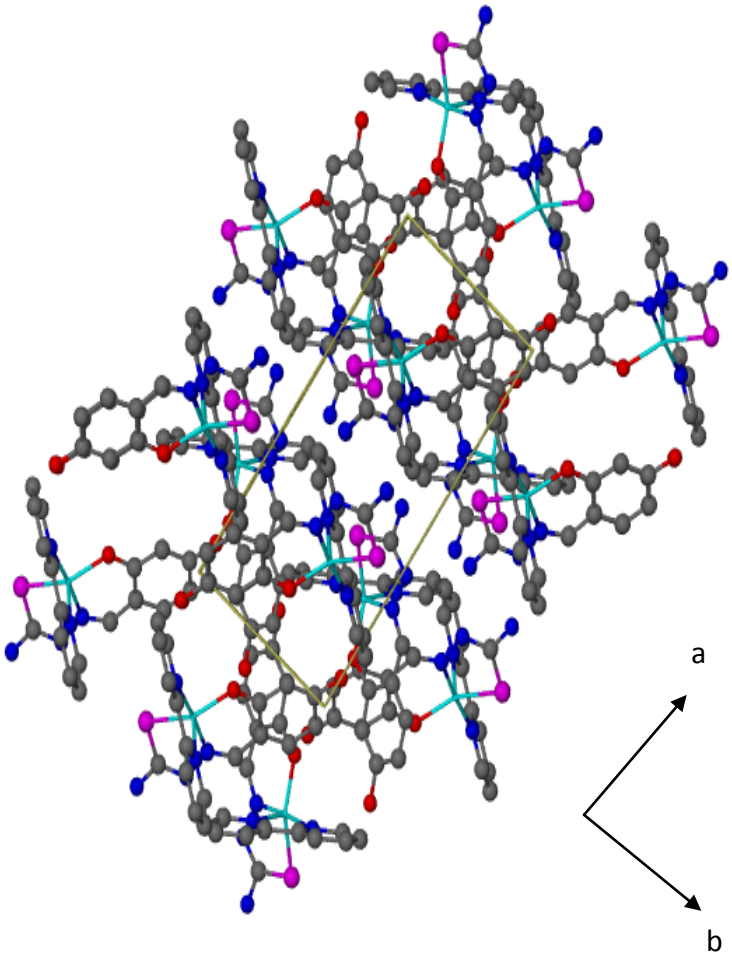

Fig. 2.13 Unit cell packing diagram of complex **5** along c axis.

Table 2.7

Selected bond lengths (Å) and angles (˚) for [Zn(bipy)(HT)](**5**)

Bond lengths		Bond angles	
Zn1—O1	1.983 (4)	O1—Zn1—N1	90.29 (16)
Zn1—N1	2.045 (5)	O1—Zn1—N4	102.37 (18)
Zn1—N4	2.109 (5)	N1—Zn1—N4	100.70 (19)
Zn1—N5	2.112 (5)	O1—Zn1—N5	93.82 (16)
Zn1—S1	2.3911 (15)	N1—Zn1—N5	175.77 (18)
S1—C8	1.746 (6)	N4—Zn1—N5	77.46 (19)
O1—C1	1.329 (7)	O1—Zn1—S1	146.42 (12)
N1—C7	1.306 (7)	N1—Zn1—S1	81.14 (13)
N1—N2	1.403 (6)	N4—Zn1—S1	111.10 (15)
N2—C8	1.310 (7)	N5—Zn1—S1	95.92 (13)
N3—C8	1.355 (7)	C8—S1—Zn1	92.73 (19)
N4—C9	1.338 (8)	C1—O1—Zn1	128.1 (3)
N4—C13	1.346 (8)		
N5—C18	1.333 (7)		
N5—C14	1.340 (7)		

Table 2.8

Hydrogen-bond geometry (Å, °) for [Zn(bipy)(HT)](**5**)

D—H···*A*	*D*—H	H···*A*	*D*···*A*	*D*—H···*A*
O2—H2···O1^{i}	0.84	1.85	2.625 (5)	153
N3—H32···N2^{ii}	0.88	2.15	2.936 (7)	148

Symmetry codes: (i)− *x*, *y*−1/2, − *z*+3/2; (ii)− *x*+1, *y*+1/2, − *z*+3/2. Hydrogen atoms are placed at calculated positions.

2.3.2.4 Crystal structures of [Zn(bipy)(HP)].2H_2O (**8**)

Complex **8** crystallized into a orthorhombic lattice with space group symmetry *Pbca*. The perspective view of the complex with numbering scheme is shown in Fig. 2.14. Selected bond lengths and angles are presented in Table 2.9.

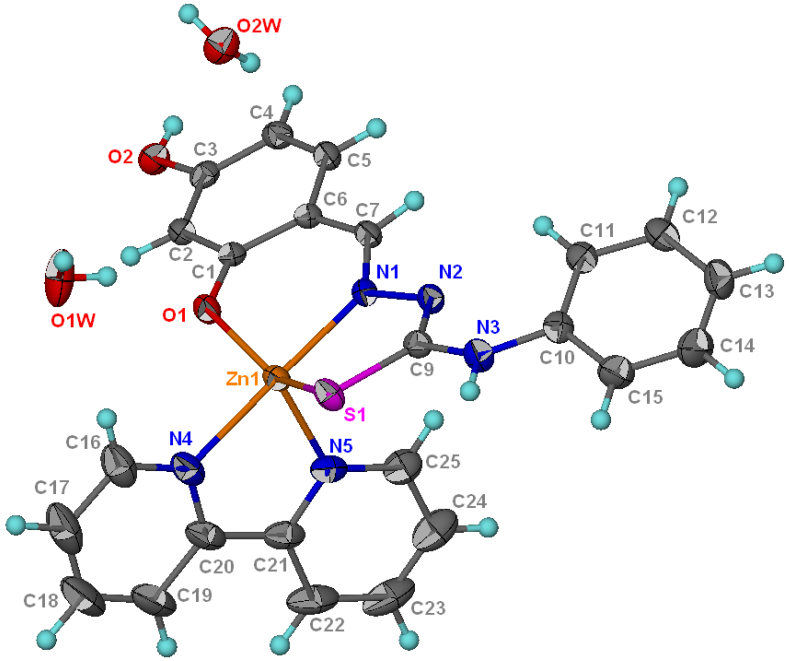

Fig. 2.14 Thermal ellipsoid (Barbour, 2001) plot of **8** drawn at the 70% probability level. Hydrogen atoms are drawn as spheres of arbitrary radii.

The complex is mononuclear and five coordinated with the doubly deprotonated thiosemicarbazone as a tridentate ligand coordinating through the phenolic oxygen, azomethine nitrogen and thiolate sulfur while 2,2'-bipyridine as the *N*,*N*'-bidentate ligand. The trigonality index τ of 0.57 for **8** indicates that the coordination geometry around zinc is intermediate between trigonal bipyramidal and square pyramidal geometries and is better described as trigonal bipyramidal distorted square based pyramid (TBDSBP). This value is similar to the value reported by Seena and Kurup (2008) for [Zn(bipy)L] where L =

salicylaldehyde 4-phenylthiosemicarbazone. Higher distortion from square pyramidal geometry is observed for complex **8** in contrast to complex **5** where the N(4) proton is unsubstituted. Higher distortion towards trigonal bipyramidal geometry for complex **8** may be due to the presence of a bulkier phenyl group at the N(4) position. The repulsion between the ligands are reduced in a trigonal bipyramidal geometry in contrast to square pyramidal.

The deviation from an ideal stereochemistry may due to the restricted bite angle imposed by both the thiosemicarbazone and bipy ligands (Seena and Kurup, 2008). The bite angle around the metal for 2,2'-bipyridine of 78.19(6)˚ may be considered larger when compared with an average value of 77˚ reported in the literature for zinc complexes with 2,2'-bipyridine (Chang and Janiak, 2001; Seena and Kurup, 2008). Zn $-N_{azomethine}$ bond length of 2.0535(14) Å is shorter than the Zn-N_{bipy} bond lengths of 2.1220(15) and 2.0954(15) Å. This indicate that the azomethine nitrogen is coordinated more strongly to zinc compared to the bipyridine nitrogen and the thiosemicarbazone moiety dominates equatorial bonding. The imine bond formation is evidenced from N1-C7 and N2-C9 distances of 1.290(2) Å and 1.306(2) Å. The C-N bond length of 1.306(2) Å and C-S bond length of 1.7500(17) is similar to those reported for coordination of thiosemicarbazone in the thiolate form (Seena and Kurup, 2008; Demirci, 2008).

Hydrogen bonding interactions for complex **8** is shown in Fig. 2.15 and 2.16. Hydrogen bonding parameters are shown in Table 2.10.

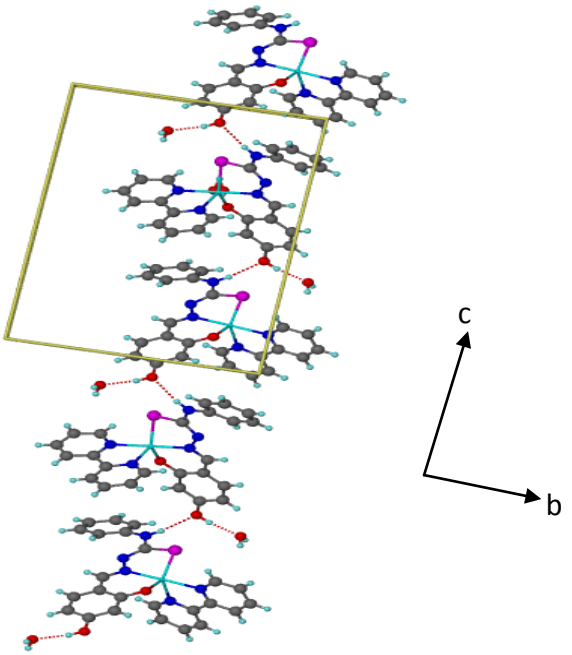

Fig. 2.15 Zig-zag chain formed from N3-H3---O2 hydrogen bonding interactions for complex **8**

The mononuclear complexes form a zig-zag chain through N3-H3---O2 hydrogen bonding as shown in Fig. 2.15 due to the presence of uncoordinated hydroxyl group. The water molecules in the crystal lattice play an important role in the crystal packing. In addition to the direct intermolecular hydrogen bonding (N3-H3---O2) between the mononuclear complexes, water molecules in the crystal lattice help to bridge the adjacent mononuclear complexes into a three-dimensional network through a series of complex hydrogen bonding interactions (O2—H2···O2w, O1w—H11···O1, O2w—H21···N2^{i} and O2w—H22···O1w^{ii}) as shown in Fig. 2.16. These observations underscore the important role played by the uncoordinated hydroxyl group in hydrogen bonding interactions which is not observed in metal complexes derived from salicyaldehyde N(4)-substituted thiosemicarbazone (Latheef *et al*. 2007 & 2008; Seena and Kurup, 2007 & 2008).

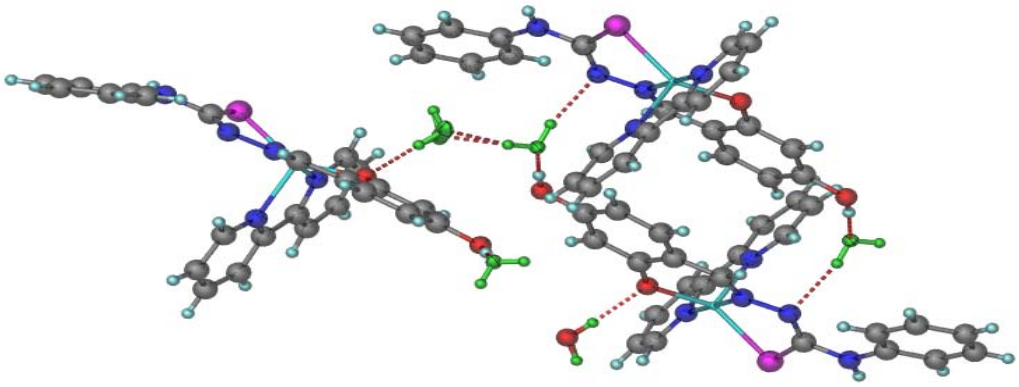

Fig. 2.16 Water molecules (green) bridging the adjacent mononuclear complexes into a three-dimensional network through hydrogen bonding.

The packing of the molecules is shown in Fig. 2.17. The molecules in the crystal lattice are stabilized by combination of hydrogen bonding and π-π interactions between aromatic rings. The expected offset or slipped stacking interactions were observed because of no substantial overlap of aromatic surface area. π stacking becomes favorable with increase in ring numbers (Janiak 2000).

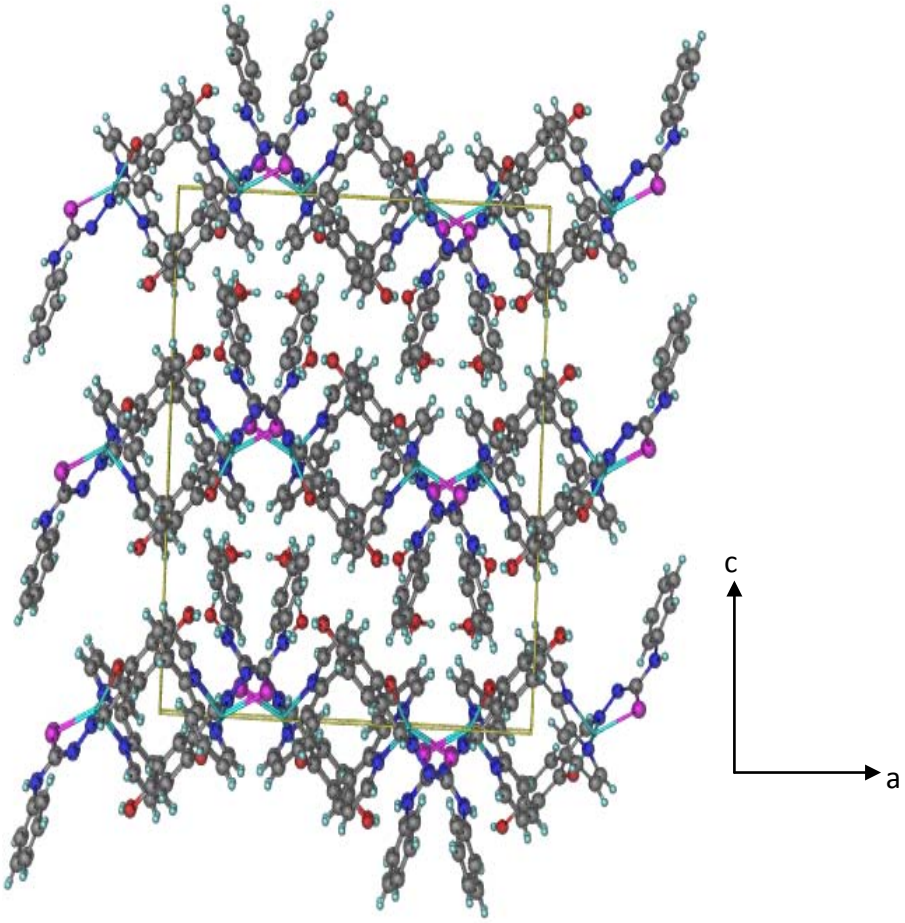

Fig. 2.17 Unit cell packing diagram of **8** view along b axis.

Table 2.9

Selected bond lengths (Å) and angles (˚) for [Zn(bipy)(HP)].2H_2O (**8**)

Bond lengths		Bond angles	
Zn1—O1	2.0069 (12)	O1—Zn1—N1	89.21 (5)
Zn1—N1	2.0535 (14)	O1—Zn1—N5	109.88 (6)
Zn1—N5	2.0954 (15)	N1—Zn1—N5	100.24 (6)
Zn1—N4	2.1220 (15)	O1—Zn1—N4	91.39 (5)
Zn1—S1	2.3657 (5)	N1—Zn1—N4	178.43 (6)
S1—C9	1.7500 (17)	N5—Zn1—N4	78.19 (6)
O1—C1	1.327 (2)	O1—Zn1—S1	144.46 (4)
O2—C3	1.364 (2)	N1—Zn1—S1	82.23 (4)
N1—C7	1.290 (2)	N5—Zn1—S1	105.58 (4)
N1—N2	1.3951 (19)	N4—Zn1—S1	98.10 (4)
N2—C9	1.306 (2)	C9—S1—Zn1	92.65 (6)
N3—C9	1.367 (2)	C1—O1—Zn1	126.12 (10)
N3—C10	1.408 (2)		
N4—C16	1.332 (3)		
N4—C20	1.350 (3)		
N5—C25	1.338 (3)		

Table 2.10

Hydrogen-bond geometry (Å, °) for [Zn(bipy)(HP)].$2H_2O$ (**8**)

D—H···*A*	*D*—H	H···*A*	*D*···*A*	*D*—H···*A*
O2—H2···O2w	0.84 (1)	1.84 (1)	2.66 (1)	172 (2)
O1w—H11···O1	0.84 (1)	1.91 (1)	2.72 (1)	161 (3)
O2w—H21···N2^{i}	0.84 (1)	2.15 (1)	2.94 (1)	159 (3)
O2w—H22···O1w^{ii}	0.83 (1)	1.88 (2)	2.70 (1)	172 (3)
N3—H3···O2^{iii}	0.87 (1)	2.19 (1)	3.04 (1)	171 (2)

Symmetry codes: (i) −*x*+1, −*y*+2, −*z*+1; (ii) −*x*+1, *y*+1/2, −*z*+3/2; (iii) *x*+1/2, −*y*+3/2, −*z*+1.

2.3.3 Infrared and electronic spectra

Important IR bands for the ligands and complexes are given in Table 2.11. IR spectra for all the ligands are shown in Fig. 2.18 while the spectra for the complexes are shown in Fig. 2.19.

The bands in the region of 3100-3500 cm^{-1} are quite difficult to assign in polyhydroxybenzaldehyde thiosemicarbazones due to the presence of complex inter and intra molecular hydrogen bonds between the amino and hydroxyl groups from ligands and solvents. Tentative assignments of bands in this region are assigned base on comparison with spectra of all the starting material and reference from literature. The bands from 3331-3478 cm^{-1} are assigned to ν(O-H) of the free ligands (West *et al.* 1993). Meanwhile, the bands from 3248-3342 cm^{-1} are assigned to ν(N(4)-H) (Lobana *et al.* 2008).

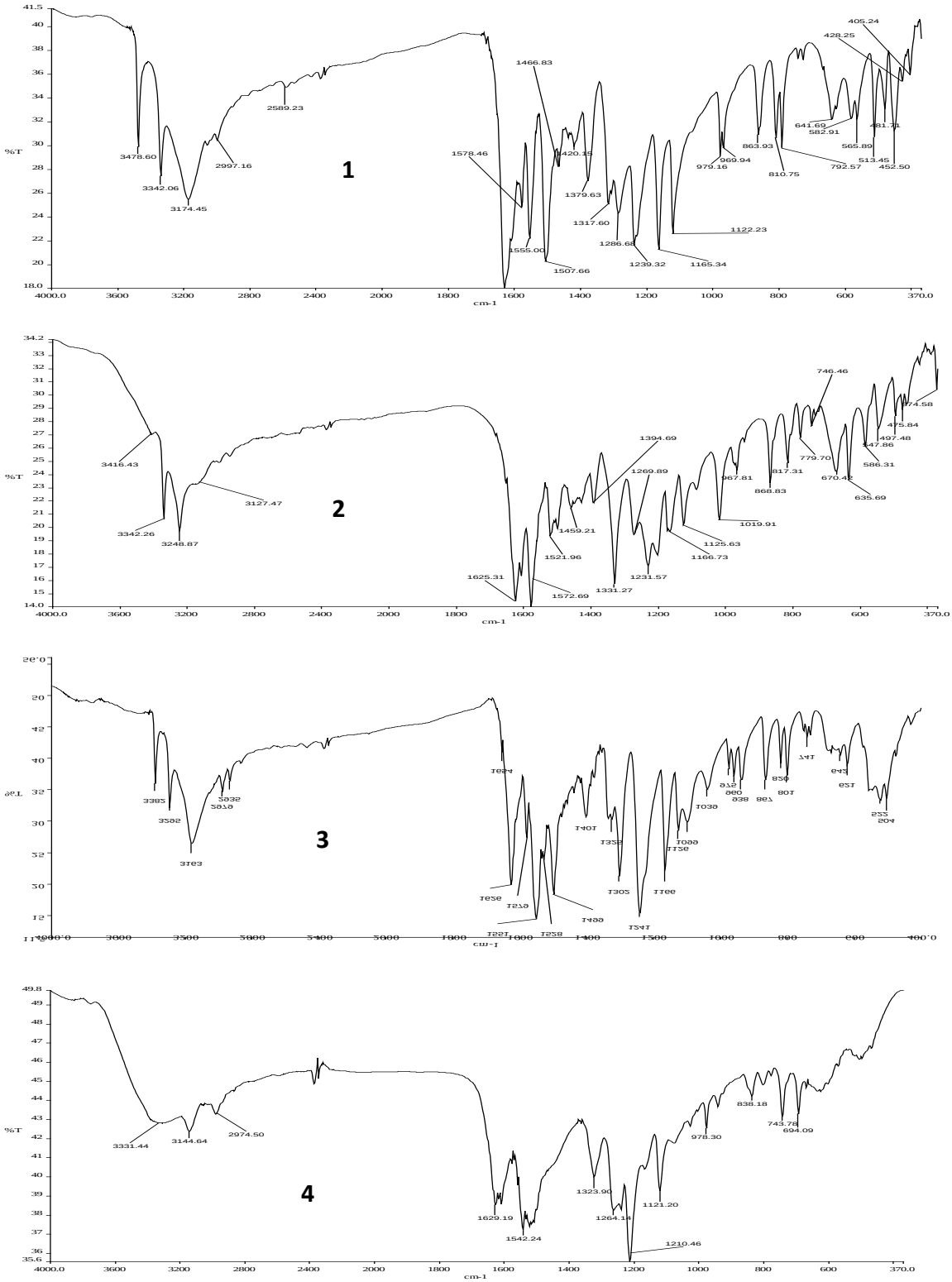

Fig. 2.18 IR spectra for the ligands

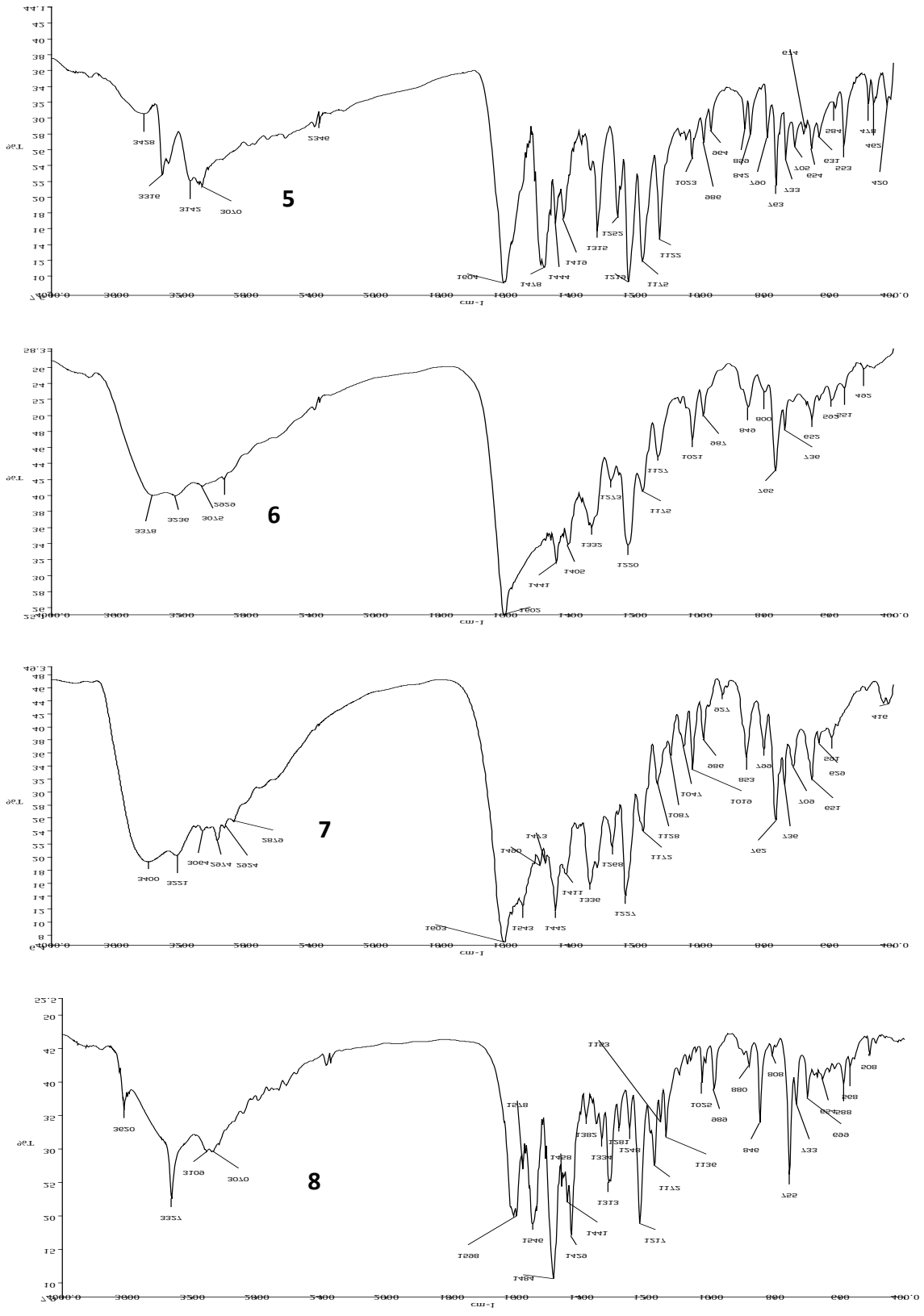

Fig. 2.19 IR spectra of all the complexes

The bands at around 3127-3174 cm^{-1} are assigned to ν(N(2)-H) (Latheef *et al.* 2007; Lobana *et al.* 2008). Thiosemicarbazones are known to exhibit thione-thiol tautomerization (Fig 3). The absence of any band around 2600-2800 cm^{-1} ν(S-H) indicates that in the solid form, all the ligands exist in the thione form (Bindu *et al.* 1999; Afrasiabi *et al.* 2005).

In contrast to complexes of salicylaldehyde thiosemicarbazone, the bands around 3380 cm^{-1} due to ν(O-H) are still seen in the spectra of all the complexes indicating that only one of the phenolic oxygen atoms from each thiosemicarbazone ligand is deprotonated and involved in coordination. The disappearance of the ν(N(2)-H) band in the spectra of all the complexes indicates the deprotonation of the hydrazinic proton which is in accordance with coordination of the sulfur atom in the thiolate form (West *et al.* 1993; Latheef *et al.* 2007 & 2008; Seena and Kurup, 2007 & 2008; Lobana *et al.* 2008).

Coordination of the azomethine nitrogen is confirmed by the shift of ν(C=N) from 1620-1629 cm^{-1} to 1598-1604 cm^{-1}. Evidence of coordination of the thiolate sulfur is further supported the decrease in frequency of the thioamide band found at around 1323-1379 cm^{-1} and 838-868 cm^{-1} to 1273-1316 and 799-849 respectively as reported by Campbell (1975). The bands from 1231-1264 cm^{-1} due to ν(C-O) decrease by 20-40 cm^{-1} upon coordination. This confirms the coordination of the phenolic oxygen to zinc (Latheef *et al.*, 2007; Seena and Kurup, 2008). The decrease in frequency of all these bands is due to the decrease in electron density upon complexation to metal. The decrease in electron density led to the weakening of the bond between carbon and nitrogen or oxygen.

The ν(N-N) band of the thiosemicarbazones is found at 1121-1166 cm^{-1}. The increase in the frequency of this band upon complexation is due to the increase in the double bond character off-setting the loss of electron density via donation to the metal and is a confirmation of the coordination of the ligand through the azomethine nitrogen atom (Latheef *et al.* 2007). The appearance of new ν(Zn-N) bands in the range of 420-450 cm^{-1} confirms the coordination through azomethine and polypyridyl nitrogens. Coordination through phenolic oxygen is confirmed by the presence of a new ν(Zn-O) band in the spectra of the complexes at 551-591 cm^{-1} (Latheef *et al.* 2007; Seena and Kurup, 2008). The mode of coordination for the ligands and complexes determined by IR spectra is in good agreement with the crystal structures of complexes **5** and **8**. Complexes **5-8** have very similar IR spectra (Fig. 2.19), this indicates that they share the similar mode of coordination. Since all the ligands have the same ligating atoms and the only variation in the structure of these complex is at the N(4)-substituent which is not involved in coordination to zinc, it is reasonable to propose that the coordination geometry around zinc for complexes **6** and **7** is intermediate between trigonal bipyramidal and square pyramidal geometries and is better described as trigonal bipyramidal distorted square based pyramid (TBDSBP).

Electronic spectral assignments for the ligands and their zinc(II) complexes in DMF are presented in Table 2.12. All the ligands and the Zn(II) complexes have a ring (phenolic and diimine) π-π^* band at around 37,593 cm^{-1} (West *et al.* 1995). No significant red shift is observed for these bands upon complexation (Swearingan and West, 2000). All the free thiosemicarbazones also have two bands at around 32,985 cm^{-1} and 29,411 cm^{-1} due to n-π^* transition of azomethine and thioamide function respectively.

Upon complexation, the n-π* band of the thioamide function is shifted above 30,000 cm^{-1} due to thioenolization and merges with the azomethine n-π* band at around 31,348 cm^{-1} (Swearingan and West, 2000). Thioenolization causes the weakening of the C=S bond attributed to the loss in double bond character. A moderately intense band in the range 26,455-27,473 cm^{-1}, found only in the spectra of the complexes, is assigned to Zn(II)→S metal to ligand charge transfer band (MLCT) (Latheef *et al.* 2007; Swearingan and West, 2000). The MLCT band for Zn(II)→O shows line broadening that runs into the visible part of the spectrum. However, the maxima of this band is not observed probably due to the overlapping with the low energy side of Zn(II)→S transitions (Latheef *et al.* 2007; Seena and Kurup, 2008). The absence of bands below 22,000 cm^{-1} due to d-d transitions is in accordance with the d^{10} electron configuration of Zn(II) ion (Latheef *et al.* 2007; Seena and Kurup, 2008).

Table 2.11

IR spectral assignments for the ligands and their zinc(II) complexes

Compound	ν(C=N)	ν(C-O)	ν(N-N)	ν (C=S)/ ν (C-S)	ν(Zn-O)	ν(Zn-N)	Bands due to bipyridine
H_3T **(1)**	1620	1239	1165	1379, 863	-	-	-
H_3M **(2)**	1625	1231	1166	1331,868	-	-	-
H_3E **(3)**	1626	1241	1166	1325, 867	-	-	-
H_3P **(4)**	1629	1264	1121	1323,838	-	-	-
[Zn(bipy)(HT)] **(5)**	1604	1219	1175	1315, 842	553	420	1419, 763
[Zn(bipy)(HM)].$3H_2O$ **(6)**	1602	1220	1175	1273, 849	551	450	1441, 765
[Zn(bipy)(HE)].$3H_2O$ **(7)**	1603	1227	1172	1316, 799	591	421	1442, 762
[Zn(bipy)(HP)].$2H_2O$ **(8)**	1598	1217	1172	1313, 846	568	450	1429, 755

Table 2.12

Electronic spectral assignments (cm^{-1}) for the ligands and their zinc(II) complexes in DMF .

Compound	π-π^*	n-π*	MLCT
H_3T (**1**)	37593	33003, 29411	
H_3M (**2**)	37593	33003, 29411	
H_3E (**3**)	37593	32895, 29240	
H_3P (**4**)	37453	32680, 28409	
[Zn(bipy)(HT)] **(5)**	37736	31250	27473
[Zn(bipy)(HM)].$3H_2O$ **(6)**	37736	31447	27027
[Zn(bipy)(HE)].$3H_2O$ **(7)**	37736	31348	27248
[Zn(bipy)(HP)].$2H_2O$ **(8)**	37593	31152	26455

2.3.4 ^{1}H and ^{13}C NMR spectra

^{1}H NMR spectral assignments for the ligands and their zinc(II) complexes in DMSO are presented in Table 2.13. All the thiosemicarbazones ligands have a sharp signal in the region of 11.14-11.79 ppm that integrates to one proton which is assigned to N(2)H. The downfield position of these protons are due to the presence of inter and intra hydrogen bonding interactions. The presence of hydrogen bonds decrease the electron density about N(2) protons and hence move the absorption down field (Ackerman *et al,* 1999). In the spectra of the thiosemicarbazones**,** the signals for the phenolic protons are found at 9.74-9.93 ppm **(**Dilović *et al.* 2008**).** These signals are broad and integrate to 2 protons in accordance to the presence of two phenolic groups in dihydroxybenzaldehyde thiosemicarbazones. Meanwhile, the azomethine protons of all the ligands are found as a sharp singlet at 8.20-8.34 ppm due to the absence of any neighboring protons. The absence of signals at around 4 ppm, due to the –SH (thiol) group, indicates that all the ligands exist

in the thione form. The signal for N(4)H appears in the region of 7.65-8.72 ppm and the value is highly dependent on the substituent groups. Compound **4** has the highest chemical shift for the N(4)H signal due to the presence of an electron withdrawing phenyl group. The N(4)H signal for other ligands appear slightly upfield due to the presence of electron donating alkyl groups. It is noteworthy that the N(4)H protons for compounds **2** and **3** exist as a doublet with a coupling constant J = 4 Hz due to the $^{3}J_{H\text{-}H}$ splitting by the alkyl group attached to the N(4) atom. This sort of coupling through a nitrogen bond is seldom seen due to N-H exchange or quadrupole broadening (Ackerman *et al*. 1999). The aromatic protons for all the ligands are found in the region of 6.22-7.82 ppm. The aromatic protons of the hydroxyl substituted ring appears slightly upfield because the presence of the hydroxyl group decreases the electron density in the aromatic ring leading to the decrease in ring current and strength of the induced field. This causes the aromatic protons to be less deshielded and absorb at a higher field (McMurry 1999).

The absence of the N(2)H peak in the spectra of all the complexes indicates the deprotonation of the hydrazinic proton and supports the coordination of sulfur in the thiolate form. The integration for phenolic protons decreases from two to one upon complexation suggesting deprotonation of one of the phenolic group and coordination of the oxygen atom to zinc. However, the phenolic proton signals for complexes **6** and **7** are not observed due to –OH exchange with the solvent. Coordination of the azomethine nitrogen is confirmed by the shifting of the -CH=N signal from 8.20-8.34 ppm in the free ligands to 8.18-8.27 ppm in the spectra of the complexes. Even though the -CH=N signal normally shifts downfield upon complexation, irregularities in this trend is not uncommon

(Lobana *et al.*, 2009). The –CH=N and N(4)H signals for complex **8** are resolved due to overlapping with the bipyridine protons signals at around 8.64-8.40 ppm. The aromatic protons on the dihydroxybenzaldehyde moiety also shifted slightly upfield upon coordination due to the decrease in electron density. Unlike aliphatic protons, aromatic protons tend to shift upfield with the decrease in electron density because the decrease in strength of the induced field, which is proportional to electron density, will cause the protons to be less deshielded. The formation of ternary complexes is shown by the presence of four signals with different multiplicity in the region of 7.48-8.62 ppm ascribed to the coordinated 2,2'-bipyridine ligand. The presence of the bipyridine moiety is also supported by elemental analyses, IR spectroscopy and confirmed by the crystal structures of complexes **5** and **8**.

Table 2.13

^{1}H NMR spectral assignments for the thiosemicarbazone ligands and their zinc(II) complexes in DMSO

Compound	Chemical shifts, δ (ppm)					
	N(2)H	OH	N(4)H	CH=N	Aromatic	Aliphatic
H_3T **(1)**	11.14 (s, 1 H)	9.74 (s, 2 H)	7.92 (s, 1 H)	8.20 (s, 1 H)	7.62 (d, 1 H)	-
			7.65 (s, 1 H)		6.25 (s, 1 H)	
					6.22 (d, 1 H)	
H_3M **(2)**	11.79 (s, 1 H)	9.88 (s, 1 H)	8.24 (t, 1 H)	8.20 (s, 1 H)	7.67 (d, 1 H)	2.95 (d, 3 H)
		9.74 (s, 1 H)			6.26 (s, 1 H)	N-C**H$_3$**
					6.24 (d, 1 H)	
H_3E **(3)**	11.16 (s, 1 H)	9.76 (s, 2 H)	8.31 (t, 1 H)	8.26 (s, 1 H)	7.72 (d, 1 H)	3.57 (m, 2H) NC**H$_2$**
					6.32 (s, 1 H)	
					6.30 (d, 1 H)	1.14 (t, 3H) NCH$_2$C**H$_3$**
H_3P **(4)**	11.54 (s, 1 H)	9.93 (s, 1 H)	8.72 (s, 1 H)	8.34 (s, 1 H)	7.82 (d, 1H)	-

		9.89 (s, 1 H)			7.53 (d, 2H) 7.33 (t, 2H) 7.16 (t, 1H) 6.29 (s, 1H) 6.27 (d, 1H)	
[Zn(bipy)(HT)] **(5)**	-	9.47 (s, 1 H)	6.03 (s, 2 H) overlap with ar-H	8.18 (s, 1 H)	8.62 (d, 2H) 8.42 (d, 2H) 8.00 (d, 2H) 7.48 (d, 2H) 6.93 (s, 1H) 6.30 (s, 1 H) 6.03 (s, 1 H)	

Compound	Chemical shifts, δ (ppm)					
	N(2)H	OH	N(4)H	CH=N	Aromatic	Aliphatic
[Zn(bipy)(HM)].3H_2O **(6)**	-	-	6.41 (s, 1 H)	8.27 (s, 1 H)	8.54 (s, 2H) 8.45 (d, 2H) 8.05 (d, 2H) 7.56 (s, 2H) 6.95 (s, 1H) 6.27 (s, 1 H) 6.02 (s, 1 H)	2.71 (d, 3 H) N-C**H_3**
[Zn(bipy)(HE)].3H_2O **(7)**	-	-	6.25 (d, 1 H)	8.22 (s, 1 H)	8.61 (s, 2H) 8.45 (d, 2H) 8.01 (d, 2H) 7.51 (s, 2H) 6.94 (s, 1H) 6.30 (s, 1 H) 6.02 (s, 1 H)	3.21 (m, 2H) NC**H_2** 1.01 (t, 3H) NCH_2C**H_3**
[Zn(bipy)(HP)].2H_2O **(8)**	-	9.61 (s, 1 H)	-overlap with bipy	-overlap with bipy	8.64 (d, 2 H) 8.41 (d, 2 H) 7.98 (t, 2 H)	-

	7.76 (d, 2 H)
	7.49 (t, 2 H)
	7.15 (t, 2 H)
	7.02 (s, 1 H)
	6.80 (t, 1 H)
	6.38 (d, 1 H)
	5.92 (s, 1 H)

Table 2.13 continued.

^{13}C NMR spectral assignments for the thiosemicarbazones in DMSO are presented in Table 2.14. All ligands show a signal in the region 175.57-177.61 ppm due to C=S. Each ligand shows two signals that correspond to C-O are observed in the region of 158.40-161.21 ppm. The formation of the Schiff base is confirmed by the presence of the azomethine carbon signal (C=N) at around 141 ppm in the spectra of all the ligands. The signals due to aromatic carbons are found at 102.81-139.64 ppm. Compound **3** has an additional peak due to N-**C**H$_3$ at 31.28 ppm while compound **4** has two signals at 15.21 and 32.20 due to NCH$_2$**C**H$_3$ and N**C**H$_2$- respectively. The total numbers of C signals in the spectra of all ligands are in agreements with the proposed structures. The values reported are similar to those in the literature (Bindu *et al.* 1998). None of the complexes were sufficiently soluble in DMSO to record acceptable ^{13}C spectra.

Table 2.14

^{13}C spectral assignments for the thiosemicarbazone ligands in DMSO.

Compound	Chemical shifts, δ (ppm)				
	C=S	C-O	C=N	Aromatic	Aliphatic
H_3T **(1)**	177.40	161.03	140.97	128.49, 112.11	-
		158.56		108.26, 102.80	
H_3M **(2)**	177.61	160.87	140.54	128.67, 112.45	31.28 (N-**C**H_3).
		158.40		108.19, 102.80	
H_3E **(3)**	176.34	160.84	140.99	128.88, 112.34	32.20 (N-**C**H_2-)
		158.40		108.32, 102.81	15.21 (NCH_2**C**$\mathbf{H_3}$)
H_3P **(4)**	175.57	161.21	141.73	139.64, 129.25	-
		158.75		126.06, 125.66	
				112.23, 108.38	
				102.84	

2.3.5 DNA binding

2.3.5.1 Duplex DNA

The interaction of the complexes with (i) duplex oligonucleotides of various specified nucleotide sequences, and (ii) quadruplex DNA of the 23-mer oligonucleotide 5'-$AG_3(T_2AG_3)_3$-3' and its corresponding duplex were investigated with CD spectroscopy. CD spectroscopy is a technique that is widely used in diagnosing changes in DNA morphology during drug–DNA interactions. This is due to the extreme sensitivity of CD in detecting changes in the conformations of DNA (Ivanov *et al*. 1973). In addition, this method is also easier, faster and relatively inexpensive compared to X-ray diffraction of crystal and NMR spectroscopy (Kypr *et al.*, 2009).

The CD spectra of all the duplex oligonucleotides show a negative band at ~250 nm due to DNA with right-handed helicity and a positive band at ~275 nm due to base-pair stacking interaction, confirming the B-form conformation of these duplexes (Table 2.15). These bands are very useful in studying small molecules interaction with DNA because simple groove binding and electrostatic interaction of small molecules show less or no perturbation on the base-stacking and helicity bands, while intercalation enhances the intensities of both bands due to stabilization of the right-handed B conformation of DNA (Maheswari and Palaniandavar, 2004).

The first investigation was to find out the DNA binding preference for CG or AT sequences by the zinc complex. Complex **5** at a complex:duplex ratio of 1:8 slightly decreases the positive (6.7%) and negative (7.2%) band of the $ds(AT)_6$ (Fig. 2.20). This suggests that binding of the complex causes a change of conformation from B to Z-like, similar to those observed in interaction of $[Cu(5,6\text{-dmp})_2]^{2+}$ with calf thymus DNA (Mahadevan and Palaniandavar, 1996). Complex **5** does not induce a significant change to the positive band (< 2%) in the CD spectrum of the $ds(CG)_6$, suggesting a retention of the B-form conformation (Fig. 2.20). This implies that complex **5** can differentiate $ds(AT)_6$ from $ds(CG)_6$ and induced different conformation change to the duplex DNA upon binding.

Interestingly, complex **6** with a methyl substituent at N(4) induced the greatest decrease (17.1%) in the negative band (helicity) of the CD spectrum of $ds(CG)_6$ (Fig. 2.21) in contrast to complexes **5**, **7** and **8**. This indicates that the binding of the

complex **6** causes the DNA to unwind more. Complex **6** also induces the same conformational change to ds$(AT)_6$ similar to complex **5** (B to Z like). However, the changes are less significant when compared to the interaction with ds$(CG)_6$. From the above discussion, complex **6** can thus be used to differentiate ds$(CG)_6$ from ds$(AT)_6$ DNA. The ability of complex **6** to show different mode of binding with AT rich and CG rich sequence of DNA is quite remarkable. Recently, Shelton *et al.* (2007) have synthesized a cationic porphyrin zinc complex, Zn(tMe_2D_4) that shows mode of binding that varies with the base content of a DNA host. This complex remains five-coordinate and binds externally when it encounters AT rich base pair. However, it will lose its axial ligand and binds by intercalation if the host only contains CG base pair. Thus, Zn(tMe_2D_4) is like complex **6**, it can differentiate DNA with AT rich bases from DNA with only CG bases.

The mode of interaction of **7** (Fig. 2.22) and **8** (Fig. 2.23) differs from complex **5**. Complexes **7** and **8** cause a slight increase and decrease in intensity of the positive and negative bands suggesting partial intercalation of the complexes to ds$(AT)_6$. This type of changes in CD has been ascribed to a conformational change from B to ψ, which is similar to those observed in [Zn(phen)edda] (Seng *et al.*, 2008) and $[Ru(NH_3)_4qdppz)]^{2+}$ (Maheswari and Palaniandavar, 2004). No significant changes were observed in the CD spectra of ds$(CG)_6$ upon interaction with complex **7**. On the other hand, complex **8** induces a conformational change from B to ψ for ds$(CG)_6$. It is noteworthy that the N(4) substituent in the thiosemicarbazones plays important role in determining the ability of the complexes in differentiating the duplex DNA base sequences and the types of structural changes to duplex DNA upon drug interaction.

Table 2.15
CD spectral bands of duplex oligo or quadruplex + zinc complex: wavelength, λ (molar ellipcity)

	λ/nm (molar ellipcity)	
	(-) band	(+) band
15 μM ds$(AT)_6$	248 (-419344)	270 (339753)
15 μM ds$(AT)_6$ + 120 μM complex **5**	249 (-387802)	269 (320390)
15 μM ds$(AT)_6$ + 120 μM complex **6**	249 (-392987)	270 (326059)
15 μM ds$(AT)_6$ + 120 μM complex **7**	249 (-401598)	270 (360260)
15 μM ds$(AT)_6$ + 120 μM complex **8**	249 (-374922)	270 (358565)
15 μM ds$(CG)_6$	252 (-585418)	278 (213799)
15 μM ds$(CG)_6$ + 120 μM complex **5**	257 (-573286)	278 (217725)
15 μM ds$(CG)_6$ + 120 μM complex **6**	253 (-482117)	279 (203453)
15 μM ds$(CG)_6$ + 120 μM complex **7**	252 (-602978)	280 (216090)
15 μM ds$(CG)_6$ + 120 μM complex **8**	253 (-582921)	279 (229141)
10 μM ds$(CGCGAATTCGCG)_2$	251 (-603665)	279 (215560)
10 μM ds$(CGCGAATTCGCG)_2$ + 120 μM complex **5**	252 (-577290)	278 (246140)
10 μM ds$(CGCGAATTCGCG)_2$ + 120 μM complex **6**	253 (-558732)	277 (236179)
10 μM ds$(CGCGAATTCGCG)_2$ + 120 μM complex **7**	251 (-520213)	278 (242670)
10 μM ds$(CGCGAATTCGCG)_2$ + 120 μM complex **8**	251 (-562839)	279 (254099)
10 μM ds$(CGCGATATCGCG)_2$	248 (-286559)	277 (174875)
10 μM ds$(CGCGATATCGCG)_2$ + 120 μM complex **5**	248 (-306538)	277 (192374)
10 μM ds$(CGCGATATCGCG)_2$ + 120 μM complex **6**	249 (-258973)	277 (171370)
10 μM ds$(CGCGATATCGCG)_2$ + 120 μM complex **7**	249 (-257970)	277 (195999)
10 μM ds$(CGCGATATCGCG)_2$ + 120 μM complex **8**	249 (-291739)	277 (212751)
20 μM G-duplex	250 (-82682)	279 (283975)
20 μM guanine rich duplex+ 120 μM complex **5**	249 (-36849)	279 (142761)
20 μM guanine rich duplex+ 120 μM complex **6**	250 (-113866)	278 (289906)
20 μM guanine rich duplex+ 120 μM complex **7**	250 (-94748)	279 (254455)
20 μM guanine rich duplex+ 120 μM complex **8**	250 (-121369)	279 (319436)
20 μM G-quadruplex	266 (-116489)	247 (106239) 296 (180571)
20 μM G-quadruplex + complex **5**	266 (-91462)	247 (121896) 296 (212408)
20 μM G-quadruplex + complex **6**	264 (-104679)	249 (122276) 296 (217413)
20 μM G-quadruplex + complex **7**	264 (-116932)	246 (115484) 296 (213537)
20 μM G-quadruplex + complex **8**	267 (-109694)	246 (123178)

	296 (192358)
guanine rich duplex =(5’-CCAGTTCGTAGTAGTAACCC-3’)·(3'-GGTCAAGCATCATCATTGGG-5’)	

Table 2.15 continued.

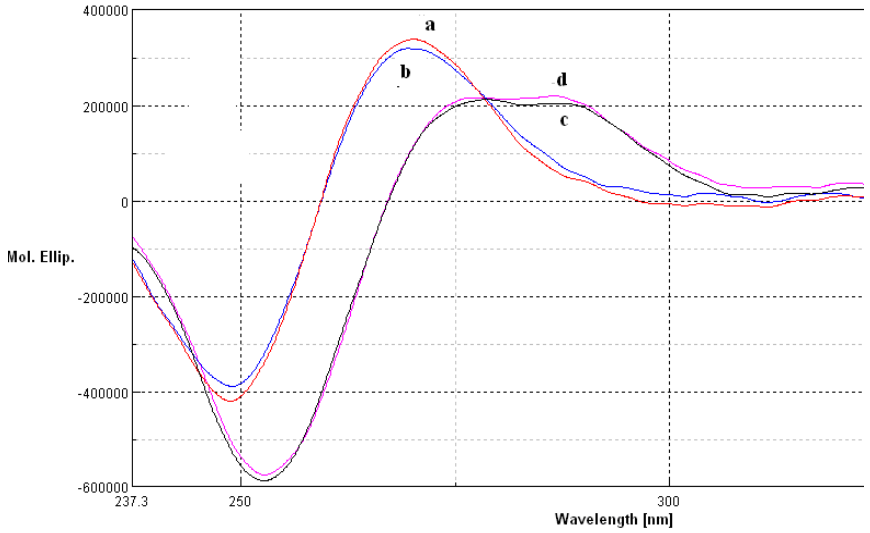

Fig. 2.20 CD spectra of 15 µM of oligonucleotide in the absence and presence of 120 µM of complex **5**; (a) ds$(AT)_6$ alone, (b) ds$(AT)_6$ with complex **5,** (c) ds$(CG)_6$ alone and (d) ds$(CG)_6$ with complex **5.**

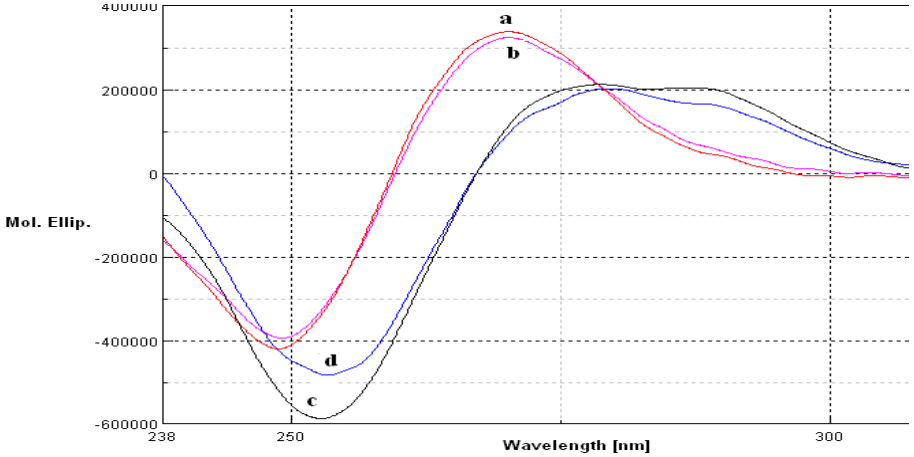

Fig. 2.21 CD spectra of 15 µM of oligonucleotide in the absence and presence of 120 µM of complex **6**; (a) ds$(AT)_6$ alone, (b) ds$(AT)_6$ with complex **6,** (c) ds$(CG)_6$ alone and (d) ds$(CG)_6$ with complex **6**

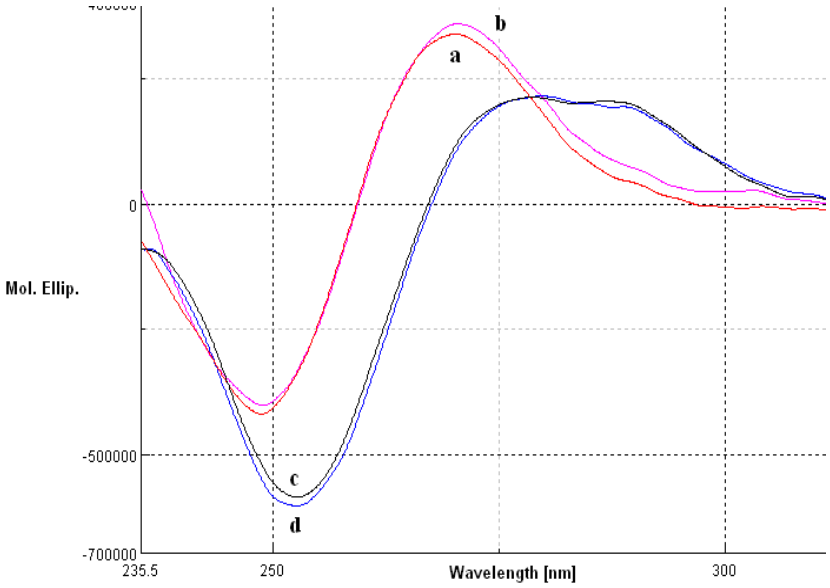

Fig. 2.22 CD spectra of 15 µM of oligonucleotide in the absence and presence of 120 µM of complex **7**; (a) ds(AT)$_6$ alone, (b) ds(AT)$_6$ with complex **7,** (c) ds(CG)$_6$ alone and (d) ds(CG)$_6$ with complex **7**

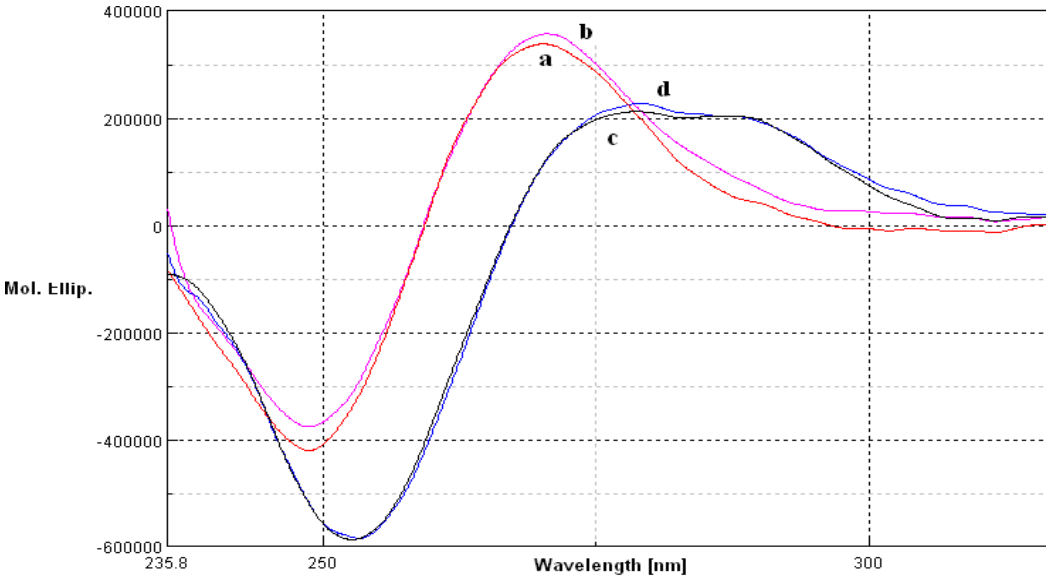

Fig. 2.23 CD spectra of 15 µM of oligonucleotide in the absence and presence of 120 µM of complex **8**; (a) ds(AT)$_6$ alone, (b) ds(AT)$_6$ with complex **8,** (c) ds(CG)$_6$ alone and (d) ds(CG)$_6$ with complex **8.**

The pair of oligonucleotides ds(CGCGAATTCGCG)$_2$ and ds(CGCGATATCGCG)$_2$ were used to investigate any binding preferences in interaction with duplex DNA as the central sequence on each chain is varied from non-alternating to alternating purine-pyrimidine bases in the grooves of the duplex. For the AATT sequence (Fig. 2.24-2.27), complexes **5-8** cause a respective increase and decrease in the positive and negative band of the CD spectra of the duplex which suggests partial intercalation of each complex to the duplex. This observation also correspond to conformational change from B to ψ, as mentioned earlier (Maheswari and Palaniandavar, 2004; Seng *et al*. 2008).

Unlike binding to DNA, with a central AATT sequence, complexes **5-8** induce a wider variety of changes to the conformation of the duplex with ATAT sequence. Complex **5** for example, causes a slight increase in both the positive and negative bands of the duplex indicating intercalation to the duplex base pair (Maheswari and Palaniandavar, 2004). For the same DNA with ATAT sequence, only complex **6** causes a decrease in the negative band with no significant changes to the positive band. This observation is similar for the interaction of complex **6** with ds(CG)$_6$ (Fig. 2.21). This observation has been ascribed to the ability of complex **6** to differentiate ds(CG) form ds(AT)$_6$. This may imply that complex **6** retains its ability in recognizing the CG sequence and bind to the CG sequence in ds(CGCGATATCGCG)$_2$ instead of the AT sequence therefore inducing similar conformational changes to the DNA. On the other hand, complex **7** induces a conformational change from B to ψ for interaction with ATAT sequence similar to its interaction with the AATT sequence. Complex **8** causes an increase in both the positive

and negative bands of the duplex with ATAT sequence suggesting the intercalation of the N(4) phenyl group in between the nucleobase pair.

Comparing the CD results of these four ds(oligos)$_2$, we can conclude that complexes **5**-**8** can bind to all the duplexes investigated in this study. In the absence of additional information such as binding constant attributed to solubility problem of these complexes, it is difficult to make conclusions about the selectivity of the complexes towards different DNA base sequences. However, the diverse changes in conformation, helicity or base stacking of DNA upon interaction with the complexes suggest that some of the complexes can differentiate DNA with different base sequences. Since electrostatic interaction is not likely because these complexes are neutral, the binding modes most likely involve a combination of partial intercalation, hydrogen bonding and groove binding that varies with complex and base sequences. Intercalation will result in an increase in the positive band of the CD spectra ascribed to base stacking. Changes in the conformation of the DNA that resulted in decrease of the positive band in the CD spectra most likely involve hydrogen bonding or groove binding. We postulate that the observed DNA recognition is conferred by the ability of the complexes to form hydrogen bonds with the DNA through various hydrogen donor and acceptor groups on the thiosemicarbazone moiety. The ability of the complexes in forming hydrogen bonds can be seen from the crystal structure of the ligands and complexes. The N(4)-substituent seems to be responsible in DNA recognition through hydrophobic interaction or groove binding because each complex has a substituent with different hydrophobicity and bulkiness (alkyl chain or aromatic ring). The size of the

molecules and the orientation of different substituted bulky group in space may affect their ability to bind into the groove (major or minor) with different cavity size or steric hindrance.

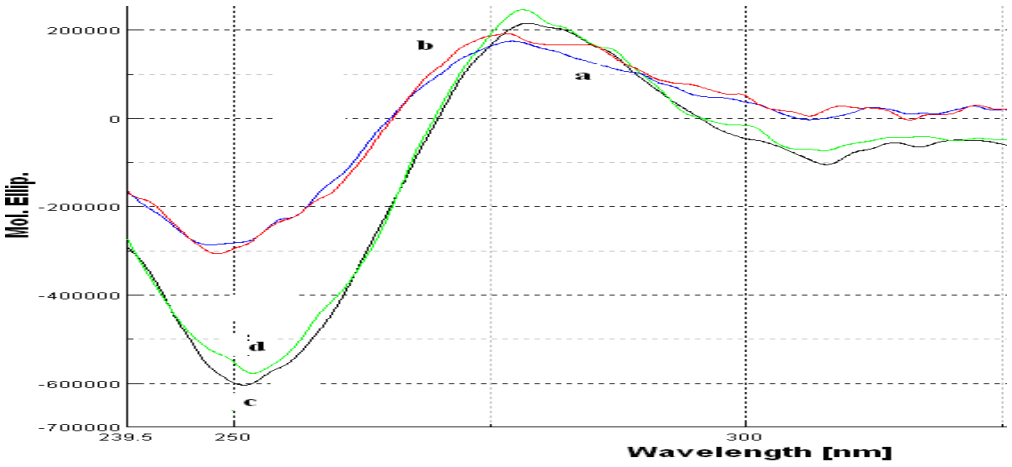

Fig. 2.24 CD spectra of 10 µM of oligonucleotides in the absence and presence of 120 µM of complex **5**; (a) ds(CGCGATATCGCG)$_2$ alone, (b) ds(CGCGATATCGCG)$_2$ with complex **5,** (c) ds(CGCGAATTCGCG)$_2$ alone and (d) ds(CGCGAATTCGCG)$_2$ with complex **5.**

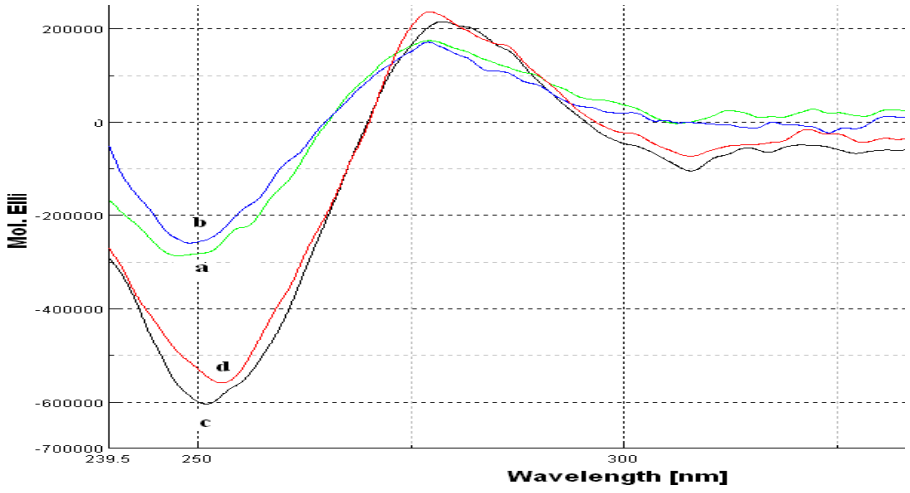

Fig. 2.25 CD spectra of 10 µM of oligonucleotides in the absence and presence of 120 µM of complex **6**; (a) ds(CGCGATATCGCG)$_2$ alone, (b) ds(CGCGATATCGCG)$_2$ with complex **6,** (c) ds(CGCGAATTCGCG)$_2$ alone and (d) ds(CGCGAATTCGCG)$_2$ with complex **6.**

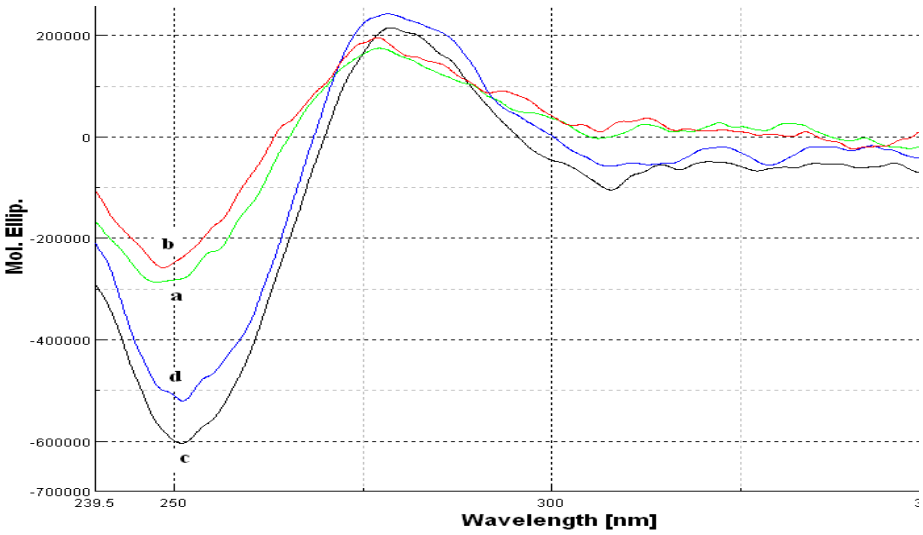

Fig. 2.26 CD spectra of 10 µM of oligonucleotides in the absence and presence of 120 µM of complex **7**; (a) ds(CGCGATATCGCG)$_2$ alone, (b) ds(CGCGATATCGCG)$_2$ with complex **7,** (c) ds(CGCGAATTCGCG)$_2$ alone and (d) ds(CGCGAATTCGCG)$_2$ with complex **7.**

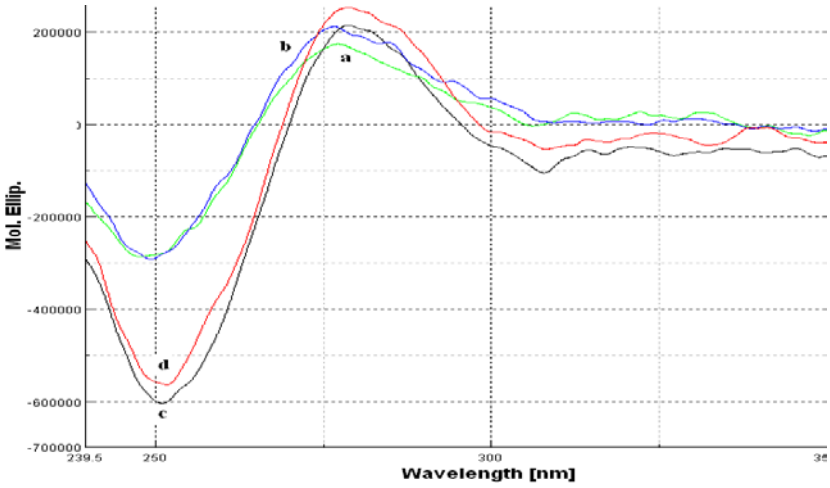

Fig. 2.27 CD spectra of 10 µM of oligonucleotides in the absence and presence of 120 µM of complex **8**; (a) ds(CGCGATATCGCG)$_2$ alone, (b) ds(CGCGATATCGCG)$_2$ with complex **8,** (c) ds(CGCGAATTCGCG)$_2$ alone and (d) ds(CGCGAATTCGCG)$_2$ with complex **8**.

2.3.5.2 G-quadruplex and guanine-rich duplex

Next, we examine the interaction of the complexes with a non-B form DNA structure. Guanine rich regions of DNA such as human telomeric DNA can be folded into higher-order DNA structure known as G-quadruplex under physiological ionic conditions (Burge *et al.* 2006). Recently, there is growing interest in compounds that can induce or stabilize quadruplex structure (Reed *et al.* 2009; Pierce *et al.* 2009; Arola and Vilar, 2008; Arola *et al.* 2008) due to the discovery that these compounds can lead to inhibition of telomerase (Neidle and Parkinson, 2002). The telomerase is a nucleoprotein that catalyzes the elongation of telomere and plays a key role in bestowing immortality to cancer cells. The telomerase is a promising target for anticancer agent because it is over expressed in 80-85% of cancer cells but not in normal somatic cells (Kim *et al.* 1994). Since the substrate of telomerase is the 3'-single-stranded overhang of telomeric DNA, the stabilisation of quadruplex DNA structures by small molecules can lead to telomerase inhibition (Reed *et al.* 2007; Neidle and Parkinson, 2002).

Therefore, we used CD spectroscopy to investigate the interaction of the zinc complexes with the single strand G-quadruplex DNA annealed from human telomeric sequence 5'-$AG_3(T_2AG_3)_3$-3' and with the duplex DNA annealed from two complementary 17 bp primers, 5'-CCAGTTCGTAGTAACCC-3' and 3'-GGTCAAGCATCATTGGG-5' to evaluate the ability of these complexes in stabilizing G-quadruplex and differentiating the guanine rich duplex structure. Single stranded quadruplexes with parallel structure has been determined by X-ray crystallography (Parkinson *et al.* 2002) whereas antiparallel structure or a mixture of both have been determined by others using NMR (Kypr *et al.* 2009,

Zhang *et al*. 2007; Baker *et al*. 2006). The structure of the quadruplex is highly dependent on the type of ion and ionic strength. Human telomeric sequence d[$G_3(T_2AG_3)_3$] can formed antiparallel quadruplex in the presence of 100 mM Na^+ but formed a hybrid mixture of parallel and antiparallel structures in the presence of K^+ (Burge *et al*. 2006). The CD spectrum of our G-quadruplex alone annealed from 5'-$AG_3(T_2AG_3)_3$-3' oligonucleotides with human telomeric sequence in the presence of Na^+ ions shows two maxima at 295 nm and 246 nm and a minimum at 267 nm (Fig. 2.28, Table 2.15). This spectrum is typical of other reported anti-parallel quadruplexes, *viz*. d$(T_2AG_3)_4$, d$(T_2AG_3)_6$ and d$AG_3(T_2AG_3)_3$ (Baker *et al*. 2006, Burge *et al*. 2006). Thus, our G-quadruplex annealed from 5'-$AG_3(T_2AG_3)_3$-3' oligonucleotides with human telomeric sequence in the presence of 100 mM Na^+ ions should have an antiparallel structure as revealed by NMR earlier (Wang and Patel, 1993). The CD positive band at 297 nm for the antiparallel G-quadruplex has been ascribed to G-G base stacking (Kypr *et al*. 2009; Burge *et al*. 2006)

The CD spectra of the antiparallel G-quadruplex 5'-$AG_3(T_2AG_3)_3$-3' (20 μM) with different complexes (120 μM) were obtained. The intensity of the positive band for G-quadruplex at 296 nm is enhanced while the negative band at 267 nm decreases upon addition of complexes **5**, **6** and **8**. Complex **7** induces an increase in both the positive and negative bands. The overall shape and the two bands position of G-quadruplex remain unchanged, suggesting retention of the antiparallel structure (Fig. 2.28, Table 2.15). The enhancement of the positive band at 296 nm due to G-G base stacking suggests partial intercalation between G-tetrads and stabilization by the zinc complex similar to enhancement of positive, base-base stacking band at ~270 nm attributed to intercalation of

the B-form duplex DNA. This observation is in contrast to those observed for the interaction of acridine and bis-acridine with G-quadruplex where the decrease in the intensity of the positive band at 293 nm was interpreted as destabilization of the quadruplex structure (Nagesh *et al*. 2003). Thus, enhancement of the positive band of the CD spectrum of the present quadruplex suggests stabilization of the antiparallel quadruplex structure by our zinc complexes as suggested by Musseti *et al.* (2009). Musseti *et al.* (2009) have monitored changes in the melting profile of the synthetic oligonucleotide (HTS) in the presence of metal ions and phenanthroline-based G-quadruplex binding ligand. Ligands that bind effectively to G-quadruplex will produce an increase in the melting temperature. An enhanced melting temperature for the oligonucleotide (HTS) in the presence of $(K34)_2Ni(II)$ which is consistent with stabilisation of G-quadruplex is confirmed by the increase in the band intensity (290 nm) of the CD spectra for G-quadruplex . In contrast, CD spectral titration of ruthenium (II) complexes with known intercalating ligands, viz. $[Ru(phen)_2(dpqC)]^{2+}$, $[Ru(phen)_2(dpq)]^{2+}$, $[Ru(phen)_2(dppz)]^{2+}$ and $[Ru(phen)_3]^{2+}$, with four stranded G-quadruplex $(TTGGGGGT)_4$ shows a significant decrease in ellipticity of both CD positive and negative bands with increasing Ru(II)-complex:G-quadruplex ratio (Talib *et al*. 2008). The positive CD band at 265 nm was found to be split into distinct bands at higher concentration of the Ru(II)-complex. These complexes have higher binding affinity towards duplex DNA than towards quadruplex.

The overall enhancement of the positive band at 296 nm in G-quadruplex by the complexes decreases in the following order: **6** > **7** > **5** > **8.** Based on the enhancement in the positive band (Fig. 2.28, Table 2.15) complex **6** is most effective in stabilizing while

complex **8** is the least effective**.** The ability of complex **6** in differentiating the CG sequence from AT in duplex DNA may be responsible in facilitating its binding to guanine rich quadruplex. The absence of cytosine in the quadruplex sequence suggests that the ability of complex **6** in recognizing the CG sequence that we observed earlier maybe related to its ability to recognize guanine. Interestingly, complex **8** shows the lowest enhancement in the positive band for G-quadruplex but the enhancement for this complex is highest when compared to the other complexes for interactions with any duplex sequences. This indicates that the presence of a planar phenyl group on the thiosemicarbazone moiety enhances the ability of the complex to bind to duplex structure through intercalation. However, this feature is unfavourable for interaction with the G-quadruplex which may be due to the greater steric effect conferred by the bulkier phenyl group making it more difficult for the molecule to approach the binding sites in the highly folded structure of G-quadruplex.

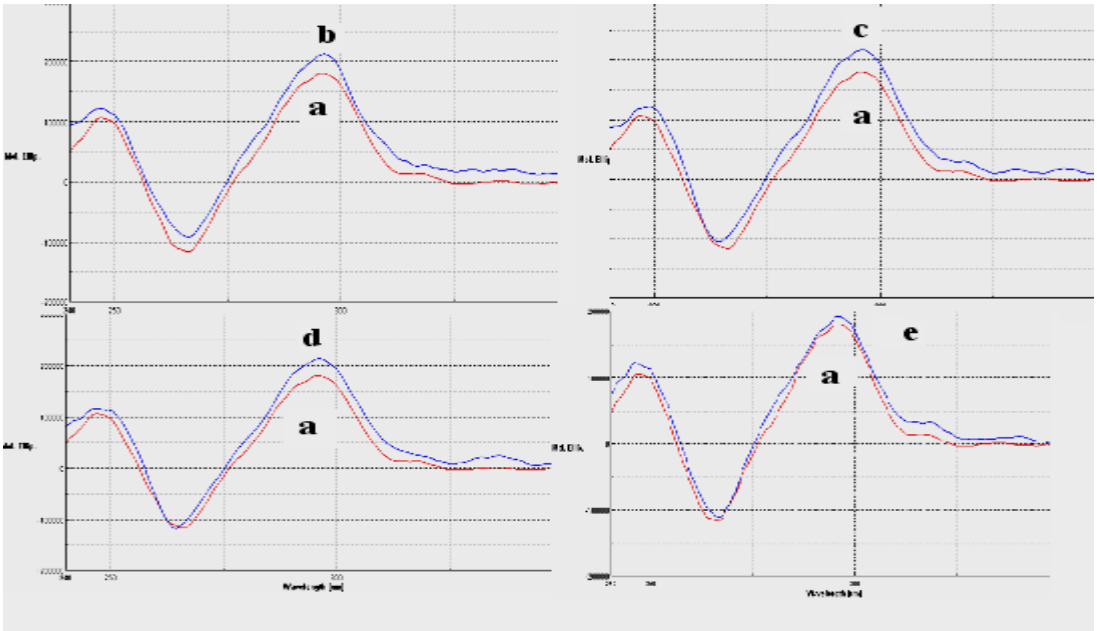

Fig. 2.28 CD spectra of 20 µM of G-quadruplex in the absence and presence of 120 µM of complex; (a) G-quadruplex alone, (b) G-quadruplex with complex **5,** (c) G-quadruplex with complex **6,** (d) G-quadruplex with complex **7** and (e) G-quadruplex with complex **8**

However, the ability of a complex to merely bind to quadruplex alone is not sufficient for it to be developed as an anticancer agent. Selectivity is always a major challenge in developing DNA binding agents for application either as DNA probes or therapeutic agents. Perhaps, the best example was shown recently by Dixon *et al.* (2007) where they managed to synthesized a pentacationic manganese(III) porphyrin complex which exhibits 10000-fold selectivity for G-quadruplex over duplex DNA. The noncovalent equilibrium binding constants of the porphyrin with duplex and quadruplex DNA were measured by surface plasmon resonance (SPR). SPR grants access to the ratio of the equilibrium binding constants, which is a measure of the G-quadruplex binding selectivity. The sensorgrams show an obvious selectivity of the complex for quadruplex DNA as the binding of the complex to GC and AT duplex DNA gives affinity constants in the 10^4 M^{-1} range, whereas it reaches 10^8 M^{-1} with quadruplex DNA. However, Talib *et al.* (2008) found that ruthenium(II) complexes with known intercalating ligands, viz. $[Ru(phen)_2(dpq)]^{2+}$, $[Ru(phen)_2(dppz)]^{2+}$ and $[Ru(phen)_3]^{2+}$ (where dpq = dipyridoquinoxaline; dppz = dipyridophenazine and phen = 1,10'-phenanthroline) complexes have higher binding affinity towards duplex DNA than towards quadruplex.

This prompted us to investigate the interaction of complexes **5–8** with guanine rich duplex DNA annealed from two complementary 17 bp primers, 5'-CCAGTTCGTAGTAACCC-3' and 3'-GGTCAAGCATCATTGGG-5'. Complex **5** (Fig. 2.29, Table 2.15) induces the greatest decrease in both positive and negative bands. This indicates that the binding of complex **5** to guanine rich duplex leads to conformational change from B-like to Z (Mahadevan and Palaniandavar, 1996). Complex **6** (Fig. 2.29, Table 2.15) that has always shown high preference to the GC rich sequence does not induce

significant increase (1.8%) to the positive band of G-duplex. However, it induces a great increase in the negative band (37.8%) of guanine rich duplex in contrast to the great decrease in negative band (17.1%) of ds$(CG)_6$ (Fig. 2.21). This suggest that besides being capable of recognizing CG sequence, complex **6** may be utilized to detect purely CG repeating sequences from the CG sequence in a mixture of other alternative nucleobase such as adenine and thymine in G-duplex. Complexes **6** and **8 (**Fig. 2.29, Table 2.15) both cause an increase in the positive and negative bands in the CD spectra of guanine rich duplex with the latter having slightly greater enhancement. This type of changes can be ascribed to a conformational change from B to ψ, which is similar to those observed in [Zn(phen)edda] (Seng *et al*., 2008) and $[Ru(NH_3)_4qdppz)]^{2+}$ (Maheswari and Palaniandavar, 2004).

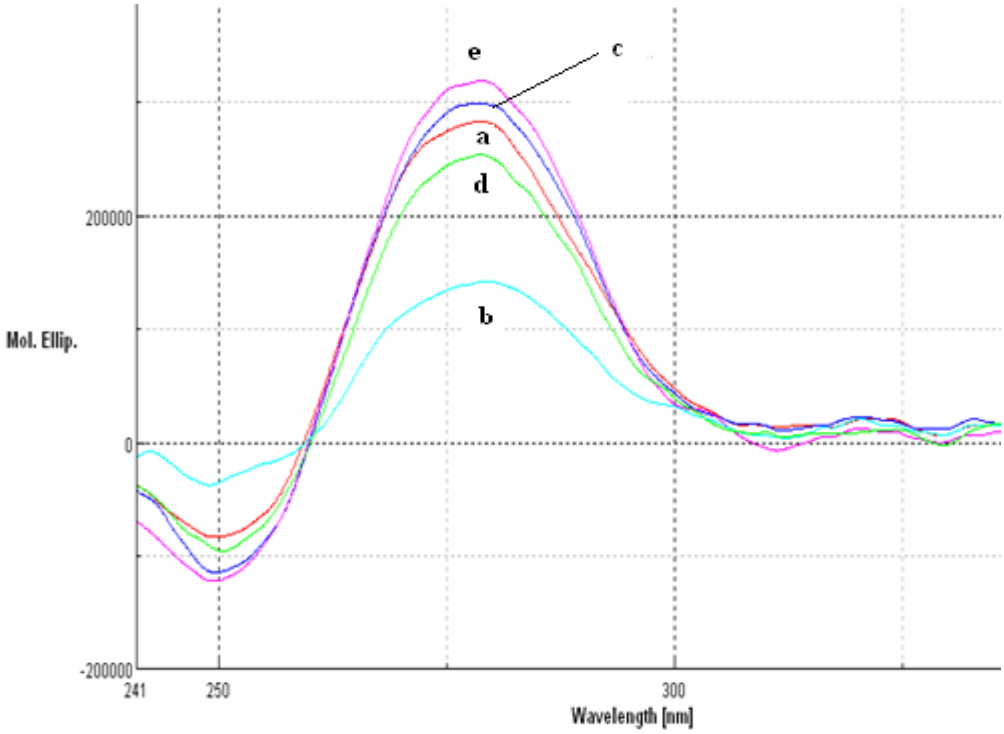

Fig. 2.29 CD spectra of 20 µM of guanine rich duplex in the absence and presence of 120 µM of complex; (a) guanine rich duplex alone, (b) guanine rich duplex with complex **5,** (c) guanine rich duplex with complex **6,** (d) rich duplex with complex **7** and (e) guanine rich duplex with complex **8**

By comparing the extent of changes induced in both the positive and negative bands of G-quadruplex and guanine rich duplex we can see that the complexes can differentiate G-quadruplex from G-duplex. Since the complexes can bind to both structures and induced different conformational change, it is not possible to compare their selectivity based on CD data alone. However, we still can conclude that complexes **6** and **7**, with alkyl group favor the stabilization of quadruplex with complex **6** being slightly more effective than **7**. Similar observations has been reported by Talib *et al.* (2008) when they studied the interaction of duplex and quadruplex DNA with platinum complexes with methylated phenanthroline ligands. It was found that introduction of a methyl groups onto the phenanthroline greatly enhanced the binding affinity towards DNA. It is noteworthy that the least reactive platinum complex towards both duplex DNA and quadruplex DNA was $[Pt(en)(phen)]^{2+}$, while the most reactive was $[Pt(en)(Me_4phen)]^{2+}$. This highlights the important role that hydrophobic interactions can play in determining overall binding affinities towards DNA. While complex **5** can bind to quadruplex with similar enhancement of base stacking as for complexes **6** and **7**, it is not a good candidate for a quadruplex binding agent because it may bind strongly to duplex DNA resulting in a great conformational change of the duplex DNA as observed in the CD spectrum. Finally, complex **8** which has a hanging pendant planar aromatic ring, which favors intercalation, is proven to bind to all the duplexes with greatest enhancement of positive band (Table 2.15). However, the binding to quadruplex is less favourable when compared to complexes **5**, **6** and **7**. This again is consistent with the idea that metal complexes do not interact with quadruplex DNA *via* the standard intercalative mode and the conceptual design used in molecules that bind to duplex DNA may not apply to quadruplex DNA.

2.3.6 Nucleolytic study

Zinc complexes that can hydrolytically cleave DNA and RNA have been extensively studied due to their biological relevance to various metalloenzymes (Bazzicalupi *et al*. 2008; Mancin *et al*. 2007; Qian *et al*. 2007). However, some zinc complexes need activation by an exogeneous agent or a change in chemical environment or reaction conditions for DNA cleavage to occur (Ramakrisnan *et al*. 2008; Seng *et al*. 2008). Although many mononuclear and multinuclear zinc(II) complexes can bind to DNA and induce hydrolytic cleavage DNA or model substrate, the ability to do so is highly dependent on the unsaturated coordination sphere of zinc and its ability to activate labile bonded nucleophiles (Liu *et al*. 2004; Mancin *et al*. 2007; He *et al*. 2009).

In this study, we examine the ability to cleave pBR322 under hydrolytic conditions and in the presence of exogenous agents, i.e. sodium ascorbate and hydrogen peroxide, using gel electrophoresis. When circular plasmid DNA is subjected to electrophoresis, relatively fast migration will be observed for the intact supercoil form (form I). If scission occurs on one strand (nicking), the supercoil will relax to generate a slower moving open circular form (form II). If both strands are cleaved, a linear form (form III) that migrates between form I and form II will be generated (Seng *et al.* 2008). Incubating the zinc complexes with pBR322 at varying concentrations of the zinc complex (10 – 1000 μM) for 24 h at 37 ^{o}C, no DNA cleavage was observed except for complex **6** (Fig. 2.30, Lane L8 & L9) and **8** (Fig. 2.31: Lane L8). Complex **6** started to show cleavage at 500 μM with the appearance of a nicked band with very low intensity and the amount of cleavage increased with the increase in concentration of the complex. Complex **8** is less active compared to **6**

because the appearance of a very low intensity nicked band can only be observed at the very high complex concentration of 1000 μM. Both the complexes are very weak hydrolytic cleavage agents.

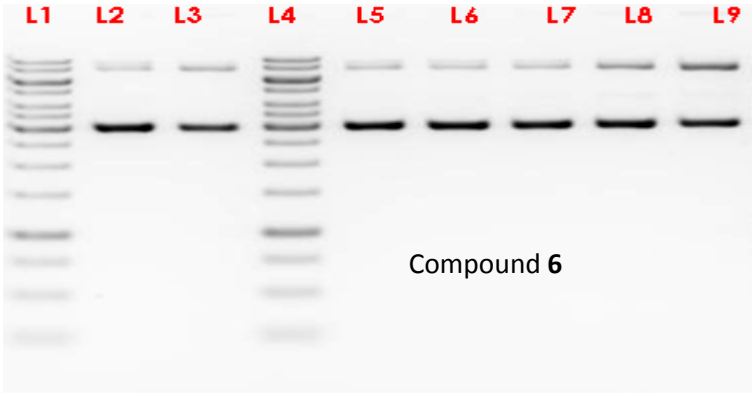

Fig. 2.30 Electrophoresis results of incubating pBR322 (0.5 μg/μL) in the presence of complex **6** in TN buffer (5 mM Tris, 50 mM NaCl) pH 7.5 at 37 ^{o}C for 24 h. L1 & L4, gene ruler 1 Kb DNA ladder; L2, DNA alone; L3, DNA + 1000 μM $ZnCl_2$; DNA + various complex concentrations L5-L9: L5, 10 μM; L6, 50 μM; L7, 200 μM; L8, 500 μM; L9, 1000 μM.

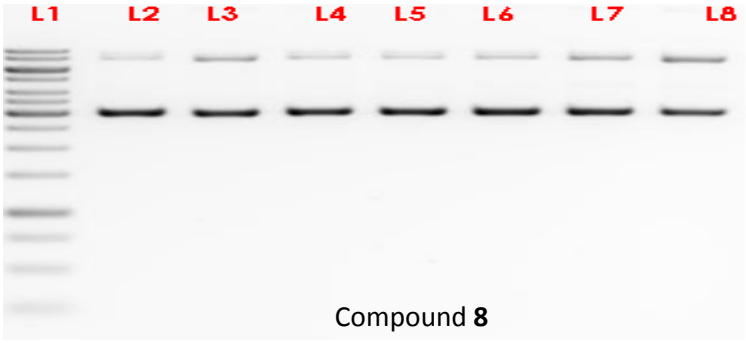

Fig. 2.31 Electrophoresis results of incubating pBR322 (0.5 μg/μL) in the presence of complex **8** in TN buffer (5 mM Tris, 50 mM NaCl) pH 7.5 at 37 ^{o}C for 24 h. L1, gene ruler 1 Kb DNA ladder; L2, DNA alone; L3, DNA + 1000 μM $ZnCl_2$; DNA + various complex concentrations L4-L8: L4, 10 μM; L5, 50 μM; L6, 200 μM; L7, 500 μM; L8, 1000 μM.

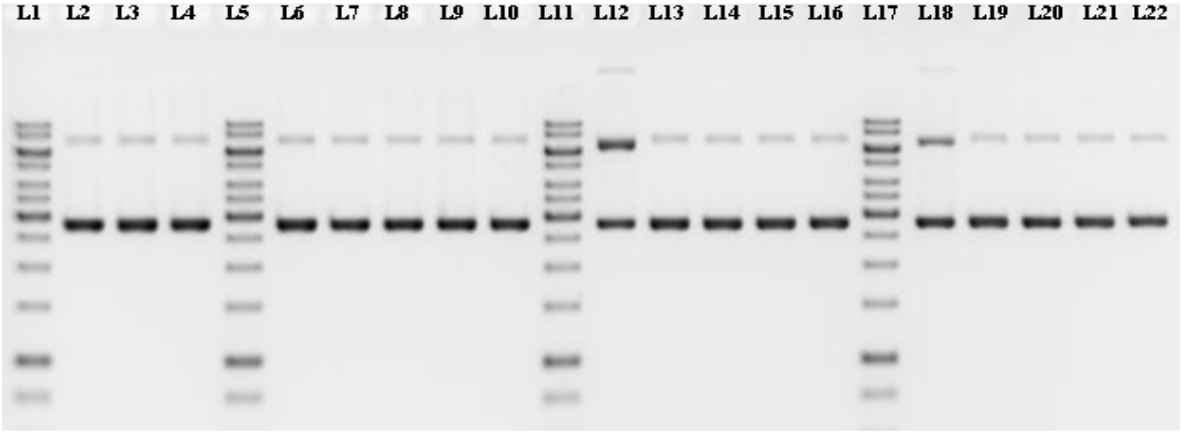

Fig. 2.32 Electrophoresis results of incubating pBR322 (0.5 μg/μL) with $ZnCl_2$ or complexes **5-8** in TN buffer (5 mM Tris, 50 mM NaCl) pH 7.5 at 37 ^oC for 2 h in the absence and presence of exogenous agents: Lane 1, 5, 11, 17 gene ruler 1 Kb DNA ladder; Lane 2, DNA alone (0.5 μg/μL) control; Lane 3, DNA + 30μM sodium ascorbate; Lane 4, DNA + 30μM H_2O_2; Lane 6, DNA + 300μM $ZnCl_2$; Lane 7, DNA + 300μM **7;** Lane 8, DNA + 300μM **6;** Lane 9, DNA + 300μM **8;** Lane 10, DNA + 300μM **5;** Lane 12, DNA + 300μM $ZnCl_2$ + 30μM sodium ascorbate; Lane 13, DNA + 300μM **7**+ 30μM sodium ascorbate; Lane 14, DNA + 300μM **6**+ 30μM sodium ascorbate; Lane 15, DNA + 300μM **8**+ 30μM sodium ascorbate; Lane 16, DNA + 300μM **5**+ 30μM sodium ascorbate; Lane 18, DNA + 300μM $ZnCl_2$ + 30μM H_2O_2; Lane 19, DNA + 300μM **7**+ 30μM H_2O_2; Lane 20, DNA + 300μM **6**+ 30μM H_2O_2; Lane 21, DNA + 300μM **8** + 30μM H_2O_2; Lane 22, DNA + 300μM **5**+ 30μM H_2O_2

When the DNA was incubated with 300 μM of zinc complex in the presence of 30 μM NaAsc or 30 μM H_2O_2, no activation of zinc complexes towards DNA cleavage by sodium ascorbate or hydrogen was observed as the gel pattern is the same as that for DNA alone (Fig. 2.32, lane L2). No cleavage was observed even when the concentration of hydrogen peroxide was varied from 250 μM to 500 μM by maintaining the complex concentration at 300 μM (results not shown).

2.3.7 Topoisomerase I inhibition assay

Topoisomerases are important nuclear enzymes that modify the topological state of DNA by catalyzing the relaxation of negative supercoils and the negative supercoiling of DNA (Wang *et al*. 1998). DNA cleavage by all topoisomerases involves the formation of a transient phosphodiester bond between a tyrosine residue in the protein and one of the ends of the broken strand. DNA topology can be modified during the lifetime of the covalent intermediate, and the enzyme is released as the DNA is religated. Those enzymes that cleave only one strand of the DNA are defined as type I and are further classified as either type IA subfamily members if the protein link is to a 50 phosphate (formerly called type I-50) or type IB subfamily members if the protein is attached to a 30 phosphate (formerly called type I-30). Topoisomerases that cleave both strands to generate a staggered double-strand break are grouped together in the type II subfamily of topoisomerases (Champoux, 2001). These enzymes play essential roles in mitosis, particularly in DNA transcription and replication (Nitiss, 1998). Topoisomerases have been identified as important targets in cancer chemotherapy and microbial infections (Kumar Singh *et al*. 2007). In fact, topoisomerase I inhibitors are quoted as having a wide range of antitumor activities and are among the most widely used anticancer drugs clinically (Sunani *et al*. 2009; Rothenberg 1997; Beretta *et al*. 2008). However, very few metal complexes have been reported to inhibit topoisomerases and even fewer zinc complexes have been reported to inhibit topoisomerase I and II (Kikuta *et al*. 2000; Chuang *et al*. 1996).

Supercoiled plasmid DNA pBR322 is a suitable substrate for study with topoisomerase I, which is a one strand DNA cutter. The supercoiled pBR322 (Form I) is

very compact and moves faster in the gel during electrophoresis. When one strand of the supercoilded DNA is cut, the resultant unwound, more relaxed open circular pBR322 (Form II) is formed and this nicked DNA moves slower. When two strands of the supercoiled DNA are cut, the linear DNA (Form III) is formed and it moves at intermediate speed. The commercial pBR322 (4.4 kb) has a small amount of both more relaxed Form II and Form III DNA (Fig. 2.33, lanes L1). In our DNA relaxation assay, one unit of human topo I can completely convert all the supercoiled plasmid pBR322 (4.4 kb) to fully relaxed topoisomer, which is the completely unwound covalently bonded closed circular DNA (Fig. 2.33, lane L7). This is found in the slowest moving DNA band (labelled Form II) which contains the fully relaxed closed circular pBR322 and the originally present, small amount of nicked DNA. No cleavage or unwinding of the DNA was observed when pBR322 was incubated with 40 μM of complexes **5-8** alone (Fig. 2.33, lane L2-L5). As can be seen from Fig. 2.33 (lane L10) only complex **8**, Zn(bipy)(HP) is capable of inhibiting topo I with total disappearance of the nicked band (containing nicked and fully relaxed DNA).

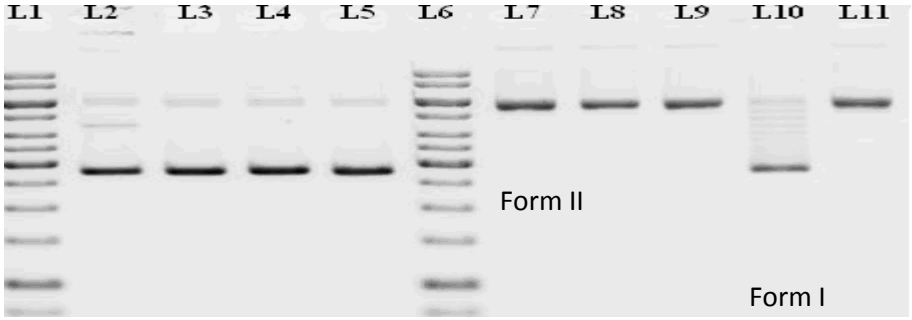

Fig. 2.33 Human topoisomerase I inhibition assay by gel electrophoresis. Electrophoresis results of incubating human topoisomerase I (1 unit/21μL) with pBR322 in the absence or presence of 40 μM of complex: Lane 1 & 6, gene ruler 1 Kb DNA ladder; Lane 2, DNA + 40μM **7** (control);Lane 3, DNA + 40μM **6** (control); Lane 4, DNA + 40μM **8** (control); Lane 5, DNA + 40μM **5** (control); Lane 7, DNA+ 1 unit Human Topoisomerase I (control); Lane 8, DNA + 40μM **7**+ 1unit Human Topoisomerase I; Lane 9, DNA + 40μM **6**+ 1unit Human Topoisomerase I; Lane 10, DNA + 40μM **8** + 1unit Human Topoisomerase I; Lane 11, DNA + 40μM **8** + 1 unit Human Topoisomerase I

As a preliminary investigation into the mechanism of action of the above topo I inhibition, we used three variations of mixing the DNA, topo I and the zinc complex **8** (at 40 μM) for the topo I inhibition assay. When the three components are mixed simultaneously, there is slight inhibition of topo I as seen by the presence of the fastest moving band with low intensity (Form I) which consists of supercoiled DNA and poorly relaxed DNA (Fig. 2.34, lane L5). The bands of topoisomers with different degrees of relaxation can also be seen in between Form I and Form II. Secondly, when complex **8** was incubated first with topo I before the addition of DNA, the intensity of the fastest moving band is the highest with almost total disappearance of the slowest moving band (Form II), suggesting that almost total inhibition of topo I (Fig. 2.34, lane L6). Finally, when the DNA is first incubated with the zinc complex for 30 minutes before adding the topo I (Fig. 2.34, lane L7), the fastest moving band (Form I) almost totally disappears. The intensity of Form II is slightly lower compared to the control in lane L4. The presence of relaxed topoisomers just below the fully relaxed topoisomer band (Form II) indicates that inhibition of topo I is less than the two methods of mixing earlier. These observed differences in inhibition of topo I suggest initial binding of the zinc complex to either the topo I or the DNA giving rise to differences in mode of action. Therefore, two pathways of toposisomerase inhibitions are suggested, one involves the binding of complex to DNA while the other involves the binding to toposiomerase. By comparing lane L6 and L7, we can infer that since greater inhibition of topo I is observed when the complex is incubated with topo first, the inhibition process involving the binding of the complex to the toposiomerase enzyme may be a more dominant pathway. However, further investigation is crucial to confirm this.

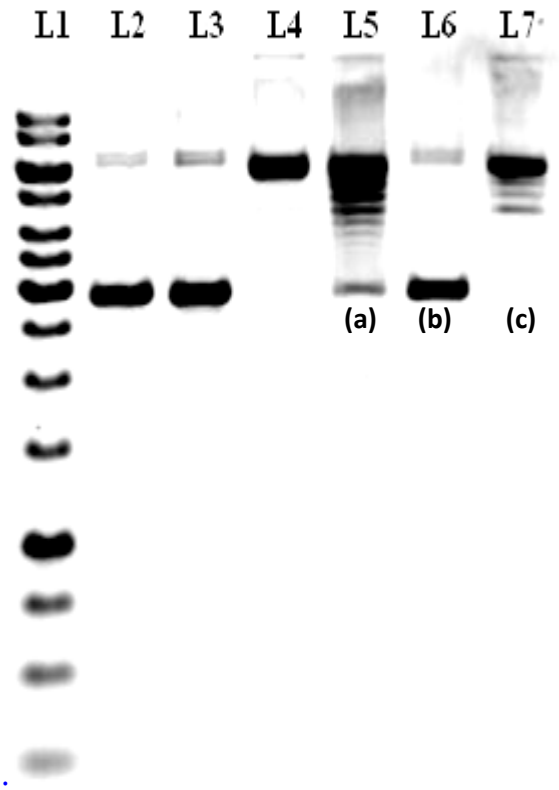

Fig. 2.34 Effect of sequence of mixing for the human topoisomerase I inhibition assay of complex **8**. Electrophoresis results of incubating human topoisomerase I (1 unit/21µL) with pBR322: Lane 1, 1 kb DNA ladder; Lane 2, Plasmid DNA pBR 322 (control); Lane 3, DNA + 40µM complex (control); Lane 4, DNA+ 1unit Human Topoisomerase I (control); (a) All components mixed at the same time; Lane 5, DNA + 40µM complex + 1 unit Human Topoisomerase I ; (b) Complex + TopoI incubated for 30 minutes first before DNA is added; Lane 6, DNA + 40µM complex + 1unit Human Topoisomerase I; (c) Complex + DNA incubated for 30 minutes first before TopoI is added; Lane 7, DNA + 40µM complex + 1unit Human Topoisomerase I

2.3.8 Antibacterial and antifungal assay

2.3.8.1 Antibacterial activity

The urge to discover new classes of antibacterial compounds is driven by the emergence of bacterial pathogens resistant to multiple antibacterial drugs in both the hospital and community setting (Tse-Dinh, 2009). Thiosemicarbazones and their metal complexes are good candidates for this purpose because of their well known antibacterial activity and

limited usage in clinical practice (Rodríguez *et al.* 2009; Joseph *et al.* 2004 & 2006; Jeragh and El-Dissouky, 2005). Therefore, the antibacterial activity of ligands and complexes were assessed against two species of Gram positive bacteria and four species of Gram negative bacteria to tap into the potential antibacterial activity of our compounds. All the ligands and complexes had some degree of inhibitory activity against the bacteria tested (Table 2.16).

Table 2.16.

Mean MIC value (μg/ml) towards microbes tested.

Compound	Bacteria					
	S. aureus	*B. cereus*	*P. aeruginosa*	*K. pneumoniae*	*E. coli* (penicillin-sensitive strain)	*E. coli* (penicillin-resistant strain)
1	62.50	62.50	62.50	62.50	62.50	62.50
2	125.00	62.50	125.00	62.50	62.50	62.50
3	62.50	62.50	62.50	62.50	62.50	62.50
4	62.50	31.25	62.50	31.25	62.50	62.50
5	62.50	62.50	62.50	62.50	62.50	62.50
6	62.50	62.50	62.50	62.50	62.50	62.50
7	62.50	62.50	62.50	62.50	62.50	62.50
8	15.63	15.63	31.25	15.63	62.50	62.50
$ZnCl_2$	-	-	-	-	-	-
bipy	125.00	62.50	62.50	62.50	62.50	62.50
Drug	8.00	4.00	4.00	4.00	4.00	4.00

" - " : no activity

Drug used in antibacterial assay = Chloramphenicol

Among the four ligands tested, ligand **4** shows the highest inhibition against *B. cereus* and *K. pneumonia* with MIC value 31.25 μg/ml. This may be due to the presence of

a more hydrophobic phenyl substituent that can enhance membrane permeability. The planar phenyl substituent may also enhance binding of the compound towards the DNA of the bacteria through intercalation. Ligands **1**, **2** and **3** show very weak antibacterial activity with MIC value of 62.50 μg/ml towards most of the bacteria except *S. aureus* and *P. aeruginosa.* These two bacteria are very resistant towards compound **2**, showing MIC value of 125.0 μg/ml.

Upon complexation, improvement of antibacterial activity is seen for complex **8**. Complexes **5-7** have the same degree of inhibitory activity against six species of bacteria with MIC value 62.50 μg/ml. But complex **8** exhibited higher inhibitory activity against *S. aureus*, *B. cereus* and *K. pneumonia* with MIC value 15.63 μg/ml and towards *P. aeruginosa* with MIC value of 31.25 μg/ml. The high antibacterial activity of complex **8** is compatible with its ability to inhibit topoisomerase I. Similar correlation of increased antibacterial activity with topoisomerase inhibition has been reported by Kikuta *et al.* (2000). The recent discovery that the accumulation of the covalent cleavage complex of bacterial topo I could indeed lead to rapid bacterial cell death has helped to validate bacterial type IA topoisomerases as useful targets for discovery of novel bactericidal compounds (Tse-Dinh, 2009). Therefore, complex **8** has the potential to be developed as antibacterial agent that targets topoisomerase. Bacterial topoisomerase inhibitors continue to be actively developed as clinical antibacterial agents, largely owing to the success of the currently marketed inhibitors, the quinolones, and the increasing resistance to these agents (Bradbury and Pucci, 2008).

2.3.8.2 Antifungal activity

The antifungal activity of ligands and complexes were assessed against four species of fungi. All the ligands and complexes had some degree of inhibitory activity against the fungi tested (Table 2.17). The antifungal property of the ligands is very dependent on the N(4) substituent and strains of fungal used in the assay. This indicates that the ligands are more selective towards certain fungal than the other. Ligands **2** and **3** which are alkyl substituted show moderate antifungal activitiy towards *C. albicans, C. parapsilosis* and *C. neoformans* with a MIC value of 31.25 µg/ml while their antifungal activity towards *A.niger is* very weak with a MIC value of 62.50 µg/ml. Compound **1** which is unsubstituted show similar activity with ligands **2** and **3** with the exception of *C. parapsilosis* with a MIC value of 62.50 µg/ml. This indicates that alkyl substitution of the free ligands does not play important role in improving their antifungal property. However, a drastic improvement can be seen in compound **4** when a phenyl substituent is attached to the N(4) atom. Compound **4** shows very good antifungal towards *C. neoformans* with a MIC value of 7.81 µg/ml and moderate antifungal towards *A. niger* with a MIC value of 31.25 µg/ml which is much higher compared to the other ligands. This may due to the greater hydrophobicity conferred to the ligand by the phenyl ring.

Table 2.17.
Mean MIC value (µg/ml) towards fungi tested.

Compound	Fungi			
	C. albicans	*C. parapsilosis*	*C. neoformans*	*A.niger*
1	31.25	62.50	31.25	62.50
2	31.25	31.25	31.25	62.50
3	31.25	31.25	31.25	62.50
4	31.25	62.50	7.81	31.25
5	31.25	62.50	15.63	62.50
6	15.63	31.25	15.63	62.50
7	31.25	62.50	15.63	62.50
8	31.25	15.63	7.81	31.25
$CuCl_2$	-	-	-	-
$ZnCl_2$	-	-	-	-
bipy	15.63	15.63	31.25	31.25
Drug	1.00	2.00	1.00	4.00

" - " : no activity

Drug used in antifungal assay = fluconazole

Upon complexation, the antifungal property remains unchanged for most of the complexes. Improvement is only seen for complexes **5-7** towards *C. neoformans* with all of them having a MIC value of 15.63 µg/ml which is lower than the MIC value of free bipyridine and their respective free thiosemicarbazones ligands. Improvement of biological property for a free ligand upon complexation is normally attributed to the increase in lipophilicity or synergistic effect from a bioactive metal centre (Liberta and West, 1992). An anomaly is seen in complex **7** towards *C. parapsilosis* where the complex is less potent than the free ligand (compound **3**). This may suggest that the antifungal property of compound **3** towards the particular strain of fungal is different from other ligands. The antifungal property of this ligand may lies in its ability to chelate free metal ion. Complexation removes its chelation ability therefore leads to decrease in its antifungal

property. Complex **8** which is derived from ligand **4** is the most potent antifungal agent with the lowest MIC value towards *C. parapsilosis, C. neoformans* and *A.niger*. However, the antifungal property of complex **8** does not surpass the activity of 2,2'-bipyridine towards *C. parapsilosis* and *A.niger*. Therefore, the complexation of the free ligands does not result in improved antifungal properties.

2.4 Conclusions

Spectroscopic and crystallographic data show that the free thiosemicarbazones ligands exist in the thione form. The zinc complexes are five-coordinated with the doubly deprotonated thiosemicarbazones ligands behaving as tridentate ligands coordinating through the phenolic oxygen, azomethine nitrogen and thiolate sulfur atoms, while the 2,2'-bipyridine ligand is coordinated in the *N,N'*-bidentate mode. The coordination geometry around the zinc complexes is intermediate between trigonal bipyramidal and square pyramidal geometries and is better described as trigonal bipyramidal distorted square based pyramid (TBDSBP).

Results from biological tests indicate that the nature of the N(4) substituent plays a crucial role in determining the selectivity and potency of zinc(II) complexes of 2,4-dihydroxybenzaldehyde N(4)-substituted thiosemicarbazones and 2,2-bipyridine. We can conclude that the complexes can differentiate DNA with different base sequences or structure. Complex **8** has the greatest potential to be developed as a drug due to its highest affinity in binding towards duplex DNA, ability to inhibit topoisomerase I and highest

antibacterial and antifungal properties. Complex **8** also holds the promise to be developed as an anticancer agent because compounds that can inhibit topoisomerase I and most compounds that show antifungal property are normally cytotoxic. This indicates that the presence of a phenyl group at the N(4) atom is crucial in elevating biological activities of this class of complex except for binding to G-quadruplex. On the other hand, complex **6,** which can recognize CG sequence, has better potential to be developed into a quadruplex binding and stabilizing agent because of its selectivity towards G-quadruplex is higher over G-duplex. The presence of an alkyl group at the N(4) atom is a desirable feature in developing complexes that bind selectively to G-quadruplex.

Chapter 3

Synthesis, characterization and biological properties of zinc(II) complexes of 2,4-dihydroxybenzaldehyde N^4-substituted thiosemicarbazones and 1,10-phenanthroline

3.1. Introduction

Previously, we observed that the N(4) substituent play a role in determining the ability of zinc(II) complexes of 2,4-dihydroxybenzaldehyde N(4)-substituted thiosemicarbazones and 2,2-bipyridine in DNA sequence and structure recognition (chapter 2). The N(4) substituents seem to affect their biological activities from changing or stabilizing the conformation of duplex DNA, quadruplex binding, topoisomerase I inhibition, antibacterial to antifungal property. In the study of interactions of ternary complexes with DNA, another common strategy is to vary the *N,N'*-heterocyclic ligands with different intercalating capability. Normally, marked improvement in DNA interaction is observed when ligand like 2,2'-bipyridine is replaced by ligands with extended aromatic ring such as 1,10-phenanthroline (phen), dipyrido[3,2-d:2′,3′-f] quinoxaline (dpq), dipyrido[3,2-a:2′,3′-c]phenazine (dppz) and naphtha[2,3-a]dipyrido[3,2-h:2′, 3′-f]phenazine-5,18-dione (qdppz). Metal complexes with intercalating ligands normally have higher binding constants in contrast to those of 2,2'-bipyridine derivatives. These intercalating ligands can promote better binding to DNA by deeper insertion of extended aromatic ring between nucleobase pair or simply by increased in π-π interaction with nucleobase attributed to increase in overlapping of the aromatic ring (Ramakrishnan and Palaniandavar, 2008; Roy *et al.* 2007; Patra *et al.* 2005; Dhar *et al.* 2005; Thomas *et al.* 2003). Sometimes, the intercalating ligand can even act as a recognition domain (Gao *et al.* 2008). Recently, Gao *et al.* (2008) have prepared a DNA intercalating Ru(II) polypyridine

complex, $[Ru(bipy)_2(appo)]^{2+}$ (appo = 11-aminopteridino[6,7-f][1,10]phenanthrolin-13(12H)-one) that showed higher selectivity towards GC sequences. The sequence selectivity is hypothesized to be conferred by hydrogen bonding interaction between the introduced guanine group in the intercalating ligand (appo) and GC base pairs of DNA.

Therefore in this chapter, we report the effect of varying the N(4) substituent of the thiosemicarbazones from hydrogen, methyl, ethyl to phenyl towards the chemical and biological properties (DNA binding, nucleolytic, topoisomerase I inhibition and antimicrobial) of ternary Zn(II) complexes containing 1,10-phenanthroline . Cross comparison with the 2,2'-bipyridine analog in chapter 2 will be carried out to evaluate the effect of changing 2,2'-bipyridine to 1,10-phenanthroline on their biological properties.

3.2. Experimental

3.2.1. Materials and solutions

The materials used were the same as mentioned in chapter 2.

3.2.2. Physical measurements

IR spectra were recorded as KBr pellets by using a Perkin-Elmer Spectrum RX-1 spectrophotometer. NMR spectra were recorded in deuterated DMSO-d6 on a JEOL JNM-LA400 or ECA 400 MHz instrument. Elemental analyses were performed on a Thermo Finnigan Eager 300 CHNS elemental analyzer. UV–visible spectroscopic measurements

were carried out on a Perkin–Elmer Lambda 40 spectrophotometer. The circular dichroism study of the interaction of metal complexes with ds(oligonucleotide) was carried out with a 1.0 cm or 1.0 mm quartz cells respectively using a Jasco J-810 spectropolarimeter.

3.2.3 Syntheses

3.2.3.1 Synthesis of (4-Hydroxy-2-oxidobenzaldehyde thiosemicarbazonato)-(1,10-phenanthroline)zinc(II) monohydrate, [Zn(phen)(HT)].H_2O **(9)**

Zinc acetate dihydrate (0.22 g, 1 mmol) and 1,10-phenanthroline (0.20 g, 1 mmol) were heated in ethanol (20 ml) for 1 hour followed by addition of 2,4-dihydroxybenzaldehyde thiosemicarbazone (0.21 g, 1 mmol) in hot ethanol (20 ml) and the mixture was refluxed for another 3 hours. The yellow complex that separated was filtered, washed with cold methanol and ether, dried in air and kept in a desiccator over silica gel. (Yield: 0.38 g, 81%). Anal. Calc. for $C_{20}H_{17}N_5O_3SZn$: C, 50.80; H, 3.62; N, 14.81. Found: C, 50.78; H, 3.36; N, 14.63%. IR (KBr disc, cm^{-1}): 3450 w, 3338 m, 3280 w, 3155 w, 3069w, 1603 s, 1474 s, 1426 s, 1318 m, 1260 m, 1219 s, 1181 m, 1119 m, 847 m, 726 m, 554 w, 426 w (s, strong; m, medium; w, weak). Complex **9** is not sufficiently soluble in DMSO-d6 to acquire good NMR spectrum.

3.2.3.2 Synthesis of (4-Hydroxy-2-oxidobenzaldehyde 4-methylthiosemicarbazonato)-(1,10-phenanthroline)zinc(II) monohydrate, [Zn(phen)(HM)]. H_2O **(10)**

Complex **10** was similarly prepared as complex **9** by using 2,4-dihydroxybenzaldehyde 4-methylthiosemicarbazone (0.23 g, 1 mmol) as the Schiff base ligand.

(Yield: 0.40 g, 82%). Anal. Calc. for $C_{21}H_{19}N_5O_3SZn$: C, 51.80; H, 3.93; N, 14.38. Found: C, 51.50; H, 3.71; N, 14.42%. IR (KBr disc, cm^{-1}): 3385 s (broad), 3249 w, 3014 w, 1601 s, 1490 s, 1426 w, 1400 s, 1279 w, 1238 m, 1200 s, 1184 m, 848 m, 726 m, 550, 430 w (s, strong; m, medium; w, weak).

Characteristic ^{1}H-NMR signals (DMSO-d6, TMS, p.p.m.): 9.05 (s, broad, 1H, OH), 8.89 (s, broad, 2H, phen), 8.78 (s, broad, 2H, phen), 8.39 (s, 1H, CH=N), 8.15 (s, broad, 2H, phen), 8.02 (s, broad, 2H, phen), 6.95 (d, 1H, aromatic, J = 8 Hz), 6.21 (s, broad, 1H, N**H**-CH_3), 5.66(s, 1H, aromatic), 5.88(d, 1H, aromatic, J = 8 Hz), 2.73 (d, 3H, NH-C**H**$_3$, J = 4 Hz)

3.2.3.3 Synthesis of (4-Hydroxy-2-oxidobenzaldehyde 4-ethylthiosemicarbazonato)-(1,10-phenanthroline)zinc(II) monohydrate, [Zn(phen)(HE)].H_2O **(11)**

Complex **11** was similarly prepared as complex **9** by using 2,4-dihydroxybenzaldehyde 4-ethylthiosemicarbazone (0.24 g, 1 mmol) as the Schiff base ligand.

(Yield: 0.38 g, 76%). Anal. Calc. for $C_{22}H_{21}N_5O_3SZn$: C, 52.75; H, 4.23; N, 13.98. Found: C, 52.54; H, 4.35; N, 14.22%. IR (KBr disc, cm^{-1}): 3501 w, 3458 w, 3331 w, 3048 w, 2962 w, 1601 s, 1481 s, 1425 s, 1343 m , 1273 m, 1205 s, 1121 m, 845 m, 725 m 553 m, 421 m (s, strong; m, medium; w, weak).

Characteristic ^{1}H-NMR signals (DMSO-d6, TMS, p.p.m.): 8.99 (s, broad, 1H, OH), 8.86 (s, broad, 2H, phen), 8.77 (s, broad, 2H, phen), 8.35 (s, 1H, CH=N), 8.13 (s, broad, 2H, phen), 8.00 (s, broad, 2H, phen), 6.92 (d, 1H, aromatic, J = 8 Hz), 6.16 (s, 1H, N**H**-CH_2CH_3) 5.62(s, 1H, aromatic), 5.85(d, 1H, aromatic, J = 8 Hz), 3.22 (m, 2H, NHC**H**$_2$-CH_3, J = 4 Hz), 1.01 (t, 3H, $NHCH_2$-**C**$\mathbf{H_3}$, J = 4 Hz)

3.2.3.4 Synthesis of (4-Hydroxy-2-oxidobenzaldehyde 4-phenylthiosemicarbazonato)-(1,10-phenanthroline)zinc(II) monohydrate, [Zn(phen)(HP)]. H_2O **(12)**

Complex **12** was similarly prepared as complex **9** by using 2,4-dihydroxybenzaldehyde 4-phenylthiosemicarbazone (0.29 g, 1 mmol) as the Schiff base ligand.

(Yield: 0.41 g, 77%). Anal. Calc. for $C_{26}H_{19}N_5O_3SZn$: C, 58.82; H, 3.61; N, 13.19. Found: C, 58.54; H, 3.31; N, 13.35%. IR (KBr disc, cm^{-1}): 3394 m, 3053 w, 1603 s, 1532 m, 1484 s, 1423 s, 1337 w, 1310 m, 1241 m, 1171 m, 849 m, 726 m, 503 w (s, strong; m, medium; w, weak).

Characteristic ^{1}H-NMR signals (DMSO-d6, TMS, p.p.m.): 9.15 (s, broad, 1H, OH), 8.95 (s, broad, 2H, phen), 8.80 (s, broad, 2H, phen), 8.56 (s, 1H, N**H**-C_6H_5), 8.52 (s, 1H, CH=N), 8.17 (s, broad, 2H, phen), 8.03 (s, broad, 2H, phen), 7.81 (d, 2H, aromatic, J = 8 Hz), 7.18 (t, 2H, aromatic, J = 8 Hz), 7.04 (d, 1H, aromatic, J = 8 Hz), 6.82 (t, 1H, aromatic, J = 8 Hz), 5.91(d, 1H, aromatic, J = 8 Hz), 5.67 (s, 1H, aromatic)

3.2.4. X-ray crystallography

Yellowish crystals for complexes **9a** and **11a** were recrystallised from DMSO and DMF respectively. The unit cell parameters and the intensity data were collected on a Bruker SMART APEX CCD diffractometer, equipped with Mo Kα X-ray source (λ=0.71073 Å). The APEX2 software was used for data acquisition and the SAINT software for cell refinement and data reduction (Bruker, 2007). Absorption corrections on the data were made using SADABS (Sheldrick, 1996). The structures were solved and refined by SHELXL97 (Sheldrick, 2008). Molecular graphics were drawn by using XSEED (Barbour,

2001). Material for publication was prepared using publCIF (Westrip, 2009). The structures were solved by direct-methods and refined by a full-matrix least-squares procedure on F^2 with anisotropic displacement parameters for non-hydrogen atoms. Hydrogen atoms in their calculated positions were refined using a riding model. All the hydrogen atoms for **9a** were fixed at calculated positions. Whereas, for the hydroxy and amino H-atoms for **11a** were located in a difference Fourier map.

3.2.5 DNA binding

PAGE grade self-complimentary 12-mer oligonucleotides $(CG)_6$, $(AT)_6$, (CGCGAATTCGCG), (CGCGATATCGCG), HPLC grade 22-mer oligonucleotide 5'-AGGGTTAGGGTTAGGGTTAGGG-3', and 17-mer complementary pair of oligonucleotides 5'-CCAGTTCGTAGTAACCC-3, 3'-GGTCAAGCATCATTGGG-5' were annealed, to give the respective duplexes and G-quadruplex, as specified by the suppliers, 1st BASE and Eurogentec Ait. The circular dichroism spectra were obtained by scanning Tris-NaCl buffered solutions of the DNA without and with the zinc complexes.

3.2.6 Nucleolytic study

Nucleolytic study was carried out according to the methods in chapter 2.

3.2.7 Human Topoisomerase I inhibtion assay

The human DNA topoisomerase I inhibitory activity was determined according to the methods in chapter 2.

3.2.8 Antibacterial and antifungal assay

The antibacterial and antifungal activities of the ligands and complexes were assessed against several strains of Gram-positive bacteria, Gram-negative bacteria, and fungi. A colorimetric broth microdilution method using *p*-iodonitrotetrazolium violet (INT) as the growth indicator was employed to quantify the minimum inhibitory concentration (MIC) value of the complexes in the assay. The test was performed as mentioned in chapter 2.

3.3. Results and discussion

3.3.1 Synthesis of the complexes

The stoichiometries, colors and partial elemental analyses of the complexes are shown in Table 3.1. Proposed structures for all the compounds with IUPAC numbering scheme are shown in Fig. 3.1. Results from partial elemental analyses are in good agreement with the proposed formulation of Zn(phen)L where phen = 1,10-phenanthroline and L is the doubly deprotonated thiosemicarbazones. The complexes exist as a monohydrate and are yellow. Complexes **9-12** were prepared in high yield by refluxing zinc acetate dihydrate, 1,10-phenanthroline and the thiosemicarbazones in ethanol. Spectroscopic and crystallographic data show that all the free ligands exist in the thione tautomer form in both solid and

solution. However, all complexes were isolated with the ligands coordinated in the thiolate form. In the absence of acetate, reactions of similar ligands with zinc chloride is known to form dinuclear complex with the thiosemicarbazone moiety coordinating in the thione form (Tan *et al.* 2009). All complexes are insoluble in common polar and non-polar solvents but are soluble in DMF and DMSO.

9 R' = H **10** R' = $-CH_3$ **11** R' = $-C_2H_5$ **12** R' = $-C_6H_5$

Fig. 3.1 Proposed structure for all the complexes

Table 3.1

Stoichiometries, color and partial elemental analyses of the zinc(II) complexes

Compound	Stoichiometries	Color	Anal. Calc.	(Found)%	
			C	H	N
[Zn(phen)(HT)].H_2O **(9)**	$C_{20}H_{17}N_5O_3SZn$	Yellow	50.80(50.78)	3.62(3.36)	14.81(14.63)
[Zn(phen)(HT)].H_2O. DMSO **(9a)**	$C_{22}H_{23}N_5O_4S_2Zn$	Yellow	47.96(48.31)	4.21(4.46)	12.71(13.04)
[Zn(phen)(HM)].H_2O **(10)**	$C_{21}H_{19}N_5O_3SZn$	Yellow	51.80(51.50)	3.93(3.71)	14.38(14.42)
[Zn(phen)(HE)].H_2O **(11)**	$C_{22}H_{21}N_5O_3SZn$	Yellow	52.75(52.54)	4.23(4.35)	13.98(14.22)
[Zn(phen)(HE)].H_2O .DMF**(11a)**	$C_{25}H_{28}N_6O_4SZn$	Yellow	52.31(52.63)	4.92(4.65)	14.64(14.33)
[Zn(phen)(HP)].H_2O **(12)**	$C_{26}H_{19}N_5O_3SZn$	Green Yellow	58.82(58.54)	3.61(3.31)	13.19(13.35)

3.3.2 Crystal structure analysis

3.3.2.1 Crystal structures of [Zn(phen)(HT)].H_2O.DMSO (**9a**)

Complex **9a** crystallised into a triclinic lattice with space group symmetry *P*$\bar{1}$**.** The perspective view of the complex with numbering scheme is shown in Fig. 3.2. The complex is mononuclear and five coordinated with the doubly deprotonated 2,4-dihydroxybenzaldehyde thiosemicarbazone as a tridentate ligand coordinating through the phenolic oxygen, azomethine nitrogen and thiolate sulfur atoms while 1,10-phenanthroline coordinates as the *N*,*N*'-bidentate ligand**.**

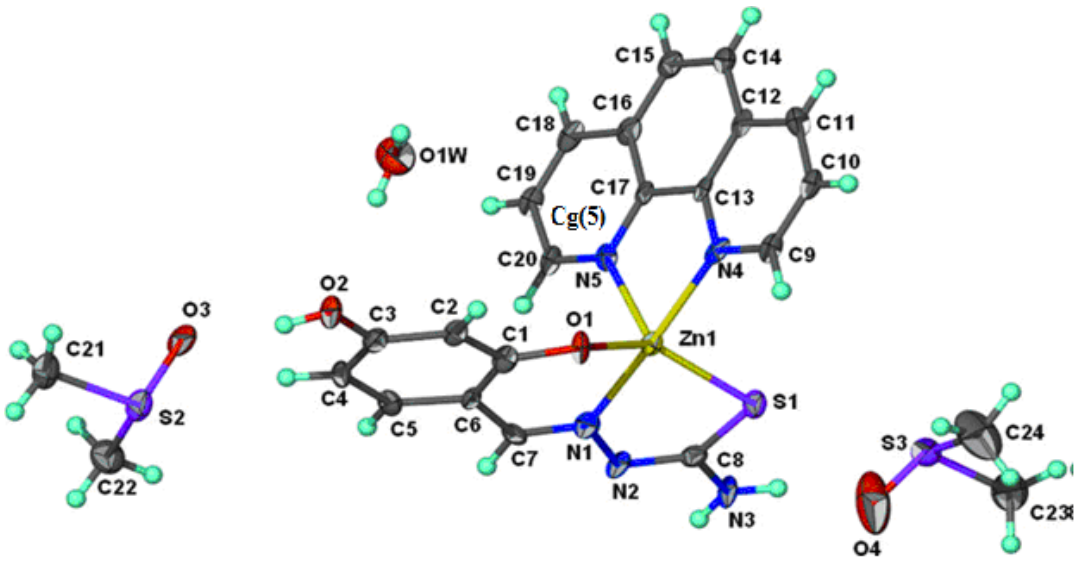

Fig. 3.2 Thermal ellipsoid (Barbour, 2001) plot of **9a** drawn at the 70% probability level. Hydrogen atoms are drawn as spheres of arbitrary radii.

The trigonality index τ of 0.47 for **9a** indicates that the coordination geometry around zinc is intermediate between trigonal bipyramidal and square pyramidal geometries and we described it as trigonal bipyramidal distorted square based pyramid (TBDSBP). This value is very close to its 2,2'-bipyridine analog (complex **5**) with trigonality index τ of 0.49. This implies that the variation of the polypyridyl ligand has not much effect on the coordination geometry. On the other hand, complex **13a** which is the copper and 2,2'-bipyridine analog of complex **9a** has a trigonality index τ of 0.03 which is close to a perfect square pyramidal. This shows that the metal ion exerts a great influence on the coordination geometry of a complex compared with these ligands. The deviation from an ideal stereochemistry may be attributed to the restricted bite angle imposed by both the thiosemicarbazone and 1,10-phenanthroline ligands (Seena and Kurup, 2008). The bite

angle around the metal for *N,N'*-heterocycle of 78.60(19)° may be considered smaller when compared with an average value of 79.33(11)° reported in the literature for zinc complexes with phenanthroline (Chang and Janiak, 2001).

Selected bond lengths and angles are presented in Table 3.3. Zn $-N_{azomethine}$ bond length of 2.081(5) Å is shorter than the Zn-N_{phen} bond lengths of 2.143(5) and 2.157(5) Å. This indicates that the azomethine nitrogen is coordinated slightly stronger to zinc compared to the phenanthroline nitrogen and the thiosemicarbazone moiety dominates equatorial bonding. The imine bond formation is evidenced from the N1-C7 and N2-C8 distances of 1.282 (8) Å and 1.324(8) Å. The C-N bond length of 1.324(8) Å and C-S bond length of 1.744(7) Å is similar to those reported for coordination of other thiosemicarbazones in the thiolate form (Seena and Kurup, 2008; Demirci, 2008).

Hydrogen bonding interactions for complex **9a** is shown in Fig. 3.3 (Table 3.4). Hydrogen bonds link the mononuclear molecule, the water and the dimethylsulphoxide (DMSO) molecules into a linear chain motif. These hydrogen bonding interactions may be responsible in DNA base sequence recognition as suggested by Gao *et al.* (2008) in their $[Ru(bipy)_2(appo)]^{2+}$ complex.

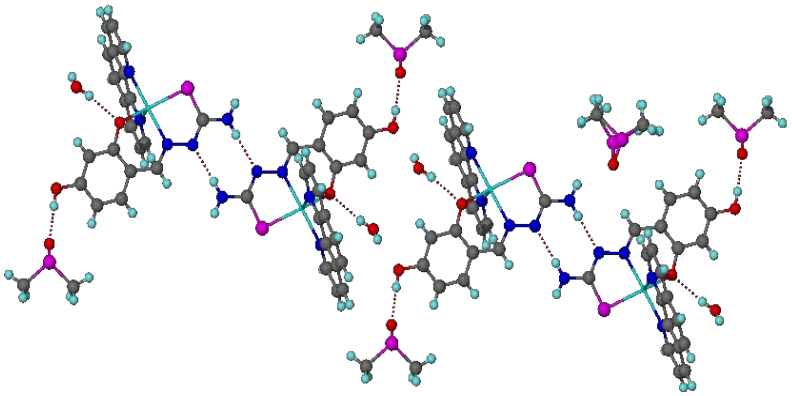

Fig. 3.3 Hydrogen bonding interactions for complex **9a**

The packing of the molecules is stabilized by the combination of hydrogen bonding and π-π interactions between aromatic rings as shown in Fig. 3.4.

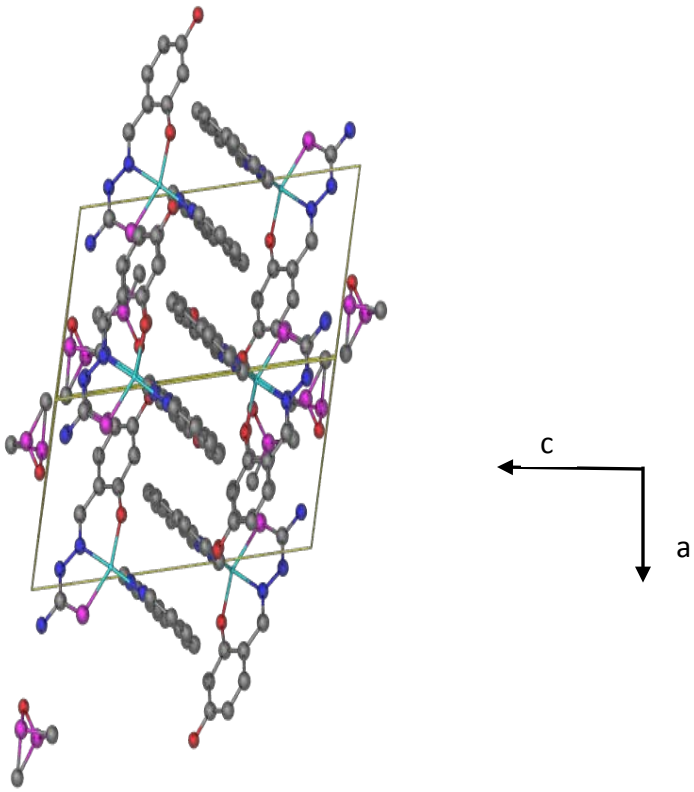

Fig. 3.4 Unit cell packing diagram of **9a** along b axis.

Table 3.2

Crystal data and structure refinement parameters for complex **9a** and **11a.**

Complex	[Zn(phen)(HT)].H_2O. 2 DMSO (**9a**)	[Zn(phen)(HE)].H_2O.DMF (**11a**)
Empirical formula	$C_{24}H_{29}N_5O_5S_3Zn$	$C_{25}H_{28}N_6O_4SZn$
Formula weight	629.07	573.96
Crystal system	Triclinic	Monoclinic
Space group	$P\bar{1}$	$P2_1/c$
Unit cell dimensions		
a (Å)	9.3582 (5)	10.3744 (2)
b (Å)	9.8181 (5)	26.5703 (5)
c (Å)	15.2913 (8)	9.2815 (2)
α (°)	73.641 (3)	90
β (°)	82.482 (4)	97.080 (1)
γ (°)	88.059 (4)	90
Volume, V ($Å^3$)	1336.49 (12)	2538.95 (9)
Z	2	4
F(0 0 0)	652	1192
Density (calculated), (mg m^{-3})	1.563	1.502
Absorption coefficient, μ(mm^{-1})	1.2	1.09
Temperature, T (K)	293 (2)	100 (2)
Crystal size (mm)	0.05 × 0.01 × 0.01	0.45 × 0.10 × 0.03
Reflections collected	12760	17571
Independent reflections	6125	5688
	[R(int) = 0.097]	[R(int) = 0.028]
Data/restraints/parameters	6125/15/356	5688/5/349
$R[F^2 > 2\sigma(F^2)]$	0.073	0.033
$wR(F^2)$	0.209	0.100
S	0.97	1.08
Largest difference peak and hole (e $Å^{-3}$)	1.5 and −1.28	0.40 and −0.60

Table 3.3

Selected bond lengths (Å) and angles (˚) for [Zn(phen)(HT)].H_2O. DMSO (**9a**)

Bond lengths		Bond angles	
Zn1—O1	1.976 (4)	O1—Zn1—N1	89.26 (19)
Zn1—N1	2.081 (5)	O1—Zn1—N5	104.24 (19)
Zn1—N5	2.143 (5)	N1—Zn1—N5	94.5 (2)
Zn1—N4	2.157 (5)	O1—Zn1—N4	95.45 (18)
Zn1—S1	2.3541 (18)	N1—Zn1—N4	172.4 (2)
S8—C1	1.744(7)	N5—Zn1—N4	78.60 (19)
O1—C1	1.330 (7)	O1—Zn1—S1	143.98 (15)
O2—C3	1.372 (8)	N1—Zn1—S1	82.37 (15)
N1—C7	1.282 (8)	N5—Zn1—S1	111.28 (14)
N1—N2	1.383 (7)	N4—Zn1—S1	97.11 (14)
N2—C8	1.324 (8)	C8—S1—Zn1	94.0 (2)
N3—C8	1.348 (8)	C1—O1—Zn1	122.6 (4)
N4—C9	1.343 (8)		
N5—C17	1.356 (8)		

Table 3.4
Hydrogen-bond geometry (Å, °) for [Zn(phen)(HT)].H_2O. DMSO (**9a**)

D—H···*A*	*D*—H	H···*A*	*D*···*A*	*D*—H···*A*
O2—H2···O3	0.84	1.85	2.679 (6)	171
N3—H31···N2^{i}	0.88	2.11	2.986 (8)	175
N3—H32···O4	0.88	2.33	3.075 (8)	143
O1W—H1W1···O1^{ii}	0.84	2.11	2.910 (7)	160
O1W—H1W2···O2	0.84	2.25	3.056 (7)	161

Symmetry codes: (i) −*x*+2, −*y*+2, −*z*+2; (ii) −*x*+1, −*y*+2, −*z*+1. Hydrogen atoms are placed at calculated positions.

3.3.2.2 Crystal structures of [Zn(phen)(HE)].H2O.DMF (**11a**)

Complex **11a** crystallised into a monoclinic lattice with space group symmetry $P2_1/c$. The perspective view of the complex with numbering scheme is shown in Fig. 3.5.

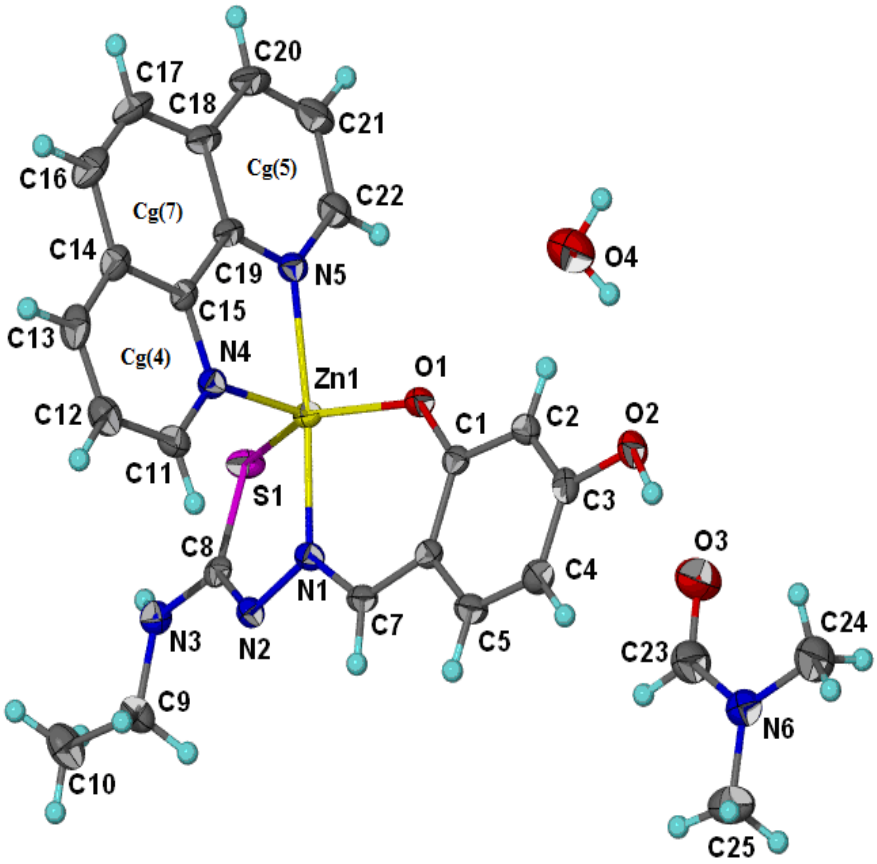

Fig. 3.5 Thermal ellipsoid (Barbour, 2001) plot of **11a** drawn at the 70% probability level. Hydrogen atoms are drawn as spheres of arbitrary radii.

The complex is mononuclear and five coordinated with the doubly deprotonated thiosemicarbazone as a tridentate ligand coordinating through the phenolic oxygen, azomethine nitrogen and thiolate sulfur while 1,10-phenanthroline as the *N*,*N*'-bidentate ligand**.** Complex **11a** with trigonality index τ of 0.58 can thus be described as trigonal bipyramidal distorted square based pyramid (TBDSBP). The τ value of **11a** is slightly

higher than that of complex **9a**. This could be attributed to the presence of an ethyl group in the N(4) position resulting in greater repulsion between the ligands. In order to minimize this repulsion, the geometry of the complex is distorted more towards a trigonal bipyramidal geometry.

Selected bond lengths and angles are presented in Table 3.5. The imine bond formation in the complex is evidenced from N2-C8 and N1-C7 distances of 1.310 (3) and 1.287 (3) Å. The C8-N2 bond length of 1.333(2) for the free ligand decreases to 1.310(3) while C8-S1 increases from 1.683(19) to 1.754(2) Å upon complexation owing to partial loss and gain of double bond character in accordance to coordination of thiosemicarbazone in the thiolate form. Hydrogen bonds link the mononuclear molecule, the water and the dimethylformamide (DMF) molecules into a linear chain motif (Fig. 3.6)

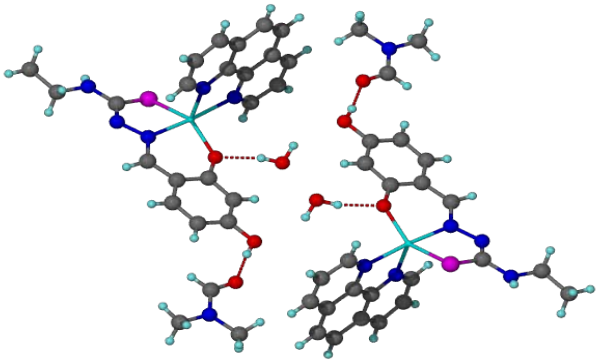

Fig. 3.6 Hydrogen bonding interactions for complex **11a**

The molecules of **11a** in the packing form infinite 2-dimensional array through extensive π-π stacking between the aromatic rings of 1,10-phenanthroline as shown in Fig. 3.7.

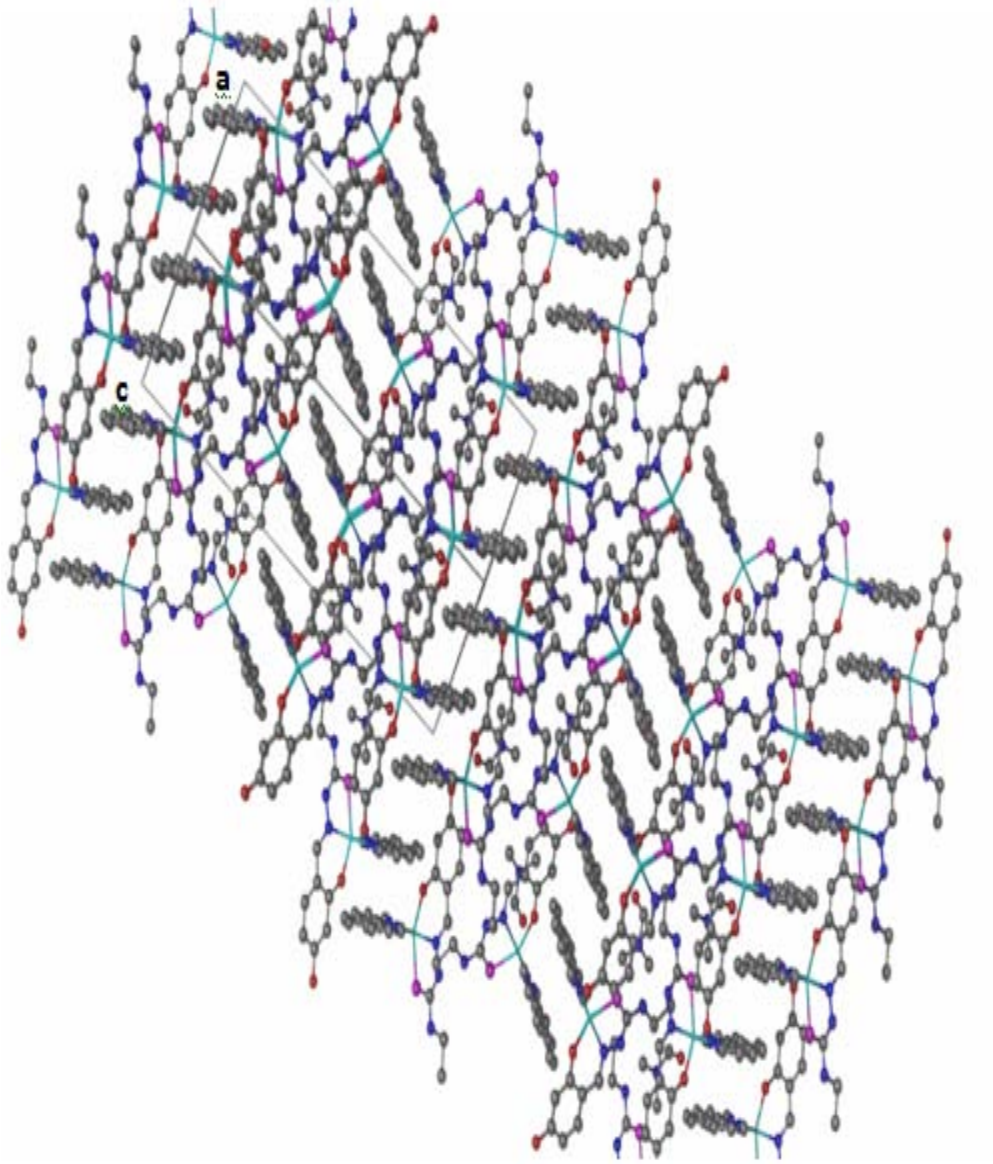

Fig. 3.7 Unit cell packing diagram of **11a** view down in between a and c axes.

Table 3.5

Selected bond lengths (Å) and angles (°) for [Zn(phen)(HE)].H_2O.DMF (**11a**)

Bond lengths		Bond angles	
Zn1—O1	1.9636 (16)	O1—Zn1—N1	90.55 (7)
Zn1—N1	2.0719 (17)	O1—Zn1—N4	111.50 (7)
Zn1—N4	2.1165 (18)	N1—Zn1—N4	96.27 (7)
Zn1—N5	2.1583 (18)	O1—Zn1—N5	93.26 (7)
Zn1—S1	2.3508 (6)	N1—Zn1—N5	174.04 (7)
S1—C8	1.754 (2)	N4—Zn1—N5	78.06 (7)
O1—C1	1.321 (3)	O1—Zn1—S1	139.27 (5)
O2—C3	1.371 (3)	N1—Zn1—S1	81.66 (5)
N1—C7	1.287 (3)	N4—Zn1—S1	109.08 (5)
N1—N2	1.398 (2)	N5—Zn1—S1	98.34 (5)
N2—C8	1.310 (3)	C8—S1—Zn1	92.59 (8)
N3—C8	1.363 (3)	C1—O1—Zn1	126.70 (13)
N3—C9	1.458 (3)		
N4—C11	1.327 (3)		
N4—C15	1.351 (3)		
N5—C22	1.329 (3)		

Table 3.6

Hydrogen-bond geometry (Å, °) for [Zn(phen)(HE)].H_2O.DMF (**11a**)

D—H···*A*	*D*—H	H···*A*	*D*···*A*	*D*—H···*A*
O2—H2···O3	0.847 (10)	1.874 (11)	2.716 (3)	173 (3)
O4—H41···O2	0.888 (10)	2.290 (17)	3.064 (3)	146 (3)
O4—H42···O1^{i}	0.889 (10)	1.931 (11)	2.804 (3)	167 (3)

Symmetry codes: (i) −*x*+1, −*y*+1, −*z*+1.

3.3.3 Infrared and electronic spectra

IR spectra for all the complexes are shown in Fig. 3.8. Important IR bands for the ligands and zinc complexes are listed in Table 3.7. In contrast to complexes of salicylaldehyde thiosemicarbazone, the bands around 3380 cm^{-1} due to ν(O-H) are still seen in the spectra of the complexes indicating that only one the phenolic oxygen from the ligands are deprotonated and involved in coordination. The deprotonation of the hydrazinic proton in accordance with coordination of the sulfur atom in the thiolate form is shown by the disappearance of the ν(N(2)-H) band in the spectra of all the complexes. (West *et al.*, 1993; Latheef *et al.*, 2007, 2008; Seena and Kurup, 2007, 2008; Lobana *et al.*, 2008).

Coordination of the azomethine nitrogen is confirmed by the shift of ν(C=N) from 1620-1629 cm^{-1} to 1601-1604 cm^{-1}. The coordination of the thiolate sulfur is supported the decrease in frequency of the thioamide band found at around 1302-1331 cm^{-1} and 867-868 cm^{-1} to 1273-1327 and 800-848 respectively as reported by Campbell (1975). The bands from 1231-1241 cm^{-1} due to ν(C-O) decrease by 20-40 cm^{-1} upon coordination confirm the coordination of the phenolic oxygen to zinc. The decrease of all these bands is due to the decrease in electron density upon complexation to the metal. The ν(N-N) of the thiosemicarbazones is found at 1121-1166 cm^{-1}. Complexation will results in the increase in the frequency of this band upon due to the increase in the double bond character off-setting the loss of electron density via donation to the metal and is a confirmation of the coordination of the ligand through the azomethine nitrogen atom (Latheef *et al.*, 2007).

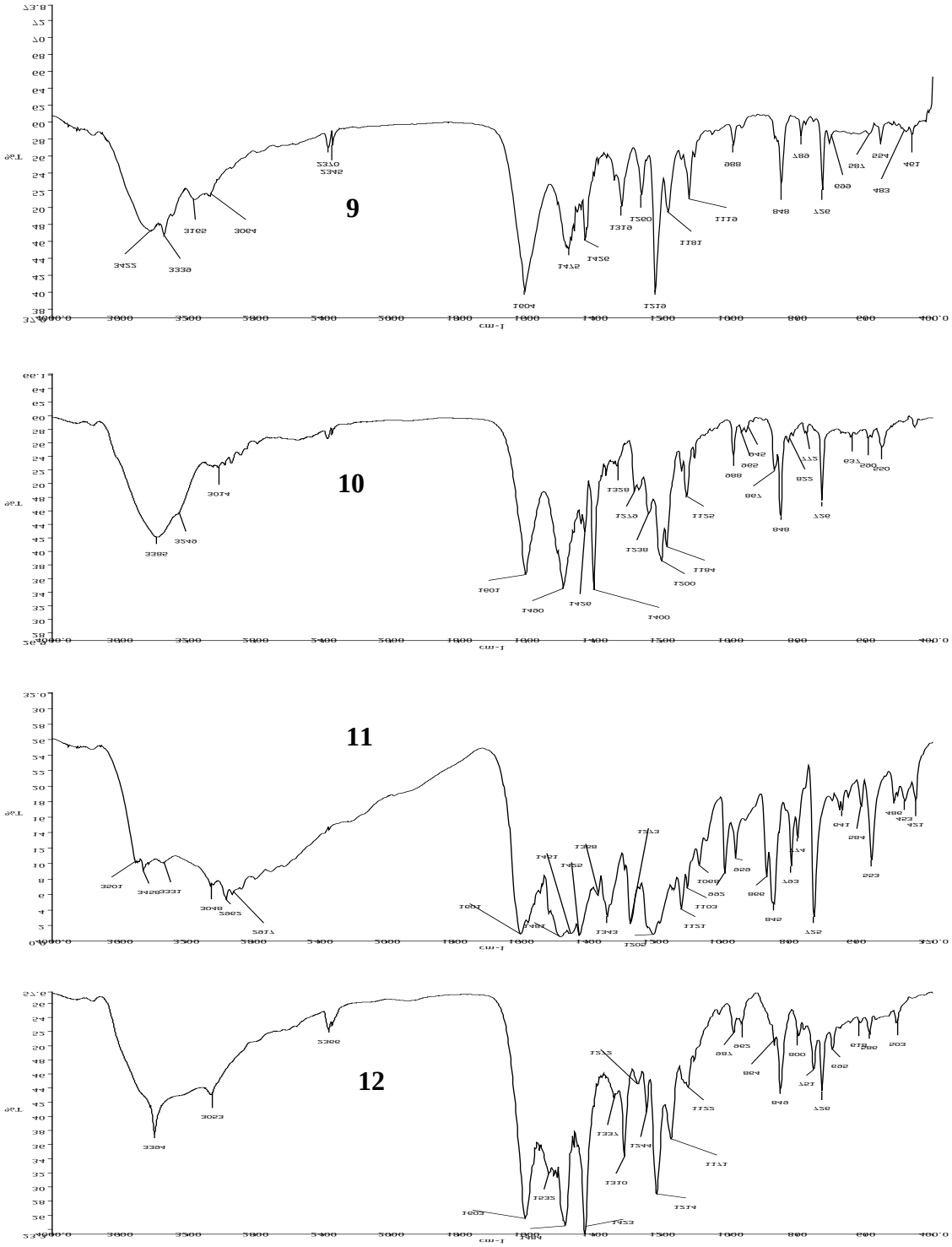

Fig. 3.8 IR spectra of the zinc complexes

Table 3.7

IR spectral assignments (cm^{-1}) for the ligands and their zinc(II) complexes

Compound	ν(C=N)	ν(C-O)	ν(N-N)	ν (C=S)/ ν (C-S)	ν(Zn-O)	ν(Zn-N)	Bands due to phenanthroline
H_3T **(1)**	1620	1239	1165	1379, 863	-	-	-
H_3M **(2)**	1625	1231	1166	1331,868	-	-	-
H_3E **(3)**	1626	1241	1166	1302, 867	-	-	-
H_3P **(4)**	1629	1264	1121	1323,838	-	-	-
[Zn(phen)(HT)].H_2O **(9)**	1604	1219	1181	1319, 848	554	426	1426, 726
[Zn(phen)(HM)].H_2O **(10)**	1601	1200	1184	1279, 848	550	430	1426, 726
[Zn(phen)(HE)].H_2O **(11)**	1601	1205	1121	1273, 845	554	421	1426, 726
[Zn(phen)(HP)].H_2O **(12)**	1603	1214	1171	1310, 800	503	-	1423, 726

The appearance of new ν(Zn-N) bands in the range of 421-426 cm^{-1} confirms the coordination through azomethine and polypyridine nitrogens. The presence of a new ν(Zn-O) band in the spectra of the complexes at 503-554 cm^{-1} is attributed to coordination of the phenolic oxygen (Latheef *et al.*, 2007; Seena and Kurup, 2008).

Electronic spectral assignments for the ligands and their zinc(II) complexes in DMF are presented in Table 3.8. All the ligands and the Zn(II) complexes have a ring (phenolic and diimine) π-π^* band at around 37,593 cm^{-1} (West *et al.*, 1995). No significant red shift is observed for these bands upon complexation (Swearingan and West, 2000). All the thiosemicarbazones also have two bands at around 32,985 cm^{-1} and 29,411 cm^{-1} due to n-π* transition of azomethine and thioamide function respectively. Upon complexation, the n-π* band of the thioamide function is shifted above 30,000 cm^{-1} due to thioenolization and merges with the azomethine n-π* band at around 31,348 cm^{-1}(Swearingan and West, 2000).

Thioenolization causes the weakening of the C=S bond. A moderately intense band in the range 26,178-27,174 found only in the spectra of all the complexes is assigned to Zn(II)→S metal to ligand charge transfer band (MLCT) (Latheef *et al.*, 2007; Swearingan and West, 2000). The MLCT band for Zn(II)→O shows line broadening that runs into the visible part of the spectrum. However, the maxima of this band is not observed probably due to the overlapping with the low energy side of Zn(II)→S transitions (Latheef *et al.*, 2007; Seena and Kurup, 2008). The absence of bands below 22,000 cm^{-1} due to d-d transitions is in accordance with the d^{10} electron configuration of Zn(II) ion (Latheef *et al.*, 2007; Seena and Kurup, 2008).

Table 3.8

Electronic spectral assignments (cm^{-1}) for the ligands and their zinc(II) complexes in DMF .

Compound	π-π^*	n-π^*	MLCT
H_3T (**1**)	37593	33003, 29411	
H_3M (**2**)	37593	33003, 29411	
H_3E (**3**)	37593	32895, 29240	
H_3P (**4**)	37453	32680, 28409	
[Zn(phen)(HT)].H_2O (**9**)	37313	31646	26881
[Zn(phen)(HM)].H_2O (**10**)	37313	31348	27100
[Zn(phen)(HE)].H_2O (**11**)	37593	31348	27174
[Zn(phen)(HP)].H_2O (**12**)	37453	30769	26178

3.3.4 ^{1}H NMR spectra

^{1}H NMR spectral assignments for the ligands and their zinc(II) complexes in DMSO are presented in Table 3.9. The absence of the N(2)H signal in the spectra of all the complexes indicates the deprotonation of the hydrazinic proton and supports the coordination of sulfur in the thiolate form. The integration for phenolic protons decreases from two to one upon complexation suggesting deprotonation of one of the phenolic group and coordination of the oxygen atom to zinc. Coordination of the azomethine nitrogen is confirmed by the downfield shift of the -CH=N signal from 8.20-8.34 ppm in the free ligands to 8.35-8.52 ppm in the spectra of the complexes due to a decrease in electron density around the proton of the azomethine linkage. Signal broadening resulted in inaccurate integration for these signals unlike those reported by Latheef *et al.* (2007) and observed by us in the bypyridine derivatives (chapter 2). However, the presence of the 1,10-phenanthroline moiety is supported by elemental analyses, IR spectroscopy and confirmed by the crystal structures of **9a** and **11a**. None of the complexes are sufficiently soluble in DMSO to record acceptable ^{13}C spectra.

Table 3.9

^{1}H NMR spectral assignments for the ligands and their zinc(II) complexes in DMSO

Compound	Chemical shifts, δ (ppm)					
	N(2)H	OH	N(4)H	CH=N	Aromatic	Aliphatic
H_3T **(1)**	11.14 (s, 1 H)	9.74 (s, 2 H)	7.92 (s, 1 H) 7.65 (s, 1 H)	8.20 (s, 1 H)	7.62 (d, 1 H) 6.25 (s, 1 H) 6.22 (d, 1 H)	-
H_3M **(2)**	11.79	9.88 (s, 1 H)	8.24 (t, 1 H)	8.20	7.67 (d, 1 H)	2.95 (d, 3 H)

	(s, 1 H)	9.74 (s, 1 H)		(s, 1 H)	6.26 (s, 1 H)	N-C**H$_3$**
					6.24 (d, 1 H)	
H_3E **(3)**	11.16	9.76 (s, 2 H)	8.31 (t, 1 H)	8.26	7.72 (d, 1 H)	3.57 (m, 2H) NC**H$_2$**
	(s, 1 H)			(s, 1 H)	6.32 (s, 1 H)	1.14 (t, 3H)
					6.30 (d, 1 H)	NCH_2C**H$_3$**
H_3P **(4)**	11.54	9.93 (s, 1 H)	8.72 (s, 1 H)	8.34	7.82 (d, 1H)	-
	(s, 1 H)	9.89 (s, 1 H)		(s, 1 H)	7.53 (d, 2H)	
					7.33 (t, 2H)	
					7.16 (t, 1H)	
					6.29 (s, 1H)	
					6.27 (d, 1H)	
[Zn(phen)(HT)].H_2O **(9)**	Not sufficiently soluble in DMSO					
[Zn(phen)(HM)].H_2O **(10)**	-	9.04 (s, 1 H)	6.21(s, 1 H)	8.39	8.89 (s, 2 H)	2.73 (d, 3 H)
				(s, 1 H)	8.78 (s, 2 H)	N-C**H$_3$**
					8.15 (s, 2 H)	
					8.02 (s, 2 H)	
					6.95 (d, 1 H)	
					5.66 (s, 1 H)	
					5.88 (d, 1 H)	

Compound	Chemical shifts, δ (ppm)					
	N(2)H	OH	N(4)H	CH=N	Aromatic	Aliphatic
[Zn(phen)(HE)].H_2O **(11)**	-	8.99 (s, 1 H)	6.16 (s, 1 H)	8.35	8.86 (s, 2 H)	3.21 (m, 2H) NC**H$_2$**
				(s, 1 H)	8.77 (s, 2 H)	1.01 (t, 3H)
					8.13 (s, 2 H)	NCH_2C**H$_3$**
					8.02(s, 2 H)	
					6.92 (d, 1 H)	
					5.62 (s, 1 H)	
					5.85 (d, 1 H)	
[Zn(phen)(HP)].H_2O **(12)**	-	9.15 (s, 1 H)	8.56 (s, 1 H)	8.52	8.95 (s, 2 H)	-
				(s, 1 H)	8.80 (s, 2 H)	
					8.17 (s, 2 H)	
					8.03(s, 2 H)	

	7.81 (d, 2 H)
	7.18 (t, 2 H)
	7.04 (d, 1 H)
	6.82 (t, 1 H)
	5.91 (d, 1 H)
	5.67 (s, 1 H)

Table 3.9 continued

3.3.5 DNA binding.

3.3.5.1 Duplex DNA

The interaction of complexes **10** and **11** with (i) duplex DNA of various specified nucleotide sequences, and (ii) quadruplex DNA of the 23-mer oligonucleotide 5'-$AG_3(T_2AG_3)_3$-3' and its corresponding duplex were investigated by using CD spectroscopy. Complexes **9** and **12** could not be studied due to limited solubility in DMF and buffer mixtures.

Each of the CD spectra of all the duplex DNA show a negative band at ~250 nm due to DNA with right helicity and a positive band at ~275 nm due to base-pair stacking interaction, confirming the B-form conformation of these duplexes (Table 3.10). These bands are very useful in studying small molecules interacting with DNA because simple groove binding and electrostatic interaction of small molecules show less or no perturbation on the base-stacking and helicity bands, while intercalation enhances the intensities of both the bands due to stabilization of the right-handed B conformation of DNA (Maheswari and Palaniandavar, 2004).

As in chapter 2, the first investigation was to find out the DNA binding preference for CG or AT sequences by zinc complexes **10** and **11** (Table 3.10). Complex **10** at a complex:duplex ratio of 1:8 causes a significant change to the CD spectrum of ds$(AT)_6$. Complex **10** induces a decrease in the negative band and a drastic increase of the positive band accompanied by a red shift of 5 nm from 270 nm (Fig. 3.9). Similar changes with greater magnitude are observed for complex **11** with a red shift of the positive band from 270 nm to 276 nm in the Cd spectrum of ds$(AT)_6$ (Fig. 3.10). These changes are consistent with **a** change of confirmation from B-like to A-like which is surprisingly not observed in its 2,2'-bipyridine analog (complexes **6** and **7**) (Maheswari and Palaniandavar, 2004). Since complexes **10** and **11** induced similar conformation changes to ds$(AT)_6$, we can compare their binding strength to AT rich sequence based on the changes in intensity of the positive band in the CD spectra. The increase in intensity of the positive band for complex **11** (62%) is much greater compared to complex **10** (18%). This suggests that complex **11** binds more strongly to ds$(AT)_6$. Seng *et al.* (2009) have studied the binding selectivity of bis(3-methylpicolinato)(1,10-phenanthroline)-zinc(II), [Zn(3-Me-pic)$_2$(phen)] towards ds(oligonucleotide) with different base sequences by using CD and ethidium bromide displacement assay (binding constant determination). The greater enhancement of positive band in the CD spectra seems to be directly proportional to the apparent binding constant obtained from ethidium bromide displacement assay for [Zn(3-Me-pic)$_2$(phen)], towards different ds(oligonucleotide).

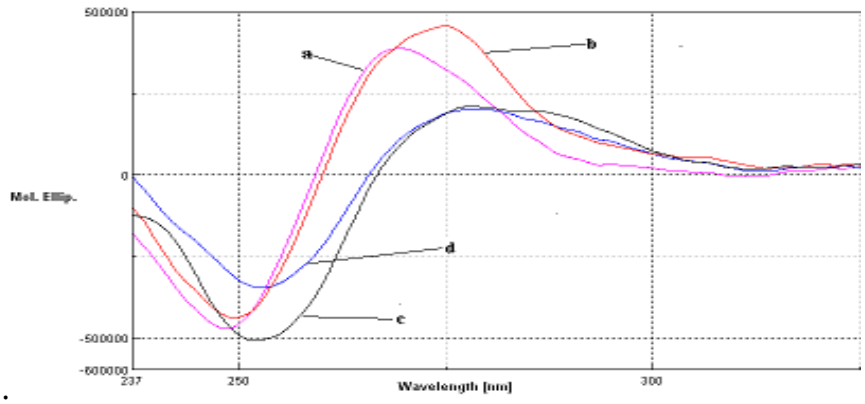

Fig. 3.9 CD spectra of 15 μM of oligonucleotide in the absence and presence of 120 μM of complex **10**; (a) ds(AT)$_6$ alone, (b) ds(AT)$_6$ with complex **10,** (c) ds(CG)$_6$ alone and (d) ds(CG)$_6$ with complex **10.**

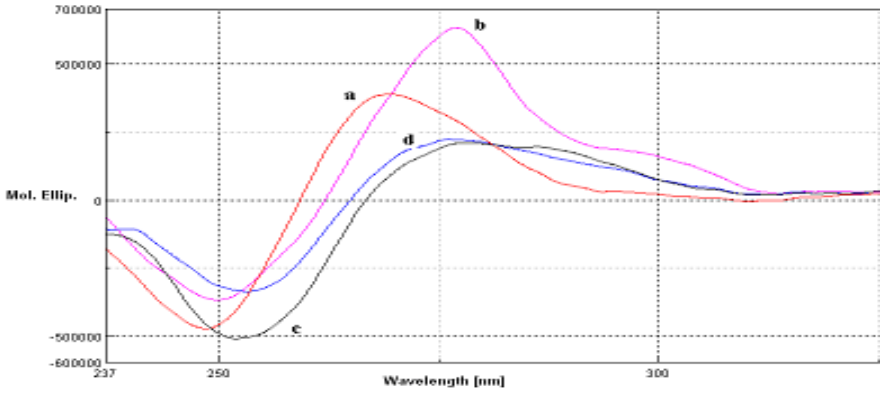

Fig. 3.10 CD spectra of 15 μM of oligonucleotide in the absence and presence of 120 μM of complex **11**; (a) ds(AT)$_6$ alone, (b) ds(AT)$_6$ with complex **11,** (c) ds(CG)$_6$ alone and (d) ds(CG)$_6$ with complex **11**

On the other hand, complexes **10**, Zn(phen)(HM), and **11**, Zn(phen)(HE), show a significant decrease in the negative band (helixcity) of the CD spectrum of ds(CG)$_6$ without appreciable changes to the positive band. Similar observations have been reported for complex **6**, Zn(bipy)(HM). However, complex **7**, Zn(bipy)(HE) does not induce such changes. The distinct differences in their interactions with DNA between complex **7,** Zn(bipy)(HE) and complex **11**, Zn(phen)(HE) derived from H_3E suggest that the presence

of the 1,10-phenanthroline moiety can also alter mode of binding as well as the ability of a complex in recognizing different DNA sequences. By comparing the changes of the positive and negative bands in the CD spectra of the CG and AT rich sequences, we can infer that complexes **10** and **11** can effectively differentiate CG from AT rich sequence base on their different mode of interaction with the DNA. Since three out of four zinc complexes in our study derived form alkyl substituted thiosemicarbazone induced similar unwinding of ds$(CG)_6$, it is possible that the alkyl substituent at the N(4) position plays a key role in recognizing CG rich sequence.

We next utilised oligonucleotides such as ds$(CGCGAATTCGCG)_2$ (referred to as AATT sequence) and ds$(CGCGATATCGCG)_2$ (referred to as ATAT sequence) to investigate any binding preferences in interactions with duplex DNA as the sequence on each chain is varied from non-alternating to alternating purine-pyrimidine bases in grooves of the duplex. For the AATT sequence (Fig. 3.11), complex **10** causes a respective decrease and increase in the negative and positive bands of the CD spectra of the duplex which correspond to conformational change from B to ψ, which we mentioned earlier (Maheswari and Palaniandavar, 2004; Seng *et al.* 2008). This observation also suggests partial intercalation of complex **10** to the duplex. However, complex **11** shows a decrease in the negative band without significant changes to the positive band. This indicates that complex **11** binds to the AATT sequence and causes the unwinding of the DNA similar to its interaction with ds$(CG)_6$ discussed earlier. For the interaction with ATAT rich sequence, complex **10** and **11** show an increase for both the positive and negative bands which is consistent with intercalation mode of binding to DNA (Maheswari and Palaniandavar,

2004; Seng *et al*. 2008). Greater enhancement of the positive band by complex **11** suggests that it binds more strongly to the ATAT sequence compared with complex **10**. Comparing the results for interactions with AATT and ATAT sequence, we can infer that complex **10** and **11** can differentiate ATAT from AATT sequence (Seng *et al*. 2009).

Comparing the CD results of these four ds(oligos)$_2$, we can conclude that complex **10**, Zn(phen)(HM) and **11**, Zn(phen)(HE) can differentiate ds(oligonucleotide) with different base sequences. However, the order of selectivity for each ds(oligonucleotide) is not clear since the complex can induce different conformational changes to oligonucleotides with different base sequences. In addition, we also noticed that complex **11** always induces greater changes (%) to the CD spectra of the four ds(oligos)$_2$ when compared with complex **10**. This may be attributed to the higher hydrophobicity of complex **11** with an ethyl substituent**.** This observation again underscores the role of hydrophobicity in enhancing drug-DNA interactions (Talib *et al.* 2008; Maheswari *et al.* 2006).

We postulate that the observed DNA recognition is conferred by the ability of the complexes to form hydrogen bonds with the DNA through various hydrogen donor and acceptor groups on the thiosemicarbazone moiety. The different length of the alkyl group of the N(4)-substituent seems to be responsible in DNA recognition through hydrophobic interaction or grooves binding because each complex has substituent with different hydrophobicity. The size of the molecules and the orientation of different substituted bulky

group in space may affect their ability to bind into the groove (major or minor) with different cavity size or steric hindrance.

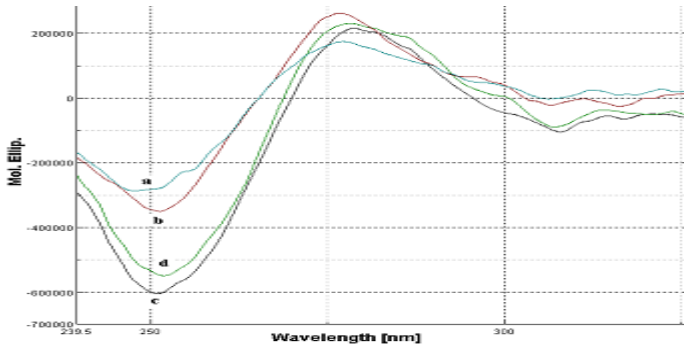

Fig. 3.11 CD spectra of 10 μM of oligonucleotides in the absence and presence of 120 μM of complex **10**; (a) ds(CGCGATATCGCG)$_2$ alone, (b) ds(CGCGATATCGCG)$_2$ with complex **10,** (c) ds(CGCGAATTCGCG)$_2$ alone, and (d) ds(CGCGAATTCGCG)$_2$ with complex **10.**

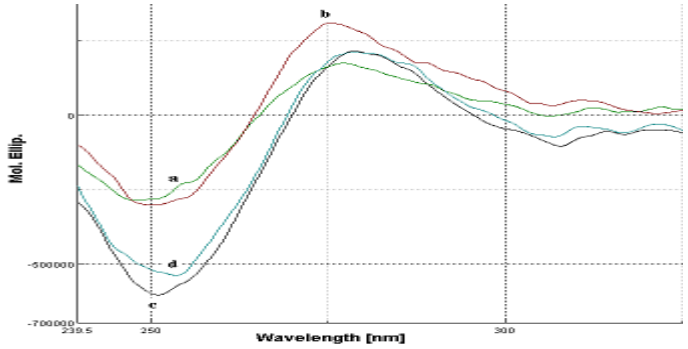

Fig. 3.12 CD spectra of 10 μM of oligonucleotides in the absence and presence of 120 μM of complex **11**; (a) ds(CGCGATATCGCG)$_2$ alone, (b) ds(CGCGATATCGCG)$_2$ with complex **11,** (c) ds(CGCGAATTCGCG)$_2$ alone, and (d) ds(CGCGAATTCGCG)$_2$ with complex **11**.

3.3.5.2 G-quadruplex and guanine-rich duplex

As mentioned in section 2.3.5, the guanine-rich region of DNA such as in human telomeric DNA, can be folded into higher-order DNA structure known as G-quadruplex under physiological (ionic) conditions (Burge *et al.* 2006). There is growing interest in complexes

that can induce or stabilize quadruplex structure due to the discovery that these complexes can lead to inhibition of telomerase (Neidle and Parkinson, 2002). Even though most of these initial studies involve the interaction of quadruplex with organic molecules having aromatic rings (Pivetta *et al.* 2008; White et al. 2007; Yamashita *et al.* 2005; Nagesh and Krishnaiah, 2003), increasing interest regarding interaction with metal complexes has been observed in recent publications (Reed *et al.* 2009; Pierce *et al.* 2009; Arola and Vilar, 2008; Arola *et al.* 2008). A peculiar similarity among these complexes is most them involve metal complexes containing phenanthroline that may favour π-π stacking interactions with the guanine quartet (Reed *et al.* 2009 and 2007; Musetti *et al.* 2009; Talib *et al.* 2008; Shi *et al.* 2008). We are curious whether interactions of metal complexes containing phenanthroline with G-quadruplex can be improved with the presence of a secondary ligand such as a thiosemicarbazone.

The CD spectra of the 20 μM of the antiparallel G-quadruplex 5'-$AG_3(T_2AG_3)_3$-3' with complexes of **10** and **11** (120 μM) were monitored. The intensity of the positive band for G-quadruplex at 296 nm is greatly enhanced while the negative band at 265 nm also increases in intensity upon addition of complexes **10** and **11**. A blue shift of 3 nm is observed for the negative band at 265 nm. Furthermore, an induced peak at 280 nm is observed for the interaction of both complexes with G-quadruplex. This induced peak may be attributed to presence of an additional chromophore on the chiral DNA backbone upon strong binding of the complex to DNA. The presence of an induced CD signal is commonly observed in binding of achiral porphyrins to chiral DNA (Yamashita *et al.* 2005). The overall shape of the G-quadruplex remains unchanged, suggesting retention of the antiparallel structure (Fig. 3.13, Table 3.10).

Table 3.10
CD spectral bands of duplex oligo or quadruplex + copper complex: wavelength, λ (molar ellipcity)

	λ/nm (molar ellipcity)	
	(-) band	(+) band
15 μM ds$(AT)_6$	248 (-472333)	270 (389404)
15 μM ds$(AT)_6$ + 120 μM complex **10**	249 (-438211)	275 (458228)
15 μM ds$(AT)_6$ + 120 μM complex **11**	250 (-366571)	276 (633852)
15 μM ds$(CG)_6$	253 (-346082)	278 (211135)
15 μM ds$(CG)_6$ + 120 μM complex **10**	253 (-568230)	280 (203041)
15 μM ds$(CG)_6$ + 120 μM complex **11**	253 (-335693)	276 (224090)
10 μM ds$(CGCGAATTCGCG)_2$	251 (-603665)	279 (215560)
10 μM ds$(CGCGAATTCGCG)_2$ + 120 μM complex **10**	252 (-584490)	278 (230681)
10 μM ds$(CGCGAATTCGCG)_2$ + 120 μM complex **11**	252 (-537811)	279 (213212)
10 μM ds$(CGCGATATCGCG)_2$	248 (-286559)	277 (174875)
10 μM ds$(CGCGATATCGCG)_2$ + 120 μM complex **10**	251 (-349413)	276 (262921)
10 μM ds$(CGCGATATCGCG)_2$ + 120 μM complex **11**	250 (-302377)	275 (310441)
20 μM G-duplex	250 (-82682)	279 (283975)
20 μM guanine-rich duplex+ 120 μM complex **10**	252 (-32694)	279 (175916)
20 μM guanine-rich duplex+ 120 μM complex **11**	251 (-145729)	280 (603383)
20 μM G-quadruplex	265 (-151753)	247 (75789) 295 (161061)
20 μM G-quadruplex + complex **10**	262 (-232022)	245 (27533) 280 (248906) 295 (273842)
20 μM G-quadruplex + complex **11**	262 (-229848)	245 (45920) 280 (333735) 295 (309068)

Guanine-rich duplex =(5'-CCAGTTCGTAGTAGTAACCC-3')·(3'-GGTCAAGCATCATCATTGGG-5')

The possibility of the formation of a mixture of parallel and antiparallel components or G-quadruplex structures is ruled out because the induced positive peak is at 280 nm and not at 272 nm which is characteristic of parallel structure. Furthermore, there is a significant increase in the negative band at 262 nm that disagreed with the formation of parallel structure. Therefore, it is very likely that the induced peak at 280 nm is from the strong absorbance of the complex at 267 nm (Shi *et al.* 2008).

Shi et al. (2008) have suggested that the induced CD signal that they observed at 272 nm may be induced through the strong absorbance of $Ru_2(obip)L_4$ (obip = 2-(2-pyridyl)imidazo[4,5-*f*][1,10]-phenanthroline) at about 280 nm.

The enhancement of the positive band at 296 nm due to G-G base stacking suggests partial intercalation of phenanthroline between G-tetrads by the zinc complex similar to enhancement of positive, base-base stacking band at ~270 nm attributed to intercalation of the B-form duplex DNA. This observation is in contrast to those observed for the interactions of acridine and bis-acridine with G-quadruplex where the decrease in the intensity of the positive band at 293 nm was interpreted as destabilization of the quadruplex structure (Nagesh *et al.* 2003). Thus, enhancement of the positive band of the CD spectrum of the present quadruplex suggests stabilization of the antiparallel quadruplex structure by our zinc complexes as suggested by Musseti *et al.* (2009). The greater enhancement of the positive band at 295 nm in contrast to its 2,2'-bipyridine analog (chapter 2) implies that the presence of an extended aromatic ring on the phenanthroline moiety enhances the ability of the complex to bind to the quadruplex structure through intercalation. The greater enhancement of the positive band for complex **11** compared with complex **10** suggests that complex **11** binds more strongly to the G-quadruplex. This may be attributed to the presence of a more hydrophobic ethyl group in complex **11** in contrast to the methyl group at the N(4) position in complex **10**.

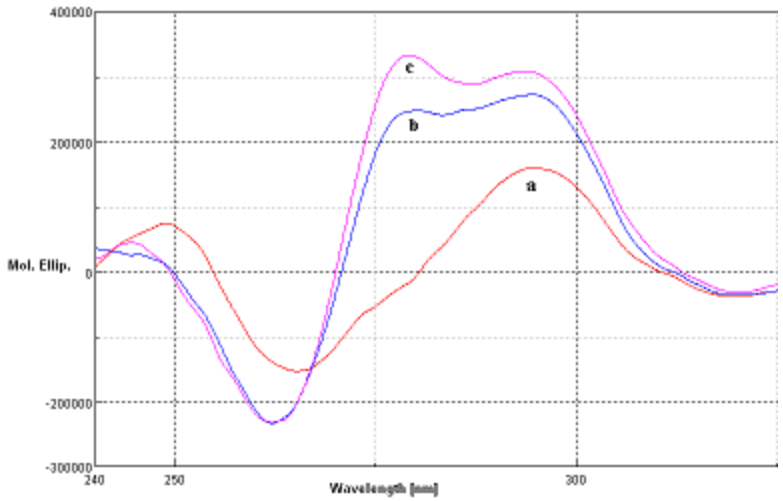

Fig. 3.13 CD spectra of 20 μM of G-quadruplex in the absence and presence of 120 μM of complex; (a) G-quadruplex alone, (b) G-quadruplex with complex **10**, (c) G-quadruplex with complex **11**

Talib *et al.* (2008) found that ruthenium(II) complexes with known intercalating ligands, viz. $[Ru(phen)_2(dpqC)]^{2+}$, $[Ru(phen)_2(dpq)]^{2+}$, $[Ru(phen)_2(dppz)]^{2+}$ and $[Ru(phen)_3]^{2+}$ complexes have higher binding affinity towards duplex DNA than towards quadruplex. This has prompted us to carry out preliminary investigation regarding the interaction of complexes **10** and **11** with guanine-rich duplex DNA annealed from two complementary 17 bp primers, 5'-CCAGTTCGTAGTAACCC-3' and 3'-GGTCAAGCATCATTGGG-5'. Complex **10** (Fig. 3.14, Table 3.10) induces a great decrease in both the positive and negative bands. This indicates that complex **10** binds to guanine-rich duplex and the binding leads to conformational change from B like to Z (Mahadevan and Palaniandavar, 1996). Complex **11** (Fig. 3.14, Table 3.10) shows drastic increase in both the positive and negative bands which indicates strong intercalation to the guanine-rich duplex (Maheswari and Palaniandavar, 2004). These observations again

illustrate the ability of the N(4) substituent in altering the interaction of the zinc complex with DNA.

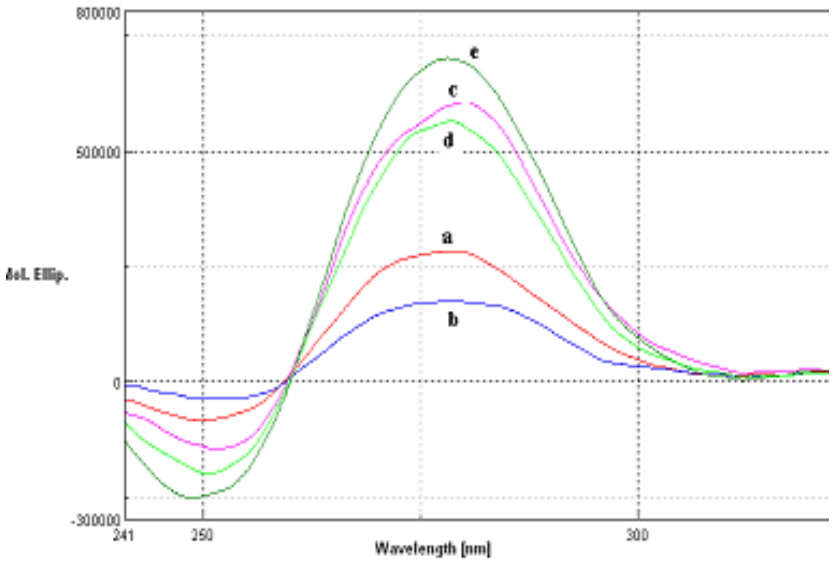

Fig. 3.14 CD spectra of 20 μM of guanine-rich duplex in the absence and presence of 120 μM of complex; (a) guanine-rich duplex alone, (b) guanine-rich duplex with complex **10**, (c) guanine-rich duplex with complex **11,** (d) guanine-rich duplex with complex **18** and (e) guanine-rich duplex with complex **19**

By comparing the extent of changes induced in both the positive and negative bands of G-quadruplex and guanine-rich duplex when they interact with the complexes, we cannot conclude the selectivity of the complexes towards different DNA structures. This is attributed to the difference in conformational changes of quadruplex and duplex DNA upon binding to the complexes. The selectivity towards different DNA structures can be easily determined with CD if the complexes only bind to either duplex or quadruplex structure. The selectivity can also be determined if the complex induced similar conformational changes to quadruplex and duplex DNA. When the conformational changes are the same, the strength of binding to the DNA structure can be derived by comparing the percentage

changes in either the positive or negative band of the CD spectra. However, we can still conclude that complexes **10** and **11** can differentiate guanine-rich duplex structure from G-quadruplex.

3.3.6 Nucleolytic study

As in chapter 2, we similarly examine the ability of complexes **10** and **11** to cleave pBR322 under hydrolytic conditions and in the presence of exogenous agents, sodium ascorbate and hydrogen peroxide, using gel electrophoresis. Complexes **9** and **12** could not be studied due to their limited solubility in DMF and other buffer mixtures. Incubating the zinc complexes with pBR322 at varying concentrations of the zinc complex (10 – 1000 μM) for 24 h at 37 ^{o}C, slight DNA cleavage was observed for complexes **10** (Fig. 3.15, Lane L8 & L9) and **11** (Fig. 3.16: Lane L5, L8 & L9). Complexes **10** and **11** can cleave the DNA at 500 μM with the appearance of a nicked band with very low intensity. Interestingly, complex **11** started to show very weak cleavage at 10 μM (Fig. 3.16: Lane L5) that diminished at 50 and 200 μM. The exact nature of this cleavage at such low concentrations is not clear but it could be attributed to slight dissociation of the complex to another species.

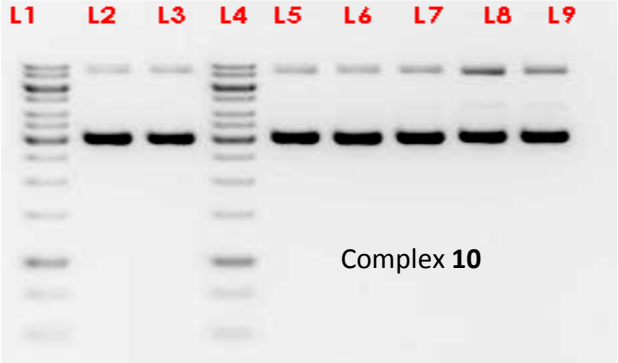

Fig. 3.15 Electrophoresis results of incubating pBR322 (0.5 μg/μL) in the presence of complex **10** in TN buffer (5 mM Tris, 50 mM NaCl) pH 7.5 at 37 ^{o}C for 24 h. L1 & L4, gene ruler 1 Kb DNA ladder; L2, DNA alone; L3, DNA + 1000 μM $ZnCl_2$; DNA + various complex concentrations L5-L9: L5, 10 μM; L6, 50 μM; L7, 200 μM; L8, 500 μM; L9, 1000 μM.

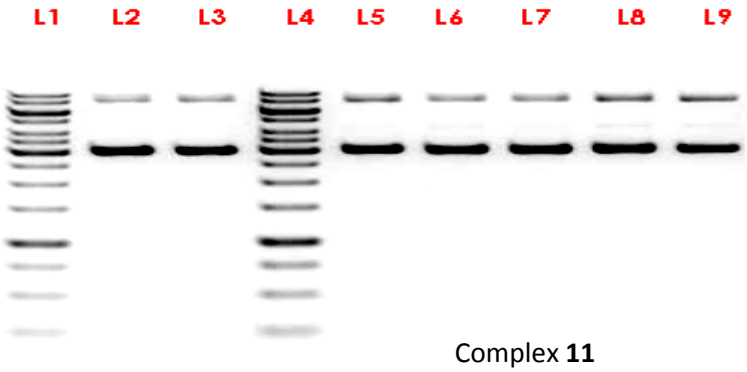

Fig. 3.16 Electrophoresis results of incubating pBR322 (0.5 μg/μL) in the presence of complex **11** in TN buffer (5 mM Tris, 50 mM NaCl) pH 7.5 at 37 ^{o}C for 24 h. L1 & L4, gene ruler 1 Kb DNA ladder; L2, DNA alone; L3, DNA + 1000 μM $ZnCl_2$; DNA + various complex concentrations L5-L9: L5, 10 μM; L6, 50 μM; L7, 200 μM; L8, 500 μM; L9, 1000 μM.

When the DNA was incubated with 300 μM of zinc complex in the presence of 30 μM sodium ascorbate or 30 μM hydrogen peroxide no activation of zinc complexes towards DNA cleavage by sodium ascorbate or hydrogen peroxide is observed as the gel pattern is the same as that for DNA alone (results not shown). No cleavage was observed even when

the concentration of hydrogen peroxide was varied from 250 μM to 500 μM by maintaining the complex concentration at 300 μM (results not shown).

3.3.7 Topoisomerase I inhibition assay

Of the four complexes **9-12**, only complexes **10** and complex 11 can be studied due to solubility problem (see previous section). As a preliminary investigation into the mechanism of action of topo I inhibition by **10** and **11**, we used three variations of mixing the DNA, topo I and the zinc complexes (at 40 μM). When the three components are mixed simultaneously for complex **10**, there is slight inhibiton of topo I as seen by the presence of various bands of DNA with different degree of relaxation between Form I and Form II (Fig. 3.17, lane L5). Secondly, when complex **10** was incubated first with topo I before the addition of DNA; the intensity of the slowest moving band (Form II) was the lowest suggesting best inhibition of topo I (Fig. 3.17, lane L6). Further, when the DNA is first incubated with complex **10** for 30 minutes before adding the topo I (Fig. 3.17, lane L7), the fastest moving band (Form I) almost totally disappears. The intensity of Form II is slightly lower compared to lane L5 but slightly higher than lane L6. This implies that the degree of topoisomerase inhibition is intermediate between those observed for the first and second methods of mixing. Therefore the order of topoisomerase inhibition decreases with the following sequence of mixing; (b) > (c) > (a) (Fig. 3.17).

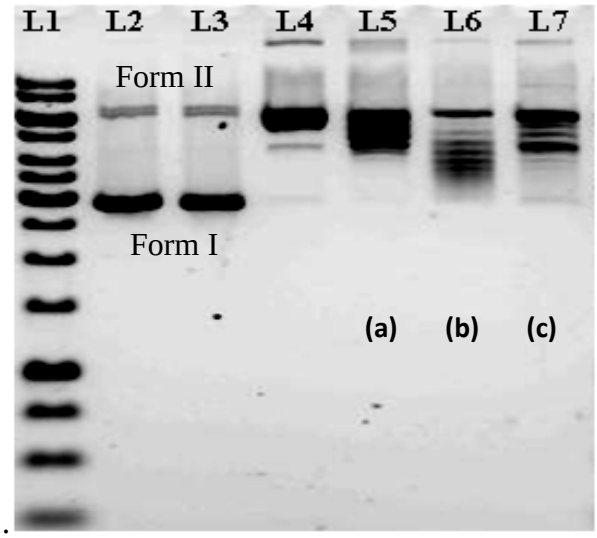

Fig. 3.17 Effect of sequence of mixing for the human topoisomerase I inhibition assay of complex **10**. Electrophoresis results of incubating human topoisomerase I (1 unit/21μL) with pBR322: Lane 1, 1 kb DNA ladder; Lane 2, Plasmid DNA pBR 322 (control); Lane 3, DNA + 40μM complex (control); Lane 4, DNA+ 1 unit Human Topoisomerase I (control); (a) All components mixed at the same time; Lane 5, DNA + 40μM complex + 1 unit Human Topoisomerase I ; (b) Complex + TopoI incubated for 30 minutes first before DNA is added; Lane 6, DNA + 40μM complex + 1 unit Human Topoisomerase I; (c) Complex + DNA incubated for 30 minutes first before TopoI is added; Lane 7, DNA + 40μM complex + 1 unit Human Topoisomerase I

When the experiment was repeated with complex **11**, a similar order of inhibitions is seen. However, complex **11** (Fig. 3.18, lane L6) shows better topoisomerase I inhibition activity when compared with complex **10**, (Fig. 3.17, lane L6) as seen from the greater intensity in the fastest moving band (Form I) and lower intensity in the slowest moving band (Form II). The disappearance of the fastest moving band (Form I) for complex **10**, (Fig. 3.17, lane L6) further supports better inhibition of topoisomerase I by complex **11**. Unlike complexes **10** and **11**, its 2,2'-bipyridine analogs (complex **6** and **7**) do not show any topoisomerase inhibition. This shows that incorporation of a 1,10-phenanthroline moiety in the ternary zinc complex has led to improvement in topoisomerase inhibition, most probably owing to its improved binding strength to AT rich sequence.

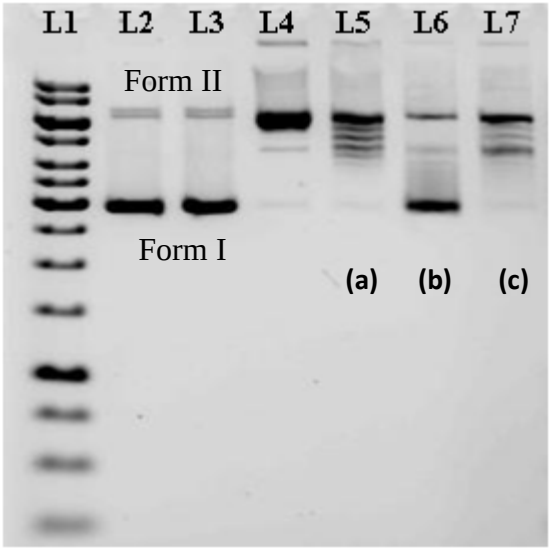

Fig. 3.18 Effect of sequence of mixing for the human topoisomerase I inhibition assay of complex **11**. Electrophoresis results of incubating human topoisomerase I (1 unit/21µL) with pBR322: Lane 1, 1 kb DNA ladder; Lane 2, Plasmid DNA pBR 322 (control); Lane 3, DNA + 40µM complex (control); Lane 4, DNA+ 1 unit Human Topoisomerase I (control); (a) All components mixed at the same time; Lane 5, DNA + 40µM complex + 1 unit Human Topoisomerase I ; (b) Complex + TopoI incubated for 30 minutes first before DNA is added; Lane 6, DNA + 40µM complex + 1 unit Human Topoisomerase I; (c) Complex + DNA incubated for 30 minutes first before TopoI is added; Lane 7, DNA + 40µM complex + 1 unit Human Topoisomerase I

These observed differences in inhibition of topo I suggest initial binding of the zinc complex to either the topo I or the DNA give rise to differences in mode of action. Therefore, two pathways of toposisomerase inhibition are suggested, one involves the binding of complex to DNA while the other involves the binding to toposiomerase. By comparing lanes L6 and L7, we infer that since greater inhibition of topo I is observed when the complex is incubated with topo first, the inhibition process involving the binding of the complex to the topoisomerase enzyme may be a more dominant pathway. However, further investigation is crucial to confirm this.

3.3.8 Antibacterial and antifungal assays

3.3.8.1 Antibacterial activity

The antibacterial activity of the ligands and complexes **10** and **11** were assessed against two species of Gram positive bacteria and four species of Gram negative bacteria (Table 3.11). Complexes **9** and **12** could not be studied due to limited solubility in DMF and buffer mixture.

Table 3.11.

Mean MIC value (μg/mL) towards microbes tested.

Complex	Bacteria					
	S. aureus	*B. cereus*	*P. aeruginosa*	*K. pneumoniae*	*E. coli* (penicillin-sensitive strain)	*E. coli* (penicillin-resistant strain)
1	62.50	62.50	62.50	62.50	62.50	62.50
2	125	62.50	125.00	62.50	62.50	62.50
3	62.50	62.50	62.50	62.50	62.50	62.50
4	62.50	31.25	62.50	31.25	62.50	62.50
10	62.50	31.25	52.08±18.04	31.25	62.50	62.50
11	62.50	15.63	31.25	31.25	31.25	31.25
$ZnCl_2$	-	-	-	-	-	-
phen	62.50	15.63	15.63	15.63	15.63	15.63
Drug	8.00	4.00	4.00	4.00	4.00	4.00

" - " : no activity . Drug used in antibacterial assay = Chloramphenicol

All thiosemicarbazones ligands are less potent than 1,10-phenanthroline ligand since their MIC values are either two times or much higher than 1,10-phenanthroline alone.

Complex **10**, Zn(phen)(HM) shows improved antibacterial activity towards *B. cereus*, *P. aeruginosa* and *K. pneumoniae* compared with its free thiosemicarbazone ligand (H_3E)(Table 3.11). On the other hand, complex **11**, Zn(phen)(HE) shows improvement in antibacterial activity towards all the strains in our study except for *S. aureus* when compared to ligand **3**, H_3E. However, the MIC values for both complexes are higher than the free 1,10-phenanthroline ligand for all the bacteria except for complex **11** against *B. cereus*. This implies that the ternary complexes did not achieve the desired improvement in antibacterial activity because its potency did not surpass both Schiff base and 1,10-phenanthroline ligands. However, complex **11** with a more hydrophobic ethyl chain still shows better antibacterial activity for most of the bacteria strains when compared with complex **10** with a methyl chain. Furthermore, complexes **10** and **11** also show better antibacterial activity than their 2,2'-bipyridine analog probably owing to the increase in hydrophobicity, stronger binding to AT rich sequences and topoisomerase I inhibition capability of these complexes that resulted from substitution of 2,2'-bipyridine with 1,10-phenanthroline. Recently, Mazumder *et al.* (2004) have studied the antibacterial activity of some mononuclear ruthenium complexes with the general formula of $[Ru(B)_2L]Cl_2$ (B = 1,10-phenanthroline or 2,2'-bipyridine; L = aze = acetazolamide; r-tsc = 4-substituted thiosemicarbazides; nmit = *N*-methyl-isatin-3-thiosemicarbazone and icpl = isatin-3-(4-chlorophenyl) thiosemicarbazone). They found that 1,10-phenanthroline imparted greater biological activity to the complexes than their 2,2'-bipyridine containing analogs. In addtition, complexes bearing bulky ligands such as nmit and icpl were found to be more biologically active than complexes with aze. Thus, it seems that the antibacterial activity of the complexes is influenced by size and the substituent groups in the ligands as reported by us.

Since the site of action of thiosemicarbazone is ribonucleotide reductase (RR) (Finch *et al.* 1999), one of the possible mechanisms of the present compounds could be inhibition of DNA synthesis by controlling the inhibition of RR as suggested by Pandeya *et al.* (1999). RR is responsible in catalyzing the reduction of the 2-carbon atoms of the D-ribose portion of the ribonucleotide directly reduced to form the 2-deoxyribonucleotides derivative. Inactivation of RR in general leads to the reduction of intracellular pools of deoxyribonucleotides and that will affect the biosynthesis of DNA and thus the death of the bacteria.

The antibacterial activity of both complexes **10** and **11** can be attributed to their ability to inhibit toposiomerase I. Toposiomerase I has been gaining popularity lately as a good target for the development of antibacterial drug (Tse-Dinh, 2009). This could be attributed to the success of the currently marketed inhibitors such as the quinolones dervatives (Bradbury and Pucci, 2008).

3.3.8.2 Antifungal activity

The antifungal activity of the ligands and complexes **10** and **11** were assessed against four species of fungi. Complexes **9** and **12** could not be studied due to limited solubility in DMF and buffer mixture. All ligands and complexes had some degree of inhibitory activity against the fungi tested (Table 3.12).

Complex **10** only shows marked improvement in antifungal activity towards *C. neoformans* with MIC value of 7.81 µg/mL when compared with 1,10-phenanthroline and its free thiosemicarbazone ligand. Whereas, complex **11** shows improvement in antifungal properties towards *C. neoformans* and *A. niger*. In general, antifungal activity of complex **11** is better than complex **10** towards *C. parapsilosis* and *A.niger*. This again shows that the presence of a longer alkyl chain in complex **11** makes it a better antifungal agent than complex **10 f**or *C. parapsilosis* and *A. niger* fungal strain. The ability of complexes **10** and **11** in inhibiting *A. niger* is noteworthy since other ligands and complexes derived from salicylaldehyde thiosemicarbazones are inactive towards this strain (Valdes-Martinez *et al.* 1996**).** Both complexes show very good antifungal property towards *C. neoformans* with MIC value of 7.81 µg/mL. Complexes **10** and **11** also have lower MIC value compared with their 2,2'-bipyridine analogs. This implies that the presence of the phenantroline moiety can also lead to improvement in antifungal activity**.**

Table 3.12.
Mean MIC value (µg/mL) towards fungi tested.

Compound	Fungi			
	C. albicans	*C. parapsilosis*	*C. neoformans*	*A.niger*
1	31.25	62.50	31.25	62.50
2	31.25	31.25	31.25	62.50
3	31.25	31.25	31.25	62.50
4	31.25	62.50	7.81	31.25
10	15.63	31.25	7.81	62.50
11	15.63	15.63	7.81	7.81
$ZnCl_2$	-	-	-	-
phen	3.91	3.91	31.25	31.25
Drug	1.00±	2.00	1.00	4.00

" - " : no activity . Drug used in antifungal assay = fluconazole

3.4 Conclusion

Spectroscopic and crystal data reveal that all the zinc complexes are five-coordinated with the doubly deprotonated thiosemicarbazones acting as a tridentate ligand that coordinated through one phenolic oxygen, azomethine nitrogen and thiolate sulfur atoms while the 1,10-phenanthroline is coordinated as the *N,N'*-bidentate ligand. The coordination geometry around these zinc complexes is intermediate between trigonal bipyramidal and square pyramidal geometries and is better described as trigonal bipyramidal distorted square based pyramid (TBDSBP). The coordination geometry around zinc complexes with 2,2'-bipyridine is retained when 2,2'-bipyridine is substituted by 1,10-phenanthroline.

Results from biological tests indicate that the N(4) substituent play crucial role in determining the selectivity and potency of zinc(II) complexes of 2,4-dihydroxybenzaldehyde N(4)-substituted thiosemicarbazones and 1,10-phenanthroline. Only the biological properties for complexes **10** and **11** can be studied attributed to their better solubility in DMF and buffer mixtures. Complex **11** has better selectivity for AT rich sequence and binds stronger to most duplex DNA sequence than complex **10**. In addition, complex **11** also has better antibacterial, antifungal and toposiomerase I inhibition activities compared with complex **10**. Since the major difference between these two complexes is just the length of the alkyl chain at the N(4) substituent, we can infer that the difference in hydrophobicity can exert a great effect on the biological potency of thiosemicarbazones and its ternary zinc complexes. Complexes **10** and **11** have the potential to be developed as an anticancer agent because complexes that can inhibit topoisomerase I and most complexes that show good antifungal property are normally cytotoxic.

When the biological properties of complexes **10** and **11** were compared with their 2,2'-bipyridine analogs, a drastic improvement in all assays is observed. This implies that the extended aromatic ring in the 1,10-phenanthroline moiety bestows a complex with better biological properties that can be attributed to enhanced hydrophobicity or intercalating capability which is known in extended polypyridine ligands like phen, dpq or dppz. Even though the 1,10-phenanthroline moiety has led to improvement of a wide spectrum of biological activities, but this strategy has it limitations. The enhanced hydrophobicity has led to a decrease in water solubility which is a major challenge in biological assays. Complex **12**, which is the analog of complex **8** with good biological

properties could not be tested owing to solubility problems. Therefore, care must be taken in juggling between features that can enhance biological properties with those that can affect water solubility in the design of metal-based drugs.

Chapter 4

Synthesis, characterization and biological properties of copper(II) complexes of 2,4-dihydroxybenzaldehyde N^4-substituted thiosemicarbazones and 2,2'-bipyridine

4.1. Introduction

The results in chapter 2 show that the N(4) substituents in zinc(II) complexes of 2,4-dihydroxybenzaldehyde N(4)-substituted thiosemicarbazones and 2,2-bipyridine (Zb(bipy)L) can affect their biological activities, viz. DNA sequence recognition, quadruplex binding, topoisomerase I inhibition, antibacterial and antifungal properties. However, these zinc complexes are lacking in nucleolytic efficiency. Since the biological properties of metal complexes with similar ligands are known to vary with the central metal ion (Bal *et al*. 2000; Kong and Xie, 2000; Roy *et al*. 2007; Seng *et al*. 2008), we replaced the zinc(II) ion with copper(II) ion in an attempt to improve the biological activities of these complexes that we mentioned earlier. Copper complexes containing heterocyclic base are well known for its ability to cleave DNA in the presence or absence of exogenous agents (Dhar *et al*. 2005; Patra *et al*. 2005 & 2007; Rao *et al*. 2007 & 2008). Previously, Seng *et al.* (2008) have shown that nucleolytic efficiency order of M(phen)(edda) (in the presence of hydrogen peroxide) is Cu(phen)(edda) > Co(phen)(edda) >Zn(phen)(edda) > Ni(phen)(edda). Whereas in the presence of 1 μM ascorbic acid, the DNA cleavage of 50 μM Cu(phen)(edda) was greatly enhanced as nearly all the supercoiled plasmid was converted to nicked and linear. The addition of this amount of ascorbic acid did not affect the nucleolytic efficiency of the other metal complexes. Furthermore, copper(II) ion was chosen because its known to enhance the anticancer properties of thiosemicarbazones (West *et al*. 1993; Bindu *et al*. 1998; Wang and Guo, 2006). Cross comparison of the

chemical and biological properties of this series with the zinc(II) series in chapter 2 may help in understanding the effect of varying the metal ions in complexes with same ligand.

Therefore in this chapter, we report the effect of varying the N(4) substituent of the thiosemicarbazone ligand, L from proton, methyl, ethyl to phenyl towards the chemical and biological properties (DNA binding, nucleolytic, topoisomerase I inhibition and antimicrobial) of Cu(bipy)L.

4.2. Experimental

4.2.1. Materials and solutions

Similar materials were used as reported in chapter 2.

4.2.2. Physical measurements

Spectroscopic measurements and elemental analyses were similarly carried out as reported in chapter 2.

4.2.3. Syntheses

4.2.3.1 Synthesis of (4-Hydroxy-2-oxidobenzaldehyde thiosemicarbazonato)-(2,2-bipyridine)copper(II) monohydrate , [Cu(bipy)(HT)]H_2O **(13)**

Copper acetate dihydrate (0.22 g, 1 mmol) and 2,2-bipyridine (0.16 g, 1 mmol) were reacted with 2,4-dihydroxybenzaldehyde thiosemicarbazone (0.21 g, 1 mmol) as reported in chapter 2.

(Yield: 0.23 g, 52 %). Anal. Calc. for $C_{18}H_{16}N_5O_3SCu$: C, 48.37; H, 3.83; N, 15.67. Found: C, 48.38; H, 3.40; N, 16.94 %. IR (KBr disc, cm^{-1}): 3436 w, 3352 m, 3277 w, 3158 w, 3087 w, , 1602 s, 1496 s, 1442 m, 1313 m, 1257 m, 1223 s, 1179s , 1123 m, 841 w, 762 m, 555 w, 430 w (s, strong; m, medium; w, weak).

4.2.3.2 Synthesis of (4-Hydroxy-2-oxidobenzaldehyde 4-methylthiosemicarbazonato)-(2,2-bipyridine)copper(II) monohydrate, [Cu(bipy)(HM)]. H_2O **(14)**

Complex **14** was similarly prepared as complex **13** by using 2,4-dihydroxybenzaldehyde 4-methylthiosemicarbazone (0.23 g, 1 mmol) as the Schiff base.

(Yield: 0.35 g, 75 %). Anal. Calc. for $C_{19}H_{19}N_5O_3SCu$: C, 49.50; H, 4.15; N, 15.19. Found: C, 49.68; H, 3.76; N, 15.62 %. IR (KBr disc, cm^{-1}): 3392 m (broad), 3069 w, 1603 s, 1444 m, 1401 m, 1365 w, 1262 m, 1221 m, 1181 m, 841 w , 763 m, 652 w 554 w, 479 w

(s, strong; m, medium; w, weak).

4.2.3.3 Synthesis of (4-Hydroxy-2-oxidobenzaldehyde 4-ethylthiosemicarbazonato)-(2,2-bipyridine)copper(II) semihydrate, [Cu(bipy)(HE)].0.5H_2O **(15)**

Complex **15** was similarly prepared as complex **13** by using 2,4-dihydroxybenzaldehyde 2,4-dihydroxybenzaldehyde 4-ethylthiosemicarbazone (0.24 g, 1 mmol) as the Schiff base.

(Yield: 0.36 g, 72 %). Anal. Calc. for $C_{20}H_{20}N_5O_{2.5}SCu$: C,51.55; H, 4.33; N, 15.03. Found: C, 50.93; H, 4.76; N, 15.33 %. IR (KBr disc, cm^{-1}): 3422 (broad) m, 3224 m, 3059 w, 2933 w, 1592 s, 1441 m, 1344 m, 1260 m, 1215 m, 1186 m, 842 m, 787 w, 765 m, 589 w, 465 w, 432 w (s, strong; m, medium; w, weak).

4.2.3.4 Synthesis of (4-Hydroxy-2-oxidobenzaldehyde 4-phenylthiosemicarbazonato)-(2,2-bipyridine)copper(II) dihydrate, [Cu(bipy)(HP)].2 H_2O **(16)**

Complex **16** was similarly prepared as complex **13** by using 2,4-dihydroxybenzaldehyde 4-phenylthiosemicarbazone (0.29 g, 1 mmol) as the Schiff base.

(Yield: 0.43 g, 80 %). Anal. Calc. for $C_{24}H_{23}N_5O_4SCu$: C, 53.27; H, 4.28; N, 12.94. Found: C, 53.28; H, 4.57; N, 13.04 %. IR (KBr disc, cm^{-1}): 3398 m, 3335 w, 3070 w, 1602 s, 1496 s, 1431 s, 1311 m, 1219 s, 1172 m, 852 m, 755 w, 588 w, 505 w, 466 w, 426 w

(s, strong; m, medium; w, weak).

4.2.4. X-ray crystallography

Green crystal for complex **13a** was recrystallised from dimethylformamide. Data collection was carried out as repoted in chapter 2. The structure was solved by direct-methods and refined by a full-matrix least-squares procedure on F^2 with anisotropic displacement parameters for non-hydrogen atoms. Hydrogen atoms in their calculated positions were refined using a riding model. The hydroxy and amino H-atoms were located in a difference Fourier map.

4.2.5 DNA binding

DNA binding was carried out as reported in chapter 2.

4.2.6 Nucleolytic study

Agarose gel electrophoresis experiments were carried out on supercoiled plasmid DNA pBR322 (4.4 kb) using a horizontal gel system as described in chapters 2 and 3.

4.2.7 Human Topoisomerase I inhibtion assay

The human DNA topoisomerase I inhibitory activity was determined by using a horizontal gel system as outlined in chapters 2 and 3.

4.2.8 Antibacterial and antifungal assay

The antibacterial and antifungal activities of the ligands and complexes were assessed against several strains of Gram-positive bacteria, Gram-negative bacteria, and fungi. A colorimetric broth microdilution method using *p*-iodonitrotetrazolium violet (INT) as the growth indicator was employed to quantify the minimum inhibitory concentration (MIC) value of the complexes in the assay. The test was performed as mentioned in chapter 2.

4.3. Results and discussion

4.3.1 Synthesis of the complexes

The stoichiometries, color and partial elemental analyses of the Cu(bipy)L complexes are shown in Table 4.1. Proposed structures for all the complexes with IUPAC numbering scheme are shown in Fig. 4.1 (Shown here for convenience).

13 R = H **14** R' = $-CH_3$ **15** R = $-C_2H_5$ **16** R = $-C_6H_5$

Fig. 4.1 Proposed structure for all the complexes

Results from partial elemental analyses are in good agreement with the proposed formulation of Cu(bipy)L where bipy = 2,2-bipyridine and L represents each of the doubly deprotonated thiosemicarbazones. Complex **13** exists as a monohydrate, while its crystal (**13a**) that was recrystallised from DMF solution contains a solvated DMF molecule**.** Complex **14** exists as a monohydrate, while complex **15** as a semihydrate and complex **16** as a dihydrate**.** All the complexes are green. The complexes were prepared in high yield by refluxing copper acetate dihydrate, 2,2'-bipyridine and the thiosemicarbazones in ethanol. Complexes **13-16** are insoluble in common polar and non-polar solvents but are soluble in DMF and DMSO. The room temperature magnetic susceptibility of the complexes in the polycrystalline state fall in the range of 1.82-1.84 B.M which are very close to the spin only value of 1.73 B.M for d^9 in Cu(II) (Bindu *et al*. 1999).

Table 4.1

Stoichiometries, color and partial elemental analyses of the copper(II) complexes

Complex	Stoichiometries	Color	Anal. Calc.	(Found)%		μ effective
			C	H	N	(B.M)
[Cu(bipy)(HT)].H_2O **(13)**	$C_{18}H_{16}N_5O_3SCu$	Green	48.37(48.38)	3.83(3.40)	15.67(16.94)	1.82
[Cu(bipy)(HT)].DMF **(13a)**	$C_{21}H_{22}N_6O_3SCu$	Green	50.24(50.55)	4.42(4.52)	16.74(16.43)	1.82
[Cu(bipy)(HM)].H_2O **(14)**	$C_{19}H_{19}N_5O_3SCu$	Green	49.50(49.68)	4.15(3.76)	15.19(15.62)	1.84
[Cu(bipy)(HE)].0.5H_2O **(15)**	$C_{20}H_{20}N_5O_{2.5}SCu$	Green	51.55(50.93)	4.33(4.76)	15.03(15.33)	1.84
[Cu(bipy)(HP)].2H_2O **(16)**	$C_{24}H_{23}N_5O_4SCu$	Green	53.27(53.28)	4.28(4.57)	12.94(13.04)	1.83

4.3.2 Crystal structure analysis

4. 3.2.1 Crystal structures of [Cu(bipy)(HT)].DMF(**13a**)

Complex **13a** crystallised into a monoclinic lattice with space group symmetry *P*21. The perspective view of the complex with numbering scheme is shown in Fig. 4.2. Selected bond lengths and angles are presented in Table 4.3.

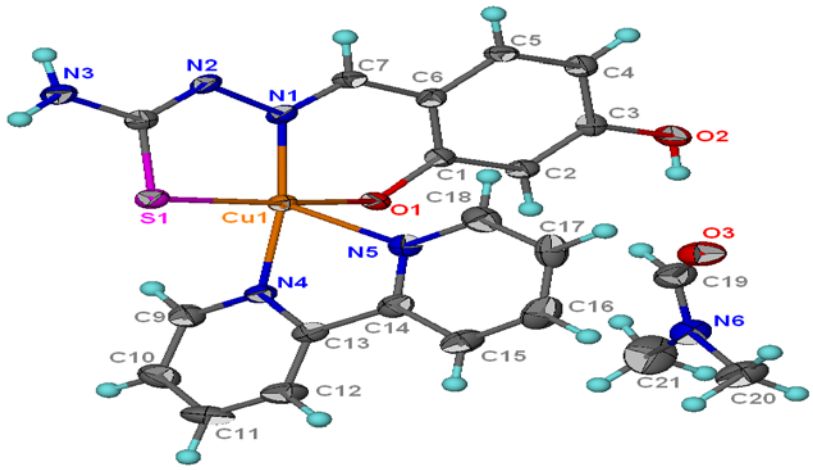

Fig. 4.2 Thermal ellipsoid (Barbour, 2001) plot of **13a** drawn at the 70% probability level. Hydrogen atoms are drawn as spheres of arbitrary radii.

The complex is mononuclear and five coordinated with the doubly deprotonated thiosemicarbazone as a tridentate ligand coordinating through the phenolic oxygen, azomethine nitrogen and thiolate sulfur atoms while 2,2-bipyridine as the *N,N'*-bidentate ligand. The trigonality index τ of 0.03 for **13a** indicates that the coordination geometry around copper is close to a perfect square pyramidal in contrast to the zinc analog, complex **9** with τ of 0.49. Complex **9** is intermediate between trigonal bipyramidal and square pyramidal geometries and is better described as trigonal bipyramidal distorted square based pyramid (TBDSBP). The τ value of complex **13a** is smaller compared to the τ value of 0.15

in [CuL^2bipy] where H_2L^2 = salicylaldehyde 3-tetramethyleneiminyl thiosemicarbazone (Latheef and Kurup, 2008). In the square pyramidal complex **13a**, copper is displaced 0.1537(3) Å above the N(1), N(4), O(1) and S(1) coordination plane and towards the elongated apical N(5) atom.

The Cu $-N_{azomethine}$ bond length of 1.960 (2) Å is shorter than the Cu-N_{bipy} bond lengths of 2.051(2) and 2.291(2) Å. This indicates that the azomethine nitrogen is coordinated more strongly to copper compared to the bipyridine nitrogen and the thiosemicarbazone moiety dominates equatorial bonding. The Cu–N_{bipy} bond lengths are similar to those reported for mononuclear copper(II) complexes (Seena and Kurup, 2007; Latheef and Kurup, 2008). The difference between the axial and equatorial Cu–N_{bipy} bond lengths may be due to the presence of Jahn-Teller effect in copper complex with d^9 electronic configuration. This is not seen in the zinc complexes with d^{10} electronic configuration in chapter 2 (complexes **5** and **8**)**.** The imine bond formation is evidenced from N1-C7 and N2-C8 distances of 1.296(3) Å and 1.308(3) Å respectively. The N2-C8 bond length of 1.308(3) Å and C-S bond length of 1.744 (2) is similar to those reported for coordination of thiosemicarbazone in the thiolate form (Seena and Kurup, 2007; Latheef and Kurup, 2008; Seena and Kurup, 2008; Bal-Demirci, 2008).

Hydrogen bonding parameters are shown in Table 4.4 while hydrogen bonding interactions for complex **13** are shown in Fig. 4.3 and Fig. 4.4. A solvated dimethylformamide (DMF) molecule is linked to complex **13** through an O2—H2···O3

hydrogen bond. The N3—H32···O2 hydrogen bonds link the mononuclear molecules into an infinite linear chain motif parallel to c axis as shown in Fig. 4.3.

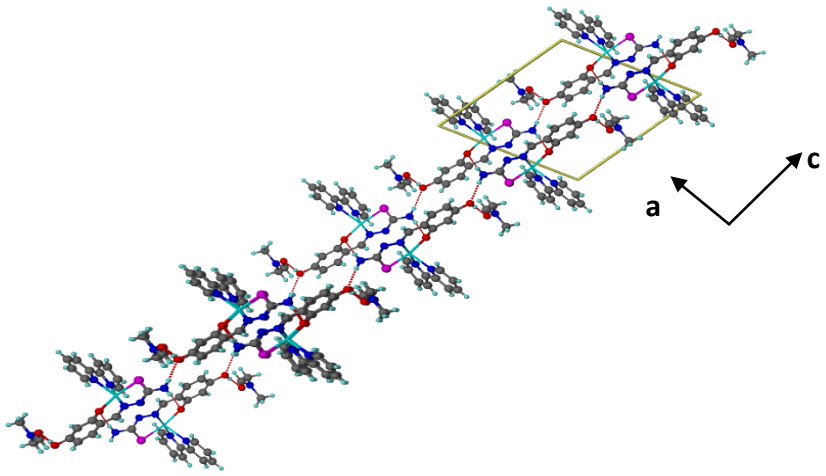

Fig. 4.3 Linear chain formed from N3—H32···O2 hydrogen bonding interactions for complex **13a** view down from b-axis.

The molecules along this linear chain are further connected to the adjacent molecule through N3—H31···O1 hydrogen bonds to form another infinite linear zigzag chain along b-axis as shown in Fig. 4.4. Combinations of these hydrogen bonds lead to the formation on an infinite two dimensional array. The packing of the molecules is stabilized by hydrogen bonding interactions (Fig. 4.5). No π-π interactions are observed in this system.

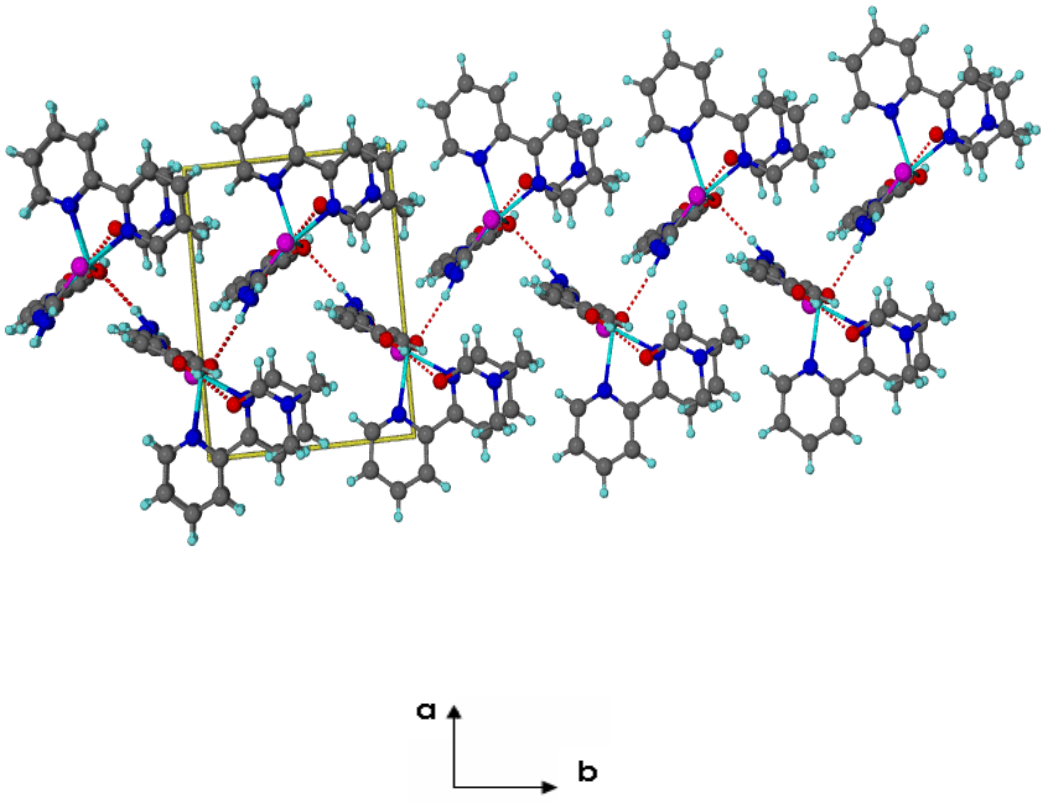

Fig. 4.4 Zig-zag chain from N3—H31···O1 hydrogen bonding interactions for complex **13a** view down from c axis.

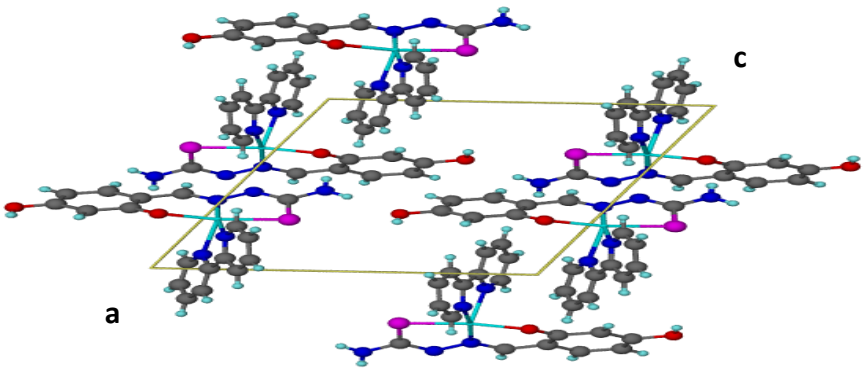

Fig. 4.5 Packing diagram of **13a** along b-axis.

Table 4.2

Crystal data and structure refinement parameters for complex **13a**

Complex	[Cu(bipy)(HT)].DMF(13)
Empirical formula	$C_{21}H_{22}CuN_6O_3S$
Formula weight	502.05
Crystal system	Monoclinic
Space group	$P2_1$
Unit cell dimensions	
a (Å)	11.8131 (3)
b (Å)	8.40790 (10)
c (Å)	12.2719 (3)
β (°)	116.5900 (10)
Volume, V ($Å^3$)	1089.97 (4)
Z	2
F(0 0 0)	518
Density (calculated), (mg m^{-3})	1.530
Absorption coefficient, μ(mm^{-1})	1.13
Wavelength, λ (Å)	0.71073
Temperature, T (K)	118 (2)
Crystal size (mm)	0.20 × 0.20 × 0.03
Reflections collected	7639
Independent reflections	4629 [R(int) = 0.020]
Data/restraints/parameters	4629/4/303
$R[F^2 > 2\sigma(F^2)]$	0.027
$wR(F^2)$	0.068
S	1.05
Largest difference peak and hole (e $Å^{-3}$)	0.27 and −0.23

Table 4.3

Selected bond lengths (Å) and angles (˚) for [Cu(bipy)(HT)].DMF (**13a**)

Bond lengths		Bond angles	
Cu1—O1	1.9562 (16)	O1—Cu1—N1	92.21 (7)
Cu1—N1	1.960 (2)	O1—Cu1—N4	91.80 (7)
Cu1—N4	2.051 (2)	N1—Cu1—N4	171.57 (8)
Cu1—S1	2.2856 (6)	O1—Cu1—S1	169.65 (5)
Cu1—N5	2.291 (2)	N1—Cu1—S1	84.77 (6)
S1—C8	1.744 (2)	N4—Cu1—S1	89.99 (6)
O1—C1	1.311 (3)	O1—Cu1—N5	90.52 (7)
O2—C3	1.362 (3)	N1—Cu1—N5	111.97 (8)
N1—C7	1.296 (3)	N4—Cu1—N5	75.39 (8)
N1—N2	1.390 (3)	S1—Cu1—N5	99.80 (5)
N2—C8	1.308 (3)	C8—S1—Cu1	93.98 (8)
N3—C8	1.353 (3)	C1—O1—Cu1	124.89 (14)
N4—C9	1.339 (3)		
N4—C13	1.346 (3)		
N5—C18	1.333 (3)		
N5—C14	1.340 (3)		

Table 4.4
Hydrogen-bond geometry (Å, °) for [Cu(bipy)(HT)].DMF (**13a**)

D—H···*A*	*D*—H	H···*A*	*D*···*A*	*D*—H···*A*
O2—H2···O3	0.838 (10)	1.827 (11)	2.661 (3)	173 (3)
N3—H31···O1^{i}	0.886 (10)	2.089 (11)	2.968 (3)	172 (2)
N3—H32···O2^{ii}	0.868 (10)	2.138 (11)	3.003 (3)	174 (2)

Symmetry codes: (i) − *x*+1, *y*+1/2, − *z*+2; (ii) *x*, *y*, *z*−1. Hydrogen atoms are placed at calculated positions.

4.3.3 Infrared and electronic spectra

Important IR bands for the ligands and complexes are given in Table 4.5. IR spectra for all the complexes are shown in Fig. 4.6. Thiosemicarbazones are known to exhibit thione-thiol tautomerization (Fig. 4.7). The absence of any band around 2600-2800 cm^{-1} ν(S-H) indicates that in the solid form, all the ligands exist in the thione form (Bindu *et al.* 1999; Afrasiabi *et al.* 2005). Analysis of the IR spectra of the complexes revealed that the thiosemicarbazones are coordinating through the phenolic oxygen, azomethine nitrogen and thiolate sulfur atoms while 2,2-bipyridine as the *N,N'*-bidentate ligand as reported for the zinc complexes in chapters 2 and 3.

The appearance of new ν(Cu-N) bands in the range of 465-479 cm^{-1} confirms the coordination through azomethine and bipyridine nitrogens. Coordination through phenolic oxygen is confirmed by the presence of ν(Cu-O) band at around at around 426-430 cm^{-1} (Bindu *et al*. 1999; Seena and Kurup, 2007; Latheef and Kurup, 2008). The mode of coordination for the ligands determined by IR spectra is in good agreement with the crystal structure of complex **13a**. Complexes **13-16** have very similar IR spectra (Fig. 4.6), this indicates that they share the similar mode of coordination. Since the ligands have the same ligating atoms and the only variation in the structure of these complex is at the N(4)-substituent which is not involved in coordination to copper, it is reasonable to propose that the coordination geometry around copper for each of the complexes **13-16** is distorted square pyramidal.

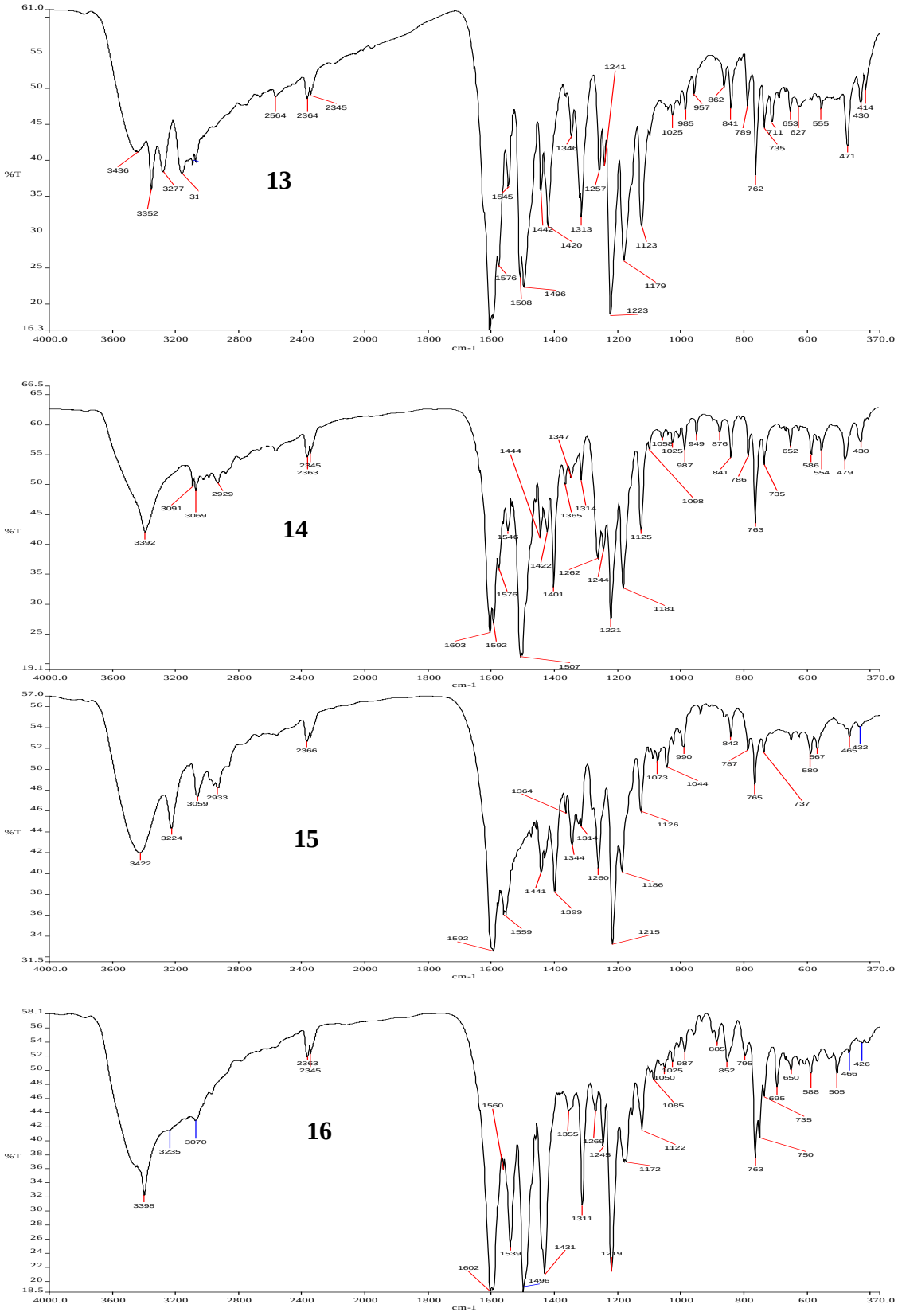

Fig. 4.6 IR spectra of complexes **13-16**

Fig. 4.7 Thione-thiol tautomerization for the ligands

Table 4.5

IR spectral assignments (cm^{-1}) for the ligands and their copper(II) complexes

Compound	ν(C=N)	ν(C-O)	ν(N-N)	ν (C=S)	ν(Cu-O)	ν(Cu-N)	Bands due to bipyridine
H_3T **(1)**	1620	1239	1165	1379, 863	-	-	-
H_3M **(2)**	1625	1231	1166	1331,868	-	-	-
H_3E **(3)**	1626	1241	1166	1325, 867	-	-	-
H_3P **(4)**	1629	1264	1121	1323,838	-	-	-
[[Cu(bipy)(HT)].H_2O **(13)**	1603	1223	1179	1313, 841	430	471	1442, 762
[Cu(bipy)(HM)].H_2O **(14)**	1603	1221	1181	1314, 841	430	479	1444, 763
[Cu(bipy)(HE)].0.5H_2O **(15)**	1592	1215	1186	1314, 842	432	465	1441, 765
[Cu(bipy)(HP)].2H_2O **(16)**	1602	1219	1172	1311, 795	426	466	1431, 763

Electronic spectral assignments for the ligands and their copper(II) complexes in DMF are presented in Table 4.6. All the ligands and the Cu(II) complexes have a ring (phenolic and diimine) π-π^* band at around 37,593 cm^{-1} (West *et al.* 1995). No significant red shift is observed for these bands upon complexation (Swearingan and West, 2000). All the thiosemicarbazones also have two bands at around 32,985 cm^{-1} and 29,411 cm^{-1} due to n-π* transition of azomethine and thioamide function, respectively. Upon complexation, the n-π* band of the thioamide function is shifted above 30,000 cm^{-1} due to thioenolization and merges with the azomethine n-π* band at around 31,348 cm^{-1}(Swearingan and West, 2000). Thioenolization causes the weakening of the C=S bond. A moderately intense band in the range 25840-26666 cm^{-1} found only in the spectra of the complexes is assigned to Cu(II)→S metal to ligand charge transfer band (MLCT) (Swearingan and West, 2000; Seena and Kurup, 2007). The MLCT band for Cu(II)→O shows line broadening that runs into the visible part of the spectrum. However, the maxima of this band is not observed probably due to the overlapping with the low energy side of Cu(II)→S transitions (Seena and Kurup, 2007). The copper complexes show a d-d band at 17153-17544 cm^{-1} due to $d_{x^2-y^2} \rightarrow d_{xz}$, d_{yz} and $d_{x^2-y^2} \rightarrow d_{z^2}$ transitions characteristic of five coordinate copper(II) complexes with square pyramidal geometry (Bindu *et al.*, 1999; Seena and Kurup, 2007; Latheef and Kurup, 2008).

Table 4.6

Electronic spectral assignments (cm^{-1}) for the ligands and their copper(II) complexes in DMF .

Complex	π-π^*	n-π*	MLCT	d-d transition
H_3T (**1**)	37593	33003, 29411	-	-
H_3M (**2**)	37593	33003, 29411	-	-
H_3E (**3**)	37593	32895, 29240	-	-
H_3P (**4**)	37453	32680, 28409	-	-
[[Cu(bipy)(HT)].H_2O **(13)**	37736	30769	26596	17483
[Cu(bipy)(HM)].H_2O **(14)**	37594	30769	26666	17153
[Cu(bipy)(HE)].0.5H_2O **(15)**	37594	30769	26455	17544
[Cu(bipy)(HP)].2H_2O **(16)**	35211	30581	25840	17182

4.3.4 DNA binding

4.3.4.1 Duplex DNA

The interaction of the complexes with (i) duplex oligonucleotides of various specified nucleotide sequences, and (ii) quadruplex DNA of the 23-mer oligonucleotide 5'-$AG_3(T_2AG_3)_3$-3' and its corresponding duplex were investigated with CD spectroscopy.

As was routinely done in the work presented in chapters 2 and 3, the first investigation was to find out the DNA binding preference for CG or AT sequences by the copper complex. Complexes **13** (Fig. 4.8) and **14** (Fig. 4.9) at a complex:duplex ratio of 1:8 induce a decrease in the intensity of the positive and negative bands of the $ds(AT)_6$, and

this suggests that binding of the complexes cause a change of conformation from B to Z-like conformation similar to those observed in interaction of $[Cu(5,6\text{-dmp})_2]^{2+}$ with calf thymus DNA (Mahadevan and Palaniandavar, 1996). On the other hand, complexes **15** (Fig. 4.10) and **16** (Fig. 4.11) cause a decrease and increase of the negative and positive band, respectively. This type of changes is normally attributed to a change of conformation from B to A-like if accompanied by a shift in the peak maxima of the positive band (Ivanov *et al*. 1973; Maheswari and Palaniandavar, 2004). However, no shift in the peak maxima of the positive band suggests that complex **15** and **16** bind to the DNA through partial intercalation and induce a slight unwinding of the helical twist of the $ds(AT)_6$. Complex **16** induces a greater increase (9.4 %) in the intensity of the positive band of the CD spectrum of $ds(AT)_6$ compared with complex **15** (3.5 %). This implies that complex **16** binds more strongly to $ds(AT)_6$ in contrast to complex **15**. This is attributed to the higher hydrophobicity and surface area conferred to complex **16** by the phenyl substituent. However, other factors may be responsible for the increase in the positive band of $ds(AT)_6$.

We now look at the results for $ds(CG)_6$. Complexes **13**, Cu(bipy)(HT) and **14**, Cu(bipy)(HM) only cause a slight increase (2-3.5 %) to the positive band of $ds(CG)_6$ which is too weak to suggest intercalation. Both complexes cause a decrease to the negative band with the greatest decrease of 18.6 % observed in complex **14** indicating that complex **14** causes more unwinding of DNA than complex **13**. Interestingly, similar observation is seen in complex **6** which is the zinc analog of complex **14** with methyl substituent at N(4). Complex **15**, Cu(bipy)(HE) causes a slight decrease in both the positive and negative bands of $ds(CG)_6$ suggesting a very weak transition from B like to Z like conformation

(Mahadevan and Palaniandavar, 1996). No significant changes is observed for the interaction of complex **16**, Cu(bipy)(HP) with ds$(CG)_6$.

By comparing the changes induced by complexes **13-16** in both the positive and negative bands in the CD spectra of ds$(AT)_6$ and ds$(CG)_6$, we can infer that complex **13-16** can differentiate ds$(AT)_6$ from ds$(CG)_6$. Complexes that induce similar conformation change suggest similar binding mode to the ds(oligonucleotides) and vice-versa. These results show that the N(4) substituent play a role in determining the mode of binding of the complexes with ds(oligonucleotides) with a particular base sequence. The strength of binding is also affected by the N(4) substituent because complexes that induce similar conformation change to a particular ds(oligonucleotides) also show differences in percentage of changes in both the positive and negative bands in the CD spectra. At present, this explanation seems reasonable. No other alternative can account for the observed results.

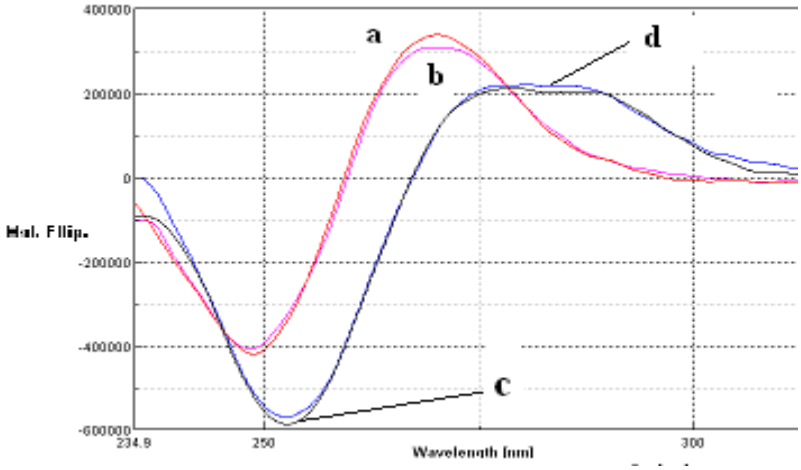

Fig. 4.8 CD spectra of 15 µM of oligonucleotide in the absence and presence of 120 µM of complex **13**; (a) ds$(AT)_6$ alone, (b) ds$(AT)_6$ with complex **13,** (c) ds$(CG)_6$ alone and (d) ds$(CG)_6$ with complex **13.**

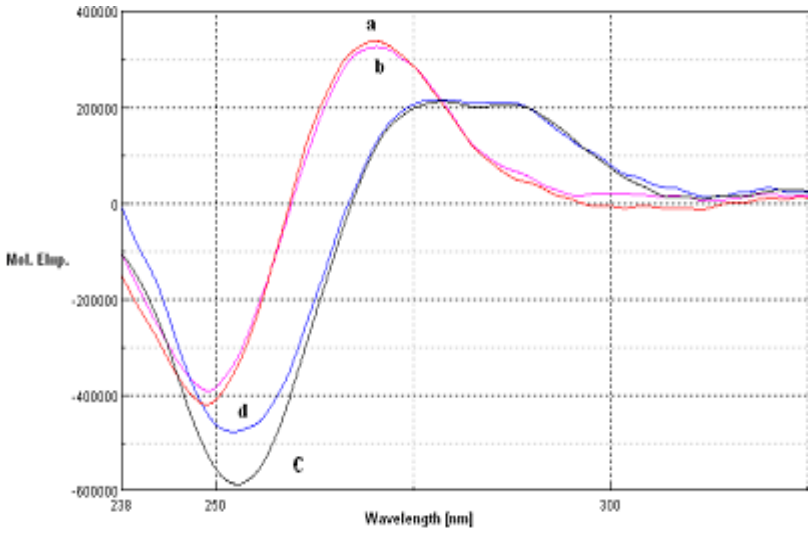

Fig. 4.9 CD spectra of 15 µM of oligonucleotide in the absence and presence of 120 µM of complex **14**; (a) ds(AT)$_6$ alone, (b) ds(AT)$_6$ with complex **14,** (c) ds(CG)$_6$ alone and (d) ds(CG)$_6$ with complex **14**

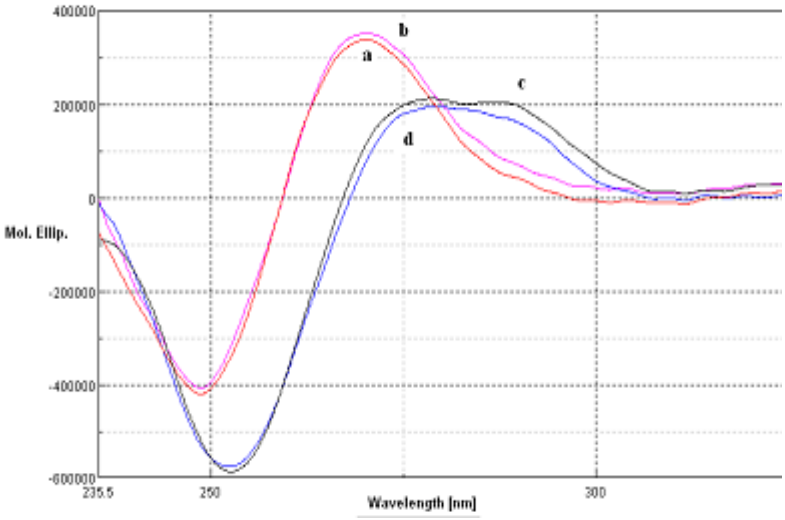

Fig. 4.10 CD spectra of 15 µM of oligonucleotide in the absence and presence of 120 µM of complex **15**; (a) ds(AT)$_6$ alone, (b) ds(AT)$_6$ with complex **15,** (c) ds(CG)$_6$ alone and (d) ds(CG)$_6$ with complex **15**

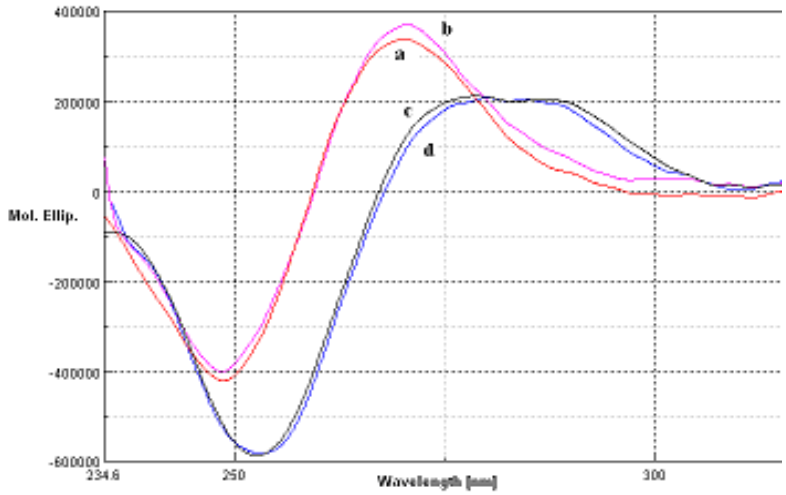

Fig. 4.11 CD spectra of 15 µM of oligonucleotide in the absence and presence of 120 µM of complex **16**; (a) ds$(AT)_6$ alone, (b) ds$(AT)_6$ with complex **16,** (c) ds$(CG)_6$ alone and (d) ds$(CG)_6$ with complex **16.**

Next oligonucleotides such as ds$(CGCGAATTCGCG)_2$ and ds$(CGCGATATCGCG)_2$ were utilized in order to investigate any binding preferences in interactions with duplex DNA as the sequence on each chain is varied from non-alternating to alternating purine-pyrimidine bases in grooves of the two duplexes. To investigate the above factors, we assume that the complexes can bind in the DNA grooves. For the AATT sequence (Fig. 4.12-4.15), complexes **13-16** show decrease and increase in the negative and positive bands of the CD spectra of the duplex which is consistent with the conformational change from B to ψ (Maheswari and Palaniandavar, 2004; Seng *et al*. 2008). The great enhancement of the positive band (≈ 20 %) for complexes **15** and **16** suggest partial intercalation of either the Schiff base or 2,2'-bipyridine to the duplex. Both the schiff base and 2,2'-bipyridine moieties have planar aromatic rings that favours intercalation. Greater enhancement of positive band for complexes **15** and **16** (≈ 20 %) compared to complexes **13** and **14** (≈ 8 %) suggests that base stacking interaction for this particular AATT sequence

is favoured by higher hydrophobicity of the N(4) substituent (ethyl and phenyl). Greater enhancement of the negative band is observed for complexes **13** and **14,** in contrast to their positive band, with the highest enhancement shown by complex **13**. This observation suggests that the binding of the complex **13** that is the least hydrophobic to the AATT sequence will result in greater unwinding of the helical twist of the ds(oligonucleotides) than complexes **14-16**.

For the ATAT sequence, complexes **13** and **14** also show a decrease and increase in the negative and positive bands respectively. This is consistent to conformational change from B to ψ (Maheswari and Palaniandavar, 2004; Seng *et al*. 2008) which was similarly observed for the interaction of these two complexes with the AATT sequence earlier. However, complexes **15** and **16** show an increase in both the positive and negative bands which implies intercalation and stabilization of the B form DNA (Maheswari and Palaniandavar, 2004). This implies that complex **15** and **16** can effectively differentiate AATT from ATAT sequence based on their different mode of binding to these different ds(oligonucleotide).

Comparing the CD results of these four ds(oligos)$_2$, we can conclude that complexes **13-16** can differentiate ds(AT)$_6$ from ds(CG)$_6$ whereas only complex **15** and **16** can effectively differentiate the AATT from ATAT sequence. Complexes **13** and **14** is less effective in differentiating AATT from ATAT sequence because both complexes induce same conformational change from B to ψ for these two duplexes. This implies that

complexes that are more hydrophobic can effectively differentiate more DNA base sequences. We think that one of the contributing factors in the observed DNA recognition is conferred by the ability of the complexes to form hydrogen bonds with the DNA through various hydrogen donor and acceptor groups on the thiosemicarbazone moiety. The N(4)-substituent seems to be responsible in DNA recognition through hydrophobic interaction or grooves binding because each complex has a substituent with different hydrophobicity and bulkiness (alkyl chain or aromatic ring). The size of the molecules and the orientation of different substituted bulky group in space may affect their ability to bind into the groove (major or minor) with different cavity size or steric hindrance.

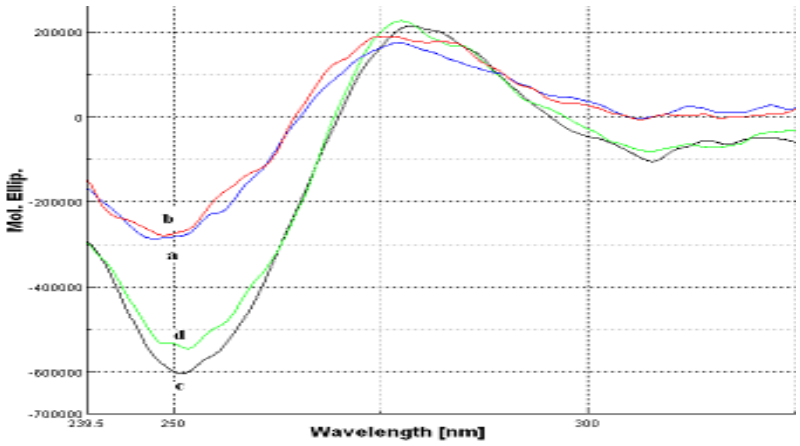

Fig. 4.12 CD spectra of 10 µM of oligonucleotides in the absence and presence of 120 µM of complex **13**; (a) ds(CGCGATATCGCG)$_2$ alone, (b) ds(CGCGATATCGCG)$_2$ with complex **13,** (c) ds(CGCGAATTCGCG)$_2$ alone and (d) ds(CGCGAATTCGCG)$_2$ with complex **13.**

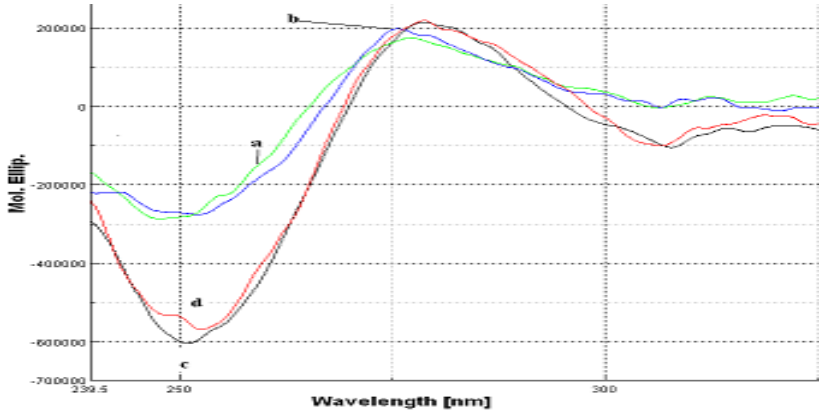

Fig. 4.13 CD spectra of 10 µM of oligonucleotides in the absence and presence of 120 µM of complex **14**; (a) ds(CGCGATATCGCG)$_2$ alone, (b) ds(CGCGATATCGCG)$_2$ with complex **14,** (c) ds(CGCGAATTCGCG)$_2$ alone and (d) ds(CGCGAATTCGCG)$_2$ with complex **14.**

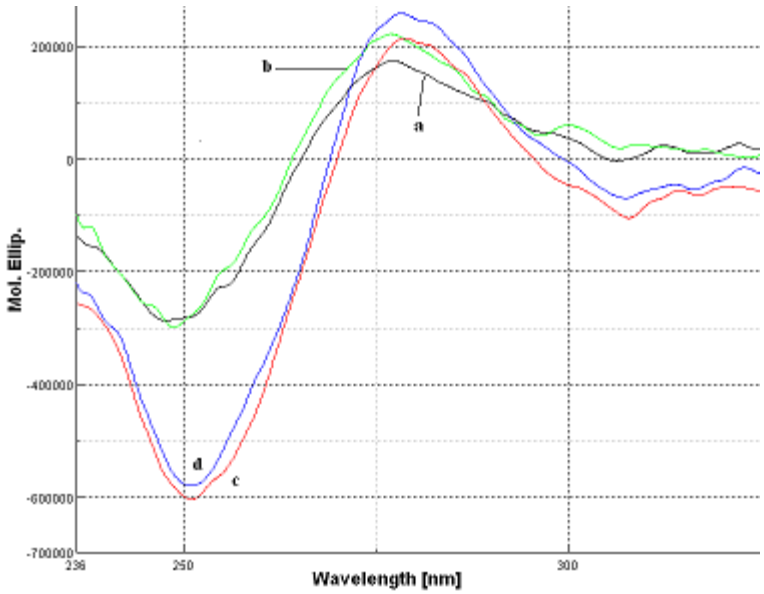

Fig. 4.14 CD spectra of 10 µM of oligonucleotides in the absence and presence of 120 µM of complex **15**; (a) ds(CGCGATATCGCG)$_2$ alone, (b) ds(CGCGATATCGCG)$_2$ with complex **15**, (c) ds(CGCGAATTCGCG)$_2$ alone and (d) ds(CGCGAATTCGCG)$_2$ with complex **15.**

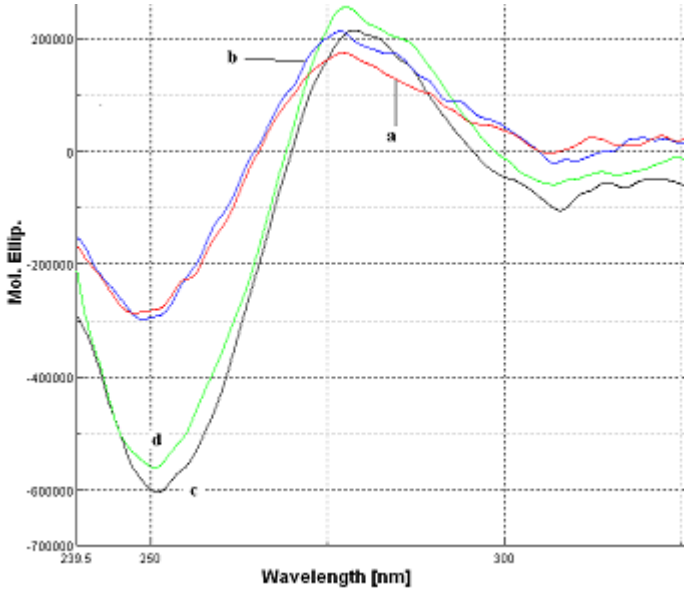

Fig. 4.15 CD spectra of 10 µM of oligonucleotides in the absence and presence of 120 µM of complex **16**; (a) ds(CGCGATATCGCG)$_2$ alone, (b) ds(CGCGATATCGCG)$_2$ with complex **16**, (c) ds(CGCGAATTCGCG)$_2$ alone and (d) ds(CGCGAATTCGCG)$_2$ with complex **16**.

Table 4.7
CD spectral bands of duplex oligo or quadruplex + copper complex: wavelength, λ (molar ellipcity)

	λ/nm (molar ellipcity)	
	(-) band	(+) band
15 μM ds$(AT)_6$	248 (-419344)	270 (339753)
15 μM ds$(AT)_6$ + 120 μM complex **13**	249 (-406033)	269 (307784)
15 μM ds$(AT)_6$ + 120 μM complex **14**	249 (-390550)	270 (327403)
15 μM ds$(AT)_6$ + 120 μM complex **15**	249 (-406640)	270 (352262)
15 μM ds$(AT)_6$ + 120 μM complex **16**	249 (-398382)	270 (372043)
15 μM ds$(CG)_6$	252 (-585418)	278 (213799)
15 μM ds$(CG)_6$ + 120 μM complex **13**	257 (-568230)	280 (221230)
15 μM ds$(CG)_6$ + 120 μM complex **14**	253 (-475805)	279 (216996)
15 μM ds$(CG)_6$ + 120 μM complex **15**	252 (-574558)	279 (195609)
15 μM ds$(CG)_6$ + 120 μM complex **16**	253 (-581489)	280 (209792)
10 μM ds$(CGCGAATTCGCG)_2$	251 (-603665)	279 (215560)
10 μM ds$(CGCGAATTCGCG)_2$ + 120 μM complex **13**	252 (-532365)	277 (226497)
10 μM ds$(CGCGAATTCGCG)_2$ + 120 μM complex **14**	253 (-568922)	279 (219396)
10 μM ds$(CGCGAATTCGCG)_2$ + 120 μM complex **15**	251 (-578551)	278 (259217)
10 μM ds$(CGCGAATTCGCG)_2$ + 120 μM complex **16**	251 (-560689)	279 (255896)
10 μM ds$(CGCGATATCGCG)_2$	248 (-286559)	277 (174875)
10 μM ds$(CGCGATATCGCG)_2$ + 120 μM complex **13**	249 (-278584)	277 (189419)
10 μM ds$(CGCGATATCGCG)_2$ + 120 μM complex **14**	252 (-274954)	276 (198449)
10 μM ds$(CGCGATATCGCG)_2$ + 120 μM complex **15**	249 (-299115)	277 (222815)
10 μM ds$(CGCGATATCGCG)_2$ + 120 μM complex complex **16**	249 (-297319)	277 (213912)
20 μM guanine-rich duplex	250 (-82682)	279 (283975)
20 μM guanine-rich duplex + 120 μM complex **13**	249 (-69010)	276 (204189)
20 μM guanine-rich duplex + 120 μM complex **14**	251 (-119879)	279 (373394)
20 μM guanine-rich duplex + 120 μM complex **15**	250 (-213321)	279 (584026)
20 μM guanine-rich duplex + 120 μM complex **16**	250 (-55187)	279 (129537)
20 μM G-quadruplex	266 (-116489)	247 (106239) 296 (180571)
20 μM G-quadruplex + complex **13**	265 (-97017)	248 (106105) 296 (184718)
20 μM G-quadruplex + complex **14**	264 (-115677)	248 (89027) 297 (178264)
20 μM G-quadruplex + complex **15**	264 (-100287)	246 (105507) 296 (187905)
20 μM G-quadruplex + complex **16**	265 (-99265)	246 (124286)

	296 (202926)

guanine-rich duplex = (5’-CCAGTTCGTAGTAGTAACCC-3’)·(3'-GGTCAAGCATCATCATTGGG-5’)

Table 4.7 Continued.

4.3.4.2 G-quadruplex and guanine-rich duplex

The CD spectra of the 20 μM of the antiparallel G-quadruplex 5’-$AG_3(T_2AG_3)_3$-3’ with complexes **13-16** (120 μM) were monitored. The intensity of the positive band for G-quadruplex at 296 nm is enhanced while the negative band at 267 nm decreases upon addition of each of the complexes **13**, **15** and **16**. Complex **14** does not induce any significant change to the CD spectrum. The overall shape of G-quadruplex remains unchanged, suggesting retention of the antiparallel structure (Fig. 4.16, Table 4.7). The enhancement of the positive band at 296 nm due to G-G base stacking suggests partial intercalation between G-tetrads by the copper complex similar to enhancement of the positive, base-base stacking band at ~270 nm attributed to intercalation of B-form duplex DNA (Maheswari and Palaniandavar, 2004). This observation is in contrast to those observed for the interaction of acridine and bis-acridine with the G-quadruplex where the decrease in the intensity of the positive band at 293 nm was interpreted as destabilization of the quadruplex structure (Nagesh *et al*. 2003). Thus, enhancement of the positive band of the CD spectrum of the present quadruplex suggests stabilization of the antiparallel quadruplex structure by the copper complexes as suggested by Musseti *et al.* (2009).

Based on the enhancement in the positive band (Fig. 4.16, Table 4.7), complex **16** with a phenyl substituent is the most effective in stabilizing G-quadrupex while complex **14**

is the least effective. Since complex **16** can bind strongly to AT-rich base sequence, there is a possibility that this complex binds to the TTA loop in G-quadrupex. Furthermore, complex **8**, which is the zinc analog of complex **16**, is known as the weakest quadruplex binder (chapter 2). This implies the significant role of the metal ion in altering the binding strength of complexes with a general formulation of [M(bipy)(L)] where M = zinc or copper and L = 2,4-dihydroxybenzaldehyde N(4)-substituted thiosemicarbazone towards the quadruplex. This could be attributed to the difference in coordination geometry of the zinc and copper complexes. Results from X-ray crystallography for complexes (**5**, **8**, **9**, **11**, **12**, **13** and **17**) and literature survey (John *et al.* 2004; Thomas *et al.* 2004; Seena and Kurup, 2007 & 2008; Latheef and Kurup, 2008) for similar complexes show that a five coordinate copper complex with a bidentate N,N'-heterocycle and a tridentate ONS-schiff base tends to adopt a distorted square pyramidal geometry with τ value less than 0.35 whereas a similar zinc complex would have a greater distortion towards a trigonal bipyramidal geometry with τ value greater than 0.4.

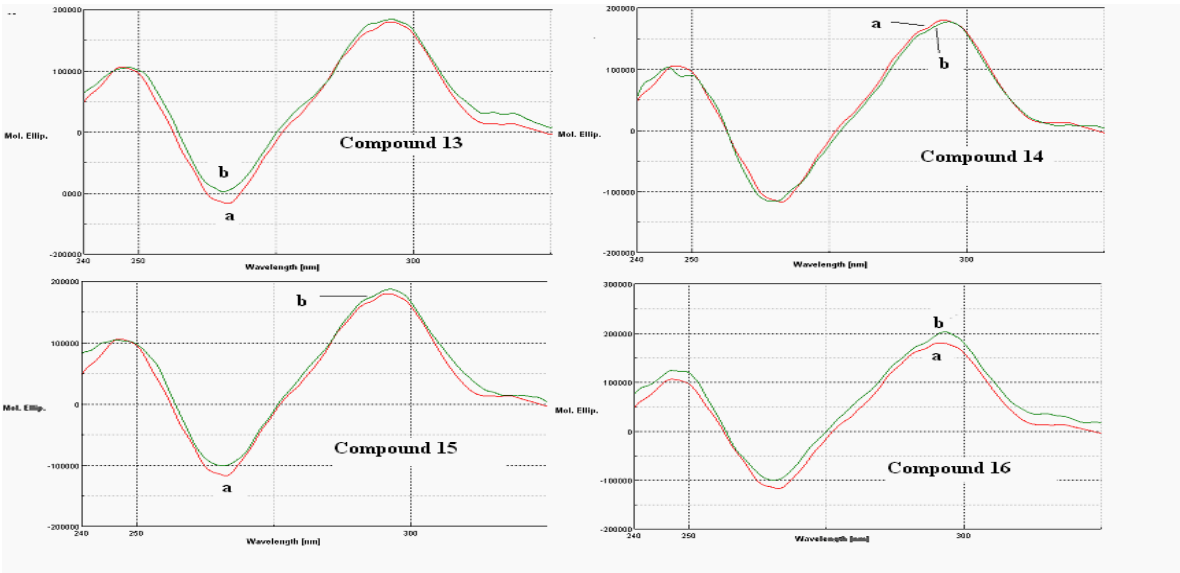

Fig. 4.16 CD spectra of 20 µM of G-quadruplex in the absence and presence of 120 µM of complex **13-16**; (a) G-quadruplex alone, (b) G-quadruplex with complex

The results from the interactions with guanine-rich duplex indicate that complexes **13** and **16** show decrease in the intensity of both the negative and positive bands with a greater decrease in the latter. This is consistent with conformational change from B to Z-like conformation (Mahadevan and Palaniandavar, 1996). Meanwhile, complexes **14** and **15** show a great increase in both the positive and negative CD spectral bands. This implies that complexes **14** and **15** intercalate strongly to the duplex and stabilize the B form of the guanine-rich duplex **(**Maheswari and Palaniandavar, 2004). The distinct difference in the conformational change induced by these two sets of complexes suggests different modes of binding towards guanine-rich duplex. This different mode of binding seems to be dependent on the N(4) substituent. It seems that complexes **13**, Cu(bipy)(HT), and **16**, Cu(bipy)(HP), without the alkyl substituent could induce conformational change from B to Z-like. Whereas, complexes **14** (methyl) and **15** (ethyl), that are alkyl substituted, will intercalate in between the guanine-rich duplex base pair. The magnitude of changes induced by these complexes towards the guanine-rich duplex is much higher compared to their zinc analogs (complexes **5-8**). This show that besides altering the base sequence recognition, the change of metal ion may also alter the binding strength of a complex towards DNA.

By comparing the extent of changes induced in both the positive and negative bands of the G-quadruplex and guanine-rich duplex, we can see that these complexes can possibly differentiate G-quadruplex from guanine-rich duplex. Since the complexes can bind to both structures and induced different conformational changes, it is not possible to determine their selectivity based on CD data alone. The feature that seems to favor stabilization of the G-quadruplex such as the presence of an alkyl substituent in the zinc series (chapter 2) does

not apply in this copper series. However, the presence of alkyl substituent in the copper series seems to promote intercalation to the guanine-rich duplex that is not seen in the zinc series either. Interestingly, in this copper series [Cu(bipy)(L)], the complex that is most effective in stabilizing G-quadruplex has a phenyl substituent while the least effective has a methyl substituent but the reverse pattern is seen in the zinc series, [Zn(bipy)(L)]. These observations show that the mode of interactions of the metal complexes with guanine-rich duplex and G-quadruplex are greatly dependent to the central metal ion. This can be attributed to the different in coordination geometry between the zinc and copper complexes as shown in the crystallographic studies.

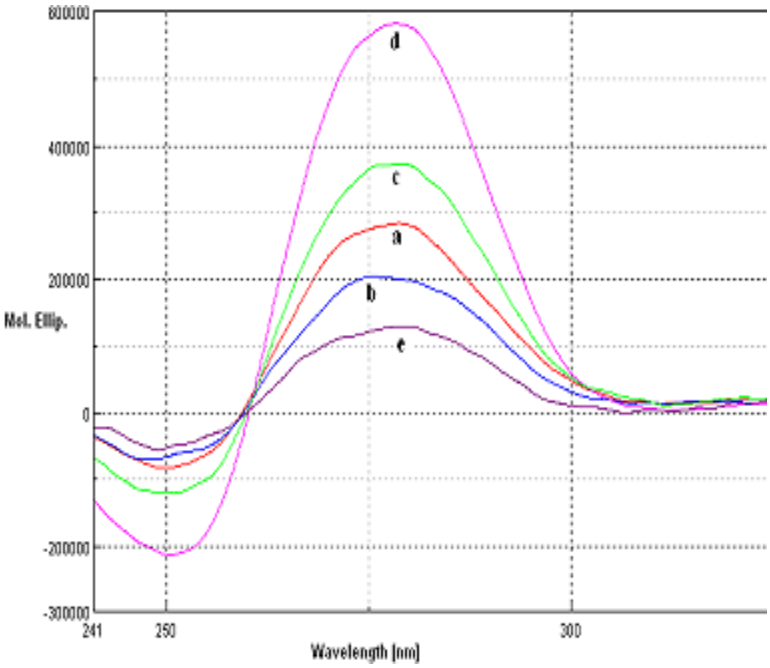

Fig. 4.17 CD spectra of 20 µM of guanine-rich duplex in the absence and presence of 120 µM of complex; (a) guanine-rich duplex alone, (b) guanine-rich duplex with complex **13,** (c) guanine-rich duplex with complex **14,** (d) guanine-rich duplex with complex **15** and (e) guanine-rich duplex with complex **16**

4.3.5 Nucleolytic study

In this study, we examine the ability of the complexes to cleave pBR322 under hydrolytic conditions and in the presence of exogenous agents, sodium ascorbate and hydrogen peroxide, using gel electrophoresis.

In the absence of exogenous agent, no cleavage was observed (results not shown) when the copper complexes were incubated with pBR322 for 24 h at 37 ^{o}C with increasing concentrations of the copper complex (10 – 1000 μM). When the DNA was incubated with 300 μM of copper complex in the presence of 30 μM sodium ascorbate, no activation of copper complexes towards DNA cleavage by sodium ascorbate is observed for complexes **15** (Fig. 4.18, lane L13) and **14** (Fig. 4.18, lane L14). However, complexes **13** and **16** can cleave the DNA in the presence of sodium ascorbate, which is evidenced from the distinct increase in intensity of the nick band (Fig. 4.18). These results imply that the presence of an electron donating alkyl group as the N(4) substituent in complexes **14** and **15** can actually stabilize the Cu(II) oxidation state whereas the presence of an electron withdrawing phenyl group in complex **16** will destabilize the 2+ oxidation state, making the complex more susceptible to reduction by sodium ascorbate. Similar observation in stabilisation of the higher oxidation state by electron donating groups has been reported by Velusamy *et al.* (2004) in their study of iron(III) complexes of sterically hindered tetradentate monophenolate ligands.

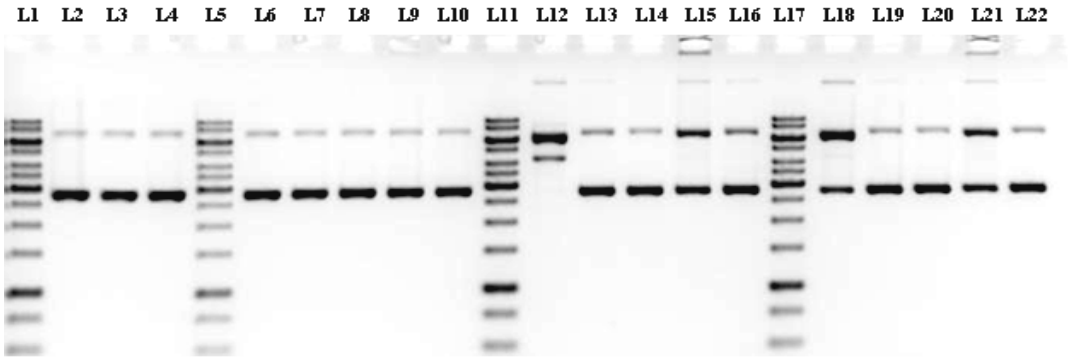

Fig. 4.18 Electrophoresis results of incubating pBR322 (0.5 μg/μL) with $CuCl_2$ or complex **13-16** in TN buffer (5 mM Tris, 50 mM NaCl) pH 7.5 at 37 ^oC for 2 h in the absence and presence of exogenous agents: Lane 1, 5, 11, 17 gene ruler 1 Kb DNA ladder; Lane 2, DNA alone (0.5 μg/μL) control; Lane 3, DNA + 30μM sodium ascorbate; Lane 4, DNA + 30μM H_2O_2; Lane 6, DNA + 300μM $CuCl_2$; Lane 7, DNA + 300μM **15;** Lane 8, DNA + 300μM **14;** Lane 9, DNA + 300μM **16;** Lane 10, DNA + 300μM **13;** Lane 12, DNA + 300μM $CuCl_2$ + 30μM sodium ascorbate; Lane 13, DNA + 300μM **15** + 30μM sodium ascorbate; Lane 14, DNA + 300μM **14** + 30μM sodium ascorbate; Lane 15, DNA + 300μM **16** + 30μM sodium ascorbate; Lane 16, DNA + 300μM **13** + 30μM sodium ascorbate; Lane 18, DNA + 300μM $CuCl_2$ + 30μM H_2O_2; Lane 19, DNA + 300μM **15** + 30μM H_2O_2; Lane 20, DNA + 300μM **14** + 30μM H_2O_2; Lane 21, DNA + 300μM **16** + 30μM H_2O_2; Lane 22, DNA + 300μM **13** + 30μM H_2O_2

Further, complex **16** (Fig. 4.18, lane L15) is more efficient in cleaving the DNA compared with complex **13** (Fig. 4.18, lane L16) based on the greater intensity of the observed nick band. If our previous assumption that an electron withdrawing group could destabilize the Cu(II) oxidation state is true, then the higher activity of complex **16** can be accounted for since it has a phenyl substituent which is more electron withdrawing compared to the two protons at N(4) in complex **13**. Another possibility is complex **16** may bind more strongly to DNA in contrast to complex **13** resulting in greater DNA cleavage. This possibility is supported by the greater enhancement of the positive band (Table 4.7) in the CD spectra for most of the tested ds(oligonucleotides) upon binding to complex **16**. The greater enhancement of the positive bands attributed to base stacking interactions suggest a

stronger mode of binding through intercalation or partial intercalation. Previously, Thomas *et al.* (2004) have studied the DNA binding and cleavage properties of ternary copper(II) complexes of formulation [Cu(Ph-tsc)phen] and [Cu(Me-tsc)phen] (H_2Ph-tsc = salicylaldehyde N(4)-phenylthiosemicarbazone and H_2ME-tsc = salicylaldehyde N(4)-ethylthiosemicarbazone). The cleavage efficiency of [Cu(Ph-tsc)phen] is greater compared with [Cu(Me-tsc)phen] which is consistent with their DNA binding strength obtained from ethidium bromide displacement assay.

When the DNA was incubated with 300 μM of copper complex in the presence of 30 μM hydrogen peroxide no activation of copper complexes towards DNA was observed for the complexes except for complex **16** (Fig. 4.18, lane L21). To determine whether all the complexes can be activated by hydrogen peroxide, the concentration of hydrogen peroxide was varied from 250 μM to 500 μM by maintaining the complex concentration at 300 μM. DNA cleavage is observed for complex **16** (Fig. 4.19, lane L15) in the presence of 250 μM hydrogen peroxide with the appearance of a nick band with very high intensity. When the concentration of hydrogen peroxide was further increased to 500 μM, complex **16** (Fig. 4.19, lane L21) converted almost all the supercoiled DNA to the nick form. Complexes **15**, **14** and **13** (Fig. 4.19, lane L19, L20 and L22) also start to cleave DNA at this hydrogen peroxide concentration based on the appearance of nick bands with similar intensity. This indicates that the copper complexes can be activated by hydrogen peroxide at high concentration and complex **16** posses the best nucleolytic efficiency in the presence of hydrogen peroxide. The zinc analog of this series cannot be activated by hydrogen peroxide. The nucleolytic efficiency of $CuCl_2$ in the presence of sodium ascorbate (Fig.

4.18, Lane L12) or hydrogen peroxide (Fig. 4.19, Lane L12) is greater compared with the ternary copper complexes. The reduced nucleolytic property of Cu(II) can be attributed to the stabilization of the 2+ oxidation state upon coordination to bipyridine and thiosemicarbazones.

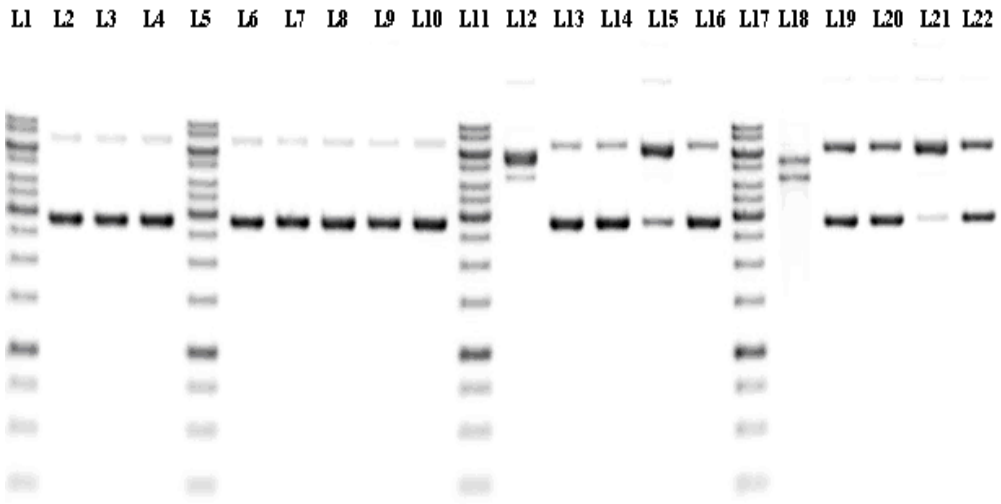

Fig. 4.19 Electrophoresis results of incubating pBR322 (0.5 μg/μL) with $CuCl_2$ or complex **13-16** in TN buffer (5 mM Tris, 50 mM NaCl) pH 7.5 at 37 ^oC for 2 h in the absence and presence of increasing hydrogen peroxide concentrations: Lane 1, 5, 11 and 17, gene ruler 1 Kb DNA ladder; Lane 2, DNA alone (0.5 μg/μL) control; Lane 3, DNA + 250μM H_2O_2; Lane 4, DNA + 500μM H_2O_2; Lane 6, DNA + 300μM $CuCl_2$; Lane 7, DNA + 300μM **15;** Lane 8, DNA + 300μM **14;** Lane 9, DNA + 300μM **16;** Lane 10, DNA + 300μM **13;** Lane 12, DNA + 300μM $CuCl_2$ + 250μM H_2O_2; Lane 13, DNA + 300μM **15** + 250μM H_2O_2; Lane 14, DNA + 300μM **14** + 250μM H_2O_2; Lane 15, DNA + 300μM **16** + 250μM H_2O_2; Lane 16, DNA + 300μM **13** + 250μM H_2O_2; Lane 18, DNA + 300μM $CuCl_2$ + 500μM H_2O_2; Lane 19, DNA + 300μM **15** + 500μM H_2O_2; Lane 20, DNA + 300μM **14** + 500μM H_2O_2; Lane 21, DNA + 300μM **16** + 500μM H_2O_2; Lane 22, DNA + 300μM **13** + 500μM H_2O_2;

Since complex **16** has the greatest nucleolytic efficency, further tests were carried out to elucidate the cleavage mechanism. Complex **16** was incubated with neocuprione (Cu(I) ion chelator), thiourea (·OH radical-specific scavenger), sodium azide (a singlet oxygen radical scavenger) and Tiron (a superoxide anion radical scavenger) in the presence

of exogenous agent. When sodium ascorbate was used as an activating agent, addition of sodium azide (Fig. 4.20, Lane L5) leads to almost total inhibition of DNA degradation. This indicates the involvement of singlet oxygen in the cleavage mechanism. No inhibition of DNA cleavage is observed when neocuproine (Fig. 4.20, Lane L6) was added, this ruled out the involvement of oxidation of Cu(I) to Cu(II) in the generation of reactive oxygen species.

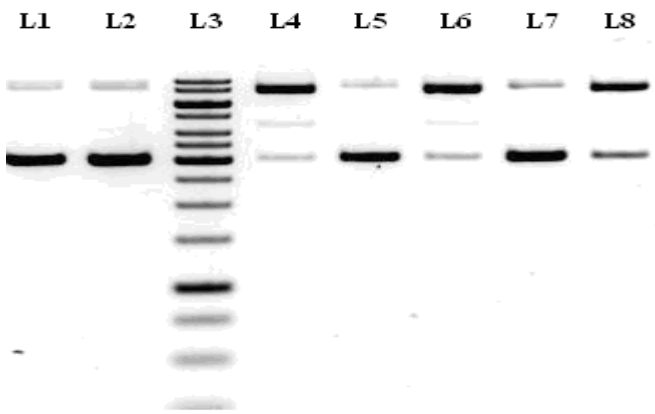

Fig. 4.20 Electrophoresis results of incubating pBR322 (0.5 μg/μL) with complex **16** in TN buffer (5 mM Tris, 50 mM NaCl) pH 7.5 at 37 ^{o}C for 2 h in the presence of sodium ascorbate and scavenging agents: Lane 1, plasmid DNA pBR322 (0.25μg/μl); Lane 2, DNA + 30 μM sodium ascorbate; Lane 3, 1kb DNA ladder; Lane 4, DNA + 300 μM complex + 30 μM sodium ascorbate (control); Lane 5, DNA + 300 μM complex + 2mM sodium azide + 30 μM sodium ascorbate; Lane 6, DNA + 300 μM complex + 2mM Neocuproine + 30 μM sodium ascorbate; Lane 7, DNA + 300 μM complex + 2mM Tiron+ 30 μM sodium ascorbate; Lane 8, DNA + 300 μM complex + 2mM Thiourea + 30 μM sodium ascorbate;

Tiron can also block the DNA cleavage (Fig. 4.20, Lane L7), this indicates the formation of superoxide radical in the cleavage mechanism. Hydroxyl radical scavengers

like thiourea can also inhibit the DNA cleavage (Fig. 4.20, Lane L8), this suggests the involvement of diffusible hydroxyl radicals in the DNA cleavage. The inhibition of DNA cleavage decreases with the following scavengers: sodium azide > Tiron > thiourea. This indicates that the major pathway in the DNA cleavage involves singlet oxygen.

Thomas *et al*. (2004) have studied the oxidative DNA cleavage activity of the some ternary copper(II) complexes with formulation of [Cu(L)B] (B = 1,10-phenanthroline, phen; dipyridoquinoxaline, dpq; dipyridophenazine, dppz; L = Ph-H_2tsc, salicylaldehyde-N(4)-phenylthiosemicarbazone) and Me-H_2tsc, salicylaldehyde-(4)-methylthiosemicarbazone) by gel electrophoresis using supercoiled (SC) pUC19 DNA in Tris–HCl buffer (pH, 7.2) in the presence of a reducing agent like mercaptopropionic acid (MPA). The complexes show significant cleavage of DNA in the dark in the presence of MPA. Mechanistic study using DMSO as hydroxyl radical scavenger revealed that the reaction pathway also involves a hydroxyl radical that can be inhibited by DMSO. In addition, Thomas *et al*. (2004) also studied light induced DNA cleavage by these complexes. Their result shows that the complexes are cleavage inactive under argon atmosphere. However, under aerobic conditions, sodium azide shows significant inhibition. The cleavage activity is also enhanced in D_2O. The results suggest the involvement of singlet oxygen ($^1O_2$) as a reactive species.

When hydrogen peroxide was used as an activating agent for the reaction with complex **16**, addition of sodium azide (Fig. 4.21, Lane L5) leads to a slight inhibition of DNA degradation. This indicates the involvement of singlet oxygen in the cleavage

mechanism. No inhibition of DNA cleavage is observed when neocuproine (Fig. 4.21, Lane L6) was added, this ruled out the involvement of oxidation of Cu(I) to Cu(II) in the generation of reactive oxygen species. Tiron shows the greatest inhibitions in the DNA cleavage, suggesting the formation of superoxide radical as the key mechanism in DNA cleavage (Fig. 4.21, lane L7). No involvement of diffusible hydroxyl radicals in the DNA cleavage is observed (Fig. 4.21, Lane L8).

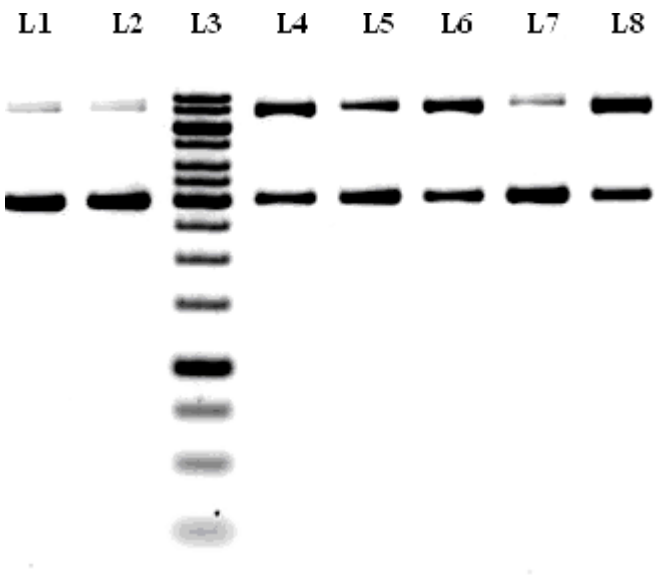

Fig. 4.21 Electrophoresis results of incubating pBR322 (0.5 μg/μL) with complex 16 in TN buffer (5 mM Tris, 50 mM NaCl) pH 7.5 at 37 ^{o}C for 2 h in the presence of hydrogen peroxide and scavenging agents: Lane 1, plasmid DNA pBR322 (0.25μg/μl); Lane 2, DNA + 30 μM hydrogen peroxide; Lane 3, 1kb DNA ladder; Lane 4, DNA + 300 μM complex + 30 μM hydrogen peroxide (control); Lane 5, DNA + 300 μM complex + 2mM sodium azide + 30 μM hydrogen peroxide; Lane 6, DNA + 300 μM complex + 2mM Neocuproine + 30 μM hydrogen peroxide; Lane 7, DNA + 300 μM complex + 2mM Tiron+ 30 μM hydrogen peroxide; Lane 8, DNA + 300 μM complex + 2mM Thiourea + 30 μM hydrogen peroxide;

4.3.6 Topoisomerase I inhibition assay

Topoisomerases are gaining prominence as a target for anticancer drugs owing to clinical successes of the camptothecin derivatives that target these enzymes. Despite the successful

approach of inhibiting DNA topoisomerase I (Topo I) in the design of anticancer agents, a significant need for less toxic and more chemically stable Topoisomerase I inhibitors still persists (Dexheimer & Pommier, 2008). However, very few metal complexes have been reported to inhibit topoisomerases (Kikuta *et al*. 2000; Chuang *et al*. 1996). Previously, we learnt that some of our ternary zinc complexes derived from N(4)-substituted thiosemicarbazone and heterocyclic base such as 2,2'-bipyridine or 1,10-phenanthroline (chapters 2 and 3) can inhibit topoisomerase I with the right combinations of ligands. Continuing our efforts to develop more ternary complexes that can inhibit topoisomerase I, the effect of varying the metal of these complexes from zinc to copper is studied.

In our DNA relaxation assay, one unit of human topoisomerase I can completely convert all the supercoiled plasmid pBR322 (4.4 kb) to fully relaxed topoisomer, which is the completely unwound covalently bonded closed circular DNA (Fig. 4.22, lane L7). This is found in the slowest moving DNA band (labelled Form II) which contains the fully relaxed closed circular pBR322 and the originally present, small amount of nicked DNA. No cleavage or unwinding of the DNA was observed when pBR322 was incubated with 40 μM of complexes **13-16** alone (Fig. 4.22, lane L2-L5). As can be seen from Fig. 4.22 (lane L10 and L11), complexes **16** and **13** are capable of inhibiting topo I. The topoisomerase inhibition property of complex **16** (Table 4.7) could be attributed to its ability to bind strongly to AT-rich sequence (Kikuta et al. 2000). Minor groove binders, such as distamycin A and 4,6-diamidino-2-phenylindole *(*DAPI*)* can suppress Topo I-linked DNA breaks. These minor groove binders, recognize AT-rich regions of DNA mainly by hydrogen bondings. However, the ability of complex **13** in inhibiting topoisomerase I is not

clear since it does not show significantly stronger binding to the AT-rich sequence compared with complexes **12** and **14**. Interestingly, the zinc analog of complex **13** cannot inhibit topoisomerase I indicating the importance of copper. This could be attributed to the different in coordination geometry between zinc and copper for our ternary complexes as shown by crystallography data.

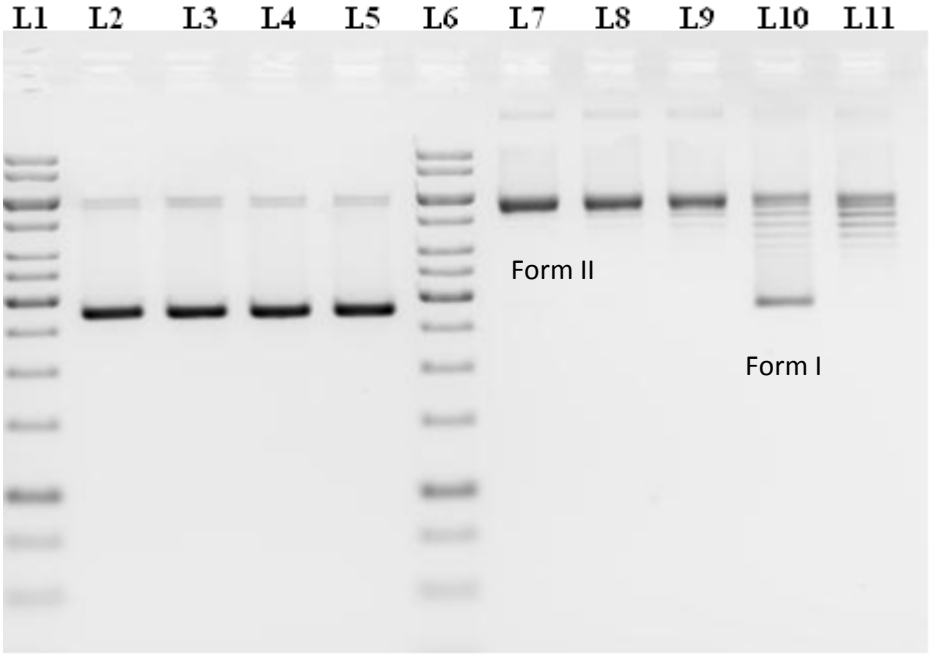

Fig. 4.22 Human topoisomerase I inhibition assay by gel electrophoresis. Electrophoresis results of incubating human topoisomerase I (1 unit/21μL) with pBR322 in the absence or presence of 40 μM of complex: Lane 1 & 6, gene ruler 1 Kb DNA ladder; Lane 2, DNA + 40μM **15** (control);Lane 3, DNA + 40μM **14** (control); Lane 4, DNA + 40μM **16**(control); Lane 5, DNA + 40μM **13**(control); Lane 7, DNA+ 1unit Human Topoisomerase I (control); Lane 8, DNA + 40μM **15**+ 1unit Human Topoisomerase I; Lane 9, DNA + 40μM **14** + 1unit Human Topoisomerase I; Lane 10, DNA + 40μM **16** + 1unit Human Topoisomerase I; Lane 11, DNA + 40μM **13** + 1unit Human Topoisomerase I

As a preliminary investigation into the mechanism of action of the above topoisomerase I inhibition, we used three variations of mixing the DNA, topoisomerase I and the copper complexes (at 40 μM) for the inhibition assay. When the three components

were mixed simultaneously, there is slight inhibiton of topoisomerase Iby complexes **13** and **16** as seen by the presence of the fastest moving band with low intensity (Form I) which consists of supercoiled DNA and poorly relaxed DNA (Fig. 4.23, lane L5). The bands of topoisomers with different degree of relaxation can also be seen in between Form I and Form II. Secondly, when the complex was incubated first with topoisomerase I before the addition of DNA; the intensity of the fastest moving band is the highest for complexes **13** and **16** with almost total disappearance of the slowest moving band (Form II), suggesting almost total inhibition of topoisomerase I (Fig. 4.23, lane L6). The inhibition of complex **16** is slightly better compared with complex **13** with this sequence of addition based on the intensity of the fastest moving band (form I).

Finally, when the DNA was first incubated with copper complex for 30 minutes before the addition of topoisomerase I (Fig. 4.23, lane L7), the fastest moving band (Form I) almost disappears completely for complex **13** whereas the fastest moving band can still be seen in complex **16**. This again indicates that complex **16** is a better topoisomerase I inhibitor. The intensity of Form I is lower for both complexes in contrast to the second method of mixing. These observed differences in inhibition of topoisomerase I suggest initial binding of the copper complex to either the topoisomerase I or the DNA give rise to differences in mode of action. By comparing lanes L6 and L7, we infer that since greater inhibition of topoisomerase I is observed when the complex is incubated with topo first, the main pathway in inhibition process most likely involves the binding of complex to the enzyme. However, further investigation is required to confirm this.

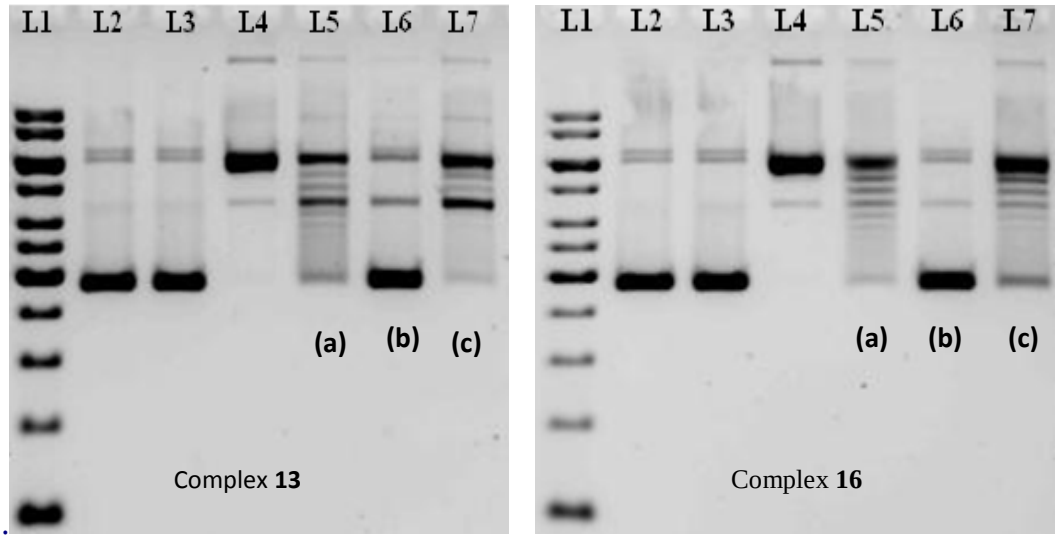

Fig. 4.23 Effect of sequence of mixing for the human topoisomerase I inhibition assay of complex **13** and **16**. Electrophoresis results of incubating human topoisomerase I (1 unit/21μL) with pBR322: Lane 1, 1 kb DNA ladder; Lane 2, Plasmid DNA pBR 322 (control); Lane 3, DNA + 40μM complex (control); Lane 4, DNA+ 1unit Human Topoisomerase I (control); (a) All components mixed at the same time; Lane 5, DNA + 40μM complex + 1unit Human Topoisomerase I ; (b) Complex + TopoI incubated for 30 minutes first before DNA is added; Lane 6, DNA + 40μM complex + 1unit Human Topoisomerase I; (c) Complex + DNA incubated for 30 minutes first before TopoI is added; Lane 7, DNA + 40μM complex + 1unit Human Topoisomerase I

4.3.7 Antibacterial and antifungal assay

4.3.7.1 Antibacterial activity

As seen in section 3.3.8.1, the antibacterial activity of ligands and complexes were assessed against the same six species. All ligands and complexes had some degree of inhibitory activity against the bacteria tested (Table 4.8). Among the four thiosemicarbazones ligands tested, ligand **4** shows the highest inhibition against *B. cereus* and *K. pneumonia* with MIC value 31.25 μg/ml.

Table 4.8.

Mean MIC value (μg/ml) towards microbes tested.

Compound	Bacteria					
	S. aureus	*B. cereus*	*P. aeruginosa*	*K. pneumonia*	*E. coli* (penicillin-sensitive strain)	*E. coli* (penicillin-resistant strain)
1	62.50	62.50	62.50	62.50	62.50	62.50
2	125.00	62.50	125.00	62.50	62.50	62.50
3	62.50	62.50	62.50	62.50	62.50	62.50
4	62.50	31.25	62.50	31.25	62.50	62.50
13	62.50	62.50	104.17	62.50	62.50	62.50
14	31.25	31.25	31.25	250.00	62.50	62.50
15	15.63	15.63	15.63	31.25	62.50	62.50
16	31.25	26.04±9.02	62.50	62.50	62.50	62.50
$CuCl_2$	-	-	-	-	-	-
bipy	125	62.50	62.50	62.50	62.50	62.50
Drug	8.00	4.00	4.00	4.00	4.00	4.00

" - " : no activity

Drug used in antibacterial assay = Chloramphenicol

Upon complexation, improvement of antibacterial activity towards *S. aureus, B. cereus, P. aeruginosa* and *K. pneumonia* are seen for complexes **14-16** compared with the free thiosemicarbazones or bipyridine ligands. However, a few exceptions are seen for the *K. pneumoniae* strain. The antibacterial property of complexes **14** and **16** towards *K. pneumonia* was less in contrast to the free ligands. However, no improvement is seen for complex **13** and the antibacterial activity towards *P. aeruginosa* even decreases to 104.17 μg/ml. None of the complexes showed improvement in efficacy towards *E.coli* compared

with their corresponding thiosemicarbazones ligands. Complex **14** shows good antibacterial activity towards *S. aureus*, *B. cereus* and *P. aeruginosa* with MIC value of 31.25 μg/ml. Complex **15** is twice as effective as complex **14** with MIC values of 15.63 μg/ml towards these three strains of bacteria. This suggests that elongation of alkyl chain in complex **15** helps to improve its antibacterial activity correlated with increasing hydrophobicity. Similar improvement in antibacterial activity with the increase in the length of alkyl chain has been reported by Kim *et al.* (1997) in their study of chitosan derivatives with quaternary ammonium salts. This increased activity has been ascribed to the contribution of the increased hydrophobic properties of the derivatives.

Complex **15**, [Cu(bipy)(HE)], with an ethyl substituent at the N(4) atom, is the most potent antibacterial complex in this copper series with the lowest MIC value towards *S. aureus*, *B. cereus*, *K. pneumonia* and *P. aeruginosa*. However, for a similar system with zinc , complex **8**, [Zn(bipy)(HP)], with a phenyl substituent is the most active. This shows that the trend in antibacterial activity for metal complexes with the same series of ligands will differ with the change in central metal ion. Copper complexes (**14** and **15**) derived from ligands **2** and **3** also show better antibacterial activity compared with their zinc analogs (complex **6** and **7**). The antibacterial activity of complex **15**, [Cu(bipy)(HE)], is not compatible with topoisomerase I inhibition unlike complex **8** from the zinc series. Toposiomerase I has been implicated as a good target for the development of antibacterial drug (Tse-Dinh, 2009). This could be attributed to the success of the currently marketed inhibitors such as the quinolones dervatives (Bradbury and Pucci, 2008). This suggests that the mode of action for the antibacterial activity of copper complexes may not be similar to

zinc. Recently, Rodríguez-Argüelles *et al*. (2009) have studied the antibacterial activity of metal complexes of 2-acetyl-butyrolactone and 2-furancarbaldehyde thiosemicarbazones. Their results show that the activity of the copper complexes is always better compared with their zinc analogs and they suggest that the observed biological activity for copper may involve redox processes. This argument seems reasonable given that copper complexes are usually redox active whereas zinc complexes are usually inert.

4.3.7.2 Antifungal activity

In the previous section, the antibacterial property of the copper complexes was discussed. This section presents the results and discussion of their antifungal property. All complexes had some degree of inhibitory activity against the fungi tested (Table 4.9).

Most of the tested complexes do not show better antifungal properties than the free 2,2'-bipyridine ligand even though their antifungal properties are mostly better than the free thiosemicarbazones ligands. This implies that formation of ternary complexes does not lead to much improvement in antifungal properties. The antifungal property for complexes **13** and **16** is the same as the ligand for *C. albicans.* The same is observed for complex **15** towards *C. parapsilosis* and *C. neoformans*. Complex **14** is the only complex that shows better antifungal property towards both *C. neoformans* and *A.niger* when compared with its free ligands (**2** and 2,2'-bipyridine). Complex **14** possesses the lowest MIC value of 7.81 µg/ml towards *C. neoformans.* This makes it the most active antifungal agent in our assay. Complexes **13** and **16** show better antifungal properties towards *C. neoformans* and *A.niger*

respectively in contrast to their free ligands (thiosemicarbazones and 2,2'-bipyridine). Both complexes have MIC value of of 15.63 µg/ml. Generally, most of the copper complexes in this series posses better antifungal property than their zinc analogs (chapter 2). Similar trends have been reported by Rodríguez-Argüelles *et al*. (2009) for metal complexes of 2-acetyl-butyrolactone and 2-furancarbaldehyde thiosemicarbazones.

Table 4.9
Mean MIC value (µg/ml) towards fungi tested.

Compound	Fungi			
	C. albicans	*C. parapsilosis*	*C. neoformans*	*A.niger*
1	31.25	62.50	31.25	62.50
2	31.25	31.25	31.25	62.50
3	31.25	31.25	31.25	62.50
4	31.25	62.50	7.81	31.25
13	31.25	31.25	15.63	31.25
14	15.63	15.63	7.81	15.63
15	15.63	31.25	31.25	31.25
16	31.25	31.25	15.63	15.63
$CuCl_2$	-	-	-	-
Bipy	15.63	15.63	31.25	31.25
Drug	1.00	2.00	1.00	4.00

All values are expressed as mean ± standard deviation of three replicates

" - " : no activity. Drug used in antifungal assay = fluconazole

4.4 Conclusion

Four new copper complexes with the formulation Cu(bipy)L where bipy = 2,2'-bipyridine and L are the doubly deprotonated thiosemicarbazones have been successfully synthesized and characterized. All copper complexes are five-coordinated with the doubly deprotonated thiosemicarbazones ligands behaving as a tridentate ligand coordinating through one phenolic oxygen, azomethine nitrogen and thiolate sulfur while the 2,2'-bipyridine is coordinated as the *N,N'*-bidentate ligand. However, the coordination geometry around the copper complexes is square pyramidal in contrast to their zinc analogs (Zn(bipy)L) that adopt trigonal bipyramidal distorted square based pyramid (TBDSBP) geometry.

Complexation of the ligands with copper lead to formation of a series of ternary complexes Cu(bipy)L with better biological properties compared with their zinc analogs. Complex **14**, Cu(bipy)(HM), which is the copper analog for complex **6**, Zn(bipy)(HM), retains its ability to effectively recognize CG rich sequence in DNA. The modes of binding towards base sequences for complexes **13**, **14**, **15** and **16** are quite different from those observed for their zinc analogs. The greatest difference is observed in binding towards the G-quadruplex. This again underscores that the synergistic effect of metal and ligand could be an underlying factor in molecular recognition of a DNA sequence or structure since a slight variation in the central metal ion for complexes with same ligands could lead to such diverse modes and strengths of binding. Unlike their zinc analogs, the copper complexes can be activated by sodium ascorbate or hydrogen peroxide to induce DNA cleavage. The nucleolytic efficiency is enhanced with the presence of an electron withdrawing group (phenyl) as the N(4) substituent. The mechanism for topoisomerase I inhibition most likely

involved the binding of the complex to topoisomerase I as the main pathway. Most of the copper complexes exhibit wider spectrum of antibacterial and antifungal properties with better MIC values compared to their zinc analogs. Complex **16**, Cu(bipy)(HP), has a good potential to be developed as a drug or DNA probe owing to its strong binding towards the AT-rich region in DNA, topoisomerase I inhibition activity and nucleolytic efficiency. It is noteworthy that complex **8**, Zn(bipy)(HP) which is the zinc analog for complex **16**, also possesses topoisomerase I inhibition activity, the best antibacterial and antifungal properties in the zinc series. This further substantiate the role of the phenyl group at the N(4) position in bestowing desirable biological activities to a complex regardless of its metal centre.

Chapter 5

Synthesis, characterization and biological properties of copper(II) complexes of 2,4-dihydroxybenzaldehyde N^4-substituted thiosemicarbazones and 1,10-phenanthroline

5.1. Introduction

In an earlier chapter (chapter 2), we showed that the N(4) substituents play a role in determining the selectivity and potency of zinc(II) complexes of 2,4-dihydroxybenzaldehyde N(4)-substituted thiosemicarbazones and 2,2'-bipyridine with the general formulation of Zn(bipy)(L). These complexes exhibit interesting biological activities from DNA sequence recognition, quadruplex binding, topoisomerase I inhibition, antibacterial to antifungal property. However, these zinc complexes are lacking in nucleolytic efficiency. When the zinc(II) ion was replaced with copper(II) ion we observed some improvements in biological activities of these complexes, Cu(bipy)(L) particularly their nucleolytic efficiency (chapter 4). These encouraging results have spurred us to introduce further modifications to these complexes by replacing 2,2'-bipyridine with 1,10-phenanthroline. We hope that this modification will result in complexes that can bind more strongly to DNA and hence wth better nucleolytic property as mentioned earlier. (Ramakrishnan and Palaniandavar, 2008; Roy *et al.* 2007; Patra *et al.* 2005; Dhar *et al.* 2005; Thomas *et al.* 2003).

Therefore, continuing our interest in improving the biological properties of these complexes, we report the effect of varying the N(4) substituent from proton, methyl, ethyl to phenyl upon the chemical and biological properties (DNA binding, nucleolytic,

topoisomerase I inhibition and antimicrobial) of ternary Cu(II) complexes containing 1,10-phenanthroline as the heterocyclic base. Cross comparison of the chemical and biological properties of this series (Cu(phen)(L)) with the zinc(II) series (Zn(phen)(L)) in chapter 3 will be carried out to study the effect of varying the metal ions in same ligand environment whereas comparison with its 2,2'-bipyridine analogs (Cu(bipy)(L)) in chapter 4 could help us in studying the effect of varying the polypyridyl ligand.

5.2. Experimental

5.2.1. Materials and solutions

Similar materials were used as reported in chapter 2.

5.2.2. Physical measurements

Spectroscopic measurements and elemental analyses were similarly carried out as reported in chapter 2.

5.2.3 Syntheses

5.2.3.1 Synthesis of (4-Hydroxy-2-oxidobenzaldehyde thiosemicarbazonato)-(1,10-phenanthroline)copper(II)monohydrate [Cu(phen)(HT)].H_2O **(17)**

Copper acetate dihydrate (0.22 g, 1 mmol) and 1,10-phenanthroline (0.20 g, 1 mmol) were heated in ethanol (20 ml) for 1 hour followed by addition of 2,4-dihydroxybenzaldehyde

thiosemicarbazone (0.21 g, 1 mmol) in hot ethanol (20 ml). The mixture was refluxed for another 3 hours.

(Yield: 0.33 g, 80%). Anal. Calc. for $C_{20}H_{17}N_5O_3SCu$: C, 51.00; H, 3.64; N, 14.87. Found: C, 50.88; H, 3.60; N, 14.68%. IR (KBr disc, cm^{-1}): 3450 w, 3350m, 3277 w, 3170 w, 3058w, 1602 s, 1491 s, 1425 m, 1318 m, 1222 s, 1184 m, 1122 m, 842 m, 726 m, 595 w, 553w, 473 w (s, strong; m, medium; w, weak).

5.2.3.2 Synthesis of (4-Hydroxy-2-oxidobenzaldehyde 4-methylthiosemicarbazonato)-(1,10-phenanthroline)copper(II) monohydrate, [Cu(phen)(HM)]. H_2O **(18)**

Complex **18** was similarly prepared as complex **17** by using 2,4-dihydroxybenzaldehyde 4-methylthiosemicarbazone (0.23 g, 1 mmol) as the Schiff base.

(Yield: 0.39 g, 80%). Anal. Calc. for $C_{21}H_{19}N_5O_3SCu$: C, 52.00; H, 3.95; N, 14.44. Found: C, 51.82; H, 3.73; N, 14.25%. IR (KBr disc, cm^{-1}): 3422 (broad), 3329 m, 3058 w, 1598 s, 1524s, 1426 w, 1404 m, 1327 m, 1267 m, 1216 s, 1279 w, 1182 m, 1122 m, 843 m, 727 m, 593 w, 553w, 471 w, (s, strong; m, medium; w, weak).

5.2.3.3 Synthesis of (4-Hydroxy-2-oxidobenzaldehyde 4-ethylthiosemicarbazonato)-(1,10-phenanthroline)copper(II) monohydrate, [Cu(phen)(HE)].H_2O **(19)**

Complex **19** was similarly prepared as complex **17** by using 2,4-dihydroxybenzaldehyde 4-ethylthiosemicarbazone (0.24 g, 1 mmol) as the Schiff base.

(Yield: 0.39 g, 78%). Anal. Calc. for $C_{22}H_{21}N_5O_3SCu$: C, 52.95; H, 4.24; N, 14.03. Found: C, 52.45; H, 4.24; N, 13.70%. IR (KBr disc, cm^{-1}): 3457 m, 2964 m, 1602 s, 1490s, 1425 s,

1342 m , 1280 m m, 1209 s, 1123 m, 841 m, 726 m, 554 m, 462 w, 420 w (s, strong; m, medium; w, weak).

5.2.3.4 Synthesis of (4-Hydroxy-2-oxidobenzaldehyde 4-ethylthiosemicarbazonato)-(1,10-phenanthroline)copper(II) monohydrate, [Cu(phen)(HP)]. H_2O **(20)**

Complex **20** was similarly prepared as complex **17** by using 2,4-dihydroxybenzaldehyde 4-phenylthiosemicarbazone (0.29 g, 1 mmol) as the Schiff base ligand.

(Yield: 0.44 g, 83%). Anal. Calc. for $C_{26}H_{19}N_5O_3SCu$: C, 59.02; H, 3.62; N, 13.24. Found: C, 58.81; H, 3.39; N, 13.65%. IR (KBr disc, cm^{-1}): 3398 m, 3058 w, 1601 s, 1541 m, 1499 s, 1430 s, 1313 m, 1220 m, 1179 m, 845 m, 726 m, 695 w, 588 w, 506 w, 420 w (s, strong; m, medium; w, weak).

5.2.4 X-ray crystallography

Greenish crystal for complex **18a** was recrystallised from DMSO. The unit cell parameters and the intensity data were collected on a Bruker SMART APEX CCD diffractometer, equipped with Mo Kα X-ray source (λ=0.71073 Å). Data collection, structure solution and refinement for complex **18a** were carried out as mentioned in chapter 2.

5.2.5 DNA binding

DNA binding was studied by using circular dichroism as reported in chapter 2.

5.2.6 Nucleolytic study

Agarose gel electrophoresis experiments were carried out on supercoiled plasmid DNA pBR322 (4.4 kb) using a horizontal gel system as described in chapter 2.

5.2.7 Human Topoisomerase I inhibtion assay

The human DNA topoisomerase I inhibitory activity was determined by measuring the relaxation of supercoiled plasmid DNA pBR322 as described in chapter 2.

5.2.8 Antibacterial and antifungal assay

For this series of Cu(phen)(L) complexes, the antibacterial and antifungal activities of the complexes were investigated as previously mentioned in chapter 2.

5.3 Results and discussions

5.3.1 Synthesis of the complexes

The stoichiometries, color and partial elemental analyses of the ligands and copper(II) complexes are shown in Table 5.1. All the complexes are prepared in high yield by

refluxing copper acetate dihydrate, 1,10-phenanthroline and the thiosemicarbazones in ethanol. Proposed structures for all the complexes with IUPAC numbering scheme are shown in Fig. 5.1. Results from partial elemental analyses are in good agreement with the proposed formulation of Cu(phen)L where phen = 1,10-phenanthroline and L are the doubly deprotonated thiosemicarbazones. The complexes exist as a monohydrate and are greenish in colour. Complex **18a** has additionally a DMSO in its lattice structure.. These complexes are insoluble in common polar and non-polar solvents but are soluble in DMF and DMSO. Magnetic susceptibility measurements indicates that the complexes are very close to the spin-only value of 1.73 B.M in accordance to d^9 configuration of copper(II) (Bindu *et al.*, 1999)

17 R = H **18** R = $-CH_3$ **19** R = $-C_2H_5$ **20** R = $-C_6H_5$

Fig. 5.1 Proposed structure for all the complexes

Table 5.1

Stoichiometries, color and partial elemental analyses of the copper(II) complexes

Complex	Stoichiometries	Color	Anal. Calc. (Found)%			μ effective
			C	H	N	(B.M)
[Cu(phen)(HT)] .H_2O **(17)**	$C_{20}H_{17}N_5O_3SCu$	Green	51.00 (50.88)	3.64 (3.60)	14.87 (14.68)	1.82
[Cu(phen)(HM)].H_2O **(18)**	$C_{21}H_{19}N_5O_3SCu$	Green	52.00 (51.82)	3.95 (3.73)	14.44 (14.25)	1.84
[Cu(phen)(HM)].H_2O .DMSO **(18a)**	$C_{23}H_{25}CuN_5O_4S_2$	Green	49.05 (49.36)	4.47 (4.26)	12.44 (12.85)	1.84
[Cu(phen)(HE)].H_2O **(19)**	$C_{22}H_{21}N_5O_3SCu$	Green	52.95 (52.45)	4.24 (4.44)	14.03 (13.70)	1.83
[Cu(phen)(HP)].H_2O **(20)**	$C_{26}H_{19}N_5O_3SCu$	Green	59.02 (58.81)	3.62 (3.39)	13.24 (13.65)	1.84

5.3.2 Crystal structure analysis

5.3.2.1 Crystal structures of [Cu(phen)(HM)].H_2O.DMSO (**18a**)

The complex is mononuclear and five coordinated with the doubly deprotonated thiosemicarbazone as a tridentate ligand coordinating through the phenolic oxygen, azomethine nitrogen and thiolate sulfur atoms. and with 1,10-phenanthroline as the *N,N'*-bidentate ligand (Fig. 5.2)**.** This complex is isomorphous with complex **11a**. Calculation of the trigonality index τ, gives a value 0.30 for **18a**. This indicates that the coordination geometry around copper is distorted square pyramidal.

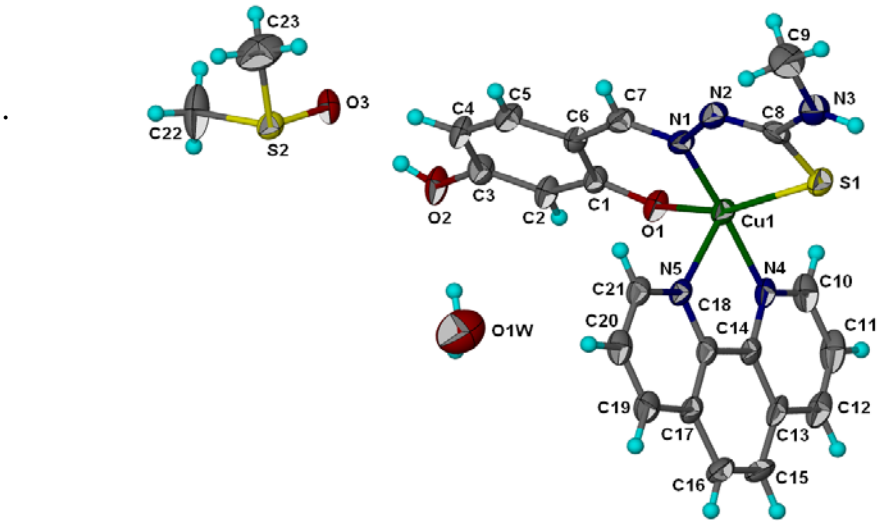

Fig. 5.2 Thermal ellipsoid (Barbour, 2001) plot of **18a** drawn at the 70% probability level. Hydrogen atoms are drawn as spheres of arbitrary radii.

Selected bond lengths and angles are presented in Table 5.3. The variation in Cu–N bond distances, Cu(1)–N(1), 1.944(4), Cu(1)–N(4), 2.040(4) and Cu(1)–N(5), 2.230(4) Å

indicate differences in the strengths of the bonds formed by each of the coordinating nitrogen atoms. The Cu–N bond lengths for N1 and N5 are shorter than those reported in mononuclear copper(II) complex, [Cu(Ph-tsc)phen] (Ph-H_2tsc = salicylaldehyde-N(4)-phenylthiosemicarbazone) by Thomas *et al.* (2004). The Cu–S bond length of 2.281(1) Å is also slightly shorter than those reported by Thomas *et al.* (2004). The imine bond formation is evidenced from N2-C8 and N1-C7 distances of 1.290(7) and 1.295(6) Å. Upon complexation, the C8-N2 bond length of 1.354(4) decreases to 1.290(7) and C8-S1 increases from 1.699(3) to 1.757(5) Å. The changes in bond length are attributed to partial loss and gain of double bond character in accordance to coordination of thiosemicarbazone in the thiolate form.

Hydrogen bonding parameters are shown in Table 5.4. Two mononuclear molecules are linked through two water molecules across a center-of-inversion. The 4-hydroxy group of the thiosemicarbazone ligand forms a hydrogen bond to the disordered DMSO solvate molecule as shown in Fig. 5.3. Formation of a hydrogen bond with DMSO hampers the formation of two or three dimensional network as seen for other complexes earlier where the hydroxyl group link the complex to adjacent mononuclear molecule through direct hydrogen bonding or through another water molecule. The packing of the molecules is stabilized by combination of hydrogen bonding and π-π interactions between aromatic rings as shown in Fig. 5.4.

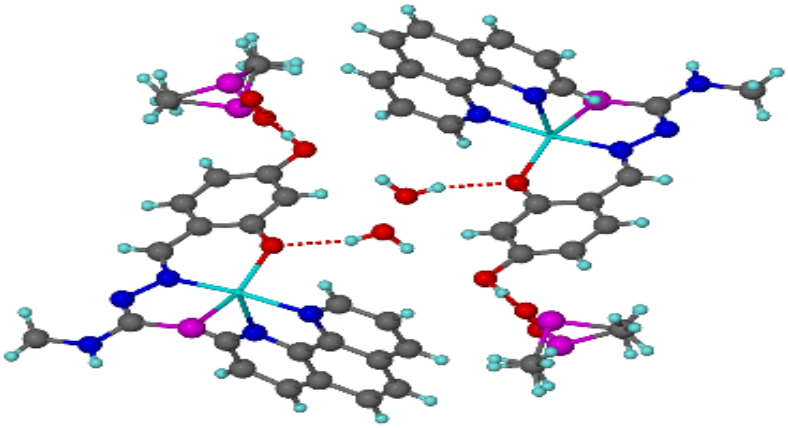

Fig. 5.3 Hydrogen bonding interactions for complex **18a**

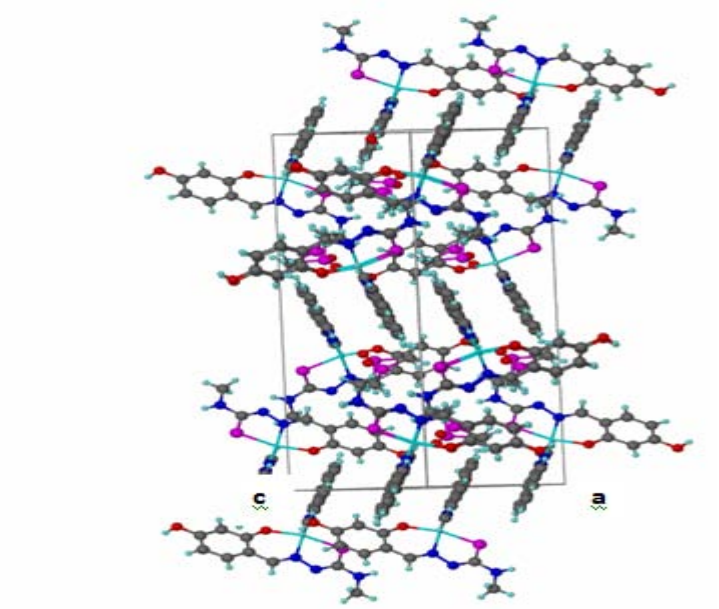

Fig. 5.4 Unit cell packing diagram of **18a** view in between c and a axis.

Table 5.2 Crystal data and structure refinement parameters for complex **18a**

Complex	[Cu(phen)(HM)].H_2O.DMSO (**18a**)
Empirical formula	$C_{23}H_{25}CuN_5O_4S_2$
Formula weight	563.14
Crystal system	Monoclinic
Space group	$P2_1/c$
Unit cell dimensions	
a (Å)	9.6205(2) Å
b (Å)	25.9915(5) Å
c (Å)	9.7074(2) Å
α (°)	93.544(2)°
Volume, V ($Å^3$)	2422.71(8)
Z	4
F(0 0 0)	1164
Density (calculated), (mg m^{-3})	1.544
Absorption coefficient, μ(mm^{-1})	1.12
Temperature, T (K)	100 (2)
Crystal size (mm)	0.28 × 0.08 × 0.04
Reflections collected	24973
Independent reflections	5569 [R(int) = 0.085]
Data/restraints/parameters	5569/10/346
$R[F^2 > 2\sigma(F^2)]$	0.059
$wR(F^2)$	0.182
S	1.10
Largest difference peak and hole (e $Å^{-3}$)	0.63 and −0.82

Table 5.3

Selected bond lengths (Å) and angles (˚) for [Cu(phen)(HM)].H_2O.DMSO (**18a**)

Bond lengths		Bond angles	
Cu1—N1	1.944 (4)	N1—Cu1—N4	172.1 (2)
Cu1—N4	2.040 (4)	N1—Cu1—N5	94.2 (2)
Cu1—N5	2.230 (4)	N1—Cu1—O1	93.3 (2)
Cu1—O1	1.965 (3)	N1—Cu1—S1	84.8 (1)
Cu1—S1	2.281 (1)	N4—Cu1—O1	90.9 (2)
S1—C8	1.757 (5)	N4—Cu1—N5	78.4 (2)
O1—C1	1.313 (6)	N4—Cu1—S1	94.4 (1)
O2—C3	1.366 (6)	N5—Cu1—O1	101.8 (2)
N1—C7	1.295 (6)	N5—Cu1—S1	104.0 (1)
N1—N2	1.409 (5)	O1—Cu1—S1	154.2 (1)
N2—C8	1.290 (7)		
N3—C8	1.369 (6)		
N3—C9	1.453 (7)		
N4—C10	1.322 (7)		

Table 5.4

Hydrogen-bond geometry (Å, °) for [Cu(phen)(HM)].H_2O.DMSO (**1a**)

D—H···*A*	*D*—H	H···*A*	*D*···*A*	*D*—H···*A*
O2—H2o···O3	0.84 (1)	1.84 (2)	2.681 (8)	173 (8)
O2—H2o···O3'	0.84 (1)	1.82 (4)	2.61 (1)	155 (8)
O1w—H1w1···O1^{i}	0.85 (1)	2.06 (4)	2.878 (6)	160 (9)
O1w—H1w2···O2	0.85 (1)	2.23 (3)	3.054 (7)	163 (9)

Symmetry codes: (i) −*x*+1, −*y*+1, −*z*+1.

5.3.3 Infrared and electronic spectra

IR spectra for all the complexes are shown in Fig. 5.5. Important IR bands for the ligands and complexes are given in Table 5.5. Thiosemicarbazones are known to exhibit thione-thiol tautomerization (Fig. 5.6). The absence of any band around 2600-2800 cm^{-1} ν(S-H) indicates that in the solid form, all the ligands exist in the thione form (Bindu *et al.* 1999; Afrasiabi *et al.* 2005). The IR spectra for the complexes are similar to their 2,2'-bipyridine derivatives discussed in chapter 2. Therefore, the mode of binding of the ligands should be the same.

Fig. 5.6 Thione-thiol tautomerization for the ligands
(Depicted again for easy reference)

The appearance of new ν(Cu-N) bands in the range of 450-479 cm^{-1} confirms the coordination through azomethine and polypyridyl nitrogens. Coordination through phenolic oxygen is confirmed by the presence of ν(Cu-O) band at around at around 426-430 cm^{-1} (Bindu *et al.* 1999; Seena and Kurup, 2007; Latheef and Kurup, 2008).

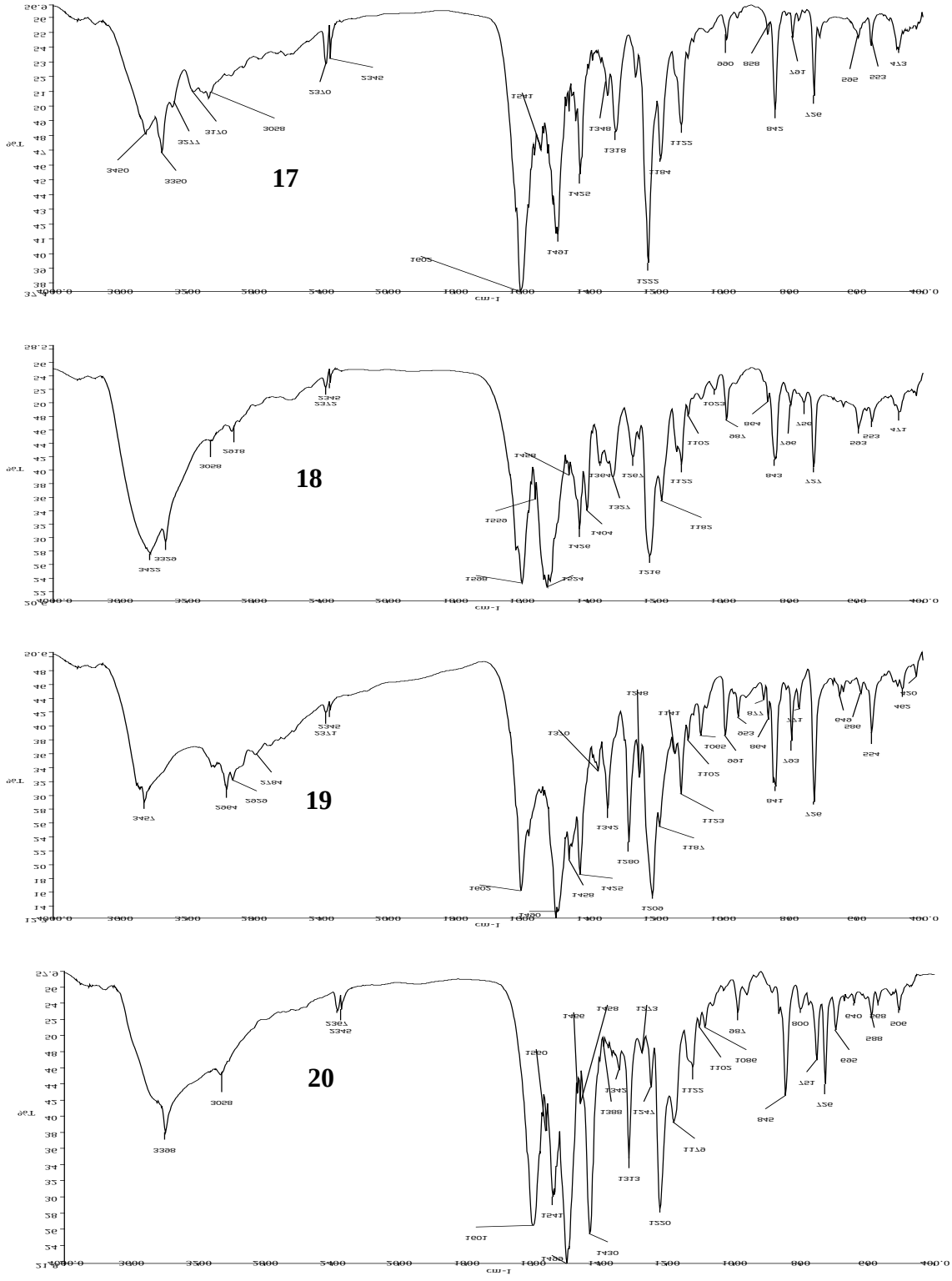

Fig. 5.5 IR spectra of all the complexes

The mode of coordination for the ligands determined by IR spectra is in good agreement with the crystal structure of complex **18a**. Complexes **17-20** have very similar IR spectra (Fig. 5.5), this indicates that they share the similar mode of coordination. Therefore, it is reasonable to propose that the coordination geometry around copper for complex **17-20** is distorted square pyramid.

Table 5.5

IR spectral assignments (cm^{-1}) for the ligands and their copper(II) complexes

Complex	ν(C=N)	ν(C-O)	ν(N-N)	ν (C=S)/ ν (C-S)	ν(Cu-O)	ν(Cu-N)	Bands due to phenanthroline
H_3T **(1)**	1620	1239	1165	1379, 863	-	-	-
H_3M **(2)**	1625	1231	1166	1331,868	-	-	-
H_3E **(3)**	1626	1241	1166	1325, 867	-	-	-
H_3P **(4)**	1629	1264	1121	1323,838	-	-	-
[Cu(phen)(HT)] (**17**)	1602	1222	1184	1318, 842	426	473	1425, 726
[Cu(phen)(HM)].H_2O (**18**)	1598	1216	1182	1327, 843	430	471	1426, 727
[Cu(phen)(HE)].H_2O (**19**)	1602	1209	1187	1280, 841	422	460	1425, 726
[Cu(phen)(HP)].H_2O (**20**)	1601	1220	1179	1313, 845	420	450	1430, 726

Electronic spectral assignments for the ligands and their copper(II) complexes in DMF are presented in Table 5.6. All the ligands and the Cu(II) complexes have a ring (phenolic and diimine) π-π^* band at around 37,593 cm^{-1} (West *et al.* 1995). No significant red shift is observed for these bands upon complexation (Swearingan and West, 2000). All the thiosemicarbazones also have two bands at around 32,985 cm^{-1} and 29,411 cm^{-1} due to n-π* transition of azomethine and thioamide function respectively. Upon complexation, the n-π* band of the thioamide function is shifted above 30,000 cm^{-1} due to thioenolization and merges with the azomethine n-π* band at around 31,348 cm^{-1} (Swearingan and West, 2000). Thioenolization causes the weakening of the C=S bond. A moderately intense band in the range 26110-27100 cm^{-1} found only in the spectra of all the complexes is assigned to Cu(II)→S metal to ligand charge transfer band (MLCT) (Swearingan and West, 2000; Seena and Kurup, 2007). The MLCT band for Cu(II)→O shows line broadening that runs into the visible part of the spectrum. However, the maxima of these band are not observed probably due to the overlapping with the low energy side of Cu(II)→S transitions (Seena and Kurup, 2007). The copper complexes show a d-d band at 17422-17825 cm^{-1} due to $d_{x^2-y^2} \rightarrow d_{xz}$, d_{yz} and $d_{x^2-y^2} \rightarrow d_{z^2}$ transitions characteristic of five coordinate copper(II) complexes with square pyramidal geometry (Bindu *et al.*, 1999; Seena and Kurup, 2007; Latheef and Kurup, 2008).

Table 5.6

Electronic spectral assignments (cm^{-1}) for the ligands and their copper(II) complexes in DMF

Complex	π-π^*	n-π*	MLCT	d-d
H_3T (**1**)	37593	33003, 29411		
H_3M (**2**)	37593	33003, 29411		
H_3E (**3**)	37593	32895, 29240		
H_3P (**4**)	37453	32680, 28409		
[Cu(phen)(HT)] (**17**)	35714	31545	27100, 26042	17422
[Cu(phen)(HM)].H_2O (**18**)	36764	32051	26525	17452
[Cu(phen)(HE)].H_2O (**19**)	36764	31348	26667	17422
[Cu(phen)(HP)].H_2O (**20**)	37453	30488	26110	17825

5.3.4 DNA binding

5.3.4.1 Duplex DNA

The interaction of more soluble **18** and **19** with (i) duplex oligonucleotides of various specified nucleotide sequences, and (ii) quadruplex DNA of the 23-mer oligonucleotide 5'-$AG_3(T_2AG_3)_3$-3' and its corresponding duplex could be investigated with CD spectroscopy. Complexes **17** and **20** could not be studied due to limited solubility in DMF and buffer mixture.

Similar to what was done in other chapters, the first investigation was to find out the DNA binding preference for CG or AT sequences by interaction with $ds(CG)_6$ and $ds(AT)_6$ duplexes by the complexes **18** and **19**. Complex **18** (Fig. 5.7) at a complex:duplex ratio of 1:8 shows decrease and increase in the positive and negative bands of the CD spectrum of

$ds(AT)_6$ which shows some resemblance to conformational change from B to C-like (Ivanov *et al.* 1973). However, complex **19** (Fig. 5.8) does not cause significant changes to CD spectrum of $ds(AT)_6$. Complex **18** shows a great decrease in intensity of the positive band of the CD spectrum of $ds(CG)_6$ without noticeable changes to the negative band which is consistent with conformational change from B to C (Ivanov *et al.* 1973). Complex **19** shows slight increase of the positive band of $ds(CG)_6$ without appreciable changes to the negative band suggesting partial intercalation of the complex to DNA. By comparing the changes induced by complexes **18** and **19** in both the positive and negative bands in the CD spectra of $ds(AT)_6$ and $ds(CG)_6$, we can infer that complex **18** binds more strongly to $ds(AT)_6$ and $ds(CG)_6$ compared with complex **19** (Table 5.7). Similar correlation between the degree of enhancement or decrease in intensity of CD bands with binding strength has been reported by Seng *et al.* (2009). Their results obtained from CD data are in good agreement with data from the ethidium bromide displacement assay and docking study.

We next utilised oligonucleotides such as $ds(CGCGAATTCGCG)_2$ and $ds(CGCGATATCGCG)_2$ to investigate further whether there is any binding preferences in interactions with duplex DNA as the sequence on each chain is varied from non-alternating to alternating purine-pyrimidine bases in the groove of the duplex. For the AATT sequence (Fig. 5.9-5.10, Table 5.7), complexes **18** and **19** show a decrease and increase in the negative and positive bands of the CD spectra of the duplex which is consistent to conformational change from B to ψ (Maheswari and Palaniandavar, 2004; Seng *et al.* 2008).

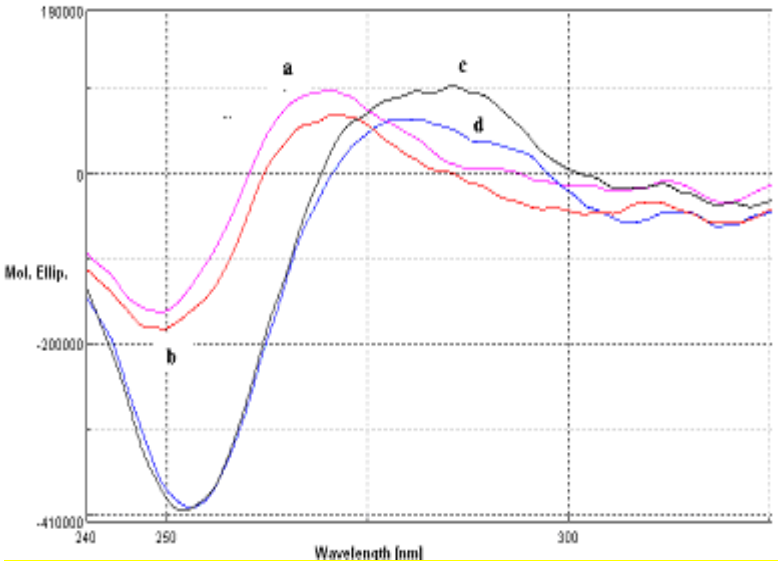

Fig. 5.7 CD spectra of 15 μM of oligonucleotide in the absence and presence of 120 μM of complex **18**; (a) ds(AT)$_6$ alone, (b) ds(AT)$_6$ with complex **18,** (c) ds(CG)$_6$ alone and (d) ds(CG)$_6$ with complex **18.**

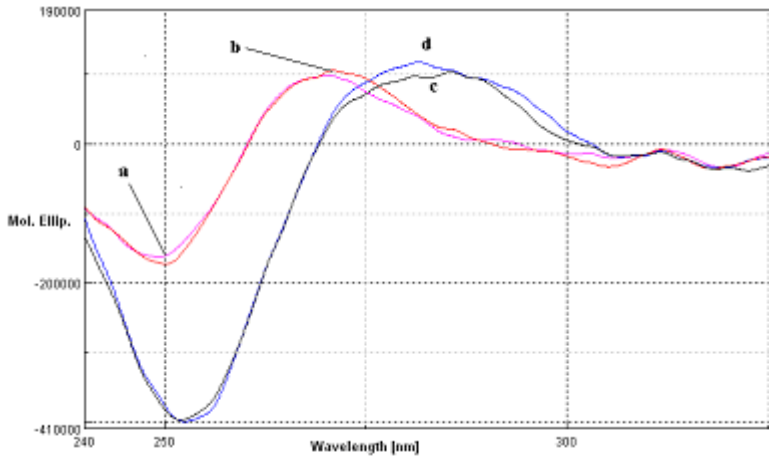

Fig. 5.8 CD spectra of 15 μM of oligonucleotide in the absence and presence of 120 μM of complex **19**; (a) ds(AT)$_6$ alone, (b) ds(AT)$_6$ with complex **19,** (c) ds(CG)$_6$ alone and (d) ds(CG)$_6$ with complex **19**

For the ATAT sequence (Fig. 5.9-5.10), complex **18** shows an increase in the positive bands of the CD spectra of the duplex without significant changes to the negative band. This suggests partial intercalation of the complex to DNA (Maheswari and

Palaniandavar, 2004; Seng *et al.* 2008). However, complex **19** shows an increase in both the positive and negative bands of the CD spectra which is consistent with intercalation mode of binding (Maheswari and Palaniandavar, 2004; Seng *et al.* 2008). Comparing the results for interaction with DNA with AATT and ATAT sequence, we found that complexes **18** and **19** can differentiate between the ATAT sequence from AATT because they induce different conformational changes to ds(oligonucleotide) with different base sequence. We also noticed that complex **18** can bind strongly to all four ds(oligonucleotides). However, complex **19** only binds strongly to AATT and ATAT sequences. This suggest that complex **19** is more selective towards these two sequence than $ds(AT)_6$ and $ds(CG)_6$. This again implies that the N(4) substituent plays an important role in recognizing base sequences, determining type of binding and strength of binding to DNA. Shape and hydrophobicity are factors long known to govern the binding of small molecules to DNA (Pyle *et al.* 1989).

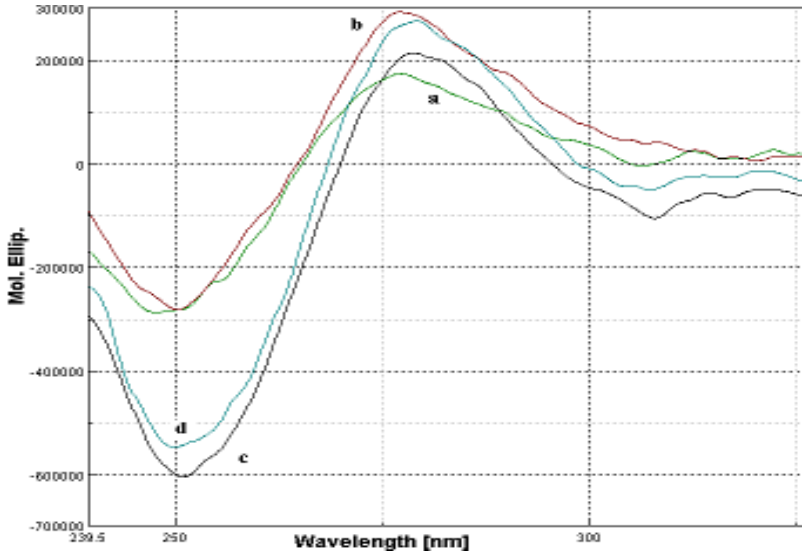

Fig. 5.9 CD spectra of 10 μM of oligonucleotides in the absence and presence of 120 μM of complex **18**; (a) ds(CGCGATATCGCG)$_2$ alone, (b) ds(CGCGATATCGCG)$_2$ with complex **18,** (c) ds(CGCGAATTCGCG)$_2$ alone and (d) ds(CGCGAATTCGCG)$_2$ with complex **18.**

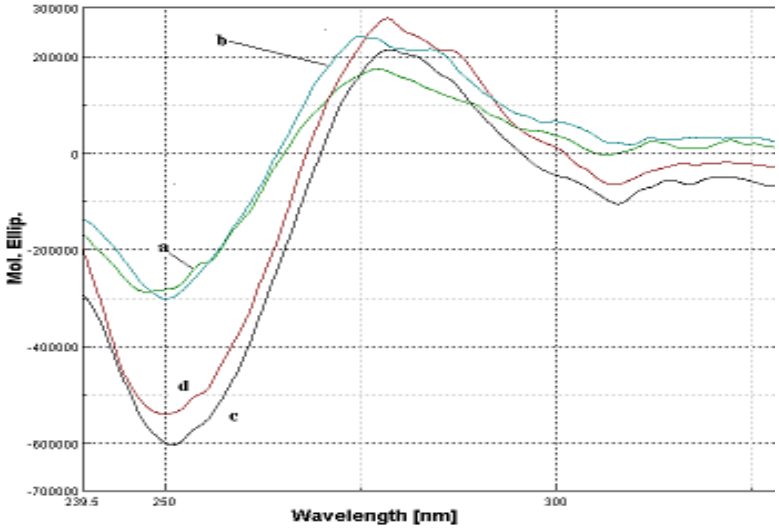

Fig. 5.10 CD spectra of 10 μM of oligonucleotides in the absence and presence of 120 μM of complex **19**; (a) ds(CGCGATATCGCG)$_2$ alone, (b) ds(CGCGATATCGCG)$_2$ with complex **19,** (c) ds(CGCGAATTCGCG)$_2$ alone and (d) ds(CGCGAATTCGCG)$_2$ with complex **19**.

Table 5.7
CD spectral bands of duplex oligo or quadruplex + copper complex: wavelength, λ (molar ellipcity)

	λ/nm (molar ellipcity)	
	(-) band	(+) band
15 μM ds$(AT)_6$	249 (-162440)	270 (98825)
15 μM ds$(AT)_6$ + 120 μM complex **18**	249 (182082)	271 (70206)
15 μM ds$(AT)_6$ + 120 μM complex **19**	250 (-172342)	271 (105235)
15 μM ds$(CG)_6$	252 (-395802)	281 (96919)
15 μM ds$(CG)_6$ + 120 μM complex **18**	253 (-392286)	281 (64133)
15 μM ds$(CG)_6$ + 120 μM complex **19**	252 (-398281)	282 (117130)
10 μM ds$(CGCGAATTCGCG)_2$	251 (-603665)	279 (215560)
10 μM ds$(CGCGAATTCGCG)_2$ + 120 μM complex **18**	250 (-546507)	279 (277015)
10 μM ds$(CGCGAATTCGCG)_2$ + 120 μM complex **19**	250 (-540857)	278 (279740)
10 μM ds$(CGCGATATCGCG)_2$	248 (-286559)	277 (174875)
10 μM ds$(CGCGATATCGCG)_2$ + 120 μM complex complex **18**	250 (-281243)	277 (294148)
10 μM ds$(CGCGATATCGCG)_2$ + 120 μM complex complex **19**	250 (-300704)	275 (241960)
20 μM G-duplex	250 (-82682)	279 (283975)
20 μM guanine-rich duplex+ 120 μM complex **18**	251 (-198287)	280 (564705)
20 μM guanine-rich duplex+ 120 μM complex **19**	249 (-250491)	278 (701158)
20 μM G-quadruplex	265 (-151753)	247 (75789) 295 (161061)
20 μM G-quadruplex + complex **18**	264 (-147796)	245 (72833) 295 (188283)
20 μM G-quadruplex + complex **19**	262 (-146047)	248 (81789) 295 (180655)

Guanine-rich duplex=(5'-CCAGTTCGTAGTAGTAACCC-3')·(3'-GGTCAAGCATCATCATTGGG-5')

5.3.4.2 G-quadruplex and guanine-rich duplex

As discussed in chapter 3, the interaction of this series of copper(II) complexes **18** and **19** (abbreviated as (Cu(phen)(L)) with G-quadruplex were similarly carried out to search for a complex that can stabilize G-quadruplex. Stabilizer of G-quadruplex can be a potential anticancer agent which functions by inhibiting telomerase.

The CD spectra of the 20 μM of the antiparallel G-quadruplex 5'-$AG_3(T_2AG_3)_3$-3' with the two different complexes (120 μM) were obtained. The intensity of the positive band for G-quadruplex at 296 nm is enhanced but no significant changes to the negative band at 267 nm are observed upon separate addition of complex **18**, Cu(phen)(HM) and **19**, Cu(phen)(HE). The overall shape of G-quadruplex remains unchanged, suggesting retention of the antiparallel structure (Fig. 5.11, Table 5.7).

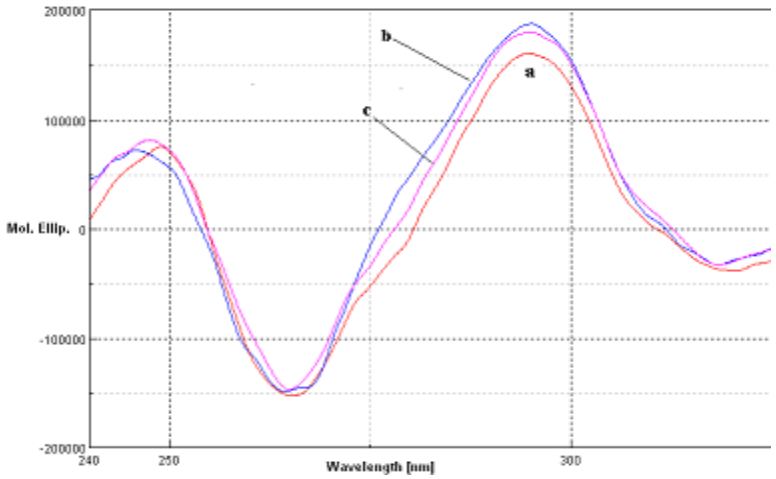

Fig. 5.11 CD spectra of 20 μM of G-quadruplex in the absence and presence of 120 μM of complex **18** and **19**; (a) G-quadruplex alone, (b) G-quadruplex with complex **18** , (c) G-quadruplex with complex **19**

The enhancement of the positive band at 296 nm due to G-G base stacking suggests partial intercalation between G-tetrads by the copper complex similar to enhancement of positive, base-base stacking band at ~270 nm attributed to intercalation of the B-form duplex DNA (Seng *et al.* 2009). Since the decrease in the intensity of the positive band at 293 nm was interpreted as destabilization of the quadruplex structure for the interaction of acridine and bis-acridine with G-quadruplex (Nagesh *et al.* 2003), the enhancement of the positive band of the CD spectrum of the present quadruplex suggests stabilization of the

antiparallel quadruplex as reported by Musseti *et al.* (2009) and Seng *et al.* (2009). Based on the enhancement in the positive band (Fig. 5.11, Table 5.7) complex **19** probably binds stronger to G-quadrupex compared with complex **18.**

Results from the study of the interaction with guanine-rich duplex indicate that complexes **18**, Cu(phen)(HM) and **19**, Cu(phen)(HE) intercalate strongly to guanine-rich duplex (Fig. 5.12, Table 5.7) based on the drastic increase in both the negative and positive bands (Maheswari and Palaniandavar, 2004). The percentage of enhancement of the positive band in the CD spectra is much higher (99-146 %) compared with their 2,2'-bipyridine analogs (31-106 %). This indicates that the 1,10-phenanthroline moiety promotes stronger binding of the complexes to guanine-rich duplex through intercalation. Complexes with phenanthroline moiety are known to bind more strongly to DNA through intercalation in contrast to those with 2,2'-bipyridine moiety (Dhar *et al*. 2002; Patra *et al.* 2005). This is attributed to the extended aromatic ring in the 1,10-phenanthroline moiety that favors π stacking interaction with nucleobase. Comparisons between the spectra for interaction with the guanine-rich duplex and G-quadruplex show that this series of complexes can differentiate the guanine-rich duplex from G-quadruplex. In addition, CD data also suggest that these complexes bind more strongly to the guanine-rich duplex than to the G-quadruplex. This is because the enhancement of the positive band in guanine-rich duplex(99-146 %) is greater compared with G-quadruplex (12-18 %). Similar observations were seen with their bipyridine analogs which implies that ternary copper complexes in our study most probably bind more strongly to guanine-rich duplex. Further, the binding of complexes **18** and **19** towards G-quadruplex are also weaker compared with their zinc

analogs (complexes **10**, Zn(phen)(HM), and **11**, Zn(phen)(HE)**).** This again implies that the central metal ion also play a role in determining the binding strength of a particular complex towards DNA. The difference in binding strength caused by the change from copper to zinc may be attributed to the change in coordination geometry since all these complexes are neutral in charge.

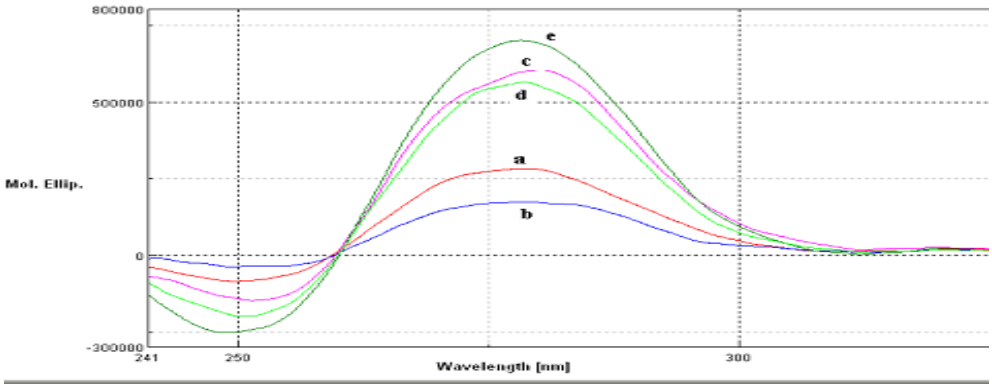

Fig. 5.12 CD spectra of 20 μM of guanine-rich duplex in the absence and presence of 120 μM of complex; (a) guanine-rich duplex alone, (b) guanine-rich duplex with complex **10,** (c) guanine-rich duplex with complex **11,** (d) guanine-rich duplex with complex **18** and (e) guanine-rich duplex with complex **19**

5.3.5 Nucleolytic study

In this study, we examine the ability of copper(II) complexes **18,** Cu(phen)(HM) and **19,** Cu(phen)(HE) to cleave pBR322 under hydrolytic conditions and in the presence of exogenous agents, sodium ascorbate and hydrogen peroxide, using gel electrophoresis. The other copper(II) complexes in the series of Cu(phen)(L) such as **17** and **20** could not be studied due to limited solubility in DMF and buffer mixture (TN buffer and DMF).

In the absence of any exogenous agent, cleavage was observed when the above two copper complexes were incubated with pBR322 for 24 h at 37 ^{o}C with increasing

concentrations of each copper complex (10 – 1000 μM). Complex **18** started to cleave DNA at a concentration of only 10 μM (Fig. 5.13, Lane L5). The amount of cleavage increases with increasing concentration of the complex from 200 μM onwards. (Fig. 5.13, Lane L7-L9) as shown by the increase in the intensity of the nicked band (Form II). At 1000 μM, total degradation of the DNA was observed through the appearance of a smeared band (Fig. 5.13, Lane L9). This implies that the amount of cleavage due to complex **18** is concentration dependent.

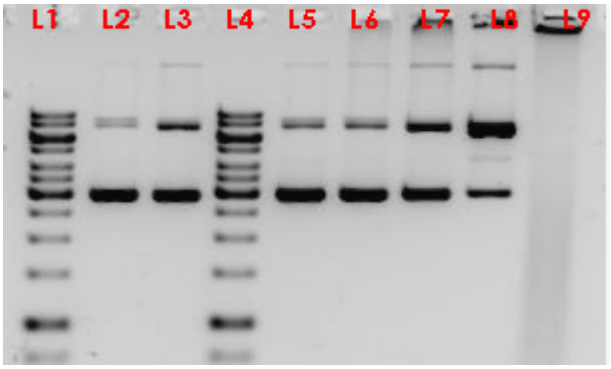

Fig. 5.13 Electrophoresis results of incubating pBR322 (0.5 μg/μL) in the presence of complex **18** in TN buffer (5 mM Tris, 50 mM NaCl) pH 7.5 at 37 ^{o}C for 24 h. L1 & L4, gene ruler 1 Kb DNA ladder; L2, DNA alone; L3, DNA + 1000 μM $CuCl_2$; DNA + various complex concentrations L5-L9: L5, 10 μM; L6, 50 μM; L7, 200 μM; L8, 500 μM; L9, 1000 μM.

On the other hand, complex **19** only started to show cleavage of the DNA at a concentration of 50 μM (Fig. 5.14, Lane L6). The amount of cleavage also increases with increase in complex concentration. (Fig. 5.14, Lane L6-L9) as shown by the increase in the intensity of the nicked band (Form II). In contrast to complex **18**, complex **19** did not cause smearing of the DNA at 1000 μM. Complex **19** converted all the supercoiled DNA (Form I) to nicked DNA (Form II) instead. This observation could imply two possibilities. The first is that, complex **18** has higher nucleolytic efficiency in the absence of exogenous agents

compared with complex **19**. However, the absence of smearing of the DNA band at very high concentration may also imply that the cleavage induced by complex **19** could be site specific.

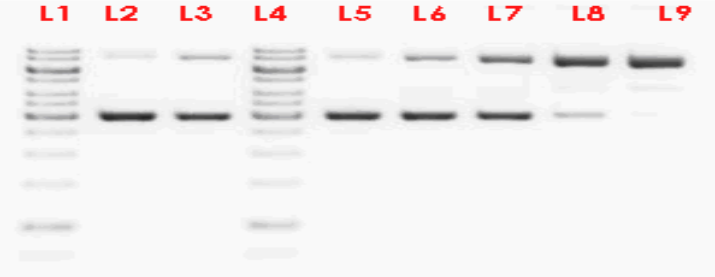

Fig. 5.14 Electrophoresis results of incubating pBR322 (0.5 μg/μL) in the presence of complex **19** in TN buffer (5 mM Tris, 50 mM NaCl) pH 7.5 at 37 ^{o}C for 24 h. L1 & L4, gene ruler 1 Kb DNA ladder; L2, DNA alone; L3, DNA + 1000 μM $CuCl_2$; DNA + various complex concentrations L5-L9: L5, 10 μM; L6, 50 μM; L7, 200 μM; L8, 500 μM; L9, 1000 μM.

Interestingly, the zinc analogs (Zn(phen)(HM) and Zn(phen)HE)) of complexes **18** and **19** can only induce mild cleavage at concentration as high as 500 μM whereas the 2,2'-bipyridine analogs (Cu(bipy)(HM) and Cu(bipy)HE)) cannot cleave the DNA in absence of exogenous agents. These results imply that double substitution of zinc with copper and 2,2'-bipyridine with 1,10-phenanthroline respectively can lead to improvement in nucleolytic efficiency in these ternary complexes. There are two possible reasons. The first is copper is redox active and the second is 1,10-phenanthroline is known to be a better intercalating ligand than 2,2'-bipyridine (Pyle *et al.* 1989). Previously, Seng *et al.* (2008) have shown that the DNA cleavage effieciency of Cu(phen)(edda) is better than Zn(phen)(edda) in the presence of hydrogen peroxide. Whereas, Thomas *et al.* (2004) have shown that the cleavage efficiency of ternary copper(II) complexes of N(4)-substituted salicylaldehyde thiosemicarbazone increase with the increase in binding strength to calf thymus DNA. This

increase in binding strength is attributed to the increase in extended aromatic ring of the intercalating ligands which escalate with the following order: phen < dpq < dppz.

To elucidate the cleavage mechanism, complexes **18** and **19** were incubated for 72 hours with DNA, neocuprione (Cu(I) ion chelator), thiourea (·OH radical-specific scavenger), sodium azide (a singlet oxygen radical scavenger) and Tiron (a superoxide anion radical scavenger) in the absence of exogenous agent. Lane L3 (Fig. 5.15) contains DNA and 500 μM complex **18** as the control. At this concentration, complex **18** can convert supercoiled DNA to the nicked and linear forms**.** The addition of sodium azide (Fig. 5.15, Lane L4) to complex **18** causes a lowering in DNA degradation. This indicates the involvement of singlet oxygen in the cleavage mechanism. No inhibition of DNA cleavage is observed when neocuproine (Fig. 5.15, Lane L5) was added. This ruled out the involvement of oxidation of Cu(I) to Cu(II) in the generation of reactive oxygen species. Neocuproine is known for its ability in stabilizing the +1 oxidation state of copper. If the mechanism in the generation of reactive oxygen species involves the oxidation of of Cu(I) to Cu(II), addition of neucuproine will lead to the decrease of Cu(I) species that can be oxidized back to Cu(II). Thus, leading to the decrease in reactive oxygen species and DNA cleavage. Very weak DNA cleavage inhibition is observed with the addition of Tiron (Fig. 5.15, Lane L6) and thiourea (Fig. 5.15, Lane L7) which indicates minor involvement of superoxide radical and hydroxyl radicals in the cleavage mechanism. The inhibition of DNA cleavage decreases with the following scavengers: sodium azide > thiourea > Tiron. From the above discussion, it can be concluded that the major pathway in the DNA cleavage involves singlet oxygen for this complex.

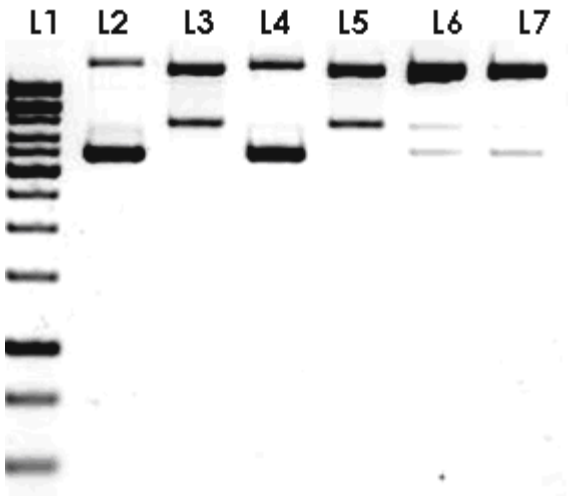

Fig. 5.15 Electrophoresis results of incubating pBR322 (0.5 µg/µL) with complex **18** in TN buffer (5 mM Tris, 50 mM NaCl) pH 7.5 at 37 ^{o}C for 72 h in the presence of scavenging agents: Lane 1, 1kb DNA ladder; Lane 2, plasmid DNA pBR322 (0.25µg/µl); Lane 3, DNA + 500 µM complex (control); Lane 4, DNA + 500 µM complex + 2mM sodium azide; Lane 5, DNA + 500 µM complex + 2mM Neocuproine; Lane 6, DNA + 500 µM complex + 2mM Tiron; Lane 7, DNA + 500 µM complex + 2mM Thiourea

As for complex **19**, addition of sodium azide (Fig. 5.16, Lane L4) causes a slight inhibition in DNA cleavage. This indicates the involvement of singlet oxygen in the cleavage mechanism. No inhibition of DNA cleavage is observed when neocuproine (Fig. 5.16, Lane L5) was added and this ruled out the involvement of oxidation of Cu(I) to Cu(II) in the generation of reactive oxygen species. The same was observed with the addition of Tiron (Fig. 5.16, Lane L6) which rules out the involvement of superoxide radical. Better DNA cleavage was observed with the addition of thiourea (Fig. 5.16, Lane L7) compared with sodium azide. This indicates that the role of singlet oxygen is more dominant in the cleavage mechanism. However, no total inhibition of DNA cleavage was observed with the addition of scavengers. Therefore, the possibility of DNA cleavage involving hydrolysis could not be ruled out. Even though the structure of complexes **18** and **19** is very similar, however it is noteworthy that the presence of an additional carbon atom at the N(4) position (ethyl) for complex **19** could results in slightly different cleavage mechanism**.** The major

pathway in the DNA cleavage for both complexes involves singlet oxygen. Further, there is a minor involvement of hydroxyl radical in both their cleavage mechanism. However, minor involvement of superoxide radical is only seen in complex **18** but not in complex 19. This implies that the N(4) substituent not only affect the nucleolytic efficiency of these two complexes but also the way they induce DNA cleavage. Further study is required in order to understand this phenomenon. The difference in cleavage mechanism pathway attributed to the change in alkyl substituent of a ligand was similarly observed by Hirohama *et al.* (2005). They have studied the DNA binding properties and nuclease activity of a series of copper(II) complexes of the type $[Cu(L)]^{2+}$, where L = N,N0–dialkyl-1,10-phenanthroline-2,9-dimethanamine and R = methyl (L1), n-propyl (L2), isopropyl (L3), sec-butyl (L4), or tert-butyl (L5) group. Mechanistic study revealed that cleavage reaction of $[Cu(L1)]^{2+}$ can be inhibited by radical scavengers such as SOD, DMSO, and NaN_3 inhibit the to the same extent. However, the reaction with $[Cu(L5)]^{2+}$ was the most inhibited by DMSO but SOD and NaN_3 fail to inhibit the cleavage under the experimental conditions employed in the pathway study. These results suggest that the cleavage reaction with $[Cu(L1)]^{2+}$ involves various oxygen species whereas that with $[Cu(L5)]^{2+}$ progresses mainly with the hydroxyl radical.

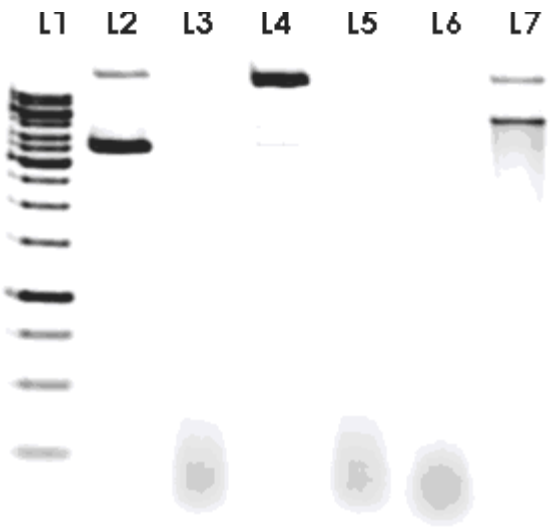

Fig. 5.16 Electrophoresis results of incubating pBR322 (0.5 µg/µL) with complex **19** in TN buffer (5 mM Tris, 50 mM NaC) pH 7.5 at 37 ^{o}C for 72 h in the presence of scavenging agents: Lane 1, 1kb DNA ladder; Lane 2, plasmid DNA pBR322 (0.25µg/µl); Lane 3, DNA + 500 µM complex (control); Lane 4, DNA + 500 µM complex + 2mM sodium azide; Lane 5, DNA + 500 µM complex + 2mM Neocuproine; Lane 6, DNA + 500 µM complex + 2mM Tiron; Lane 7, DNA + 500 µM complex + 2mM Thiourea

When the DNA was incubated with 300 µM of copper complex in the presence of 30 µM NaAsc, activation of copper complexes towards DNA cleavage by sodium ascorbate is observed for complexes **18** (Fig. 5.17, lane L14) and **19** (Fig. 5.17, lane L16). The DNA cleavage is evidenced from the increase in intensity of the nicked band. Further, complex **18** (Fig. 5.17, lane L14) is more efficient in cleaving the DNA compared with complex **19** (Fig. 5.17, lane L16) based on the total conversion of supercoiled DNA to the nicked form (Form II). For complex **19,** the band attributed to supercoil DNA can still be seen**.** If our previous assumption that an electron donating group could stabilize the Cu(II) oxidation state is true, then the lower activity of complex **19** can be accounted for since it has an ethyl substituent which is more electron donating compared with the methyl substituent in complex **18**. No DNA cleavage was observed for its zinc analogs (Fig. 5.17, lane L15 and

17) and its 2,2'-bipyridine analogs (chapter 4). This implies that the cleavage efficiency of ternary copper(II) complexes is improved with the presence of 1,10-phenanthroline moiety that enhances DNA binding.

When the DNA was incubated with 300 μM of copper complex in the presence of 30 μM hydrogen peroxide, DNA cleavage was observed for complexes **18,** Cu(phen)(HM), and **19,** Cu(phen)(HE), (Fig. 5.17, lane L21 and 23). However, a reversal in cleavage efficiency is seen for complex **19** in contrast to its cleavage efficiency with sodium ascorbate**.** Complex **19** converted (Fig. 5.17, lane L23) all the supercoiled DNA to nicked DNA and the appearance of linear DNA can also be seen. However, no linear band is seen with complex **18**. Therefore, complex **19** is a better nuclease compared with complex **18** in the presence of hydrogen peroxide. The reversal in cleavage efficiency can be attributed to the presence of a more electron donating ethyl group in complex **19**. The more electron donating ethyl group bestows the copper centre of **19** with higher electron density through inductive effect. Therefore, higher electron density led to the easier removal of electron from copper (oxidation) in complex **19** thus the increase in cleavage efficiency.

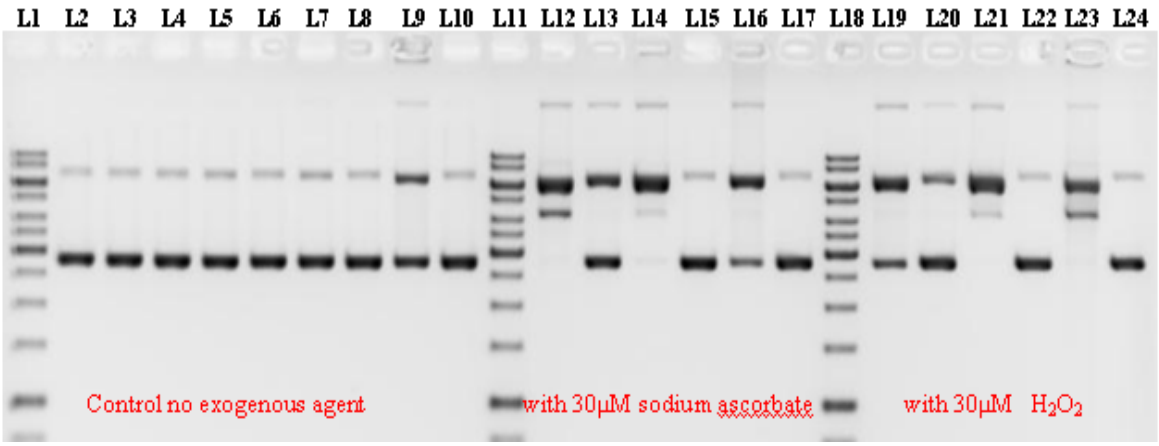

Fig. 5.17 Electrophoresis results of incubating pBR322 (0.5 μg/μL) with $CuCl_2$ or complex **10, 11, 18 and 19** in TN buffer (5 mM Tris, 50 mM NaC) pH 7.5 at 37 ^oC for 2 h in the absence and presence of exogenous agents: Lane 1, 11 and 18 gene ruler 1 Kb DNA ladder; Lane 2, DNA alone (0.5 μg/μL) control; Lane 3, DNA+ 30μM sodium ascorbate; Lane 4, DNA + 30μM H_2O_2; Lane 5, DNA + 300μM $CuCl_2$; Lane 6, DNA + 300μM $ZnCl_2$; Lane 7, DNA + 300μM of **18;** Lane 8, DNA + 300μM of **10;** Lane 9, DNA + 300μM of **19;** Lane 10, DNA + 300μM of **11;** Lane 12, DNA + 300μM $CuCl_2$ + 30μM sodium ascorbate; Lane 13, DNA + 300μM $ZnCl_2$ + 30μM sodium ascorbate; Lane 14, DNA + 300μM of **18** + 30μM sodium ascorbate; Lane 15, DNA + 300μM of **10** + 30μM sodium ascorbate; Lane 16, DNA + 300μM of **19** + 30μM sodium ascorbate; Lane 17, DNA + 300μM of **11** + 30μM sodium ascorbate; Lane 19, DNA + 300μM $CuCl_2$ + 30μM H_2O_2; Lane 20, DNA+300μM $ZnCl_2$ + 30μM H_2O_2; Lane 21, DNA + 300μM of **18** + 30μM H_2O_2; Lane 22, DNA + 300μM of **10** + 30μM H_2O_2; Lane 23, DNA + 300μM of **19** + 30μM H_2O_2; Lane 24, DNA + 300μM of **11** + 30μM H_2O_2

To determine whether the complexes can be activated by hydrogen peroxide, the concentration of hydrogen peroxide was varied from 250 μM to 500 μM while maintaining the complex concentration at 300 μM. DNA cleavage was observed for complexes **18** and **19** (Fig. 5.18, lane L14 and 16) in the presence of 250 μM hydrogen peroxide. Appearance of a nicked band with very high intensity and a linear band with low intensity is seen for complex **18** whereas smearing of the DNA band is seen for complex **19 (**Fig. 5.18, lane L21 and 23). This is consistent with our earlier result that complex **19** is a better DNA cleaving

agent than complex **18** in the presence of hydrogen peroxide. No cleavage is seen for their zinc analogs (Fig. 5.18, lane L15, 17, 22 and 24).

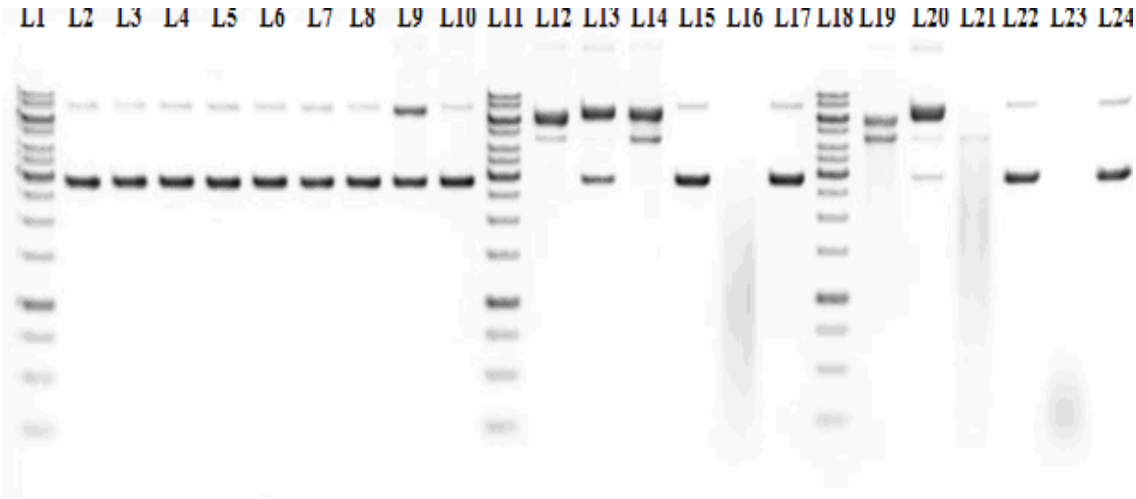

Fig. 5.18 Electrophoresis results of incubating pBR322 (0.5 μg/μL) with $CuCl_2$ or complex (**10, 11, 18** or **19)** in TN buffer (5 mM Tris, 50 mM NaCl) pH 7.5 at 37 ^oC for 2 h in the absence and presence of increasing hydrogen peroxide concentrations: Lane 1, 11 and 18 gene ruler 1 Kb DNA ladder; Lane 2, DNA alone (0.5 μg/μL) control; Lane 3, DNA + 250μM H_2O_2; Lane 4, DNA + 500μM H_2O_2; Lane 5, DNA + 300μM $CuCl_2$; Lane 6, DNA + 300μM $ZnCl_2$; Lane 7, DNA + 300μM of **18;** Lane 8, DNA + 300μM of **10;** Lane 9, DNA + 300μM of **19;** Lane 10, DNA + 300μM of **11;** Lane 12, DNA + 300μM $CuCl_2$ + 250μM H_2O_2; Lane 13, DNA + 300μM $ZnCl_2$ + 250μM H_2O_2; Lane 14, DNA + 300μM of **18** + 250μM H_2O_2; Lane 15, DNA + 300μM of **10** + 250μM H_2O_2; Lane 16, DNA + 300μM of **19** + 250μM H_2O_2; Lane 17, DNA + 300μM of **11** + 250μM H_2O_2; Lane 19, DNA + 300μM $CuCl_2$ + 500μM H_2O_2; Lane 20, DNA + 300μM $ZnCl_2$ + 500μM H_2O_2; Lane 21, DNA + 300μM of **18** + 500μM H_2O_2; Lane 22, DNA + 300μM of **10** + 500μM H_2O_2; Lane 23, DNA + 300μM of **19** + 500μM H_2O_2; Lane 24, DNA + 300μM of **11** + 500μM H_2O_2.

In order to elucidate the cleavage mechanism with exogenous agents, complexes **18** and **19** were incubated for 2 hours with DNA in the presence of the exogenous agent and scavenging agents such as neocuprione (Cu(I) ion chelator), thiourea (·OH radical-specific scavenger), sodium azide (a singlet oxygen radical scavenger) and Tiron (a superoxide anion radical scavenger) in the presence of exogenous agent.

When sodium ascorbate was used as an activating agent, addition of sodium azide (Fig. 5.19, Lane L5) and thiourea (Fig. 5.19, Lane L8) to complex **18** showed no effect on inhibition of DNA degradation. This rules out the involvement of either singlet oxygen and hydroxyl radical in the cleavage mechanism. Slight inhibition of DNA cleavage is observed when neocuproine (Fig. 5.19, Lane L6) was added, this indicates the involvement of oxidation of Cu(I) to Cu(II) in the generation of reactive oxygen species. Tiron also showed mild inhibition of DNA cleavage (Fig. 5.20, Lane L7), this indicates that the cleavage mechanism also involves the formation of superoxide radical. On the other hand, for complex **19** only thiourea showed slight inhibition to its cleavage activity (Fig. 5.20, Lane L8). This indicates that the cleavage mechanism involves hydroxyl radical but not singlet oxygen, superoxide radical and the oxidation of Cu(I) to Cu(II) in the generation of reactive oxygen species. When hydrogen peroxide was used as an activating agent, the cleavage by complex **18** can only be inhibited by sodium azide and Tiron (Fig. 5.21, L5 and 7). This indicates the involvement of singlet oxygen and superoxide radical in the cleavage mechanism. Greatest inhibition is seen with Tiron which implies that the superoxide anion dominates in the cleavage mechanism. A similar observation was encountered in complex **19** (Fig. 5.22, L4 and 6).

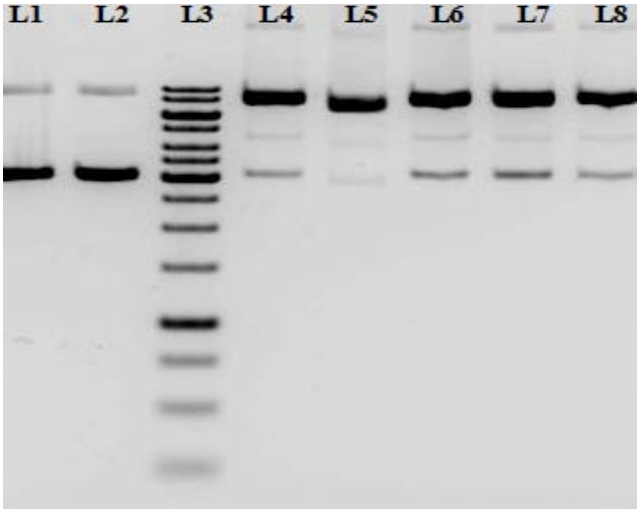

Fig. 5.19 Electrophoresis results of incubating pBR322 (0.5 μg/μL) with complex **18** in TN buffer (5 mM Tris, 50 mM NaC) pH 7.5 at 37 ^{o}C for 2 h in the presence of exogenous agent and scavenging agents: Lane 1, plasmid DNA pBR322 (0.25μg/μl); Lane 2, DNA + 30 μM sodium ascorbate; Lane 3, 1kb DNA ladder; Lane 4, DNA + 300 μM complex + 30 μM sodium ascorbate (control); Lane 5, DNA + 300 μM complex + 2mM sodium azide + 30 μM sodium ascorbate; Lane 6, DNA + 300 μM complex + 2mM Neocuproine + 30 μM sodium ascorbate; Lane 7, DNA + 300 μM complex + 2mM Tiron+ 30 μM sodium ascorbate; Lane 8, DNA + 300 μM complex + 2mM Thiourea + 30 μM sodium ascorbate

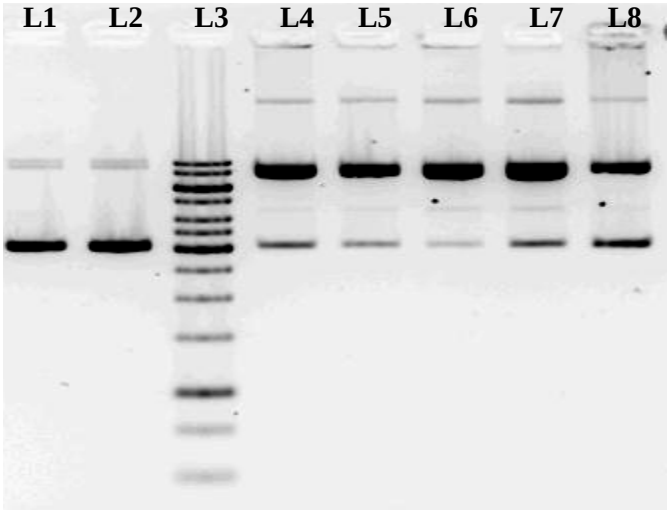

Fig. 5.20 Electrophoresis results of incubating pBR322 (0.5 μg/μL) with complex **19** in TN buffer (5 mM Tris, 50 mM NaCl) pH 7.5 at 37 ^{o}C for 2 h in the presence of exogenous agent and scavenging agents: Lane 1, plasmid DNA pBR322 (0.25μg/μl); Lane 2, DNA + 30 μM sodium ascorbate; Lane 3, 1kb DNA ladder; Lane 4, DNA + 300 μM complex + 30 μM sodium ascorbate (control); Lane 5, DNA + 300 μM complex + 2mM sodium azide + 30 μM sodium ascorbate; Lane 6, DNA + 300 μM complex + 2mM Neocuproine + 30 μM sodium ascorbate; Lane 7, DNA + 300 μM complex + 2mM Tiron+ 30 μM sodium ascorbate; Lane 8, DNA + 300 μM complex + 2mM Thiourea + 30 μM sodium ascorbate

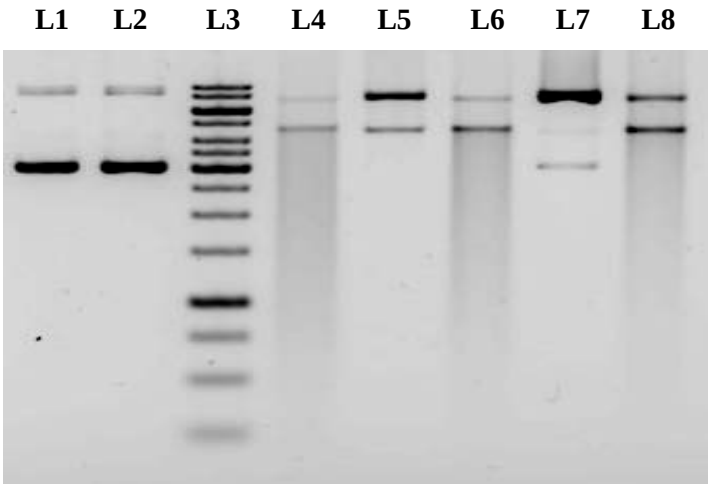

Fig. 5.21 Electrophoresis results of incubating pBR322 (0.5 μg/μL) with complex **18** in TN buffer (5 mM Tris, 50 mM NaC) pH 7.5 at 37 ^{o}C for 2 h in the presence of hydrogen peroxide and scavenging agents: Lane 1, plasmid DNA pBR322 (0.25μg/μl); Lane 2, DNA + 30 μM hydrogen peroxide; Lane 3, 1kb DNA ladder; Lane 4, DNA + 300 μM complex + 30 μM hydrogen peroxide (control); Lane 5, DNA + 300 μM complex + 2mM sodium azide + 30 μM hydrogen peroxide; Lane 6, DNA + 300 μM complex + 2mM Neocuproine + 30 μM hydrogen peroxide; Lane 7, DNA + 300 μM complex + 2mM Tiron+ 30 μM hydrogen peroxide; Lane 8, DNA + 300 μM complex + 2mM Thiourea + 30 μM hydrogen peroxide;

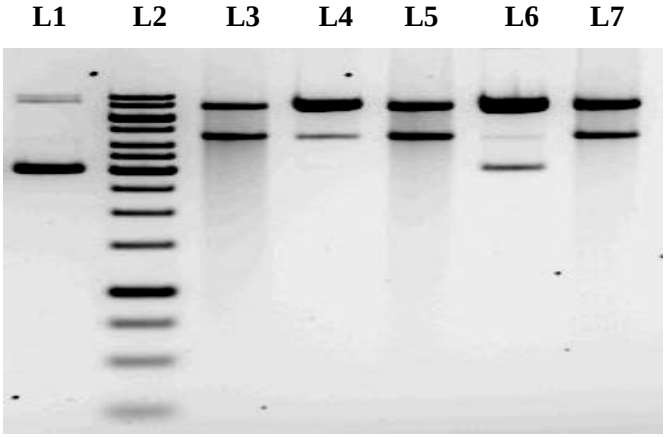

Fig. 5.22 Electrophoresis results of incubating pBR322 (0.5 μg/μL) with complex **19** in TN buffer (5 mM Tris, 50 mM NaC) pH 7.5 at 37 ^{o}C for 2 h in the presence of hydrogen peroxide and scavenging agents: Lane 1, plasmid DNA pBR322 (0.25μg/μl); Lane 2, 1kb DNA ladder; Lane 3, DNA + 300 μM complex + 30 μM hydrogen peroxide (control); Lane 4, DNA + 300 μM complex + 2mM sodium azide + 30 μM hydrogen peroxide; Lane 5, DNA + 300 μM complex + 2mM Neocuproine + 30 μM hydrogen peroxide; Lane 6, DNA + 300 μM complex + 2mM Tiron+ 30 μM hydrogen peroxide; Lane 7, DNA + 300 μM complex + 2mM Thiourea + 30 μM hydrogen peroxide

5.3.6 Topoisomerase I inhibition assay

The objective of topoisomerase I inhibition assay by complexes **18** and **19** is similar to that mentioned in previous chapters (Chapters 2, 3 and 4).

As can be seen from Fig. 5.23 (lanes L10 and L11), complex **19,** Cu(phen)(HE), is capable of almost total inhibition of topo I. The inhibition activity is better than the zinc complexes used as a comparison. Interestingly, complex **18,** Cu(phen)(HM), does not inhibit topo I in contrast to its zinc analog (complex **10)**. This implies that inhibition of topo I in ternary complexes is very dependent on the combinations of ligands and metal. A slight variation in geometry and hydrophobicity can lead to total alterations of its potency.

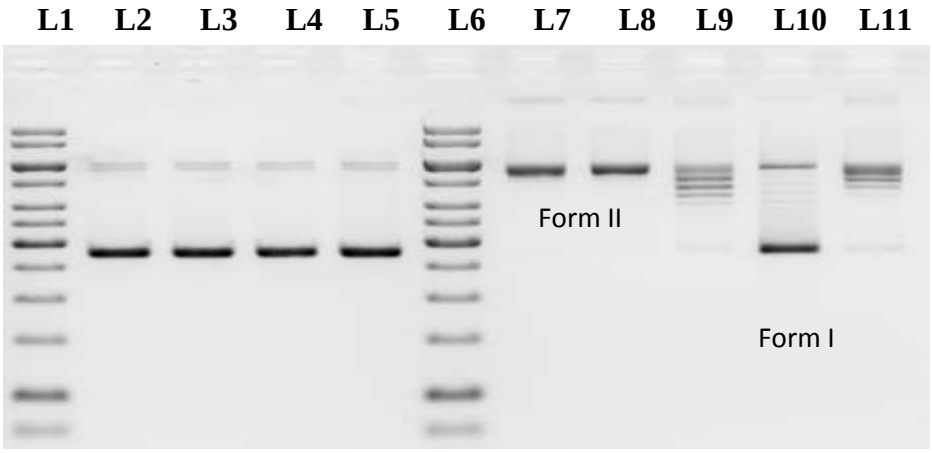

Fig. 5.23 Human topoisomerase I inhibition assay by gel electrophoresis. Electrophoresis results of incubating human topoisomerase I (1 unit/21μL) with pBR322 in the absence or presence of 40 μM of complex: Lane 1 & 6, gene ruler 1 Kb DNA ladder; Lane 2, DNA + 40μM **18**(control);Lane 3, DNA + 40μM **10**(control); Lane 4, DNA + 40μM **19**(control); Lane 5, DNA + 40μM **11**(control); Lane 7, DNA+ 1 unit Human Topoisomerase I (control); Lane 8, DNA + 40μM **18**+ 1 unit Human Topoisomerase I; Lane 9, DNA + 40μM **10** + 1 unit Human Topoisomerase I; Lane 10, DNA + 40μM **19** + 1 unit Human Topoisomerase I; Lane 11, DNA + 40μM **11** + 1 unit Human Topoisomerase I

5.3.7 Antibacterial and antifungal assays

5.3.7.1 Antibacterial activity

As a routine test in this research project, the antibacterial activity of ligands and complexes Cu(phen)(L) were screened against Gram positive bacteria Gram negative bacteria as was carried out for the other complexes. All ligands and complexes had some degree of inhibitory activity against the bacteria tested (Table 5.8). Complexes **17** and **20** could not be studied due to limited solubility in DMF and the buffer mixture therefore the antibacterial activity of complexes **18** and **19** are compared with their zinc analogs **(**complexes **10** and **11**) to study the effect of varying metal ions. All the thiosemicarbazones ligands are less potent compared with the 1,10-phenanthroline ligand.

Upon complexation of copper(II) with 1,10-phenanthroline and the thiosemicarbazones ligands (**2** and **3**), enhanced antibacterial activity is observed for complexes **18** and **19** towards *S. aureus and B. cereus* compared with 1,10-phenanthroline and their free thiosemicarbazones. On top of that, complex **19** also showed improved antibacterial activity towards *K. pneumonia and P. aeruginosa.* Since the MIC values of these complexes are lower than their free ligands, the improved antibacterial activity can be attributed to synergistic effect of metal and ligands in the complexes. The antibacterial properties of thiosemicarbazones ligands are known to improve upon complexation and this is attributed to enhance liphophilicity (Bindu *et al.* 1998; Joseph *et al.* 2006). However, a right combination of metals and ligands is essential to achieve the desired results since complexation does not always resulting in improved biological properties.

For the copper complexes in this research project, the ethyl derivative is always more active compared to the methyl derivative. Higher lipophilicity of a complex can help in permeation through the hydrophobic membrane of bacteria, thus enhancing their antibacterial activity (Kikuta *et al.*, 2000, Kasuga *et al.*, 2003).

Another important observation is that under the same ligand environment, the copper complexes will always have better antimicrobial activity compared to the zinc complexes. This may be due to the ability of the copper complexes in inducing DNA damage in the presence or absence of exogenous agent in contrast to the zinc complexes that are cleavage inactive as observed in the nucleolytic experiments.

The antimicrobial activity of the complexes in decreasing order for majority of the strains tested is **19** > **18** > **11** > **10**. A few exceptions are seen in *S. aureus, K. pneumoniae* and the *E.Coli* strains. Of the complexes tested, complex **19** showed the highest antibacterial activity. It is noteworthy that complex **19** inhibited *S. aureus* with a MIC value (7.81 μg/mL) even lower than the antibacterial drug, Chloramphenicol, used for comparison. The highest antimicrobial activity for complex **19** is understandable because **19** has an ethyl substituent which is more hydrophobic than the methyl group and it consists of a copper centre that is redox active.

Table 5.8.

Mean MIC value (μg/mL) towards microbes tested.

Complex	Bacteria					
	S. aureus	*B. cereus*	*P. aeruginosa*	*K. pneumoniae*	*E. coli* (penicillin-sensitive strain)	*E. coli* (penicillin-resistant strain)
1	62.50	62.50	62.50	62.50	62.50	62.50
2	125.00	62.50	125	62.50	62.50	62.50
3	62.50	62.50	62.50	62.50	62.50	62.50
4	62.50	31.25	62.50	31.25	62.50	62.50
10	62.50	31.25	52.08	31.25	62.50	62.50
11	62.50	15.63	31.25	31.25	31.25	31.25
18	15.63	7.81	15.63	15.63	31.25	31.25
19	7.81	6.51±2.25	7.81	6.51	15.63	15.63
$CuCl_2$	-	-	-	-	-	-
phen	62.50	15.63	15.63	15.63	15.63	15.63
Drug	8.00	4.00	4.00	4.00	4.00	4.00

" - " : no activity. Drug used in antibacterial assay = Chloramphenicol

5.3.7.2 Antifungal activity

The antifungal activity of ligands and their complexes were assessed against four species of fungi. All ligands and complexes had some degree of inhibitory activity against the fungi tested (Table 5.9). All the thiosemicarbazones ligands are less potent compared with 1,10-phenanthroline.

The antifungal trends of the complexes are dependent on the strain of the fungi. However a general trend that can still be observed is that the copper complexes are generally more active than their zinc counterpart. The complexes are most active towards *C. neoformans* with a MIC value of 7.81 µg/mL (complexes **19**, **11** and **10**) and 15.63 µg/mL (complex **18**). All four copper complexes benefited from the synergistic effect of complexation between metal with the 1,10-phenanthroline and their thiosemicarbazones ligands towards *C. neoformans* strains. These complexes have lower MIC value compared with 1,10-phenanthroline and their respective thiosemicarbazone ligands. *A.niger* showed very high resistant towards complex **18** and complex **10** suggesting that the membrane of this particular fungus is harder to permeate with shorter alkyl chain compared to other strains. Drastic improvement is observed for complex **19** and complex **11** towards *A.niger* with both showing MIC value of 7.81 ug/ml when the methyl group in complex **18** and complex **10** is replaced with an ethyl group. This example once again demonstrates the importance of lipophilicity in antifungal property as observed for antibacterial activity. Complex **19** showed the highest inhibitory activity of 7.81 ug/ml for all the fungi tested when compared with all of the complexes in this assay. However, its MIC value is higher than 1,10-phenanthroline (3.91 ug/ml) towards *C. albicans* and *C. parapsilosis*. This implies that antifungal properties of 1,10-phenanthroline towards these two fungi most likely attributed to its ability to chelate metal ions required for the survival of the fungi. Complexation removes the chelation ability of 1,10-phenanthroline hence resulted in decrease antifungal property towards these fungi.

Table 5.9
Mean MIC value (µg/mL) towards fungi tested.

Complex	Fungi			
	C. albicans	*C. parapsilosis*	*C. neoformans*	*A.niger*
1	31.25	62.50	31.25	62.50
2	31.25	31.25	31.25	62.50
3	31.25	31.25	31.25	62.50
4	31.25	62.50	7.81	31.25
10	15.63	31.25	7.81	62.50
11	15.63	15.63	7.81	7.81
18	15.63	7.81	15.63	31.25
19	7.81	7.81	7.81	7.81
$CuCl_2$	-	-	-	-
phen	3.91	3.91	31.25	31.25
Drug	1.00	2.00	1.00	4.00

All values are expressed as mean ± standard deviation of three replicates

" - " : no activity

Drug used in antifungal assay = fluconazole

5.4 Conclusion

Spectroscopic and crystal data reveal that all the copper complexes are five-coordinated with the doubly deprotonated thiosemicarbazones acting as a tridentate ligand that coordinated through one phenolic oxygen, azomethine nitrogen and thiolate sulfur atoms while the 1,10-phenanthroline is coordinated as a *N,N'*-bidentate ligand. The coordination geometry around these copper complexes is distorted square pyramidal similar to their 2,2'-bipyridine analogs Cu(bipy)(L).

Complexation of the ligands with copper lead to formation of a series of ternary complexes with better biological activities compared with their zinc analogs. Complex **18** Cu(phen)(HM) which is the copper analog for complexes **6,** Zn(bipy)(HM)**, 10,** Zn(phen)(HM), and **14,** Cu(bipy)(HM), retains its ability in recognizing CG rich sequence in DNA. The mode of binding towards DNA for complexes **18** and **19** is quite different from those observed in their zinc analog Zn(phen)L. The same is true for its bipyridine analogs Zn(bipy)L. However, greater enhancement in binding strengths is observed by substitution of bipyridine with 1,10-phenanthroline. This can be attributed to increase lipophilicity and intercalation of the 1,10-phenanthroline ligand.

Unlike their zinc analogs, Zn(phen)L, the Cu(phen)L complexes can be activated by sodium ascorbate or hydrogen peroxide to induce DNA cleavage. In addition, these copper complexes also have better nucleolytic efficiency than their 2,2'-bipyridine analogs Cu(bipy)L, because they can cleave DNA without any exogenous agents and the cleavage efficiency is much higher in the presence of exogenous agent. Topoisomerase I inhibition by complex **19**, Cu(phen)(HE), is also better than its zinc analog (complex **11** Zn(phen)(HE)). Most of the copper complexes exhibit a wider spectrum of antibacterial and antifungal properties with better MIC value compared to their zinc analog. Complex **19** has a good potential to be developed as a drug or DNA probe owing to its highest nucleolytic efficiency, topoisomerase I inhibition, antibacterial and antifungal activities. These results further substantiate the role of hydrophobicity in bestowing desirable biological activities to a complex regardless of its metal centre.

Chapter 6

Conclusion

6.1 Syntheses and characterizations of the ligands and complexes

Four thiosemicarbazones ligands (H_3T(**1**), H_3M(**2**), H_3E(**3**) H_3P(**4**)) have been prepared in good yield by refluxing 2,4-dihydroxybenzaldehyde with thiosemicarbazide or N(4)-substituted thiosemicarbazide in ethanol or methanol. From these four ligands, four new sets of ternary metal complexes (Zn(bipy)L (**5-8**); Zn(phen)L (**9-12**); Cu(bipy)L (**13-16**) and Cu(phen)L (**17-20**) with the general formulation of M(B)L have been prepared from the reactions of metal acetates with 2,4-dihydroxybenzaldehyde N(4)-substituted thiosemicarbazone in the presence of *N,N*-heterocyclic base (M^{2+} = Zn^{2+} or Cu^{2+}; B = 2,2'-bipyridine, (bipy); 1,10-phenanthroline, (phen); L^{2-} = doubly deprotonated thiosemicarbazone = 2,4-dihydroxybenzaldehyde thiosemicarbazonato, (HT); 2,4-dihydroxybenzaldehyde 4-methylthiosemicarbazonato, (HM); 2,4-dihydroxybenzaldehyde 4-ethylthiosemicarbazonato, (HE) and 2,4-dihydroxybenzaldehyde 4-phenylthiosemicarbazonato, (HP)). These compounds have been characterized by elemental analyses, IR, UV, NMR, magnetic susceptibility. The structures for some of the ligands (**2, 3**) and some of the complexes (**5**, **8, 9, 11, 13** and **18**) have been solved by single crystal X-ray crystallography.* Results from spectroscopic data and crystal structure analysis show that all of the free ligands exist in the thione form. The complexes are mononuclear and five coordinated with the doubly deprotonated thiosemicarbazone as a tridentate ligand coordinating through the phenolic oxygen, azomethine nitrogen and thiolate sulfur atoms with 2,2'-bipyridine or 1,10-phenanthroline as the *N,N'*-bidentate ligand**.** The coordination geometries vary from distorted square pyramidal to trigonal

bipyramidal distorted square based pyramid (TBDSBP). Five coordinated complexes can adopt either one of the coordination geometry and are known to interconvert through a process known as pseudo-Berry rotation. Results from our crystallography study and literature review show that the copper complexes tend to adopt distorted square pyramidal geometry while zinc complexes tend to adopt a trigonal bipyramidal distorted square based pyramid (TBDSBP). The preferred coordination geometry is conferred by several restrictions such as the strength of the ligand field, rigidity and denticity of the ligand as well as the electronic configuration of the metal ions. The combinations of these factors will dictate the possible hybridization of the metal's orbitals and hence the preferred coordination geometry. Since the copper and zinc complexes are analogs with similar ligands, the effects from the ligands such as the strength of the ligand field, rigidity and denticity should not be the driving force in dictating the final coordination geometry. Hence, the deciding factor should lie with the metal ions used in our study. Copper complexes tend to adopt a distorted square pyramidal geometry while zinc complexes tend to adopt a geometry towards trigonal bipyramidal. This could be attributed to the difference in electron configurations for copper and zinc that leads to the stabilization of particular coordination geometry since the energy difference between square pyramidal and trigonal bipyramidal is quite small. For copper with a d^9 electronic configuration, the energy difference is 0.25 $\beta_\sigma S_\sigma^2$. The zinc(II) ion with d^{10} electronic configuration is not subjected to tetragonal distortion of its coordination geometry due to Jahn-Teller effect unlike copper with a d^9 electronic configurations. The presence of Jahn-Teller effect in the copper complexes is confirmed by the elongation of the apical Cu-N bond lengths. The copper complexes show two different sets of Cu-N(heterocycle) bond length with one being

slightly longer than the other. As for the zinc complexes, similar Zn-N(heterocycle) bond lengths are observed.

* Structures for the following compounds have been published: **2**, **3**, **5** and **9** (Appendix)

6.2 Biological activities

The effect of varying (i) the N(4) substituent from methyl, ethyl to phenyl, (ii) metal ions and (iii) polpyridyl ligand towards the chemical and biological properties (DNA binding, nucleolytic, topoisomerase I inhibition and antimicrobial) have been studied. By comparing the results of 12 complexes in each type of screening that span over four chapters, some generalizations can be made on the role of metal ions, type of N(4) substituent and type of polypyridyl ligand in determining the ability to recognize different DNA base sequence and potency of a particular complex towards a particular biological property or activity.

6.2.1 DNA binding

Results from CD experiments show that the mode of binding and recognizing capability of the complexes to different DNA sequences or structures are dependent on the N(4) substituent because the variation of the substituent would change the hydrophobicity, surface area, shape, size and steric effect of a particular complex. The ability of a complex to differentiate base sequences and DNA structure (e.g.s quadruplex) is found to be dependent on the N(4) substituent. The mode of binding strength as well as the binding strength of a complex is also dependent on the N(4) substituent. Besides the N(4)

substituent, recognition capability of a complex is also dependent on polypyridyl ligands or metal ions. The shape of a complex and how that shape matches the DNA is known as the most critical factor in determining binding affinity (Pyle *et al.* 1989).

As for the effect of varying polypyridyl ligand, incorporation of a 1,10-phenanthroline moiety in place of a 2,2'-bipyridine moiety in Zn(bipy)L led to formation of Zn(phen)L that show higher selectivity for the $ds(AT)_6$ sequence for the N(4) alkyl substituted thiosemicarbazones. The non-substituted thiosemicarbazones complexes containing phenanthroline could not be studied owing to solubility problem. This also implies that though the phenanthroline moiety can promote DNA binding with its better intercalating capability, it can also pose a problem in biological testing of neutral complexes. The increased hydrophobicity in a neutral complex owing to the presence of extended aromatic ring can render it insoluble in water. Our study also shows that most of the complexes that are more hydrophobic (containing phenyl as N(4) substituent or phenanthroline) normally bind more strongly to the various duplex structures. Our results also show that most zinc complexes (Zn(bipy)L and Zn(phen)L) induce a greater increase in the positive band of the CD spectra of G-quadruplex compared with their copper analogs (Cu(bipy)L and Cu(phen)L). This suggests that zinc complexes are better in stabilizing the G-quadruplex structure. Since the major difference between the zinc and the copper complexes is their coordination geometry, the shape of the complex with same ligand may be important in determining its ability to bind to G-quadruplex.

6.2.2 Nucleolytic study

Results from nucleolytic experiments show that the zinc complexes are very weak DNA cleaving agents that only show mild cleavage of the DNA at very high concentration in the absence of exogenous agents. Not much difference is observed in the cleavage efficiency between the 2,2'-bipyridine and 1,10-phenanthroline derivatives of zinc. None of the complexes can be activated to induce DNA cleavage by the exogenous agents. Interestingly, when zinc in the Zn(bipy)L series was replaced by copper to form Cu(bipy)L, drastic improvement is seen in the cleavage efficiency in the presence of exogenous agents used. The copper complex with unsubstituted thiosemicarbazone and N(4)-phenylthiosemicarbazone can induce DNA cleavage in the presence of sodium ascorbate. The copper complexes with alkyl substituted thiosemicarbazones (Cu(bipy)(HM) and Cu(bipy)(HE)) are incapable of DNA degradation most probably owing to its ability to stabilize the Cu(II) oxidation state from reduction by sodium ascorbate. All copper complexes can be activated to induce DNA scission in the presence of hydrogen peroxide. Cleavage efficiency for complex **16** Cu(bipy)(HP) is the highest in the presence of an exogenous agent most probably owing to its ability to intercalate to DNA with its hanging phenyl substituent. None of the copper complexes Cu(bipy)L show hydrolytic cleavage of DNA. When the 2,2'-bipyridine moiety in complex **14**, Cu(bipy)(HM), and **15**, Cu(bipy)(HE) was substituted with a 1,10-phenanthroline moiety, great improvement in cleavage efficiency is seen. This could be attributed to stronger binding of the complexes to DNA. The resultant 1,10-phenanthroline derivatives (complex **18**, Cu(phen)(HM), and **19**, Cu(phen)(HE)) can cleave DNA in the absence of exogenous agents. Complex **18** has better cleavage efficiency in the absence of exogenous agent. Radical scavenging experiments for

complex **18** show that the cleavage mechanism involves a combination of reactive oxygen species such as singlet oxygen, superoxide anion and hydroxyl radical. However, no total inhibition was observed with the addition of scavengers. Therefore, the possibilities of DNA cleavage involving hydrolysis can not be ruled out. Complexes (**18** and **19**) can also be activated by hydrogen peroxide and sodium ascorbate. The mechanism of cleavage is different in the presence of different exogenous agents as seen from the scavenging experiments. Complex **18** shows better cleavage efficiency in the presence of sodium ascorbate whereas complex **19** shows better cleavage efficiency in the presence of hydrogen peroxide. These results imply that the best way of elevating cleavage efficiency for these complexes is to use a redox active metal such as copper and a better intercalating ligand such as phenanthroline. The incorporation of ligands such as dpq or dppz may further enhance its cleavage efficiency. However, solubility problem may arise from higher hydrophobicity.

6.2.3 Topoisomerase I inhibition assay

Results from topoisomerase I inhibitions show that six (Zn(bipy)(HP) (**8**), Zn(phen)(HM) (**10**), Zn(phen)(HE) (**11**), Cu(bipy)(HT) (**13**), Cu(bipy)(HP) (**16**), Cu(phen)(HE) (**19**)) out of twelve of the complexes tested can inhibit the enzyme. The ability of these complexes to inhibit the enzyme may be attributed to (i) their ability to bind to DNA and cause various conformational changes to the DNA or (ii) blocking the binding site of the enzyme. However, the preliminary mechanistic study suggests that the main pathway in inhibition of the enzymes is likely attributed to the binding of the complexes to the enzymes since greater inhibition was observed when the complexes were incubated

with topoisomerase I first before the addition of DNA. Both pathways seem to be occurring simultaneously. Similar to results from DNA binding, the factors that favor topoisomerase I inhibition is not straight forward. However, in the absence of the 1,10-phenanthroline moiety, two of the complexes that inhibited the enzymes contain a thiosemicarbazone moiety with phenyl substituent that favors intercalation to DNA. The third complex is a copper complex with unsubstituted thiosemicarbazone. Another implication that maybe derived from this observation is none of them are alkyl substituted. This suggests that alkyl substitution disfavor topoisomerase I inhibition in 2,2'-bipyridine derivatives.

However, a very contradicting observation is seen in the 1,10-phenanthroline analog of these alkyl substituted complexes. Three out of four of these complexes (Zn(phen)(HM) (**10**), Zn(phen)(HE) (**11**) and Cu(phen)(HE) (**19**)) can inhibit topoisomerase I. This suggests that the 1,10-phenanthroline moiety can bestow the following inactive complexes (Zn(bipy)(HM)(**6**), Zn(bipy)(HE)(**7**) and Cu(bipy)(HM)(**14**)) with topoisomerase inhibiton activity by substituting the 2,2'-bipyridine moiety. The exact nature of this improvement is not fully understood. However, such improvement may be attributed to better binding to DNA or topoisomerase I with the presence of 1,10-phenanthroline moiety with higher hydrophobicity and intercalating capability.

6.2.4 Antibacterial and antifungal activity

The antibacterial and antifungal activity of the free thiosemicarbazones ligands are very dependent on the N(4) substituent. Greater degree of substitution or presence of a

more hydrophobic substituent led to an increase in inhibitory activity. Drastic enhancement is seen in overall inhibitory activity of the complexes compared with their free thiosemicarbazones ligands. However, most of these complexes have MIC values either higher or similar to the polypyridyl ligands. This implies that the inhibitory activities of these complexes are most likely conferred by the polypyridyl ligands. Most complexes that show good antibacterial activity in our study are also topoisomerase I inhibitor. Better activity is seen in complexes with more hydrophobic substituent group (ethyl and phenyl). All the 1,10-phenanthroline derivatives possess better activity than their 2,2'-bipyridine analogs. Another important observation is that under the same ligand environment, the copper complexes will always have better antimicrobial activity compared to the zinc complexes. This may be due to the ability of the copper complexes in inducing DNA cleavage in the presence or absence of exogenous agent in contrast to the zinc complexes that are cleavage inactive as observed in the nucleolytic experiments. The good antifungal and antibacterial activity of complex **19** can be attributed to its redox active copper metal center and the presence of an ethyl susbstituent and 1,10-phenanthroline moiety. The ethyl substituent and 1,10-phenanthroline moiety can increase the permeability of the complex across the membrane of the microbes by elevating its hydrophobicity. In addition, the 1,10-phenanthroline moiety can also help to promote the binding of the complex to DNA in the cell. Complex **19** is the most active complex with the lowest MIC value of 7.81 μg/mL towards *S. aureus* which is even lower than the antibacterial drug, Chloramphenicol, used in the assay. Antibacterial and antifungal activities of complex **19** are good examples of the role of synergistic effect in elevating biological properties. This is attributed to the greater enhancement in biological activity of the complex in contrast to its free ion and both its free ligands (H_3E and phenanthroline).

6.3 Suggestions

Among the zinc complexes studied, complexes Zn(bipy)(HP) (**8**), Zn(phen)(HM) (**10**) and Zn(phen)(HE) (**11**) deserve further study owing to their good topoisomerase I inhibition, antibacterial and antifungal activities. Though these complexes are not efficient DNA cleavage agents, their ability to differentiate DNA sequences and induce various conformational change upon DNA binding make them good candidate as potential anticancer agent that does not cause oxidative cleavage to DNA. Complexes **10** and **11** that can bind strongly to the G-quadruplex also warrants further study as they can shed light on the requirements of zinc complexes that can stabilize G-quadruplex. As for the copper complexes, the most promising candidates are complexes Cu(bipy)(HP) (**16**), Cu(phen)(HE) **(19)** owing to their high nucleolytic efficiency, topoisomerase I inhibition, antibacterial and antifungal activities. Based on the selection of the most active complexes in each series that we have tested, (Zn(bipy)(HP)(**8**), Zn(phen)(HE)(**11**), Cu(bipy)(HP)(**16**), and Cu(phen)(HE)(**19**)) we can conclude that phenyl and alkyl substituted thiosemicarbazone complexes are always better than the non-substituted derivatives in the same series and the choice of polypyridyl ligands is crucial in determining the biological properties and water solubility of a particular complex. Further, the biological activities of the complexes seems to be cooperative since most complexes that are selective DNA binders are also good nuclease, topoisomerase I inhibitors, antibacterial and antifungal agents. Further, tests such as cytotoxicity assays can be carried out to evaluate the potential anticancer properties of the complexes that can inhibit topoisomerase I and bind strongly to G-quadruplex. Docking studies with computer simulation can also help to shed light on the mode of binding of the complexes to duplex and G-quadruplex DNA.

REFERENCES

Ackerman, L. J., Fanwick, P. E., Green, M. A., John, E., Running, W. E., Swearingen, J. K., et al. (1999). Structural and spectral studies of copper(II) and nickel(II) complexes of pyruvaldehyde mixed bis{N(4)-substituted thiosemicarbazones}. *Polyhedron, 18*, 2759-2767.

Addison, A. W., Rao, T. N., Reedijk, J., Van Rijn, J., & Verschoor, G. C. (1984). Synthesis, structure, and spectroscopic properties of copper(II) compounds containing nitrogen-sulphur donor ligands; the crystal and molecular structure of aqua[1,7-bis(N-methylbenzimidazol-2′;-yl)-2,6-dithiaheptane]copper(II) perchlorate. *J. Chem. Soc., Dalton Trans.* 7, 1349-1356

Adsule, S., Barve, V., Chen, D., Ahmed, F., Dou, Q. P., Padhye, S & Sarkar, F. H. (2006). Novel schiff base copper complexes of quinoline-2 carboxaldehyde as proteasome inhibitors in human prostate cancer cells. *J. Med. Chem., 49*, 7242-7246.

Afrasiabi, Z., Sinn, E., Chen, J., Ma, Y., Rheingold, A. L., Zakharov, L. N., Rath, N. & Padhye, S. (2004). Appended 1,2-naphthoquinones as anticancer agents 1: Synthesis, structural, spectral and antitumor activities of ortho-naphthaquinone thiosemicarbazone and its transition metal complexes. *Inorg. Chim. Acta ,357*, 271-278

Al-Kubaisi, A. H. (2002). Copper(II) complexes of 2,3-dihydroxybenzaldehyde N(4)-substituted thiosemicarbazone. *Int. J. Chem.*, 12, 213-220.

Alvero, A. B., Chen, W., Sartorelli, A. C., Schwartz, P., Rutherford, T., & Mor, G. (2006). Triapine (3-aminopyridine-2-carboxaldehyde thiosemicarbazone) induces apoptosis in ovarian cancer cells. *J. Soc. Gynecol. Invest., 13*, 145-152.

Ang W. H. and Dyson, P. J. (2006). Classical and non-classical ruthenium based anticancer drugs: Towards targeted chemotherapy. *Eur. J. Inorg. Chem.*,4003-4018.

Arola, A., & Vilar, R. (2008). Stabilisation of G-quadruplex DNA by small molecules. *Curr. Topics in Med. Chem., 8*, 1405-1415.

Arola-Arnal, A., Benet-Buchholz, J., Neidle, S., & Vilar, R. (2008). Effects of metal coordination geometry on stabilization of human telomeric quadruplex DNA by square-planar and square-pyramidal metal complexes. *Inorg. Chem. , 47*, 11910-11919

Attia, S., Kolesar, J., Mahoney, M. R., Pitot, H. C., Laheru, D., Heun, J., Huang, W., Eickhoff, J., Erlichman, C. & Holen, K. D. (2008). A phase 2 consortium (P2C) trial of 3-aminopyridine-2-carboxaldehyde thiosemicarbazone (3-AP) for advanced adenocarcinoma of the pancreas. *Invest. New Drugs, 26*, 369-379.

Baker, E. S., Bernstein, S. L. , Gabelica, V., De Pauw, E. & Bowers, M. T. (2006). G-quadruplexes in telomeric repeats are conserved in a solvent-free environment. *Int. J. Mass Spectrom*. 253, 225-237.

Bal, W., Liang, R., Lukszo, J., Lee, S., Dizdaroglu, M., & Kasprzak, K. S. (2000). Ni(II) specifically cleaves the C-terminal tail of the major variant of histone H2A and forms an oxidative damage-mediating complex with the cleaved- off octapeptide. *Chem. Res. Toxicol. , 13*, 616-624.

Bal-Demirci, T. (2008). Synthesis, spectral characterization of the zinc(II) mixed-ligand complexes of N(4)-allyl thiosemicarbazones and ′,N′,N,N - tetramethylethylenediamine, and crystal structure of the novel [ZnL2(tmen)] compound. *Polyhedron, 27*, 440-446.

Barbour, L. J. (2001). X-seed - A software tool for Supramol. crystallography. *J. Supramol. Chem., 1*(4-6), 189-191.

Barnes, K. R, Kutikov, A. and Lippard S. J. (2004). Synthesis, characterization, and cytotoxicity of a series of estrogen-tethered platinum(IV) complexes. *Chem. Biol.* 11, 557-564.

Barve, V., Ahmed, F., Adsule, S., Banerjee, S., Kulkarni, S., Katiyar, P., Anson, C. E., Powell, A. K. , Padhye, S. & Sarkar, F. H (2006). Synthesis, molecular characterization, and biological activity of novel synthetic derivatives of chromen-4-one in human cancer cells. *J. Med. Chem.*, 3800-3808.

Bauer, D.J. Ed. *Thiosemicarbazones in Chemotherapy of Virus Diseases*, Pergamon Press, Oxford 1972, Vol. *1*.

Bazzicalupi, C., Bencin, A., Bonaccini, C., Giorgi, C., Gratteri, P., Moro, S., Palumbo, A., Simionato, A., Sgrignani, J., Sissi, C. & Valtancoli, B. (2008) Tuning the activity of Zn(II) complexes in DNA cleavage: clues for design of new efficient metallo-hydrolases. *Inorg. Chem*. 47, 5473-5484.

Beraldo, H., & Gambino, D. (2004). The wide pharmacological versatility of semicarbazones, thiosemicarbozones and their metal complexes. *Mini-rev Med. Chem., 4*, 31-39.

Beretta, GL, Perego P, Zunino F (2008) Targeting topoisomerase I:molecular mechanisms and cellular determinants of response to topoisomerase I inhibitors. *Expert Opin. Ther. Targets*. 12, 1243-1256.

Bergamo, A. &, Sava, G. (2007). Ruthenium complexes can target determinants of tumour malignancy. *Dalton Trans.*, 135, 1267-1272.

Bindu, P., & Prathapachandra Kurup, M. R. (1997). E.s.r. and electrochemical studies of four- and five-coordinate copper(II) complexes containing mixed ligands. *Transition Met. Chem., 22*, 578-582.

Bindu, P., Kurup, M. R. P., & Satyakeerty, T. R. (1998). EPR, cyclic voltammetric and biological activities of copper(II) complexes of salicylaldehyde N(4)-substituted thiosemicarbazone and heterocyclic bases. *Polyhedron, 18*, 321-331.

Boer, D. R., Canals, A., & Coll, M. (2009). DNA-binding drugs caught in action: The latest 3D pictures of drug-DNA complexes. *Dalton Tran.s,* 3, 399-414.

Bradbury, B. J., & Pucci, M. J. (2008). Recent advances in bacterial topoisomerase inhibitors. *Curr. Opin. in Pharm., 8*, 574-581

Bregman, H., Carroll, P. J. & Meggers, E. (2006). Rapid access to unexplored chemical space by ligand scanning around a ruthenium center: discovery of potent and selective protein kinase inhibitors. *J. Am. Chem. Soc.* 128, 877-884.

Brewer, G. J. (2003). Copper in medicine. *Curr. Opin. in Chem. Biol.*, 7 207-212.

Brockman, R.W.; Thomson, J.R.; Bell, M.J.; Skipper, H.E. (1956). Observations on the Antileukemic Activity of Pyridine-2-carboxaldehyde Thiosemicarbazone and Thiocarbohydrazone. *Cancer Res. 16*, 167-170.

Bruijnincx, P. C. and Sadler, P. J. (2008) New trends for metal complexes with anticancer activity. *Curr. Opin. in Chem. Biol.*. 12, 197-206

Bruker (2007). APEX2 and SAINT. Bruker AXS Inc., Madison, Wisconsin, USA.

Burge, S., Parkinson, G. N., Hazel, P., Todd, A. K., & Neidle, S. (2006). Quadruplex DNA: Sequence, topology and structure. *Nucleic Acids Res.*, 34, 5402-5415.

Campbell, M. J. M. (1975). Transition metal complexes of thiosemicarbazide and thiosemicarbazones. *Coord. Chem. Rev., 15*, 279-319.

Champoux, J. J. (2001). DNA TOPOISOMERASES: Structure, Function, and Mechanism. *Annu. Rev. Biochem.* 70, 369–413

Carter, M. T., Rodriguez, M., & Bard, A. J. (1989). Voltammetric studies of the interaction of metal chelates with DNA. 2. tris-chelated complexes of cobalt(III) and iron(II) with 1,10-phenanthroline and 2,2 -bipyridine. *J. Am. Chem. Soc.* , 111, 8901-8911.

Chakravarty A. R. (2006). Photocleavage of DNA by copper(II) complexes. *J. Chem. Sci.*, 118, 443–453.

Chen, J., Huang, Y., Liu, G., Afrasiabi, Z., Sinn, E., Padhye, S. & Ma, Y. (2004). The cytotoxicity and mechanisms of 1,2-naphthoquinone thiosemicarbazone and its metal derivatives against MCF-7 human breast cancer cells. *Toxicol. Appl. Pharmacol.*,197, 40-48.

Chuang N-N, Lin C-L & Chen H-K (1996). Modification of DNA Topoisomerase I Enzymatic Activity with Phosphotyrosyl Protein Phosphatase and Alkaline Phosphatase from the Hepatopancreas of the Shrimp *Penaeus japonicus* (Crustacea: Decapoda). *Comp. Biochem. Physiol*. l14B, 145-151.

Clarke, M. J. Ruthenium metallopharmaceuticals. *Coord. Chem. Rev.* (2003). 236:209-233.

Dang, Yuanlin; Zhuo, Lihong; Chen, Xin; Li, Xin. (2002). Spectrophotometric study on the color reaction of 2,4-dihydroxybenzaldehyde thiosemicarbazone with copper and application. *Yejin Fenxi,* 22, 6-8. Journal written in Chinese

Dhar, S., Liu, Z., Thomale, J., Dai. H. and Lippard. S. J. (2008). Targeted single-wall carbon nanotube-mediated Pt(IV) prodrug delivery using folate as a homing device. *J. Am. Chem. Soc*. 13, 11467-1476.

Dhar, S., Nethaji, M., & Chakravarty, A. R. (2005). Synthesis, crystal structure and photo-induced DNA cleavage activity of ternary copper(II) complexes of NSO-donor schiff bases and N,N-donor heterocyclic ligands. *Inorg. Chim. Acta , 358,* 2437-2444.

Dilović, I., Rubc□ić, M., Vrdoljak, V., Pavelić, S. K., Kralj, M., Piantanida, I. & Cindric, M. (2008). Novel thiosemicarbazone derivatives as potential antitumor agents: Synthesis, physicochemical and structural properties, DNA interactions and antiproliferative activity. *Bioorg. and Med. Chem., 16,* 5189-5198

Dixon IM, Lopez F, Tejera AM, Esteve JP, Blasco MA, Pratviel G, Meunier B: A G-quadruplex ligand with 10 000-fold selectivity over duplex DNA. *J. Am. Chem. Soc.* 2007, 129, 1502-1503.

Dyson, P. J. & Sava, G. (2006). Metal-based antitumour drugs in the post genomic era. *Dalton Trans.,* 1929-1933.

Fahmi, N., & Singh, R. V. (1996). Spectroscopic, antifungal and antibacterial studies of some manganese heterochelates. *J. Indian Chem. Soc., 73,* 257-259.

Fan, H., Villegas, C., Huang, A., & Wright, J. A. (1998). The mammalian ribonucleotide reductase R2 component cooperates with a variety of oncogenes in mechanisms of cellular transformation. *Cancer Res., 58,* 1650-1653.

Farrell, N. (2002). Biomedical uses and applications of inorganic chemistry. An overview. *Coord. Chem. Rev. 232,* 1-4.

Feazell, R. P., Nakayama-Ratchford N, Dai. H. and Lippard. S. J. (2007). Soluble single-walled carbon nanotubes as longboat delivery systems for platinum(IV) anticancer drug design. *J. Am. Chem. Soc*. 129, 8438-8439.

Finch, R. A., Liu, M., Cory, A. H., Cory, J. G., & Sartorelli, A. C. (1999). *Triapine (3-aminopyridine-2-carboxaldehyde thiosemicarbazone; 3-AP): An inhibitor of ribonucleotide reductase with antineoplastic activity . Adv Enzyme Regul*. 39, 3–12.

Fleming, I (1967). Absolute Configuration and the Structure of Chlorophyll. *Nature* 216, 151–152.

G. Petering and G.J. van Giessen, The Biochemistry of Copper, Academic Press, New York, 1966, p. 197.

Gaggelli E, Kozlowski H, Valensin D, Valensin G. (2006). Copper homeostasis and neurodegenerative disorders (Alzheimer's, prion, and Parkinson's diseases and amyotrophic lateral sclerosis). *Chem Rev*, 106,1995-2044.

Galanello, R., Piga, A., Alberti, D., Rouan, M. -., Bigler, H., & Séchaud, R. (2003). Safety, tolerability, and pharmacokinetics of ICL670, a new orally active iron-chelating agent in patients with transfusion-dependent iron overload due to β-thalassemia. *J. Clin. Pharm., 43*, 565-572.

Gao, F., Chao, H., Zhou, F., Chen, X., Wei, Y. -., & Ji, L. -. (2008). Synthesis, GC selective DNA binding and topoisomerase II inhibition activities of ruthenium(II) polypyridyl complex containing 11-aminopteridino[6,7-f][1,10]phenanthrolin-13(12H)-one. *J. Inorg. Biochem., 102*, 1050-1059.

Gopal YNV, Konuru N, Kondapi AK. (2002). Topoisomerase II antagonism and anticancer activity of coordinated derivatives of $[RuCl_2(C_6H_6)(dmso)]$. *Arch Biochem Biophys* 2002, 401, 53-62.

Guyatt, G. H., Oxman, A. D., Ali, M., Willan, A., McIlroy, W., & Patterson, C. (1992). Laboratory diagnosis of iron-deficiency anemia: An overview. *J.Gen. Internal Med. 7*, 145-153.

Harris AL, Yang X, Hegmans A, Povirk L, Ryan J. J, Kelland L, Farrell NP. (2005). Synthesis, characterization, and cytotoxicity of a novel highly charged trinuclear platinum compound. Enhancement of cellular uptake with charge. *Inorg Chem*, 44, 9598-9600.

He, J., Sun, J., Mao, Z-W., Ji, L-N. & Sun, H. (2009). Phosphodieste hydrolysis and specific DNA binding and cleavage promoted by guanidinium-functionalized zinc complexes. *J. Inorg. Biochem*. 103, 851-858.

Heaney, R. P. (2000). Calcium, dairy products and osteoporosis. *J. Am. Coll. Nutrit., 19*(SUPPL.), 83S-99S.

Hirohama, T., Kuranuki, Y., Ebina, E., Sugizaki, T., Arii, H., Chikira, M., Tamil Selvi, P. & Palaniandavar, M. (2005). Copper(II) complexes of 1,10-phenanthroline-derived ligands: Studies on DNA binding properties and nuclease activity. *J. Inorg. Biochem, 99*, 1205-1219

Hotze A. C. G, Kariuki, B. M. & Hannon, M. J. (2006). Dinuclear double stranded metalloSupramol. ruthenium complexes: potential anticancer drugs. *Angew Chem Int Ed*., 45, 4839-4842.

Ivanov, V. I., Minchenkova, L. E., Schyolkina, A. K., & Poletayev, A. I. (1973). Different conformations of double-stranded nucleic acid in solution as revealed by circular dichroism. *Biopolymers - Peptide Science Section, 12*, 89-110.

Janiak, C. (2000). A critical account on π-π stacking in metal complexes with aromatic nitrogen-containing ligands. *J. Chem. Soc., Dalton Trans.* ,21, 3885-3896

Jenkins, Y., Friedman, A. E., Turro, N. J., & Barton, J. K. (1992). Characterization of dipyridophenazine complexes of ruthenium(II): The light switch effect as a function of nucleic acid sequence and conformation. *Biochem.* , *31*, 10809-10816.

Jeragh, B. J. A., & El-Dissouky, A. (2005). Synthesis, spectroscopic and the biological activity studies of thiosemicarbazones containing ferrocene and their copper(II) complexes. *J.Coord. Chem., 58*(12), 1029-1038.

John, R. P., Sreekanth, A., Rajakannan, V., Ajith, T. A., & Kurup, M. R. P. (2004). New copper(II) complexes of 2-hydroxyacetophenone N(4)-substituted thiosemicarbazones and polypyridyl co-ligands: Structural, electrochemical and antimicrobial studies. *Polyhedron, 23*(16), 2549-2559

Joseph, M., Kuriakose, M., Kurup, M. R. P., Suresh, E., Kishore, A., & Bhat, S. G. (2006). Structural, antimicrobial and spectral studies of copper(II) complexes of 2-benzoylpyridine N(4)-phenyl thiosemicarbazone. *Polyhedron, 25*(1), 61-70.

Joseph, M., Suni, V., Prathapachandra Kurup, M. R., Nethaji, M., Kishore, A., & Bhat, S. G. (2004). Structural, spectral and antimicrobial studies of copper(II) complexes of 2-benzoylpyridine N(4)-cyclohexyl thiosemicarbazone. *Polyhedron, 23*, 3069-3080

Kageyama, Y., Yamazaki, Y., & Okuno, H. (1998). Novel approaches to prodrugs of anticancer diaminodichloroplatinum(II) complexes activated by stereoselective enzymatic ester hydrolysis. *J. Inorg. Biochem. , 70*, 25-32.

Kalinowski and Richardson. (2007). Future of Toxicologys Iron Chelators and Differing Modes of Action and Toxicity: The Changing Face of Iron Chelation Therapy.

Kikuta, E., Koike, T., & Kimura, E. (2000). Controlling gene expression by zinc(II)-macrocyclic tetraamine complexes. *J. Inorg. Biochem., 79*, 253-259.

Kim, N. W., Piatyszek, M. A., Prowse, K. R., Harley, C. B., West, M. D., Ho, P. L. C., Coviello, G. M., Wright, W. E., Weinrich, S. L. & Shay, J. W (1994). Specific association of human telomerase activity with immortal cells and cancer. *Science, 266* , 2011-2015.

Kim, C. H., Choi, J. W., Chun, H. J., & Choi, K. S. (1997). Synthesis of chitosan derivatives with quaternary ammonium salt and their antibacterial activity. *Polymer Bull., 38*, 387-393.

Komeda S, Moulaei T, Woods KK, Chikuma M, Farrell NP, Williams LD. (2006). A third mode of DNA binding: Phosphate clamps by a polynuclear platinum complex. *J. Am. Chem. Soc.* 128, 16092-16103.

Kong, D. & Xie, Y. (2000). Synthesis, structural characterization and potentiometric studies of divalent metal complexes with an octadentate tetraazamacrocyclic ligand and their DNA cleavage ability. *Polyhedron, 19*, 1527-1537.

Kovala-Demertzi, D., Alexandratos, A., Papageorgiou, A., Yadav, P. N., Dalezis, P., & Demertzis, M. A. (2008). Synthesis, characterization, crystal structures, in vitro and in vivo antitumor activity of palladium(II) and zinc(II) complexes with 2-formyl and 2-acetyl pyridine N(4)-1-(2-pyridyl)-piperazinyl thiosemicarbazone. *Polyhedron, 27*, 2731-2738

Kovala-Demertzi, D., Yadav, P. N., Wiecek, J., Skoulika, S., Varadinova, T., & Demertzis, M. A. (2006). Zinc(II) complexes derived from pyridine-2-carbaldehyde thiosemicarbazone and (1E)-1-pyridin-2-ylethan-1-one thiosemicarbazone. synthesis, crystal structures and antiproliferative activity of zinc(II) complexes. *J. Inorg. Biochem.. 100*, 1558-1567

Kozlowski, H., Janicka-Klos, A., Brasun, J., Gaggelli, E., Valensin, D., & Valensin, G. (2009). Copper, iron, and zinc ions homeostasis and their role in neurodegenerative disorders (metal uptake, transport, distribution and regulation). *Coord. Chem. Rev., 253*, 2665-2685

Kumar Singh S, Joshi S, Ranjan Singh A, Saxena JK, Pandey DS (2007) DNA binding and topoisomerase II inhibitory activity of water-soluble ruthenium(II) and rhodium(III) complexes. *Inorg. Chem*. 46, 10869-10876.

Kypr, J., Kenovska, I., Renciuk, D. and Vorlickova, M. (2009). Circular Dichroism and conformational polymorphism of DNA. *Nucleic Acids Res.,* 37, 1713-1725

Latheef, L., & Kurup, M. R. P. (2008). Spectral and structural studies of copper(II) complexes of thiosemicarbazones derived from salicylaldehyde and containing ring incorporated at N(4)-position. *Spectrochim. Acta - Part A: Molecular and Biomolecular Spectroscopy, 70*, 86-93.

Latheef, L., Manoj, E., & Prathapachandra Kurup, M. R. (2007). Synthesis and spectral characterization of zinc(II) complexes of N(4)-substituted thiosemicarbazone derived from salicylaldehyde: Structural study of a novel -OH free Zn(II) complex. *Polyhedron, 26,* 4107-4113.

Liberta, A. E., & West, D. X. (1992). Antifungal and antitumor activity of heterocyclic thiosemicarbazones and their metal complexes: Curr. status. *Biometals, 5,* 121-126.

Lincoln, P., & Nordén, B. (1998). DNA binding geometries of ruthenium(II) complexes with 1,10-phenanthroline and 2,2′-bipyridine ligands studied with linear dichroism spectroscopy. Borderline cases of intercalation. *J. Phys. Chem. B, 102,* 9583-9594.

Linder, M. C., & Hazegh-Azam, M. (1996). Copper biochemistry and molecular biology. *American J. Clin. Nutrit., 63,* 797S-811S.

Liu C-L, Wang M, Zhang T-L, Sun H-Z (2004) DNA hydrolysis promoted by di- and multi-nuclear metal complexes. *Coord. Chem. Reviews,* 248, 147–168

Liu, H. K., Berners-Price, S. J., Wang, F. Y., Parkinson, J. A., Xu, J. J., Bella, J. & Sadler, P. J. (2006). Diversity in guanine-selective DNA binding modes for an organometallic ruthenium arene complex. *Angew Chem Int Ed.,* 45, 8153-8156.

Lobana, T. S., Sharma, R., Bawa, G., & Khanna, S. (2009). Bonding and structure trends of thiosemicarbazone derivatives of metals-an overview. *Coord. Chem. Rev., 253,* 977-1055.

Lozoff, B., Brittenham, G. M., & Wolf, A. W. (1987). Iron deficiency anemia and iron therapy effects on infant developmental test performance. *Pediatrics, 79,* 981-995.

Lyons, T. J, Gralla, E. B. and Valentine, J. S. (1999). Biological chemistry of copper-zinc superoxide dismutase and its link to amyotrophic lateral sclerosis. *Met Ions Biol Syst,* 36, 125-177.

Ma, B., Goh, B. C., Tan, E. H., Lam, K. C., Soo, R., Leong, S. S., Wang, L.Z. ,Mo, F., Chan, A. T. C., Zee, B. & Mok, T. (2008). A multicenter phase II trial of 3-aminopyridine-2-carboxaldehyde thiosemicarbazone (3-AP, triapine®) and gemcitabine in advanced non-small-cell lung cancer with pharmacokinetic evaluation using peripheral blood mononuclear cells. *Invest.al New Drugs, 26,* 169-173.

MacDiarmid, J. A., Mugridge, N. B., Weiss, J. C., Phillips, L., Burn, A. L., Paulin, R. P., Haasdyk, J. E., Dickson, K. A., Brahmbhatt, V. N., and Pattison S.T (2007). Bacterially derived 400 nm particles for encapsulation and cancer cell targeting of chemotherapeutics. *Cancer Cell* 11, 431-445.

Mackay F. S, Woods J. A, Heringova´ P, Kapa´ rkova´ J, Pizarro A. M, Moggach S. A, Parsons, S, Brabec, V, Sadler, P. J. (2007). A potent cytotoxic photoactivated platinum complex. PNAS, 104, 20743-20748.

Mackay. F. S., Woods, J. A., Moseley, H., Ferguson, J., Dawson, A., Parsons, S. and Sadler, P. J. (2006) A photoactivated trans-diammine platinum complex as cytotoxic as cisplatin. *Chem. Eur. J.* 12, 3155-3161.

Mahadevan, S., & Palaniandavar, M. (1996). $[Cu(5,6\text{-dmp})_2]^{2+}$ selectively and reversibly converts calf thymus DNA from right-handed B to left-handed Z conformation. *Chem. Commun*., 22, 2547-2548.

Mancin F, Tecilla P (2007) Zinc(II) complexes as hydrolytic catalysts of phosphate diester cleavage: from model substrates to nucleic acids. *New J. Chem.* 31, 800-817

Mazumder, U. K., Gupta, M., Karki, S. S., Bhattacharya, S., Rathinasamy, S., & Thangavel, S. (2004). Synthesis, anticancer and antibacterial activity of some novel mononuclear Ru(II) complexes. *Chem. Pharm. Bull., 52*, 178-185.

Mazumder, U. K., Gupta, M., Bera, A., Bhattacharya, S., Karki, S., Manikandan, L. & Patra, S. (2003). Synthesis, antitumour and antibacterial activity of some $Ru(bpy)_2^{2+}$/4-substituted thiosemicarbazide complexes. *Indian J. Chem. – Sect. A 42*, 313-317.

McKeage MJ, Maharaj L, Berners-Price SJ. (2002). Mechanisms of cytotoxicity and antitumor activity of gold(I) phosphine complexes: the possible role of mitochondria. *Coord. Chem. Rev.*232, 127-135.

Meggers E, Atilla-Gokcumen GE, Bregman H, Maksimoska J, Mulcahy SP, Pagano N, Williams DS. (2007). Exploring chemical space with organometallics: Rutheniumcomplexes as protein kinase inhibitors. *Synlett*, 1177-1189.

Milacic V, Chen D, Ronconi L, Landis-Piwowar KR, Fregona D, Dou Q. P. (2006). A novel anticancer gold(III) dithiocarbamate compound inhibits the activity of a purified 20S proteasome and 26S proteasome in human breast cancer cell cultures and xenografts. *Cancer Res* 66, 10478-10486.

Musetti, C., Lucatello, L., Bianco, S., Krapcho, A. P., Cadamuro, S. A., Palumbo, M. & Sisis, C. (2009). Metal ion-mediated assembly of effective phenanthroline-based G-quadruplex ligands. Dalton Trans., 19, 3657-3660

Nagesh N, Krishnaiah A (2003) A comparative study on the interaction of acridine and synthetic bis-acridine with G-quadruplex structure. *J. Biochem. Biophys. Methods.* 57, 65-74.

Naik, A. D., Reddy, P. A. N., Nethaji, M., & Chakravarty, A. R. (2003). Ternary copper(II) complexes of thiosemicarbazones and heterocyclic bases showing

N3OS coordination as models for the type-2 centers of copper monooxygenases. *Inorg. Chim.Acta* , *349*, 149-158

Najajreh Y, Perez JM, Navarro-Ranninger C, Gibson D. (2002). Novel soluble cationic trans-diaminedichloroplatinum(II) complexes that are active against cisplatin resistant ovarian cancer celllines. *J. Med. Chem.* 2002, 45, 5189-5195.

Natile G, Coluccia M. (2001). Curr. status of trans-platinum compounds in cancer therapy. *Coord. Chem. Rev.* 2001, 216-217, 383-410.

Neidle, S., & Parkinson, G. (2002). Telomere maintenance as a target for anticancer drug discovery. *Nature Rev. Drug Discovery*, *1*, 383-393.

Neufeld, E. J. (2006). Oral chelators deferasirox and deferiprone for transfusional iron overload in thalassemia major: New data, new questions. *Blood*, 107, 3436-3441.

Nitiss, J. L. (1998). Investigating the biological functions of DNA topoisomerases in eukaryotic cells. *Biochimica et Biophysica Acta* , 1400, 63-81

Ng, C. H., Kong, K. C., Von, S. T., Balraj, P., Jensen, P., Thirthagiri, E., et al. (2008). Synthesis, characterization, DNA-binding study and anticancer properties of ternary Metal(II) complexes of edda and an intercalating ligand. *Dalton Trans*, *8*, 447-454.

Nordin, B. E. C. (1997). Calcium and osteoporosis. *Nutrition*, *13*, 664-686.

Odenike, O. M., Larson, R. A., Gajria, D., Dolan, M. E., Delaney, S. M., Karrison, T. G., Ratain, M. J. & Stock, W. (2008). Phase I study of the ribonucleotide reductase inhibitor 3-aminopyridine-2-carboxaldehyde-thiosemicarbazone (3-AP) in combination with high dose cytarabine in patients with advanced myeloid leukemia. *Invest.al New Drugs, 26*, 233-239.

Oleksi, A. G. Blanco, R. Boer, I. Uson, J. Aymami, Rodger, A., Hannon, M. J. & Coll. M. (2006) Molecular recognition of a three-way DNA junction by a metalloSupramol. helicate. *Angew. Chem. Int. Ed. Engl.* 45, 1227–1231

Orvig, C. & Abrams, M. J. (1999). Medicinal Inorganic Chemistry. *Chem. Rev.* (9)99: 2201-2203

Pandeya, S. N., D. Sriram, D. G. Nath, G. E. DeClercq, E. (1999). Synthesis, antibacterial, antifungal and anti-HIV activities of Schiff and Mannich bases derived from isatin derivatives and N-[4-(4'-chlorophenyl)thiazol-2-yl] thiosemicarbazide. *European J. Pharm. Sci.* 9, 25–31

Padyhe, S. & Kaufman G. B. (1985). Transition metal complexes of semicarbazone and thiosemicarbazones. *Coord. Chem. Rev.*, 63, 127-160.

Parkinson, G. N., Lee, M. P. H., & Neidle, S. (2002). Crystal structure of parallel quadruplexes from human telomeric DNA. *Nature, 417*, 876-880.

Pascu, G. I, Hotze, A. C. G., Sanchez-Cano, C, Kariuki, B. M., Hannon & M. J. . (2007). Dinuclear ruthenium(II) triple-stranded helicates: Luminescent Supramol. cylinders that bind and coil DNA and exhibit activity against cancer cell lines. *Angew Chem Int Ed*, 46:4374-4378.

Patra, A. K., Dhar, S., Nethaji, M., & Chakravarty, A. R. (2005). Metal-assisted red light-induced DNA cleavage by ternary L-methionine copper(II) complexes of planar heterocyclic bases. *Dalton Trans.*, 5, 896-902.

Patra, A. K., Nethaji, M., & Chakravarty, A. R. (2007). Synthesis, crystal structure, DNA binding and photo-induced DNA cleavage activity of (S-methyl-l-cysteine)copper(II) complexes of heterocyclic bases. *J. Inorg. Biochem. , 101*, 233-244.

Pierce, S. E., Kieltyka, R., Sleiman, H. F., & Brodbelt, J. S. (2009). Evaluation of binding selectivities and affinities of platinum-based quadruplex interactive complexes by electrospray ionization mass spectrometry. *Biopolymers, 91*, 233-243.

Pillarsetty, N., Katti, K. K., Hoffman, T. J., Volkert, W. A, Katti, K. V., Kamei, H. & Koide, T. (2003). In vitro and in vivo antitumor properties of tetrakis((trishydroxymethyl)phosphine)gold(I) chloride. *J. Med. Chem*., 46, 1130-1132.

Pratesi G, Perego P, Polizzi D, Righetti SC, Supino R, Caserini C, Manzotti C, Giuliani FC, Pezzoni G & Tognella S. (1999). A novel charged trinuclear platinum complex effective against cisplatin-resistant tumors: hypersensitivity of p53-mutant human tumor xenografts. *Br. J. Cancer*, 80, 1912-1919.

Pyle, A. M., Rehmann, J. P., Meshoyrer, R., Kumar, C. V., Turro, N. J., & Barton, J. K. (1989). Mixed-ligand complexes of ruthenium(II): Factors governing binding to DNA. *J. Am. Chem. Soc*., 111, 3051-3058.

Qian J, Gu W, Liu H, Gao F, Feng L, Yan S, Liao D, Cheng P (2007) The first dinuclear copper(II) and zinc(II) complexes containing novel bis-TACN: Syntheses, structures, and DNA cleavage activities. *Dalton Trans*., 1060-1066.

R.A. Tromp, S. van Boom, C.M. Timmers, S. van Zutphen, G.A. van der Marel, H.S. Overkleeft, J.H. van Boom, J. Reedijk. (2004). The β-glucuronyl-based prodrug strategy allows for its application on β-glucuronyl-platinum conjugates. *Bioorg. Med. Chem. Lett.*, 14, 4273-4276.

Ramakrishnan, S., & Palaniandavar, M. (2008). Interaction of rac-$[Cu(diimine)_3]^{2+}$ and rac-$[Zn(diimine)_3]^{2+}$ complexes with CT DNA: Effect of fluxional Cu(II) geometry on DNA binding, ligand-promoted exciton coupling and prominent DNA cleavage. *Dalton Trans.*, 29, 3866-3878.

Rao, R., Patra, A. K., & Chetana, P. R. (2007). DNA binding and oxidative cleavage activity of ternary (l-proline)copper(II) complexes of heterocyclic bases. *Polyhedron, 26*, 5331-5338.

Rao, R., Patra, A. K., & Chetana, P. R. (2008). Synthesis, structure, DNA binding and oxidative cleavage activity of ternary (l-leucine/isoleucine) copper(II) complexes of heterocyclic bases. *Polyhedron, 27*, 1343-1352.

Rao, V. A., Klein, S. R., Agama, K. K., Toyoda, E., Adachi, N., Pommier, Y. & Shacter, E. B. (2009). The iron chelator Dp44mT causes DNA damage and selective inhibition of topoisomerase IIA in breast cancer cells. *Cancer Res., 69*, 948-957.

Rebolledo, A. P., Vieites, M., Gambino, D., Piro, O. E., Castellano, E. E., Zani, C. L., Souza-Fagundes, E. M. , Teixeira, L. R. , Batista, A. A. & Beraldo, H. (2005). Palladium(II) complexes of 2-benzoylpyridine-derived thiosemicarbazones: Spectral characterization, structural studies and cytotoxic activity. *J. Inorg. Biochem. , 99*(3), 698-706

Reed, J. E., Arnal, A. A., Neidle, S. & Vilar R: Stabilization of G-quadruplex DNA and inhibition of telomerase activity by square-planar nickel(II) complexes. *J. Am. Chem. Soc.* 2006, 128, 5992-5993.

Reed, J. E., Neidle, S., & Vilar, R. (2007). Stabilisation of human telomeric quadruplex DNA and inhibition of telomerase by a platinum-phenanthroline complex. *Chem. Commun.,* (42), 4366-4368

Reed, J. E., White, A. J. P., Neidle, S., & Vilar, R. (2009). Effect of metal coordination on the interaction of substituted phenanthroline and pyridine ligands with quadruplex DNA. *Dalton Trans.,* 14, 2558-2568.

Reichard, P. (1988). Interactions between deoxyribonucleotide and DNA synthesis. *Annual Review of Biochem. , 57*, 349-374.

Rodríguez-Argu□elles, M. C., Tourón-Touceda, P., Cao, R., García-Deibe, A. M., Pelagatti, P., Pelizzi, C., & Zani, F. (2009). Complexes of 2-acetyl-γ-butyrolactone and 2-furancarbaldehyde thiosemicarbazones: Antibacterial and antifungal activity. *J. Inorg. Biochem., 103*, 35-42.

Rosenberg, B. L., VanChamp, L., Trosko, J. E. and Mansour, V. H. (1969). Platinum Compounds: A new class of potent antitumor agents. *Nature* 222, 385-386

Rothenberg ML (1997). Topoisomerase I inhibitors: review and update. *Ann. Oncol.* 8, 837-855

Roy, M., Pathak, B., Patra, A. K., Jemmis, E. D., Nethaji, M., & Chakravarty, A. R. (2007). New insights into the visible-light-induced DNA cleavage activity of

dipyridoquinoxaline complexes of bivalent 3d-metal ions. *Inorg. Chem. , 46*, 11122-11132.

S. Hanessian and J.G. Wang, (1993). Design and synthesis of a cephalosporin-carboplatinum prodrug activatable by a β-lactamase. *Can. J. Chem. Rev. Can. Chim*. 71, 896-906.

S. Neidle and G. Parkinson, *Nat. Rev. Drug Discovery*, 2002, 1, 383–393.

Sarkar, B. (1999). Treatment of Wilson and Menkes diseases. *Chem Rev*, 99, 2535-2544.

Seena, E. B., & Kurup, M. R. P. (2007). Spectral and structural studies of mono- and binuclear copper(II) complexes of salicylaldehyde N(4)-substituted thiosemicarbazones. *Polyhedron*, *26*, 829-836.

Seena, E. B., & Kurup, M. R. P. (2008). Synthesis, spectral and structural studies of zinc(II) complexes of salicylaldehyde N(4)-phenylthiosemicarbazone. *Spectrochim. Acta. - Part A: Molecular and Biomolecular Spectroscopy, 69*, 726-732

Seng, H. L., Alan Ong, H. K., Raja Noor, Z. R. A. R., Bohari, M. Y., Tiekink E. R. T., Tan, K.W., Maah, M. J., Caracelli, I. & Ng C. H (2008) Factors affecting nucleolytic efficiency of some ternary metal complexes with DNA binding and recognition domains. Crystal and molecular structure of Zn(phen)(edda). *J. Inorg. Biochem.* 102, 1997–2011.

Sheldrick, G. M. (1996). SADABS. University of Gottingen, Germany.

Sheldrick, G. M. (2007). A short history of SHELX. *Acta Crystallographica Section A: Foundations of Crystallography, 64*, 112-122.

Shelton, A. H., Rodger, A., & McMillin, D. R. (2007). DNA binding studies of a new dicationic porphyrin. insights into interligand interactions. *Biochem. , 46*, 9143-9154

Shouchun Zhang , Yangguang Zhu , Chao Tu , Haiying Wei , Zhen Yang , Liping Lin , Jian Ding , Junfeng Zhang , Zijian Guo. (2004). A novel cytotoxic ternary copper(II) complex of 1,10-phenanthroline and L-threonine with DNA nuclease activity. *J. Inorg. Biochem.* 98, 2099–2106

Singh, N. K., Srivastava, A., Sodhi, A., & Ranjan, P. (2000). In vitro and in vivo antitumour studies of a new thiosemicarbazide derivative and its complexes with 3d-metal ions. *Transition Met. Chem., 25*, 133-140.

Sun, R. W. Y., Ma, D. L., Wong, E. L. M. & Che, C. M. (2007). Some uses of metal complexes as anti-cancer and anti-HIV agents. *Dalton Trans.*, 4884-4892.

Sunami S, Nishimura T, Nishimura I, Ito S, Arakawa H, Ohkubo M (2009) Synthesis and biological activities of topoisomerase I inhibitors, 6-arylmethylamino analogues of edotecarin. *J. Med. Chem*. 52, 3225-3237.

Swearingen, J. K. and West D. X. (2000). T*ransition Met. Chem.* 25: 241-246.

Tan, K. W., Ng, C. H., Maah, M. J. & Ng, S. W. (2009). Bis(l-4-hydroxy-2-oxidobenzaldehyde 4-ethylthiosemicarbazone)- $\kappa^4O^2,N^1,S:-O^2$; $\kappa^4O^2:O^2,N^1,S$-bis[chloridozinc(II)]dimethyl sulfoxide trisolvate. *Acta Cryst.* E65, m549

Thomas, A. M., Naik, A. D., Nethaji, M., & Chakravarty, A. R. (2004). Synthesis, crystal structure and photo-induced DNA cleavage activity of ternary copper(II)-thiosemicarbazone complexes having heterocyclic bases. *Inorg. Chim. Acta , 357,* 2315-2323.

Thomas, A. M., Nethaji, M., Mahadevan, S., & Chakravarty, A. R. (2003). Synthesis, crystal structure, and nuclease activity of planar mono-heterocyclic base copper(II) complexes. *J. Inorg. Biochem., 94*, 171-178.

Tilyard, M. W., Spears, G. F. S., Thomson, J., & Dovey, S. (1992). Treatment of postmenopausal osteoporosis with calcitriol or calcium. *New England J. Med., 326*, 357-362.

Tonde, S. S., Kumbhar, A. S., Padhye, S. B., & Butcher, R. J. (2006). Self-activating nuclease activity of copper (II) complexes of hydroxyl-rich ligands. *J. Inorg. Biochem., 100*, 51-57

Tse-Dinh, Y. (2009). Bacterial topoisomerase I as a target for discovery of antibacterial compounds. *Nucleic Acids Res.*, 37, 731-737.

Tysoe, S. A., Morgan, R. J., Baker, A. D., & Strekas, T. C. (1993). Spectroscopic Invest. of differential binding modes of Δ- and Λ-$Ru(bpy)_2(dppz)^{2+}$ with calf thymus DNA. *J. Phys. Chem., 97,* 1707-1711.

Uma Maheswari, P., & Palaniandavar, M. (2004). DNA binding and cleavage properties of certain tetrammine ruthenium(II) complexes of modified 1,10-phenanthrolines - effect of hydrogen-bonding on DNA-binding affinity. *J. Inorg. Biochem. ,* 98, 219-230.

Urig S & Becker K (2006a). On the potential of thioredoxin reductase inhibitors for cancer therapy. *Semin. Cancer Biol*., 16, 452-465.

Urig S, Fritz-Wolf K, Reau R, Herold-Mende C, Toth K, Davioud-Charvet E,Becker K. (2006b). Undressing of phosphine gold(I) complexes as irreversible inhibitors of human disulfide reductases. *Angew Chem Int Ed.*, 45, 1881-1886.

Valdés-Martínez, J., Toscano, R. A., Zentella-Dehesa, A., Salberg, M. M., Bain, G. A., & West, D. X. (1996). Synthesis, crystal and molecular structure of 5-bromo-salicylaldehyde-2-methylthiosemicarbazonato(nitrato) copper(II) monohydrate. *Polyhedron, 15*, 427-431.

Valko, M., Rhodes, C. J., Moncol, J., Izakovic, M., & Mazur, M. (2006). Free radicals, metals and antioxidants in oxidative stress-induced cancer. *Chemico-Biol. Interactions, 160*, 1-40.

Vallee, B. L., & Auld, D. S. (1990). Zinc coordination, function, and structure of zinc enzymes and other proteins. *Biochem. , 29*, 5647-565.

Wagner, K. R., Sharp, F. R., Ardizzone, T. D., Lu, A., & Clark, J. F. (2003). Heme and iron metabolism: Role in cerebral hemorrhage. *J.Cerebral Blood Flow and Metabolism, 23*, 629-652.

Wang X, Wang L-K, Kingsbury WD, Johnson RK, Hecht SM (1998) Differential effects of camptothecin derivatives on topoisomerase I-mediated DNA structure modifications. *Biochem.* 3, 9399-9408.

Wang, T., & Guo, Z. (2006). Copper in medicine: Homeostasis, chelation therapy and antitumor drug design. *Curr. Med. Chem., 13*, 525-537.

Wang, Y., & Patel, D. J. (1993). Solution structure of the human telomeric repeat d[AG3(T2AG3)3] G-tetraplex. *Structure, 1*, 263-282

Waterborg J. H. & Kuyper C. M. A. (1982). Substrate specificity and mode of action of the zinc-metallo nuclease from Physarum polycephalum. *J. Biochem.* 92, 1655-1661.

Wei, L., Easmon, J., Nagi, R. K., Muegge, B. D., Meyer, L. A., & Lewis, J. S. (2006). 64Cu-azabicyclo[3.2.2]nonane thiosemicarbazone complexes: Radiopharmaceuticals for PET of topoisomerase II expression in tumors. *J. Nucl. Med., 47*, 2034-2041.

West, D. X.; Padhye, S. B.; Sonawane, P. B. In *Structure and Bonding*, Springer-Verlag: New York, 1991, Vol. *76*, pp 1-49

West, D. X., Liberta, A. E., Padhye, S. B., Chikate, R. C., Sonawane, P. B., Kumbhar, A. S. (1993). Thiosemicarbazone complexes of copper(II): Structural and biological studies. *Coord. Chem. Rev.,* 123, 49-71.

West, D. X., Ives, J. S., Krejci, J., Salberg, M. M., Zumbahlen, T. L., Bain, G. A., Liberta, A. E., Valdes-Martinez, J. S., Hernadez-Ortiz & Toscano R. A. (1995). Copper(II) complexes of 2-benzoylpyridine ^{4}N-substituted thiosemicarbazones. *Polyhedron*, 14, 2189-2200

Westrip, S. P. (2009). publCIF. In preparation

Yan, Y. K., Melchart, M., Habtemariam, A. & Sadler, P. J. (2005). Organometallic chemistry, biology and medicine: Ruthenium arene anticancer complexes. *Chem Commun*, 4764-4776.

Yang, Z., Wang, X. Y., Diao, H. J., Zhang, J. F., Li, H. Y., Sun, H .Z. and Guo, Z .J. (2007). Encapsulation of platinum anticancer drugs by apoferritin. *Chem. Commun.*, 3453-3455.

Zamble, D. B., Jacks, T. & Lippard, S. J. (1998). p53-dependent and -independent responses to cisplatin in mouse testicular teratocarcinoma cells. *Proc Natl Acad Sci* . USA , 95, 6163-6168.

Zhang, W-J., Ou, T-M., Lu Y-J., Huang, Y-Y., Wu, W-B., Huang, Z-S., Zhou, J-L., Wong, K-Y. & Gu, L-Q. (2007). 9-substituted derivatives as G-quadruplex stabilising ligands in telomeric DNA. *Bioorg. Med. Chem*. 15, 5493-5501.

Zhang, C. X. and Lippard, S. J. (2003) New metal complexes as potential therapeutics. *Curr. Opin. in Chem. Biol.*. 7, 481-489

Zhang, C., & Janiak, C. (2001). Six-coordinated zinc complexes: $[Zn(H_2O)_4(phen)]$ $(NO_3)_2{\cdot}H_2O$ and $[ZnNO_3(H_2O)(bipy)(him)]NO_3$ (phen = 1,10-phenanthroline, bipy = ′2,2 -bipyridine, and him = imidazole). *J. Chem. Crystallography, 31*, 29-35.

Zhu, X., Wang, C., Lu, Z., & Dang, Y. (1997). Synthesis, characterization and biological activity of the schiff base derived from 3,4-dihydroxybenzaldehyde and thiosemicarbazide, and its complexes with nickel(II) and iron(II). *Transition Met. Chem., 22,* 9-13.

Zutphen, S. V. and Reedijk, Jan. (2005). Targeting platinum anti-tumour drugs: Overview of strategies employed to reduce systemic toxicity. *Coord. Chem. Rev.* 249, 2485-2853

Appendix

List of publications:

1. K. W. Tan, Y. Farina, C. H. Ng, M. J. Maah & S. W. Ng (2008). *3,4-Dihydroxybenzaldehyde 4-phenylthiosemicarbazone. Acta Cryst.* E**64**, o1035.

2. K. W. Tan, C. H. Ng, M. J. Maah & S. W. Ng (2008). *2,4-Dihydroxybenzaldehyde 4-methylthiosemicarbazone. Acta Cryst.* E**64**, o2224.

3. K. W. Tan, Y. Farina, C. H. Ng, M. J. Maah & S. W. Ng (2008). *3,4-Dihydroxybenzaldehyde thiosemicarbazone. Acta Cryst.* E**64**, o1073.

4. K. W. Tan, C. H. Ng, M. J. Maah & S. W. Ng (2008). *Chlorido(2-methyl-4-oxo-4H-pyran-3-olato-κ^2O^3,O^4)(1,10-phenanthroline-κ^2N,N')copper(II). Acta Cryst.* E**64**, m1104.

5. K. W. Tan, C. H. Ng, M. J. Maah & S. W. Ng (2008). *2,5-Dihydroxybenzaldehyde 4-methylthiosemicarbazone. Acta Cryst.* E**64**, o1344.

6. K. W. Tan, C. H. Ng, M. J. Maah & S. W. Ng (2008). *2,4-Dihydroxybenzaldehyde 4-ethylthiosemicarbazone. Acta Cryst.* E**64**, o2123.

7. K. W. Tan, C. H. Ng, M. J. Maah & S. W. Ng (2009). *(4-Hydroxy-2-oxidobenzaldehyde thiosemicarbazonato-κ^3O^2,N^1,S)(1,10-phenanthroline-κ^2N,N')zinc(II) dimethyl sulfoxide disolvate monohydrate. Acta Cryst.* E**65**, m61-m62.

8. K. W. Tan, C. H. Ng, M. J. Maah & S. W. Ng (2009). *(2,2'-Bipyridine-κ^2N,N')(4-hydroxy-2-oxidobenzaldehyde thiosemicarbazonato-κ^3O^2,N^1,S)zinc(II). Acta Cryst.* E**65**, m143.

9. K. W. Tan, C. H. Ng, M. J. Maah & S. W. Ng (2009). *Bis(l-4-hydroxy-2-oxidobenzaldehyde 4-ethylthiosemicarbazone)- $\kappa^4O^2,N^1,S:-O^2$; $\kappa^4O^2:O^2,N^1,S$-bis[chloridozinc(II)]dimethyl sulfoxide trisolvate. Acta Cryst.* E**65**, m549

10. K. W. Tan, C. H. Ng, M. J. Maah & S. W. Ng (2009). *Bis(acetone 4-phenylthiosemicarbazonato-κ^2N^1,S)zinc(II). Acta Cryst.* E**65**, m969.

11. K. W. Tan, C. H. Ng, M. J. Maah & S. W. Ng (2009). *[1-(4-Hydroxy-2-oxidobenzylidene)-4-phenylthiosemicarbazonato-κ^3N,O,S](1,10-phenanthroline-κ^2N,N')zinc(II)-4,4'-bipyridine (2/1). Acta Cryst.* E**65**, m920.

12. H. L. Seng, S. Z. Von., K. W. Tan, M. J. Maah, S. W. Ng, Raja Noor Zaliha Raja Abd. Rahman, I. Caracelli, C. H. Ng (2009). Crystal structure, DNA binding studies, nucleolytic property and topoisomerase I inhibition of zinc complex with 1,10-phenanthroline and 3-methyl-picolinic acid. *Biometals*. **Published online 29 September 2009.**